NORTHWESTERN UNIVERSITY

# Engineering Spatial Patterns of Gene Expression: Fundamental Studies of Guided Cellular Processes and Applications to Tissue Regeneration

A DISSERTATION

SUBMITTED TO THE GRADUATE SCHOOL
IN PARTIAL FULFILLMENT OF THE REQUIREMENTS

for the degree

DOCTOR OF PHILOSOPHY

Field of Chemical Engineering

By

Tiffany Leigh Ray

EVANSTON, ILLINOIS

June 2008

# ABSTRACT

Engineering Spatial Patterns of Gene Expression: Fundamental Studies of Guided Cellular Processes and Applications to Tissue Regeneration

Tiffany Leigh Ray

Natural tissues can have complex architectures characterized by the organization of multiple cells into structures, such as branching networks of the vascular or nervous systems. This cellular organization arises, in part, from spatial patterns in the expression of soluble factors, which create concentration gradients that direct cellular processes during morphogenesis. Regenerative strategies for damaged tissue must recreate these cellular architectures to restore function. Biomaterials serve a central role in the engineering of functional tissue replacements, and are designed to present a combination of insoluble and soluble signals that direct tissue formation. Gradients of insoluble signals have been created at biomaterial surfaces; however, generation of gradients of soluble signals has proven more difficult. By combining non-viral gene delivery strategies with soft lithography, I have developed methods to spatially pattern gene expression. Using DNA encoding for soluble growth factors, transfection leads to localized and sustained secretion thereby creating concentration gradients as the factors diffuse. In this thesis, the systems are utilized to investigate fundamental questions in neurite guidance and are applied to the rational design of tissue engineering scaffolds. Spatial patterns of gene expression within a cluster of cells were established and the gradients formed by diffusion were mathematically modeled. Neuronal responses to NGF gradients formed by patterned expression were experimentally determined using an in vitro co-culture model, and the width of the pattern governed neuronal response. Patterns 100-250 μm in width confined neuron survival and neurite

extension to the region of localized expression. Patterns of 500-1000 μm in width guided neurite extension up the NGF gradient, with guidance dependent on the amount of NGF on the surface and the distance a neuron was cultured from the pattern. Spatial patterns of gene expression were next established within single cells, by altering the extent of transgene expression and transfection efficiency. The gene expression patterns were combined with topographically patterned scaffolds to determine the design parameters necessary for directed neurite extension during nerve regeneration strategies. Neurite guidance was governed by the topographical pattern width and the extent of transgene expression by transfected cells. Photopolymerizable hydrogels were developed to extend spatially patterned gene expression to three-dimensional systems. Hydrogels were characterized in terms of mechanical properties, DNA vector release, and in vivo cell migration and transfection. These studies demonstrate the capacity of patterned gene expression to create concentration gradients of soluble factors that can locally organize tissue formation. The systems developed in this thesis provide a platform with which to investigate concentration gradients in tissue formation, and may be applied for the engineering of functional tissue replacements.

# ACKNOWLEDGMENTS

To all of those who have provided necessary love and support the past five years, I am forever indebted. To my advisor, Lonnie Shea, thank you for your guidance and wisdom. You provided me the freedom to develop into an independent scientist and critical thinker. To my thesis committee, Guillermo, Annelise, and Phil, thank you for your direction and encouragement. To my original mentors, Angie, Zain, and Tatiana, you led by example and taught me to be strong. Thank you for taking the time to challenge me. To members of the Shea L.A.B., Chris, Jen, Alyssa, Abbie, Elizabeth, Michael, Hannah, Marina, David, Romie, Ryan, and Martha, thank you for the helpful scientific discussions, and more importantly, the laughs. To Jackie and Ariella, my hydrogel princesses, thank you for always making me smile. I know your time in the Shea lab will be filled with major scientific achievements. To my best friends, Erin, Laura, and Nisha, we have made many memories that I will forever hold close to my heart. I am lucky to have found such supportive confidants. To my parents, I owe all of my successes and accomplishments to your patience, courage, persistence, love, and support. You have given me the confidence to dream big and the humility to remember what's really important. To my sisters and very best friends, Tara and Tracy, thank you for always providing me a comical outlet and keeping me positive. To my grandfather, thank you for always believing in me and instilling in me a competitive spirit. To my in-laws, Ken and Nancy, thank you for taking me into your family as your own. Finally, to my husband, Justin, thank you for your endless love and support. I appreciate and acknowledge all of your sacrifices for me to achieve these goals, and I am the luckiest woman in the world to have you by my side.

*Dedicated to my family:*

*Justin,*

*Mom, Dad,*

*Tara and Tracy*

# TABLE OF CONTENTS

# LIST OF FIGURES

# LIST OF TABLES

# LIST OF ABBREVIATIONS

AA……*amino acid*
AAV……..*adeno-associated virus*
AFM……...*atomic force microscopy*
BDNF……...*brain derived neurotrophic factor*
BMP……*bone morphogenic protein*
CAM……..*cell adhesion molecule*
cAMP……*cyclic adenosine monophosphate*
CNS……...*central nervous system*
CSPG……*chondroitin sulfate proteoglycan*
DCC……...*deleted colorectal cancer*
DNA……...*deoxyribonucleic acid*
ECM……...*extracellular matrix*
EGF……*epidermal growth factor*
HA……*hyaluronic acid*
HEK293T……*human embryonic kidney cell line*
μCP…….....*microcontact printing*
NGF.....*nerve growth factor*
NT-3……..*neurotrophin-3*
PAM……*pressure assisted microsyringe*
PAMAM……..*poly(amido amine)*
PDMS……...*poly(dimethyl siloxane)*
PEG……..*poly(ethylene glycol)*
PEI……*poly(ethylene imine)*
PEO-PPO-PEO……*Pluronic*
PGA……*poly(glycolic acid)*
PLGA……*poly(lactic glycolic acid)*
PLL……..*poly(L-lysine)*
PLLA……*poly(L-lactic acid)*
PNS……..*peripheral nervous system*
SAM……..*self assembled monolayer*
siRNA……...*small interfering ribonucleic acid*

# Chapter 1

# Introduction: Thesis Overview

## *1.1 Motivation and Objectives*

Complex spatiotemporal patterns of gene expression guide cell differentiation and migration into organized functional structures during tissue development and repair. Patterned gene expression results in concentration gradients of guidance molecules facilitating cell orientation and instruction during morphogenesis [1], immune responses [2], wound repair [3, 4], and nervous system development [5]. The elucidation of cellular guidance mechanisms during embryogenesis and regeneration will rely on a fundamental understanding of the manner in which gradients are presented naturally, and how cells interpret gradients into functional response [6]. The mechanisms are difficult to study in vivo, limiting much of the embryogenesis research to *Drosophila*, *Xenopus*, and chick models [6]. Consequently, there exists a need for in vitro systems capable of recapitulating patterns of gene expression to characterize gradients and investigate cell responses. Recently, advances in biological patterning strategies have introduced systems to spatially pattern extracellular matrix molecules [7], adhesion peptides [8], and growth factors [9]. However, adsorption of proteins to heterogeneous hydrophobic surfaces or synthetic chemistries may alter protein structure and misrepresent the manner in which ligands are presented during normal tissue functions [10]. An in vitro system of spatially patterned gene expression within a complex cellular environment may present molecules similar to the manner in which they are presented naturally, providing an in vitro assay to study embryogenesis and regeneration. In this thesis, biological patterning strategies were combined with DNA delivery

techniques to spatially pattern non-viral DNA vectors and, subsequently, gene expression in vitro. Here, the system is employed to investigate neurite guidance and characterize the gradients formed by patterns of expression capable of eliciting a response. The thesis focuses on nerve guidance, but the system presented herein is universal and can be utilized for fundamental studies of tissue development or the rational design of tissue regeneration strategies.

Tissue engineering strategies aim to support and stimulate tissue formation that has been lost due to injury or disease. Tissue engineering scaffolds function to maintain a space at a lesion site and support cellular organization, while drug delivery strategies are incorporated to present factors that are critical to promote cell processes (adhesion, migration, differentiation, proliferation). Gene delivery from scaffolds aims to overcome disadvantages associated with traditional protein delivery, and can present therapeutic factors at elevated and sustained levels [11, 12]. Many tissues rely on a complex architecture to function properly, and tissue regeneration strategies must reestablish the architecture to regain function. Tissue engineering strategies combined with patterned gene delivery offers the potential to spatially control factors responsible for cell guidance and organization over time scales appropriate for regeneration. In this thesis, in vitro methods to pattern gene expression within regenerative scaffolds are developed. The systems are employed to determine design parameters for the rational design of tissue engineering scaffolds to optimize neurite guidance.

## *1.2 Thesis Outline and Approach*

Chapters 2-4 provide background material relevant to the experimental work. Chapter 2 details gene delivery strategies from tissue engineering scaffolds, including polymeric release and substrate-mediated delivery. Chapter 3 provides an overview of strategies to pattern

biologically relevant molecules, including soft lithography, a technique that is utilized throughout the thesis. Chapter 4 explains the fundamentals of nervous system development with a focus on growth cone guidance in response to spatial patterns of gene expression. Chapters 5-9 describe the experimental work, while Chapter 10 provides conclusions of the research presented herein and insight into future directions for the field.

An overview of the research presented in this thesis is provided in Figure 1-1. *Focus 1* applies soft lithography to spatially pattern DNA vectors and gene expression within a cluster of cells to establish gradients of diffusible factors and perform fundamental studies of neurite guidance (Chapters 5 and 6). The development of a microfluidic system to spatially pattern gene delivery is described in Chapter 5. Conditions were optimized to reduce binding of vectors to the microfluidic channel walls and maintain complex activity on the surface to achieve patterned transfection on a 100 μm-width scale. The system was characterized in terms of the protein production rates and concentration gradients that develop from localized secretion of soluble guidance factors in Chapter 6. The system was employed to correlate neurite guidance to the gradients formed by spatially patterned gene expression.

*Focus 2* details strategies to alter patterns of gene expression within single cells for the rational design of topographically patterned tissue engineering scaffolds (Chapters 7 and 8).

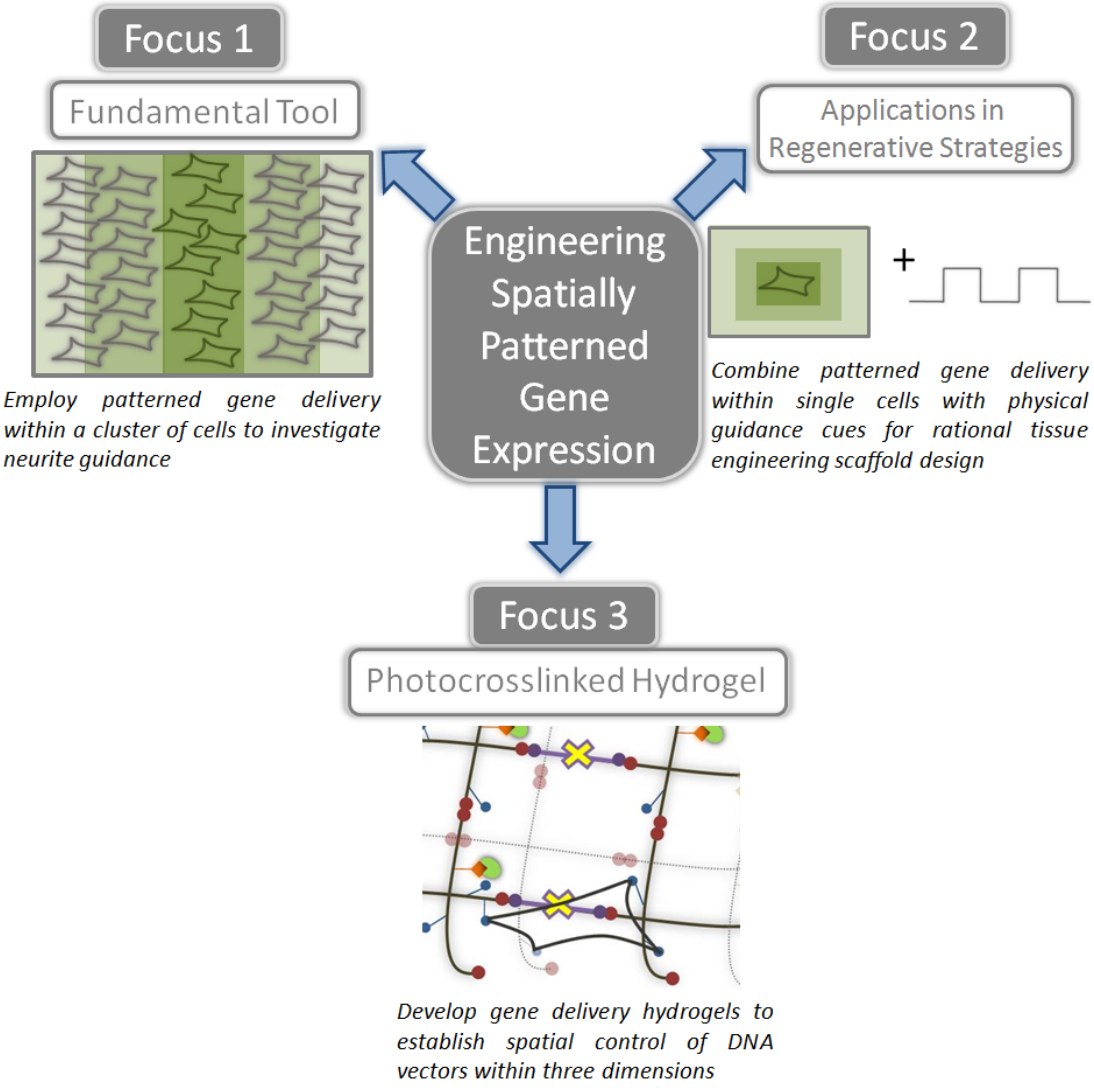


**Figure 1-1: Thesis overview.** An outline of the three foci covered in this thesis.

Methods to pattern gene delivery within topographically patterned channels were developed to investigate synergistic guidance cues in Chapter 7. Concentration gradients that arise from a single transfected cell were characterized and evaluated for guidance capabilities in Chapter 8. Knowledge gained from these studies can be applied to rational design of tissue engineering scaffolds to achieve neurite guidance.

*Focus 3* explores substrate-mediated gene delivery within photopolymerizable hydrogels and establishes techniques to achieve spatial control of DNA vectors within three dimensions. Hydrogels were developed to conform to specific design requirements: biologically inert backbone, incorporation of cell adhesion molecules, instructed cellular degradation, and affinity molecules for DNA vector retention. The hydrogel was characterized for mechanical properties, DNA vector release, and in vivo cell migration and transfection. Patterning strategies were developed to demonstrate spatial control of DNA vectors within three-dimensional constructs.

Collectively, the three foci of this thesis explore strategies to spatially pattern gene expression and define concentration gradients responsible for neuronal responses. Concentration gradients developed by spatially patterned gene delivery represent the manner in which gradients are formed naturally. Spatially patterned gene expression systems can be utilized to investigate fundamental questions in tissue development as well as define design parameters for the engineering of tissues with complex architectures.

# Chapter 2

# Gene Delivery from Tissue Engineering Scaffolds

## *2.1 Introduction*

Tissue engineering has demonstrated the potential to replace tissue loss or organ failure, which results in expenditures of billions of dollars annually in the US alone [13]. Approximately $500 million was spent by the tissue engineering industry for the 2002 calendar year [14], with industrial spending growing at an annual rate of 11% and a total investment exceeding $3.5 billion since 1990. This investment has resulted in several FDA-approved products, including Apligraf® (Organogenesis), Carticel® (Genzyme Biosurgery), Dermagraft® (ATS), and OrCel® (Ortec), with product sales estimated at $0.1 to 25 million [14]. Although these products have demonstrated some clinical benefit, many others failed to provide efficacy in phase III trials or were abandoned during phase I or II. Additionally, these products have not become profitable, despite treating many thousands of patients, and, in some instances, the clinical benefit is not greatly superior to less expensive methods. Emerging strategies that combine biomaterial scaffolds, drug delivery technology, and gene therapy have the potential to provide more effective tissue replacements with significant benefits relative to current products, confer safety advantages, and potentially lower costs relative to current therapies [15].

Tissue engineering scaffolds serve a central role in the approaches to tissue engineering, which can be broadly classified as conductive, inductive, and cell transplantation [16]. The conductive approach employs polymer scaffolds to create and maintain a space and provide a physical support that allows tissue regeneration. The inductive approach also employs the

scaffold as a drug delivery vehicle to provide a stimulus that induces tissue formation. The conductive and inductive approaches assume the presence of progenitor cells in the surrounding tissue that are capable of regenerating the tissue. Tissue engineering scaffolds can also function as vehicles for the transplantation of cells that can regenerate lost or diseased tissue. The design of these scaffolds is evolving to provide signals that direct gene expression for tissue progenitor cells, either endogenous or transplanted.

Gene therapy approaches provide a mechanism to directly alter gene expression within a developing tissue. The delivery of genes is a versatile approach capable of targeting any cellular process, and can produce prolonged expression of tissue inductive factors [17]. Delivery strategies have typically employed direct injection of viral or non-viral vectors, the gene gun, or the transplantation of *ex-vivo* genetically engineered cells. Strategies typically employ a gene that results in protein secretion (e.g., growth factor), which is capable of stimulating numerous cells in the microenvironment. Cells that express the transgene serve as bioreactors for localized protein production. Alternatively, genes encoding for intracellular proteins could be delivered to control the fate of individual cells, which may require large numbers of cells to be targeted for efficacy. Examples include genes encoding for cell surface receptors or nuclear transcription factors. Tissue-specific and inducible promoters also provide a means to restrict or control transgene expression after gene delivery. The combination of gene therapy and tissue engineering scaffolds represents a promising approach, with the scaffold providing the physical support for cell adhesion and a template for tissue formation and gene delivery functioning to induce specific cellular processes.

This Chapter examines gene delivery from tissue engineering scaffolds as a means to directly alter gene expression and stimulate tissue formation. The development of scaffolds for localized DNA delivery builds upon research into gene delivery systems [18], and also the transplantation of *ex-vivo* genetically engineered cells [19, 20]. A brief overview of scaffolds and gene delivery systems is provided, followed by current capabilities for DNA delivery from tissue engineering scaffolds. The relationship between gene delivery, transgene expression, and tissue formation is also presented. Although this Chapter focuses primarily on the development of gene releasing scaffolds to increase expression, similar approaches can be employed to reduce or eliminate gene expression through delivery of oligonucleotides or siRNA delivery [21]. Reducing gene expression with siRNA has potential therapeutically [22], and adapting the delivery systems for siRNA may significantly enhance the ability to direct tissue formation.

## *2.2 Tissue Engineering Scaffolds*

A variety of natural and synthetic materials have been employed as scaffolds for tissue engineering [23, 24]. The polymers used in scaffold fabrication can generally be categorized as either hydrophilic (e.g., hyaluronic acid (HA), collagen, poly (ethylene glycol) (PEG)) or hydrophobic (e.g., poly (lactide-co-glycolide) (PLG)). Hydrophilic polymers can assemble or be crosslinked to form hydrogels. Naturally occurring materials, such as collagen or hyaluronan, can form hydrogels and are advantageous for tissue engineering scaffolds, as they are intrinsically involved in the numerous developmental and physiological functions, such as cell attachment, differentiation, and chemotaxis. In particular, collagen and its derivatives have been used for pharmaceutical and medical applications due to their biosafety and ability to modify the physicochemical properties. Synthetic polymers provide greater versatility than natural materials

for designing tissue engineering scaffolds with controlled macrostructure, mechanical properties, and degradation time. Synthetic hydrophilic polymers (e.g., PEG) can be crosslinked and functionalized [25]. Perhaps the most widely used synthetic materials for tissue engineering scaffolds are poly-(L)-lactic acid (PLLA), polyglycolic acid (PGA), and copolymers of these materials (PLG). Copolymers of PLG have been extensively used because they are biocompatible, FDA approved, and can be designed to degrade over times ranging from a few weeks to more than a year [26]. Scaffolds can be formed as a mesh of fibers wound together or the polymer can be processed into a highly porous structure [27, 28].

Tissue engineering scaffolds must mimic the numerous functions of the natural extracellular matrix (ECM), including providing a support for cell adhesion and migration, and organizing cells into structures. Several fundamental scaffold design requirements have been identified from the variety of materials and tissue systems that have been examined [16]. These basic requirements include being biodegradable and biocompatible, having sufficient mechanical integrity, and the ability to provide a suitable environment for new tissue formation that can integrate with the surrounding tissue. Scaffolds must create and maintain a space for tissue formation, and should be resorbed or degraded at a rate that is comparable to new tissue formation. For scaffolds fabricated from natural polymers such as collagen or hyaluronic acid, cells can migrate by specific cellular interactions with the matrix, and have the ability to degrade the matrix. For synthetic polymers (e.g., PLG), scaffolds are typically highly porous, which can allow nutrient transport and cell infiltration from the surrounding tissue. Cellular infiltration from the surrounding tissue is important for integration of the engineered tissue with the host,

and also for development of a vascular network throughout the tissue to supply necessary metabolites once the tissue has developed.

The basic properties of the scaffold can be augmented to provide specific cellular cues that direct tissue formation. These signals can be presented through multiple cellular interactions with the microenvironment, and include interactions with the scaffold surface or other cells, the release of soluble factors, and mechanical stimuli. Adhesion molecules, peptides, and extracellular matrix proteins can be immobilized to the biomaterial to regulate the cellular interactions with the matrix [24, 29]. Growth factors can be released from the matrix, which can then bind to cell surface receptors and initiate a variety of cellular processes [24, 30]. Each stimulus presents unique opportunities for directing cellular functions, and the scaffold must provide the appropriate combination to coordinate gene expression that ultimately leads to tissues with the desired properties. Relative to direct protein delivery, gene delivery is a more versatile approach that may provide more sustained, localized production of tissue inductive factors. Additionally, gene delivery may produce more potent proteins capable of stimulating autocrine or paracrine loops, which play important roles in tissue development and physiology.

## *2.3 Gene Delivery*

Gene delivery requires that DNA overcome a series of extracellular and intracellular barriers that can limit efficiency. The extracellular barriers include efficient mass transport to the desired cell populations, DNA degradation, and clearance from the delivery site. Intracellular barriers include limited cellular internalization, endosomal escape, vector unpacking, and transport into the nucleus. DNA can be delivered alone (i.e., plasmid), or can be packaged using viral or non-viral vectors. These vectors consist of DNA assembled with proteins, polymers, or lipids. The

fundamentals underlying non-viral and viral delivery systems, and the more recent development of polymeric delivery systems are described in the following sections.

### *2.3.1 Non-viral Gene Delivery*

Plasmid and non-viral vectors are less toxic and immunogenic than viral vectors, and easier to prepare [31]; however, the gene delivery efficiency can also be significantly lower. Many cells can be transfected by direct injection of plasmids into the interstitial space of the tissue, however, transfection is often variable and inefficient [32]. Other physical methods, such as gene gun and electroporation, have been developed to target naked DNA locally or systemically. However, there are disadvantages to naked DNA delivery. Plasmids are large molecules ($10^3$-$10^4$ base pairs) and have a negative charge density, which can prevent the plasmid from crossing cellular membranes [33]. Furthermore, non-methylated CpG motifs in the plasmid can stimulate a dose-dependent immune response [34].

Self-assembly of plasmid with cationic lipids (e.g., DOTAP/DOPE) or cationic polymers (e.g., poly-L-lysine (PLL), poly(ethylene imine) (PEI)) forms lipoplexes or polyplexes, respectively. Complexation creates a less negative surface charge, may reduce the effective size, protects the DNA against degradation, and can facilitate intracellular trafficking (i.e., cellular internalization, endosomal escape, nuclear localization) [31]. Additionally, cationic lipids and polymers within the DNA complexes can be designed to target specific processes, such as receptor binding, nuclear localization, or modulation of an immune response [35]. The quantity of cationic polymer or lipid in the complex is often minimized to reduce cellular toxicity and the inflammatory response.

### *2.3.2 Viral Gene Delivery*

Viral vectors are the most efficient method of gene transfer in vivo [36]. Viral particles are composed of a nucleic acid genome surrounded by a capsid of proteins, with sections of the virus genome replaced with a therapeutic gene. Viruses can circulate or associate with extracellular matrix molecules prior to internalization, which typically occurs through receptor binding or membrane fusion [37]. Despite the in vivo gene delivery efficiency, viral vectors must often be modified due to safety issues. Viruses are typically engineered to be replication deficient, and are being designed to minimize the immune response.

Viruses utilized for gene delivery vectors include retrovirus, adenovirus, and adeno-associated virus (AAV) [37]. Retroviruses offer the potential for long-term gene expression through integration into the host cell genome. However, the challenges associated with retrovirus vectors include the inability to transduce non-dividing cells, obtain efficient delivery, and achieve stable expression at an appropriate level. Lentivirus is a class of retrovirus that transduces non-dividing cells and provides long term gene expression. Alternatively, adenoviral vectors can transduce non-dividing cells with transient gene expression, but often result in a strong immune response that requires the virus modification. Adeno-associated virus (AAV) transduces a variety of cells, including non-dividing cells, provides long-term gene expression, and does not induce a strong immune response. However, limitations with AAV vectors include a small packaging capacity and inefficient transgene expression due to the need for duplication of the single-stranded DNA genome.

### *2.3.3 Scaffold Delivery Systems*

Scaffold delivery systems may enhance delivery efficiency of viral and non-viral vectors by increasing residence time within the tissue, protecting against degradation, and minimizing the inflammatory response. The large size of DNA limits vector transport through tissues, resulting in diffusion coefficients on the order of $10^{-9}$ to $10^{-12}$ $cm^2$/sec [38], and promotes localized delivery when scaffolds are inserted into a tissue. Interactions with the material can provide stability against degradation, which is important considering that these vectors can have half-lives on the order of minutes to hours. DNA delivery can also stimulate an immune response targeted to the vector or transgene expressing cells [39, 40]. Scaffold delivery can limit binding of neutralizing antibodies and minimize the amount of DNA necessary for gene transfer [41], thereby reducing the immune response.

Delivery from tissue engineering scaffolds can be categorized according to two general mechanisms: polymeric release or substrate-mediated delivery (Figure 2-1). Molecular interactions between the vector and the polymer dictate whether the DNA is released from or bound to the polymer. Delivery from most scaffolds likely occurs through a combination of binding and release mechanisms, and both the vector and polymer can be designed to regulate these interactions. For polymeric release, the vector is entrapped within the material for release into the environment. The polymer may enhance gene transfer by protecting DNA from

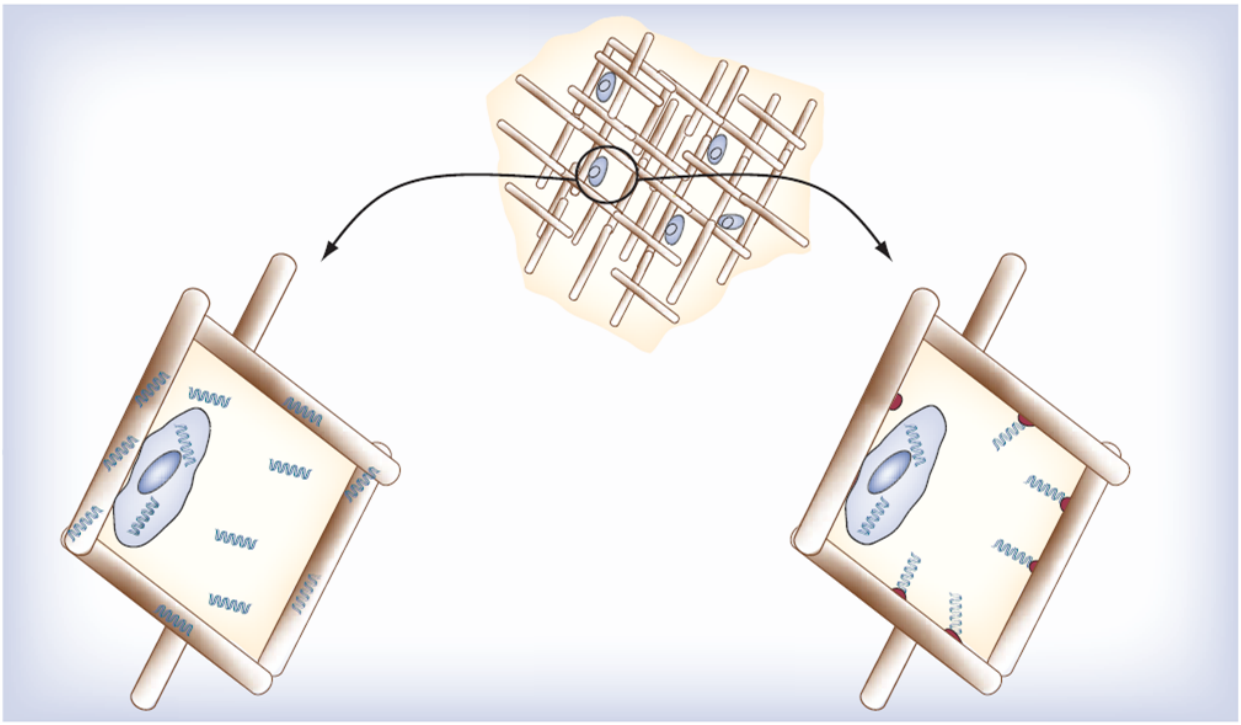

**Figure 2-1: Tissue engineering scaffold (center) for DNA delivery.** Polymeric release (left) involves an encapsulation and release of DNA into the local microenvironment. Alternatively, substrate-mediated delivery (right) employs the immobilization of DNA to the scaffold surface.

degradation, maintaining the vector at effective concentrations, and extending the opportunity for internalization. DNA release into the tissue can occur rapidly, as in bolus delivery, or extend over days to months [11, 42, 43]**.** For rapid release, levels would be expected to quickly rise and decline as the DNA is cleared or degraded. For sustained delivery, the concentration may be maintained within an appropriate range by adjusting the release to replace DNA that is cleared or degraded. Conversely, substrate-mediated delivery, also termed solid phase delivery or reverse transfection, describes the immobilization of DNA to a biomaterial or extracellular matrix, which functions to support cell adhesion as well as migration and places DNA directly in the cellular microenvironment. In substrate-mediated delivery, DNA is concentrated at the delivery site and targeted to the cells that are adhered to the substrate [44, 45]. Cells cultured on the substrate can internalize the DNA either directly from the surface, or by degrading the linkage between the vector and the polymer.

Several polymers used as tissue engineering scaffolds have also been employed as vehicles for DNA delivery. The three-dimensional scaffold may enhance the extent and duration of transgene expression by cells on the scaffold relative to a two-dimensional surface [46]. Hydrogel scaffolds often contain more than 98% water and are formed with mild processing conditions, which can maintain the activity of encapsulated vectors. These scaffolds typically release the vector by diffusion from the polymer network [43]; however, crosslinking the polymer or increasing its density can slow the release and allow network degradation to control the rate [25, 47, 48]. These hydrophilic polymers, along with some hydrophobic polymers, contain functional groups (e.g., carboxylic acids, amines) in the polymer backbone that can be readily modified, allowing interactions between the polymer and the vector to be manipulated.

Synthetic polymers such as PLG and polyanhydrides have been widely used in drug delivery applications, with release typically occurring through a combination of surface desorption, drug diffusion, and polymer degradation [49]. Importantly, the processing strategies to fabricate the scaffolds must maintain activity for the vector, while providing an effective delivery system.

## *2.4 Gene Delivery from Tissue Engineering Scaffolds*

Gene delivery from tissue engineering scaffolds has demonstrated the ability to promote gene transfer and stimulate new tissue formation. DNA loaded scaffolds can be directly implanted into an injury site for gene delivery to cells within or near the scaffold. Scaffolds can distribute the DNA throughout the three-dimensional space of the injury site, which may be more effective than injection. Alternatively, cells could be seeded onto the scaffold prior to implantation. The design and functionality of tissue engineering scaffolds for gene delivery, and their ability to promote tissue formation is described below. These systems are categorized according to the basic delivery mechanisms: polymeric release and substrate-mediated delivery, as described above.

### *2.4.1 Polymeric Release*

Sustained DNA delivery from polymer scaffolds has the capability to enhance gene transfer by protecting DNA from clearance or degradation and maintaining elevated DNA concentrations within the extracellular environment. Maintaining these elevated concentrations may extend transgene expression by repeated cellular internalization. The total quantity of DNA released by polymeric release can be greater than that delivered by injection, as the gradual release should maintain elevated, but not cytotoxic levels. However, if polymeric release can increase the delivery efficiency, the total amount of DNA could be reduced, which has been observed for

polymeric release of proteins [15]. Tissue engineering scaffolds for release of viral and non-viral vectors, with their results and applications, are summarized in Table 2-1.

#### *2.4.1.1 Polymeric release of non-viral vectors*

Collagen based delivery of plasmid and non-viral vectors has been employed to promote tissue formation in models of bone [50], cartilage [51], nerve regeneration [52], wound healing [53], and cardiovascular disease [54]. The collagen serves as a scaffold for the migration of repair cells into the matrix, and functions to either retain DNA within the scaffold [50, 52, 53, 55, 56] or provide gradual release [43, 57]. Hydrogels prepared from cationized gelatin achieved controlled release of plasmid DNA based on the hydrogel degradation following intramuscular implantation [58]. Transgene expression correlated with the release rate of DNA from the hydrogel. Sustained plasmid release (50 μg) from atelocollagen delivered intramuscularly resulted in expression for at least 60 days [57]. Collagen/plasmid constructs have been implanted into an adult rat femur [59] and a canine bone defect model [50]. Scaffolds loaded with 1 mg of DNA were capable of transfecting cells in vivo, which resulted in protein production for up to 3 weeks post implant. For the canine model, however, regeneration required significantly larger quantities of plasmid.

DNA complexed with cationic lipids or cationic polymers can also be incorporated and released from collagen-based matrices, while maintaining their activity. The release of complexes may differ significantly from that for plasmid, due to the different physical properties

| Scaffold | Vector / gene | Location / Species (Application) | Result | Reference |
|---|---|---|---|---|
| **Collagen** | Plasmid / BMP-4, hPTH1-34 | Femur / Rat (Bone) | New bone formation filling a 5-mm osteotomy gap | **[50]** |
| **Collagen / PVA** | Adenovirus / PDGF-B | Subdermal / Rat (Wound healing) | Increased granulation tissue formation | **[60]** |
| **Collagen / PVA** | Adenovirus (FGF-2 target) / PDGF-B | Subdermal / Rat (Wound healing) | Granulation tissue formation | **[61]** |
| **Collagen-gelatin** | Plasmid / PDGF-2, FGF-2 | Subdermal / Rat (Wound healing) | Increase in patent vessels supporting blood flow in flaps | **[56]** |
| **Collagen** | Plasmid / PDGF | Ear / Rabbit (Wound healing) | Granulation tissue and epithelialization | **[53]** |
| **Collagen** | Adenovirus / PDGF, FGF-2, FGF-6 | Intramuscular / Rat (Wound healing) | Early angiogenesis and skeletal muscle repair | **[62]** |
| **Collagen** | Adenovirus / PDGF-B | Subdermal / Mouse (Wound healing) | Granulation tissue and vascularization | **[63]** |
| **Collagen** | PEI, PLL, Liposome-Plasmid / Luciferase | Subdermal / Rat | Higher gene expression with PLL-pDNA loaded matrices | **[55]** |
| **Collagen** | PLL-Plasmid / FGF2, BDNF, NT-3 | Optic Nerve / Rat (Nerve regeneration) | Survival of axotomized RGCs | **[52]** |
| **Denatured collagen-PLGA** | Plasmid / GFP, β-galactosidase | Coronary Artery / Swine | Enhanced GFP expression | **[64]** |
| **Hydrogel (PEG-PLGA-PEG)** | Plasmid / TGF-β1 | Subdermal / Mouse (Wound healing) | Accelerated re-epithelialization | **[65]** |
| **Hydrogel (PEG-PLGA-PEG)** | Plasmid / Luciferase | Subdermal / Mouse | Higher and extended gene expression relative to free DNA | **[66]** |
| **PLG** | Plasmid / PDGF | Subdermal / Rat | Enhanced matrix deposition and vascularization | **[11]** |
| **PLG coated stent** | Plasmid / GFP | Coronary Artery / Swine | Localized GFP expression at arterial wall | **[54]** |

**Table 2-1:** DNA releasing polymer scaffolds (Polymeric release).

of each. Collagen matrices were loaded by pipetting solutions of plasmid, polyplexes (PEI/DNA), and lipoplexes (DOTAP/cholesterol) onto collagen [43]. Although plasmid is rapidly released in vitro, polyplexes and lipoplexes were slowly released. The addition of a protective copolymer to the polyplexes produced intermediate release kinetics, which also resulted in the highest transfection in vivo, with maximal expression occurring at 4 days and expression observed at 7 days. Alternatively, PLL/DNA complexes have been encapsulated into collagen sponges for implantation into severed optic nerves to promote neuronal survival and promote regeneration [52].

Hydrogels based on agarose, hyaluronic acid (HA), fibrin, and PEG have been employed independently as biomaterials for fabrication of tissue engineering matrices or as materials to regulate DNA delivery. Functionalized hydrogels have tremendous potential for tissue engineering, and are being developed to gel in situ, have controlled mechanical properties, modulate cell adhesion, controllable degradation, and release bioactive factors locally [67-71]. Agarose gels have provided a sustained release of lipoplexes for over 50 days [72]. Released lipoplexes transfected smooth muscle cells in vitro with an efficiency less than that obtained by freshly formed complexes, but greater than that obtained with plasmid. HA scaffolds have also demonstrated the capability of sustained release of plasmid, with release likely occurring following polymer degradation [48]. The release rate of plasmid, some of which may be associated with HA fragments, could be modulated by the extent of crosslinking in the hydrogel. Fibrin sealants have been employed for the delivery of plasmids to promote angiogenesis, with fibrin-based delivery providing similar responses to delivery in PBS solution [73]. Thermosensitive or photocrosslinkable PEG hydrogels have been used to release plasmid, which

could be modulated through hydrogel degradation or the extent of crosslinking [65, 74]. Photocrosslinked PEG-based hydrogels could produce either linear or delayed release profiles [74]. PEG hydrogels containing TGF-β1 encoding plasmid administered into excisional wounds on diabetic mice accelerated re-epithelialization at the early stage (day 5) with 56% wound closure [65]. Tissue engineering matrices based on these hydrogels, or combinations of these materials, provide a variety of approaches to regulate DNA delivery in vitro and in vivo.

Scaffolds fabricated from the synthetic polymer PLG have increased the extent of in vivo transfection and also induced tissue ingrowth within or around the systems by providing sustained DNA release [11]. PLG-mediated delivery of plasmid (50 μg) has led to 28 days of gene expression [75]. The released plasmid transfected cells in vivo adjacent to the polymeric implant, resulting in a significant increase in transgene expression (14 to 40 fold) relative to direct injection. Plasmid releasing scaffolds have been fabricated by the assembly and fusion of PLG microspheres using a gas foaming process [11, 12]. The release rate can be modulated by either lyophilizing DNA with the microspheres [11] or encapsulating DNA into the microspheres [28, 76], with encapsulation into the microsphere providing a more sustained release profile. Subcutaneous implantation of these scaffolds resulted in transfected cells within the scaffold and the tissue immediately adjacent to the scaffold for 105 days [12]. Enhanced matrix deposition and blood vessel formation was observed in the developing tissue by delivery of a PDGF-encoding plasmid [11]. Physiological effects were not observed by direct injection of equivalent quantities of plasmid. Porous PLG scaffolds have also been incorporated with encapsulated polyplexes and achieved substantial transfection in vitro [77], but with significantly altered release profiles compared to plasmid. An alternative approach to fabrication of PLG scaffolds for

DNA delivery is electrospinning [27]. Electrospinning creates non-woven, nano-fibered membranous structures that released DNA, with maximal release occurring at approximately two hours.

### *2.4.1.2 Polymeric release of viral vectors*

The ability of viral delivery to promote regeneration is decreased by the induced immune response, which may be reduced by polymeric encapsulation. Ectopic bone formation was observed by the injection of a BMP-2 containing adenovirus into the thigh muscles of nude rats [78]. However, bone formation was inhibited in immune competent rats [39]. In vivo delivery of viruses results in immune responses that target the vector or the transduced cells, thus decreasing transduction or the activity of the secreted protein [40, 79]. This immune response typically prohibits multiple administration of the vector. Vectors encapsulated in synthetic polymers had 45-fold lower anti-adenovirus titers than that obtained with direct injection of the adenovirus [41]. Similarly, encapsulation of adenovirus vectors in alginate beads or collagen minipellets showed significantly greater expression in pre-immunized mice than direct delivery of the virus, while reducing the vector-specific immune responses [80]. Polymeric encapsulation is hypothesize to shield the vector from neutralizing antibodies, and may reduce the quantities of vector required for transduction in vivo.

Encapsulation of viral vectors in biomaterials can serve to locally concentrate the virus, which may increase the efficiency and localize vector delivery. For delivery from collagen, the release of adenovirus was dependent on the collagen concentration, with minimal release obtained for collagen concentrations above 1% [42]. These adenovirus vectors remained viable in vivo, suggesting that the collagen may limit virus degradation [42]. A gelatin sponge for

delivery of canarypox virus increased expression relative to fluid injection of the virus [81], and the fluid phase delivery led to expression outside of the delivery site [61, 62, 82]. In wound healing applications, collagen hydrogels containing a PDGF-B-encoding adenovirus enhanced granulation tissue deposition and vascularization within wound beds [61, 62]. A single application of collagen scaffolds with encapsulated virus was as effective for neo-tissue induction as repeated fluid phase administration [62]. Implantation of adenovirus-loaded collagen gels into skeletal muscle defects resulted in enhanced muscle repair, with induction of angiogenesis, arteriogenesis, and myogenesis [82].

### *2.4.2 Substrate-Mediated Gene Delivery*

Substrate-mediated DNA delivery is based on the immobilization of complexes within or to a biomaterial, which serves as a substrate for cell adhesion. This delivery method places the DNA directly in the cell microenvironment for subsequent cellular internalization [83], and may function to overcome barriers to gene transfer, such as complex aggregation and mass transfer limitations. The design of substrate-immobilization systems was examined through modifying cationic polymers with biotin for the immobilization of DNA complexes to a neutravidin substrate [45, 83]. Immobilized complexes were prevented from aggregating, and transgene expression by substrate-mediated delivery was increased 100 fold relative to bolus delivery [45]. Interestingly, although immobilization increased with increasing biotin content in the complex, transfection increased with a decreasing quantity of biotin in the complex, suggesting non-specific immobilization of complexes governed expression. Immobilization of fibronectin to the substrate before non-specific complex adsorption showed an enhancement in extent of transgene expression as compared to other ECMs, potentially by targeting complex internalization through

caveolae-mediated endocytosis [84]. The ionization and hydrophobicity of the substrate were also shown to influence transgene expression, with the greatest amounts of binding and transfection observed on surfaces presenting charged, hydrophilic groups, suggesting that electrostatic interactions allow for reversible interactions between the substrate and complexes and result in efficient gene delivery [85]. Additionally, transfection has been localized to topographically patterned regions, suggesting that spatially controlled DNA delivery is possible [83], which may be important for creating complex tissue architectures [30]. Many studies with this approach have focused on system development rather than application (summarized, Table 2-2), yet this approach can be adapted to tissue engineering scaffolds with numerous applications.

#### *2.4.2.1 Substrate-mediated delivery of non-viral vectors*

Non-viral vectors have been immobilized to biomaterial substrates by drying, non-specific adsorption, and biotin/avidin binding. Polyamidoamine (PAMAM) dendrimers have been complexed with DNA and dried onto both PLG and collagen-based membranes [86]. These immobilized complexes were able to mediate transfection both in vitro and in vivo. Similarly, DNA was co-precipitated with calcium phosphate and adsorbed onto PLG scaffolds [87]. Cells cultured on PLG scaffolds were able to internalize the immobilized DNA. Finally, biotinylated

| Scaffold | Vector/gene | Location / Species (Application) | Result | Reference |
|---|---|---|---|---|
| **Collagen membranes** | PAMAM-Plasmid / Luciferase, GFP | *in vitro* (Skin) | $10^4$-$10^5$ RLU/µg total protein | **[86]** |
| **PLG** | Bacteria phage lambda | *in vitro* | Successful cellular uptake of DNA | **[87]** |
| **HA-collagen hydrogels** | PEI-Plasmid/ Luciferase, GFP | *in vitro* | Spatially controlled gene transfer | **[88]** |
| **Collagen-avidin gels** | Virus / β-galactosidase, GFP | Right Ventricle / Swine (Myocardial revascularization) | Uniform transduction and more efficient expression compared to direct injection | **[44]** |
| **Collagen coated stents** | Virus / GFP | Coronary Artery / Swine (Vascular stents) | 5.9 +/- 1.1% transduction | **[89]** |
| **Collagen coated microcoils** | Virus / β-galactosidase, GFP | Carotid Artery / Rat (Cerebral aneurysms) | 13.3 + 2.0% of cells within thrombus transduced | **[90]** |
| **Polyurethane films, collagen coated** | Virus / GFP | Pulmonary Position / Sheep (Heart valve disease, vascular disorders) | 25.1 +/- 5.7% attached cells transduced after 1 week implantation | **[91]** |

**Table 2-2:** DNA releasing polymer scaffolds (Substrate-mediated delivery).

DNA polyplexes were immobilized to a hyaluronic acid-collagen hydrogel that was modified with neutravidin [88]. Complexes bound with high efficiency to the scaffold through a combination of non-specific adsorption and biotin-neutravidin interaction. Cells cultured on the hydrogel are transfected, while cells adjacent to the hydrogel are not. Interestingly, the size of the immobilized complexes affected the number of transfected cells and the extent of transgene expression. Small complexes (≈100 nm) produced lower levels of transgene expression than large complexes (≈1000 nm), yet the percentage of transfected cells was doubled with small complexes, reaching over 50% of the cell population. These hydrogels were also topographically patterned with a series of grooves and ridges, which resulted in cell adhesion to the ridges and oriented cell growth. Thus, cellular transfection was spatially patterned on the scaffold through this controlled cell adhesion. Delivery by DNA immobilization can be extended to other materials such as cationically charged chitosan, which has been used for gene delivery by either encapsulating [92] or complexing plasmids [93].

#### *2.4.2.2 Substrate-mediated delivery of viral vectors*

Viral vectors have been immobilized to a range of collagen-coated biomaterials using antibodies capable of binding the virus. This approach has been able to achieve efficient gene delivery both in vitro and in vivo, with in vivo transduction localized to avoid distal spreading of the virus [89]. Smooth muscle cells cultured on collagen hydrogels showed significantly more localized reporter gene expression in vitro compared to non-antibody complexed controls [44]. Stents, microcoils, and prosthetic heart valve cusps have been collagen coated and modified for covalent attachment of anti-adenovirus antibodies, for the subsequent binding of adenovirus. Stainless steel coronary stents were collagen coated and modified with sulfhydryl containing

antibodies using disulfide chemistry [89]. Similarly, collagen-coated microcoils for treatment of cerebral aneurysms were modified with adenovirus [90]. After 7-day implantation in vivo, cells (13.3 ± 2.0%) within the organized thrombus were transduced. Adenovirus was also immobilized to collagen coated polyurethane, which is widely used in pulmonary heart valve replacement cusps [91]. Collagen-coated polyurethane was thiol-activated for covalent attachment of anti-adenovirus antibodies and subsequent binding of adenovirus. In vivo implantation resulted in transduction of 14.3 ± 2.5% of neo-intimal cells after one week. However, uncoated polyurethane films with virus bound to adsorbed antivector antibodies transduced 25.1 ± 5.7% of attached cells.

## *2.5 Transgene Expression and Tissue Formation*

The fundamental relationship between transgene expression and tissue formation remains a significant challenge in the design of tissue engineering scaffolds. Gene delivery from the scaffold can produce transgene expression locally, and the duration of transgene expression may be significantly longer than the duration of release (Figure 2-2). For many wound healing and tissue engineering applications, transient expression of the encoded gene is thought to be desirable, as inappropriate expression of growth factors can be associated with disease. Importantly, the expression of the transgene must be considered within the context of the signals present in the environment. As mentioned previously, the scaffold provides a support for cell adhesion and can be designed to mediate adhesion through specific receptors [68, 94]. The mechanical properties of the scaffold and mechanical stimulation of the tissue can influence

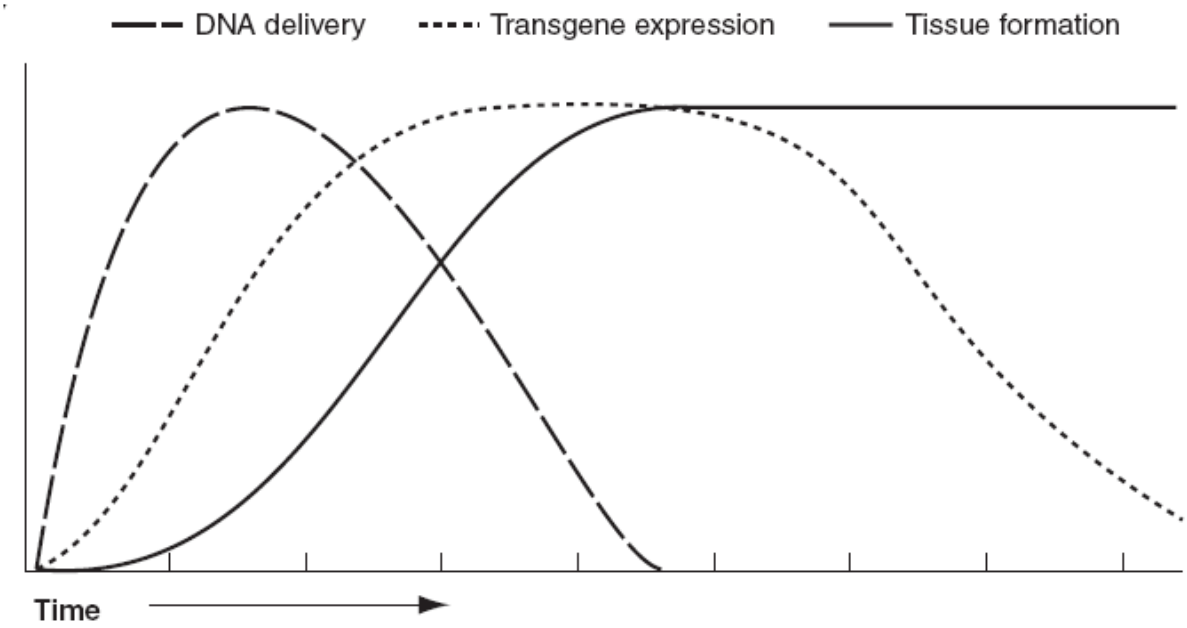


**Figure 2-2: Relative timing for gene delivery, transgene expression, and tissue formation.** Gene delivery by polymeric release or substrate-mediated delivery can enhance the local concentration of DNA, with an initial rise and a subsequent decrease due to clearance or degradation. Transgene expression is induced after gene delivery, and has the potential to persist for significantly longer times than the duration of delivery.

tissue formation [95]. Transgene expression can upregulate expression of tissue specific genes and accelerate tissue formation, which has been observed with telomerase expression in bone marrow stromal cells [96].

Although implantation of scaffolds releasing DNA has demonstrated the capability to promote tissue formation, guidelines regarding the target cell population for gene transfer, the extent of transgene expression, and the type of gene delivered are poorly understood. Some insight into these guidelines may be obtained from studies employing the transplantation of genetically engineered cells. In this approach, cells are isolated, transduced or transfected ex vivo using the described gene delivery systems, and selected for expression of a transgene for subsequent delivery to an injury site, either by direct injection or implantation of a scaffold seeded with cells. Cells for genetic engineering are selected based on their availability, expansion capacity in vitro, ability to survive following transplantation, and function at the implant site. Genetically engineered cells have been delivered in numerous models, such as bone and nerve regeneration.

Regeneration is observed independent of the cell type expressing the transgene, yet there can be benefits of expression by specific cell types. In bone regeneration, skeletal muscle cells, mesenchymal stem cells, mesodermal-derived cells, marrow stromal cells, and skin fibroblasts have been genetically engineered to express bone morphogenic proteins (BMPs) and were successful in inducing bone healing or bone formation [97-101]. Similarly, in nerve regeneration, fibroblasts, olfactory ensheathing cells, and Schwann cells engineered to express proteins (NT-3, NGF, BDNF, GDNF) can promote the growth of healthy axons when transplanted at injury sites [102]. For both examples, the cells act as bioreactors for tissue formation by progenitor cells at

the implant site. However, for nerve regeneration, fibroblasts cannot form functional relays, nor can they myelinate regenerating axons [102, 103]. Targeting of specific cell populations for gene delivery may be desirable for obtaining differentiated cell function at the injury site, or inducing differentiation toward specific fates.

The number of cells expressing the transgene and the extent of transgene expression by the cells can impact tissue formation. Ozawa *et al.* [104] demonstrated that high levels of VEGF secretion by retrovirally transduced myoblasts induced the growth of abnormal blood vessels. Decreasing the number of cells transplanted, which decreased the total dose of VEGF, served to reduce the region in which abnormal blood vessel formation was observed. However, transplantation of cells that were selected for low VEGF expression resulted in the formation of normal, mature vascular structures. These results illustrate that a discrete threshold in microenvironmental concentration determines either normal or aberrant tissue formation, and indicates that gene delivery strategies must promote an appropriate concentration of tissue inductive factors.

The type of gene (e.g., growth factor, transcription factor) delivered may also influence maximal tissue regeneration. As described earlier, many studies have investigated delivery of genes encoding growth factors to stimulate a multitude of cellular processes, such as proliferation, survival, or differentiation. Delivery of DNA encoding transcription factors that induce target protein production can present advantages relative to delivering DNA encoding for the target protein directly. Transcription factors that activate the endogenous gene would ensure that expression of all natural splice variants occurs [105]. Further, transcription factors may regulate multiple separate genes, which may prove advantageous for tissue regeneration. Zinc-

finger protein (ZFP) transcription factors have been engineered that regulate the endogenous gene encoding VEGF-A [105]. Expression of the ZFPs in vivo led to induced expression of VEGF-A and enhancement of both angiogenesis and wound healing.

## *2.6 Regeneration of Tissues with Complex Architectures*

Important in the consideration of tissue engineering system development is the ability to engineer tissues with complex architectures, such as the intricate circuits of the nervous system or the highly organized vasculature. These tissues rely on a specific architecture to function properly, and the regeneration strategy must recapitulate that architecture. During embryogenesis, proper tissue development involves instructed cell migration, proliferation, and differentiation by both spatial and temporal patterns of gene expression. Strategies to spatially pattern gene delivery within a scaffold may provide methods to recapitulate complex patterns of gene expression, and subsequently cell processes necessary for regeneration. Methods to spatially pattern biological molecules on two-dimensional tissue culture substrates and within three-dimensional biomaterials have been developed, and an overview of these systems is presented in Chapter 3.

## *2.7 Conclusions*

Tissue engineering scaffolds have been fabricated from natural and synthetic materials that deliver viral and non-viral vectors, and identification of the design parameters that regulate gene transfer is critical. Studies have examined the mechanism by which vectors traffic through the cell and into the nucleus for subsequent expression [106, 107]. Prior to cellular internalization however, the vector may interact with the polymer scaffold and other components in the

extracellular milieu. These interactions can influence vector release from the scaffold, stability, transport through the extracellular space, and ultimately internalization and trafficking. These scaffold-based gene delivery systems capitalize on both specific and non-specific interactions between the biomaterial and vector, to achieve either release into the extracellular space or immobilization at the surface. Vector and biomaterial development, combined with studies that correlate system properties (e.g., dose, release rate) with the quantity and duration of protein production, and the number and location of cells expressing the transgene will lead to molecular scale design of the scaffold and vector.

The application of these scaffolds will also require a more thorough understanding of the biological requirements for tissue regeneration. Cellular signaling within the scaffold will depend on various factors, such as implant location and cell types present. The expression of transgenes, encoding for growth factors or transcription factors, will likely influence cellular processes such as proliferation, differentiation, and migration. The integration of the transgene expression profile with other design components that influence gene expression must be considered for their cumulative effects on tissue formation. While these studies have illustrated the potential for extending the production of growth factors locally, adapting the delivery strategies to control transgene expression spatially (μm to mm) or temporally (days to months) may recreate the environmental complexity present during tissue formation [30]. These systems would also increase our understanding of the biology underlying tissue formation, and would serve to identify how gene delivery can best enhance the regenerative process.

# Chapter 3

# Spatially Patterned Biological Molecules: Techniques and Applications

## *3.1 Introduction*

Embryogenesis is marked by complex spatiotemporal patterns of gene expression that guide adhesion, migration, proliferation, and differentiation of cells into functional tissue with precise architecture. Gene expression of cell adhesion and extracellular matrix molecules, growth factors, chemokines, and cell surface receptors is continually changing over time and within the extracellular milieu. Tissue regeneration strategies must similarly guide cellular processes into structured, functional tissue. Therefore, the rational design of tissue regeneration constructs will require an understanding of the interactions between cells and spatiotemporal patterns of gene expression. Strategies to pattern adhesion molecules and growth factors have been developed to rapidly screen cellular responses to spatial patterns of biological molecules. The patterning techniques were first demonstrated on two-dimensional substrates. However, three-dimensional patterning strategies may be required to properly present molecules for regeneration of functional tissues.

Methods to spatially pattern biologically relevant molecules have also been employed for the development of high-throughput screens for bioassays. Decoding of the genome, advances in DNA separation techniques, and the discovery of RNAi has provided the foundation for the discovery of new drug targets [108, 109]. Combinatorial methods of organic synthesis have opened doors for thousands of candidate drug molecules [110] and advances in recombinant

DNA technology have facilitated the assessment of gene expression within live cells [111]. With this profusion of information, techniques to accurately and efficiently analyze data are essential. Methods to spatially pattern biomolecules (e.g., proteins, oligonucleotides, DNA vectors) have been developed for high-throughput bioassays, which had been made possible with all of the advancements.

This Chapter describes biological patterning strategies and applications. The technology to pattern biologically relevant molecules primarily descends from the microelectronics industry. Methods to pattern molecules on two-dimensional substrates include photolithography, soft lithography, and dip pen nanolithography. Additionally, two-dimensional patterning strategies have been altered to achieve three-dimensional patterns in order to present cells with a more physiologically relevant environment.

## *3.2 Two-Dimensional Patterning Strategies*

Two-dimensional patterning strategies have been developed to pattern proteins, peptides, DNA, and small molecules. The molecules are attached to a substrate via specific (covalent, biotin-avidin) [112, 113] or non-specific (hydrophobic, electrostatic interactions) [85, 114] interactions. The attachment sites are patterned to a substrate using methods of photolithography, soft lithography, and dip pen nanolithography. Photolithography was the first strategy employed to pattern biologically relevant molecules. Subsequently, soft lithography was developed to overcome discrepancies between the converging fields of photolithography and biotechnology. Dip pen nanolithography utilizes atomic force microscopy techniques to pattern molecules on the nanometer scale. The patterning strategies and applications for each are described in the following sections.

### *3.2.1 Photolithography*

Photolithography was originally developed for the microelectronics industry, and was the first strategy to be used for the patterning of biological molecules. The process of photolithography involves the topographical patterning of a photoresist that has been uniformly spin-coated to a silicon wafer. A patterned quartz mask is employed to selectively crosslink the photoresist upon application of light. A contact printer is generally used to place the photoresist in direct contact with the mask to avoid random transfer of light. Depending on the nature of the photoresist (negative or positive), the exposure of light will either stabilize or destabilize the photoresist. The destabilized photoresist is removed during development with tetramethylammonium hydroxide. A schematic depicting the photolithography process is shown in Figure 3-1. The advantages to photolithography techniques include the length scale precision that can be obtained, with resolution to tens of nanometers [115].

Photolithography was first applied to the biological field in the patterning of microarrays [116, 117]. Techniques to spatially pattern peptides on a substrate were developed by combining solid-phase chemistry, photolabile protecting groups, and photolithography [118]. Linkers attached to a glass substrate containing terminal amines with photoremovable protective groups were selectively exposed to light, and a series of peptide synthesis reactions and deprotection steps were performed to achieve a 1024-peptide array. These techniques were later adapted to fabricate DNA arrays containing 135,000 probes complementary to the 16.6-kilobase human

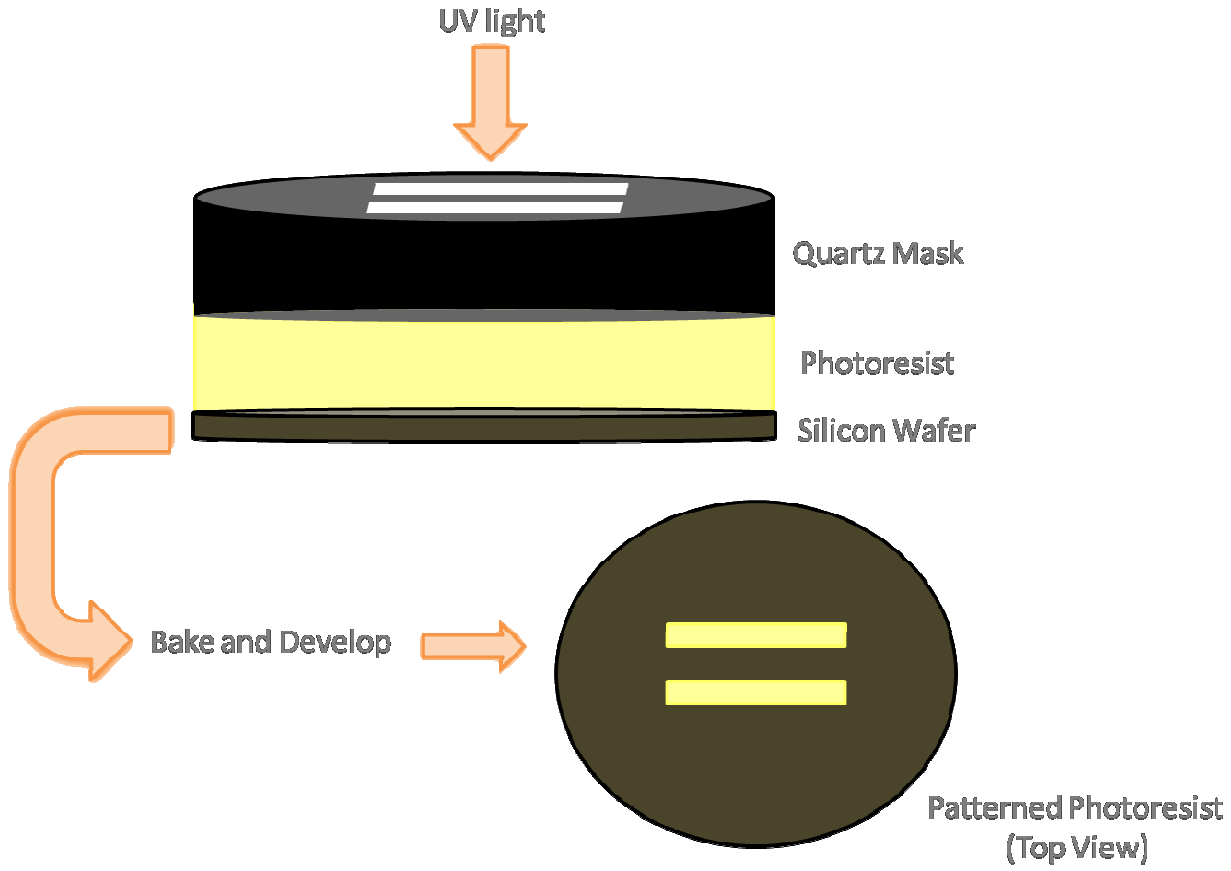


**Figure 3-1: Photolithography schematic.** An example of photolithographic patterning of a negative-tone photoresist.

mitochondrial genome [119]. Additionally, spatial control of cell adhesive molecules and subsequent control over cell adhesion has been demonstrated with photolithography techniques. Photolithography was employed to selectively oxidize regions of tissue culture polystyrene, and after treatment with Pluronic and fibronectin, cells adhered to the oxidized/fibronectin regions [114]. In a separate study, photolithography was used to create patterns of titanium dioxide within a matrix of silicon dioxide [120]. Alkane phosphates self-assembled on $TiO_2$ and supported protein adsorption, while the exposed $SiO_2$ was treated with a protein adsorption resistant molecule, PEG. Patterned protein regions supported cellular adhesion of human foreskin fibroblasts. Taken together, these finding demonstrate the utility of photolithography to pattern biologically relevant molecules for bioassays and selected cell adhesion. However, there are disadvantages associated with photolithography for the patterning of biological molecules [121]. The process is relatively expensive and inaccessible to biologists. Additionally, photolithography substrates must be planar, yielding limited control over surface properties and incompatibility with proteins and cells.

### *3.2.2 Soft Lithography*

Soft lithography was developed to overcome disadvantages associated with photolithography [121]. The technique involves the use of a patterned elastomer stamp, mold, or mask to generate micropatterns [122]. The patterned stamp is commonly fabricated with poly(dimethylsiloxane) (PDMS), a commercially available elastomer with repeating $[SiO(CH3)_2]$ monomers. PDMS is hydrophobic, but can be rendered hydrophilic via oxygen plasma treatment, which converts $SiCH_3$ groups to SiOH groups [123]. Pluronic (PEO-PPO-PEO) treatment is also utilized to render PDMS hydrophilic, by exposing hydrophilic PEO blocks on the surface [124]. PDMS

reversibly seals to biological substrates, including glass and tissue culture polystyrene (TCPS). Irreversible bonding between PDMS-PDMS or PDMS-glass can be generated by oxygen plasma treating and conformal contact, presumably by a spontaneous dehydration of SiOH groups (SiOH + HOSi → SiOSi) [125]. To utilize soft lithography techniques to pattern biological molecules, the PDMS stamp must be topographically patterned. PDMS is oftentimes patterned by replica molding techniques. A mold fabricated by photolithography is employed and cured PDMS retains the opposite features of the mold.

Soft lithographic strategies overcome the disadvantages associated with photolithography. The techniques are relatively inexpensive and are not limited to the microelectronics community. Additionally, the strategies are compatible with non-planar surfaces and can be used with a wide variety of materials and chemistries [122]. Soft lithography strategies to pattern molecules includes microcontact printing, microfluidics, and dry lift-off [121]. Details of each are discussed below.

### *3.2.2.1 Microcontact printing*

Microcontact printing (μCP) employs a topographically patterned PDMS stamp to "ink" a solution of a molecule to a substrate (Figure 3-2). The PDMS stamp possesses relief structures that are placed into the desired inking solution, and the solution deposits on the relief structures. The stamp is brought into conformal contact with a substrate, readily transferring the inked solution from the relief structures to the substrate. Once the PDMS is removed, a pattern defined by the raised bas-structure of the stamp remains [121]. Proteins have been patterned by

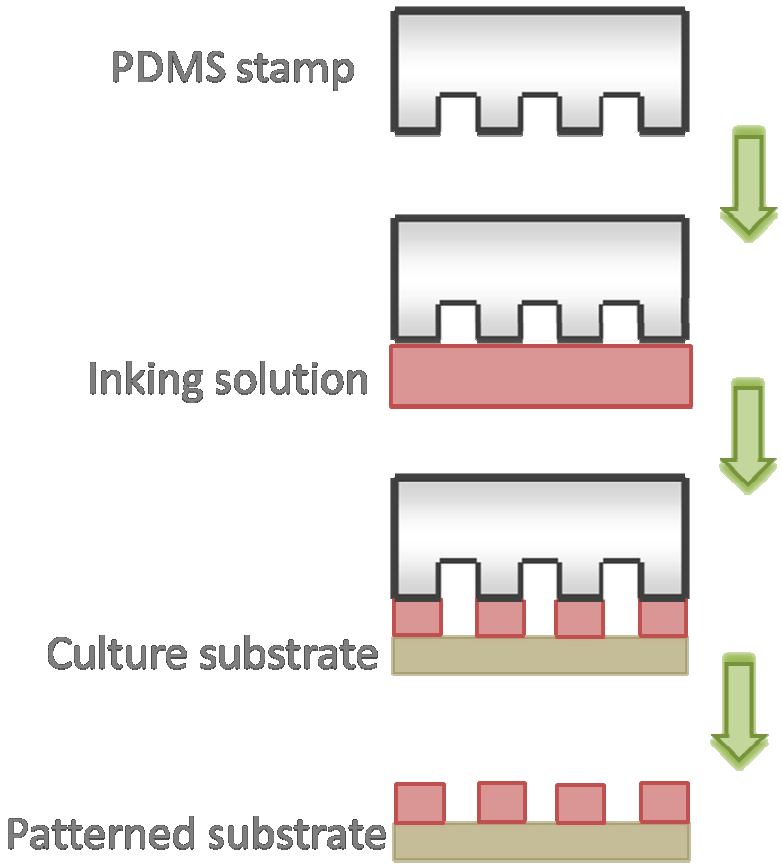


**Figure 3-2: Microcontact printing schematic.** An example of microcontact printing an inking solution (e.g., proteins) to a culture substrate.

nonspecific adsorption to glass, TCPS, or silicon substrates using μCP [126, 127], and the activity of the proteins can be 50-100% of that adsorbed directly from solution [121]. Chemically bound surface patterning techniques have been developed by combining self-assembled monolayers (SAMs) with μCP. A common SAM involves alkanethiols ($HS(CH_2)_nX$, where n = 16–18 and X = a small, nonpolar organic functional group) reacting with metal atoms on a gold surface to generate an array of thiolate groups. The surface retains the properties of the functional group, X [128]. An alkanethiol with functional group X is commonly inked onto a gold surface by μCP, followed by the addition of a second alkanethiol with functional group Y to backfill the surface.

Microcontact printing has been applied to pattern proteins, cell adhesion, and DNA complexes. Alkanethiols terminated with methyl groups were microcontact printed onto transparent gold substrates in pattern widths between 10 and 90 μm amongst a backfilled pattern of alkanethiols terminated with PEG [129]. Fibronectin selectively adhered to the methylated SAMs, and bovine capillary endothelial cells selectively adhered to the fibronectin patterns and remained patterned for up to 7 days. In a separate study, self-assembling oligopeptides with cell adhesion motifs were microcontact printed to a gold-coated surface amongst a backfilled pattern of oligopeptides terminated with PEG [130]. Human epidermoid carcinoma cells selectively adhered to the peptide bearing the adhesion motif. The self-assembling oligopeptides allowed precise presentation of cell adhesion peptide fragments rather than entire proteins for the controlled investigation of cell responses. Microcontact printing has also been used to pattern gene delivery vectors and cellular transfection. Alkanethiols with -CH3, -OH, or -COOH functional groups were patterned onto gold substrates to investigate the influence of surface

chemistry on DNA complex immobilization, release, and transfection [85]. Localized complex deposition led to patterned transfection, demonstrating utility for transfected cell arrays.

#### *3.2.2.2 Microfluidics*

PDMS microfluidic channels (microchannels) are fabricated by replica molding on photolithographic patterns (Figure 3-3). Microchannels contain inlet and outlet ports, and liquid is pumped into the microchannel via non-mechanical (e.g., capillary flow, electroosmosis) or mechanical pumping. The type of pump determines the flow profiles (parabolic, plug-like, complex). When protein or peptide solutions are passed through the microchannels, the biomolecules are deposited on the surface. PDMS must be rendered hydrophilic to improve flow rates in the microchannel and minimize biomolecule adsorption [131, 132]. The deposition of two molecules side-by-side can be patterned by flowing solutions into the microchannel and maintaining laminar flow. Gradients of molecules can be generated using complex microfluidic structures and mixing by diffusion [133], depletion of protein inside microfluidic channels by adsorption [134], and electrochemical desorption of SAMs [135].

Microfluidic networks have been employed to study cell adhesion and migration, as well as drug delivery devices. Human umbilical vein endothelial cells (HUVECs) mixed with collagen matrices were flowed into PDMS microchannels and subsequently patterned on silicon substrates [136]. This cell patterning technique is a tool to study tissue engineering strategies for

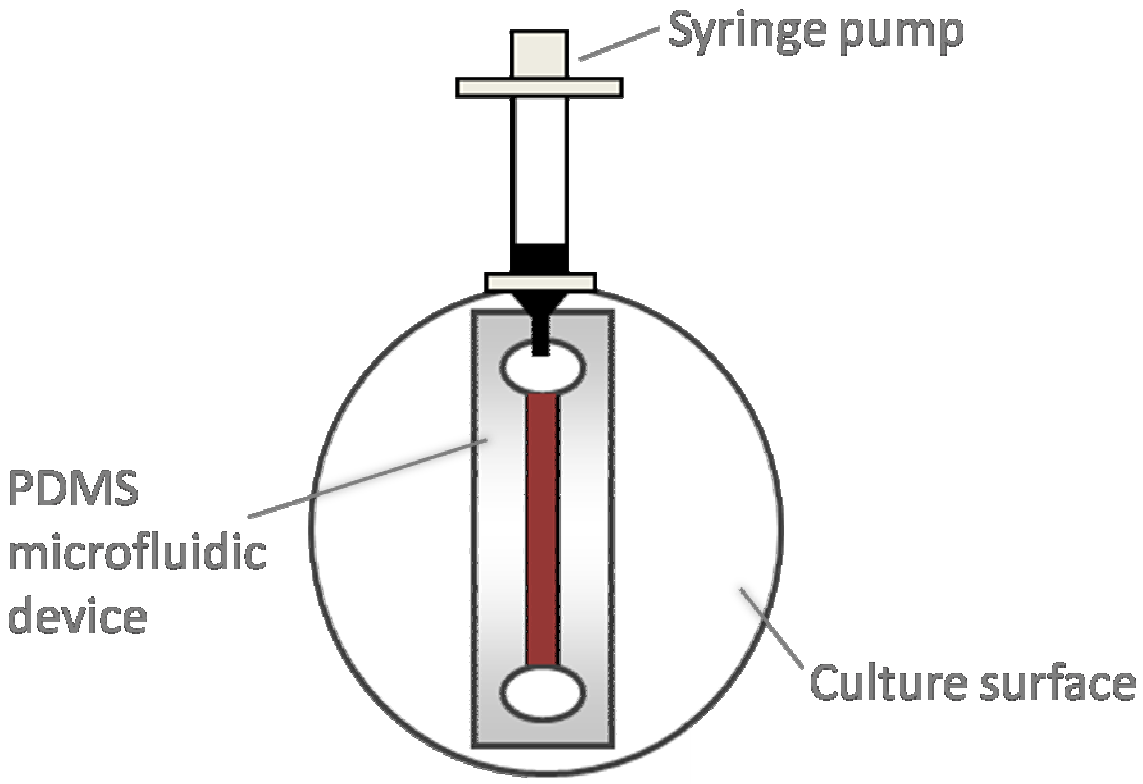


**Figure 3-3: Microfluidic device schematic.** An example of a PDMS microfluidic device. PDMS is reversibly sealed to a culture surface, and fluid is injected into the microchannel via a syringe pump.

vascularization. In a separate study, novel microfluidic chambers were developed to generate gradients of epidermal growth factor (EGF) within a 1-mm wide channel [133]. The EGF gradients induced human metastatic breast cancer chemotaxis, and breast cancer drugs were screened for their ability to slow metastasis. Furthermore, microfluidic devices were fabricated to selectively deliver small molecules and proteins to specific regions of a single cell [137]. This technique demonstrates selective manipulation of the cellular metabolic and structural machinery, and can be applied to studies in chemotaxis, drug screening, and spatially regulated signaling.

#### *3.2.2.3 Dry lift-off*

Elastomeric stamps can be manipulated to physically restrict molecule deposition, a process termed dry lift-off. Typically, elastomeric membranes are fabricated to contain through-holes. The membranes are reversibly sealed to a substrate, and the biological molecule of interest is incubated on the exposed regions of the substrate. After deposition, the membrane is peeled away, leaving behind the patterned molecules. PDMS prepolymer was spin-coated onto a photolithographically defined master, with a height shorter than the master posts and then cured [138]. The elastomeric membrane supported the patterning of a variety of materials typically difficult to pattern, including metals, sol-gels, hydrogels, and organometallic molecules. In a separate study, through-holes were mechanically punched into a PDMS stamp, and the stamp was employed to pattern DNA complex deposition and subsequently transfection [111].

### *3.2.3 Dip Pen Nanolithography*

Methods to achieve nanoscale patterns of biological molecules have recently been developed. Dip pen nanolithography (DPN) involves atomic force microscopy (AFM) to ink biological

molecules onto gold substrates [139]. Capillary transport of molecules from the AFM tip allows precise deposition. Proteins were deposited on substrates in 100- to 350-nm features using DPN [140]. Cells adhered to the nanometer-scale protein patterns and exhibited a flattened morphology. In a separate study, collagen and collagen-like peptide were patterned in 30- to 50-nm features using DPN [141]. The technique preserved the triple helical structure of collagen, and can be used to investigate the structural features of collagen and subsequent influences on cell response. Patterning proteins and cells at the nanometer scale may increase capacity for understanding interactions between biological structures (cells, proteins, viruses) and proteins [140].

## *3.3 Three-Dimensional Patterning Strategies*

The ability to pattern biologically relevant molecules within physically patterned three-dimensional constructs is important for studying cell processes in environments similar to native tissue, as well as developing strategies for tissue regeneration. Importantly, the composition and functions of adhesions in three-dimensional matrices differ from focal adhesions on two-dimensional substrates [142]. Three-dimensional adhesions displayed enhanced cell biological activities and narrowed integrin usage. Presumably, differences in cell adhesion in three dimensions versus two dimensions translate to differences in cell migration, proliferation, and differentiation.

Common strategies to pattern molecules within three-dimensional constructs involve modifications of two-dimensional lithography methods. Photocrosslinkable biomaterials have been employed to lithographically pattern three-dimensional constructs. Poly(ethylene glycol) (PEG) functionalized with photocrosslinkable moieties (e.g., methacrylate, acrylate, acrylamide)

is commonly used in three-dimensional patterning strategies. PEG is biologically inert, making the elucidation of cell responses to patterned biological molecules straightforward. Photocrosslinking strategies with PEG are almost instantaneous, allowing spatial patterning before the molecules diffuse. Additionally, some photocrosslinking strategies have been shown to be minimally toxic to cells [143] and other molecules (e.g., DNA vectors) [25]. Rapid prototyping methods have also been devised to pattern three-dimensional constructs and biological molecules. These techniques are compatible with non-photocrosslinking materials, but may be limited due to organic solvents or viscosity requirements [144]. Lithography and rapid prototyping strategies for physical patterning (i.e. complex architectures) and chemical patterning (i.e. proteins, peptides) are described below. While this overview is not intended to be exhaustive, it is important to note that other strategies have been utilized to pattern scaffold architecture, including compression molding on soft lithography elastomers, fused deposition modeling, and selective laser sintering [144].

### *3.3.1 Layer-by-Layer Lithography*

Lithography techniques have been applied to photocrosslinkable hydrogels to pattern cells and biologically relevant molecules. Three-dimensional microstructures for tissue engineering should have dimensions on the order of hundreds of microns to centimeters, to adequately investigate large populations of cells in three dimensions and fabricate implantable materials. Standard lithography strategies with photocrosslinkable hydrogels are hampered by the gel height that can be achieved due to spin coating limitations and the distance light can penetrate hydrogels in discrete patterns. Solutions of acrylated PEG were spin-coated on a layer of acrylated SAMs, and photolithography techniques were incorporated to selectively crosslink

PEG hydrogels [145]. The single-step photolithography returned hydrogels with 12 μm height features. Oftentimes, multiple rounds of photolithography are performed consecutively to increase the height of the structures and the complexity of the scaffold. Layer-by-layer photolithography was performed to create three-dimensional spatial patterns of HepG2 (human hepatocellular liver carcinoma) cells in PEG hydrogels [146]. Cells remained viable in the hydrogels after photocrosslinking, and microstructures were formed with varying shape and architecture. In a follow-up study, primary hepatocytes were patterned within PEG hydrogels using layer-by-layer techniques, and the patterns were arranged to allow single UV exposure to encapsulated cells to prevent toxicity [147]. The three-dimensional hepatocyte constructs were employed to investigate the influence of hydrogel architecture on nutrient transport. Layer-by-layer stereolithography was used to pattern RGD and heparan sulfate within PEG hydrogels [9]. Stereolithography allowed selective exposure of the hydrogel precursor solution with a precise UV laser. Patterned RGD supported selective adhesion of marrow stromal cells, while patterned heparan sulfate supported patterned adsorption of basic fibroblast growth factor. The complex three-dimensional cell structures fabricated with layer-by-layer lithography provide strategies to investigate three-dimensional cell adhesion and migration, and their effects on tissue formation.

### *3.3.2 Rapid Prototyping*

Rapid prototyping can physically pattern the location of biologically relevant molecules within materials that do not require photocrosslinking. Three-dimensional printing (3-DP) and pressure assisted microsyringe (PAM) fabrication [144] are examples of rapid prototyping. 3-DP involves depositing a binder solution onto a biomaterial powder bed using an ink jet printer [148]. Multiple layers are printed to achieve a three-dimensional structure. 3-DP was employed

to pattern a solvent on PLG powder packed with sodium chloride particles to build three-dimensional scaffolds as a series of thin two-dimensional slices [149]. The PLG scaffolds supported the co-culture of rat hepatocyte and nonparenchymal cells. Alternatively, PAM fabrication involves a capillary needle on a pressure controlled micro-syringe to deposit biomaterial structures on a surface. The micro-syringe typically deposits the biomaterial of interest dissolved in a solvent, and the polymer stream is varied by changing the syringe pressure, solution viscosity, syringe tip diameter, and motor speed [144]. More than 30 layers of a hepatocyte/gelatin mixture were laminated into a high spatial structure using PAM, and the hepatocytes remained viable and performed biological functions in the construct for more than two months.

### *3.3.3 Two-Photon Absorption Photolithography*

Strategies have been devised to circumvent the requirement of a layer-by-layer approach to achieve complex three-dimensional patterns. Two-photon absorption photolithography involves a mode-locked Ti:sapphire laser manipulated in the x-y-z planes to selectively photocrosslink hydrogels along a three-dimensional pattern [150]. The laser is programmed by the user to scan only specified regions within each focal plane. Using this technique, proteolytically degradable hydrogels were patterned with selective sites containing adhesion motifs (RGDS). Cells were shown to invade and migrate only in the three-dimensional regions containing RGDS.

## *3.4 Conclusions*

In conclusion, the microelectronics industry has provided a profusion of knowledge and strategies which biologists, chemists, and engineers have applied to the patterning of biologically relevant molecules. Two-dimensional patterning strategies are relatively mature and currently

used in functional DNA microarrays and transfected cell arrays. Protein patterning in two dimensions has been applied to investigate cell adhesion. However, proteins nonspecifically adsorbed to hydrophobic substrates may not present ligands in a natural context. SAMs aim to overcome this matter by presenting defined chemistries for adsorption. Strategies to pattern adhesion fragments, rather than the entire protein, also aim to better control ligand presentation. Three-dimensional patterning strategies more accurately depict the microenvironment of native tissue, and will be required to adequately screen tissue engineering systems. Three-dimensional patterning strategies, however, are relatively immature and will require optimizations to achieve patterns of mm-scale heights, adequate cellular viability, and proper tools for assessing cellular outputs. Patterning biologically relevant molecules offers unique strategies for high-throughput screening of drug targets, drug design, and regenerative systems.

# Chapter 4

# Axon Guidance in Development and Regeneration

## *4.1 Introduction*

The nervous system is an intricate arrangement of neural networks responsible for sensation, perception, and behavior. The nervous system is composed of nerve cells, or neurons, and a variety of supporting cells divided into two subsets: the central nervous system (CNS) and the peripheral nervous system (PNS). The central nervous system, consisting of the brain and spinal cord, is responsible for analysis and integration of sensory and motor information [151]. The peripheral nervous system is comprised of sensory neurons and motor neurons. Sensory neurons connect the brain and spinal cord to sensory receptors, while the motor neurons connect the brain and spinal cord to muscles and glands [151].

The unique, complex morphology of neurons allows the integration and analysis of information that controls all movements, senses, and thoughts. Nerve fibers, referred to as dendrites or axons or collectively as neurites, are entities of the neuron responsible for transferring information in the form of electrical signals. Synapses are sites of connection between neurons, and precise synapse formation is critical for accurate information transfer. Dendrites and the neuron cell body provide sites for synaptic contacts made by the terminals of other nerve cells; thus, are specialized to receive signals. Most neurons have multiple dendrites, which are short and highly branched. The axon is specialized for the conduction of electrical impulses, called action potentials, away from the cell body toward the axon terminus [152].

Neuroglial cells, such as astrocytes and oligodendrocytes (CNS) and Schwann cells (PNS), do not transmit electrical signals. However, as part of the nervous system, they play an important role in bundling axons (myelination), maintaining the ionic milieu, and modulating the rate of nerve signal propagation [151]. The complexity of the nervous system can be described by the sheer number of cells required to carry out functions, with billions of neurons in the vertebrate forebrain, each forming as many as a thousand connections [152, 153]. The proper wiring of this complex neural circuitry is dependent on neurite pathfinding to synaptic targets [154]. Mutations of genes responsible for neurite pathfinding are linked to several neurological diseases, such as the reading disorder, dyslexia [155], the seizure disorder, epilepsy [156], and MASA syndrome (mental retardation, aphasia, shuffling gait, and adducted thumbs) [157].

Understanding the manner in which nerve fibers migrate, and moreover how migrating neurites are directed to synaptic targets, is important in the study of developmental neurobiology and disease, as well as in the engineering of strategies to achieve functional recovery after injury. Ramon y Cajal was the first to hypothesize that axons migrate through the extracellular environment, guided by the expanded terminal structure, which he named the growth cone [158]. Conversely, others believed that long nerve fibers were a result of progressive differentiation without movement [159]. Two decades later, Granville Harrison directly observed the dynamic nature of the growth cone in vitro and confirmed Cajal's hypothesis [160]. It is now widely accepted that neurites grow toward their targets, and migration is regulated by interactions with the growth cone and extracellular guidance cues [159]. Axonal guidance molecules are either permissive or inhibitory, and exist as either soluble factors that diffuse throughout the extracellular space or nondiffusible factors presented by cells in the microenvironment or bound

to the extracellular matrix. Upon binding of guidance molecules to growth cone receptors, intracellular signaling triggers alterations in growth cone cytoskeletal dynamics, causing the axon to advance, retract, turn, and branch [161]. This Chapter examines axon guidance molecules and mechanisms of guidance. Additionally, methods in which researchers are applying this information to engineer regeneration strategies will be reviewed.

## *4.2 Axon Guidance in Embryonic Development*

The intricate formations of neural networks generated during embryogenesis are a result of axon homing to proper synaptic targets. Axons extend and turn along precise pathways constructed by guidance molecules in the extracellular space, making few navigational errors. There are four classes of guidance molecules. The molecules can be either attractive or repulsive, and diffusible (chemotactic) or contact-mediated (haptotactic) (Figure 4-1) [5]. In 1892, Ramon y Cajal was the first to hypothesize gradients of diffusible chemoattractants are presented to axons, similar to chemotaxis mechanisms in leukocytes, and elicit a relatively long range guidance signal (hundreds of micrometers) [162]. This hypothesis was not confirmed until eight decades later [163, 164]. Guidance signals presented by contact-mediated molecules, either as transmembrane proteins or the extracellular matrix, present a short range guidance signal acting on a relatively small length scale. Importantly, axons in the developing embryo may travel distances up to several centimeters to reach their targets. For this reason, axon trajectories are simplified by fragmentation into shorter steps interrupted by intermediate targets, or choice

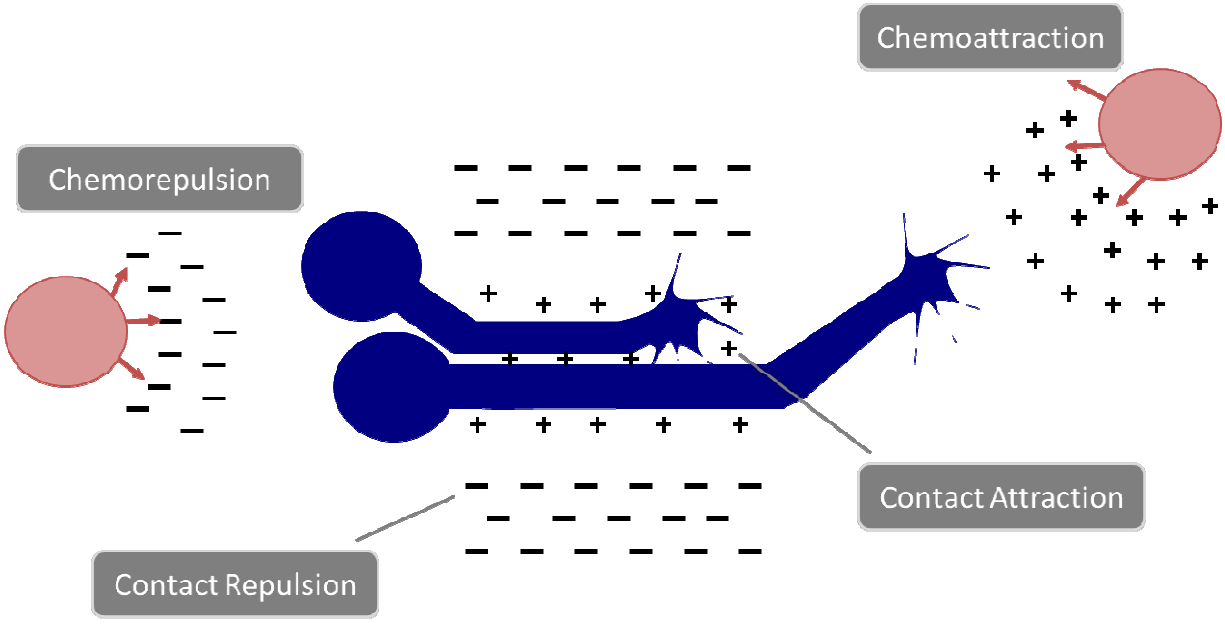


**Figure 4-1: Schematic of axon guidance molecules.** There are four general classes of axon guidance molecules: Contact attractive and repulsive and Chemo attractive and repulsive. Contact molecules signal over a relatively short range, while chemotactic molecules signal over a relatively long range. Adapted from Tessier-Lavigne [5].

points, at which tissues present critical guidance cues that direct growth cones on the next stage of their trajectory [165]. Additional complexity is introduced when determining whether a molecule is either attractive or repulsive, which does not only depend on the intrinsic properties of the molecule, but some guidance factors may function as both repellants and attractants. The function of the guidance factors depends on second messenger levels within the growth cone and the type of receptor on the growth cone surface [166, 167].

Axonal pathfinding has been implicated in the proper development of many tissues within the nervous system. During embryogenesis, the neural tube is the first structure in the central nervous system to form, and later develops into the spinal cord. The floor plate, the structure that comprises the cells occupying the ventral midline of the developing spinal cord, plays an important role in central nervous system axon guidance. Highly specialized cells in the floor plate attract spinal commissural axons from the dorsal spinal cord. Conversely, motor, spinal association, and sensory axons within the vicinity of floor plate guidance molecules are non-responsive and continue on alternative paths (reviewed in: [168])[169-171]. Axonal pathfinding has also been implicated in the development of the visual system and, in turn, the proper functioning of the eye. Guidance molecules positioned within the outer retina instruct retinal ganglia cells to extend their axons in a highly directed, radial manner toward the optic disc and through the retina to the optic fiber layer, forming the optic nerve [172]. In the mammalian neocortex, axons migrate and establish a connection with the basilar pons, a major connection that is essential for the control of motor behavior [173, 174]. This migration is controlled by guidance molecules secreted near the basilar pons [175].

In each of the cases described above, proper wiring of the neural circuitry results from a complex interplay of the four classes of guidance molecules. Attractive molecules instruct specific populations of axons to the appropriate target and repulsive molecules deter axons from an inappropriate target. Moreover, differential expression of guidance molecules and growth cone receptors [176], combined with alterations in intracellular signaling molecules [154], allow for both spatial and temporal regulation during embryogenesis. The following sections review in detail chemotactic and haptotactic guidance molecules, and the mechanisms of guidance by each.

### *4.2.1 Chemotactic Signals and Mechanisms*

Chemotactic signals are presented by cells within target tissue that express and secrete guidance molecules. Soluble guidance molecules presumably diffuse through the extracellular space, resulting in concentration gradients of the factor. The growth cone is believed to sense a concentration difference across its spatial extent, and convert this as a signal to move up or down a gradient and therefore toward or away from the target tissue [177]. While this phenomenon is widely accepted to occur during embryogenesis, only recently was the first gradient of a guidance factor, netrin-1, visualized directly in the path of commissural axons in rat, chick, and mouse spinal cords [178]. Since gradients are difficult to visualize in vivo, combined with the complex interplay of many guidance factors acting on one axon, the mechanisms of axon guidance by chemotaxis have been difficult to elucidate. The next sections describe the axon chemotactic molecules that have been identified, in vitro systems that have been developed to study this complex phenomenon, and attempts at defining the gradients capable of guiding axons.

### *4.2.1.1 Axon chemotactic molecules*

Molecules that have been identified to signal axon chemotaxis are organized into several families, most notably the Netrins, Semaphorins, and Neurotrophins [5, 179]. Considerable information has been gathered about the role each plays in axon pathfinding, along with specific receptors on the growth cone that bind the ligands. A brief overview is provided below. While this overview is not intended to be exhaustive, it is important to note that other families of diffusible molecules have been shown to guide axons, including Slits, Ephrins, and morphogens.

#### *4.2.1.1.1 Netrins*

Netrins are a small family of axon guidance molecules, bearing much resemblance to laminin, but are only ~ 600 amino acids in size. They do not bear the transmembrane domain as laminin, and therefore, are diffusible molecules. However, netrins contain a basic domain and some have hypothesized that the diffusion of the netrins may be slowed by interactions with cell surfaces or ECM [180]. Netrin-1 and netrin-2 were first identified after purification from chick brain [180, 181], and are capable of attracting some axons, while repelling others [5]. Evidence of axon guidance by netrins has been demonstrated extensively in vertebrates. Netrins are expressed by glial and neuronal cells along the ventral midline, and guide different axon populations to and away from the midline [168, 181]. Netrins have also been implicated in the guidance of cortical axons [182], as well as retinal axons at the optic disc [183]. The ability of netrins to behave as a bifunctional guidance cue is related to the receptors on the growth cone in which they bind. Members of the DCC subfamily of the Ig superfamily are components of receptors that mediate attractive effects of netrins [184], while UNC-5, a transmembrane protein that defines a distinct branch of the Ig superfamily, mediates repulsive effects [185].

Interestingly, the ability of netrin-1 bound to the DCC receptor to elicit an attractive guidance cue was switched to a repulsive cue by altering cAMP levels within the growth cone [186].

*4.2.1.1.2 Semaphorins*

Semaphorins are a relatively large family of axon guidance molecules, containing at least 30 members. Some semaphorins have a transmembrane domain, which are in turn contact-mediated guidance molecules. Others lack the transmembrane domain, and are diffusible, long range chemotactic factors [167]. Semaphorins share the same homologous domain, sema, which is a large extracellular domain approximately 500 amino acids in length. The sema members are divided into six classes, based on structural similarities, and Sema II and III are the diffusible guidance factors [187]. Most semaphorins are known only to repel growing axons, while Sema I has been suggested to provide a contact-mediated attractive cue [5]. Sema III secreted at the ventral spinal cord has been implicated in patterning sensory projections by selectively repelling axons that normally terminate dorsally [188]. The Sema III receptor, neuropilin, is a transmembrane protein [189]. Four other members of the semaphorin family were later identified to bind to neuropilin with similar affinity [190].

*4.2.1.1.3 Neurotrophins*

The family of neurotrophins, or neurotrophic factors, is characterized by the ability to maintain synaptic connections. During embryogenesis and beyond, neurotrophins are secreted at sites of synaptic connection. Neurotrophins function to maintain connections between neurons and their targets by regulating survival, growth, and differentiation. Without trophic factor support, the axons and dendrites of developing neurons atrophy and the nerve cells may eventually die [151]. The first neurotrophic factor discovered was Nerve Growth Factor (NGF),

isolated from mouse sarcoma [191, 192]. Only certain populations of neurons, however, are responsive to NGF. Other members of the neurotrophin family include brain-derived neurotrophic factor (BDNF), neurotrophin-3 (NT-3), and NT-4/5. The receptors that bind neurotrophins include the Trk family of receptor tyrosine kinases (TrkA; NGF, TrkB; BDNF and NT-4, and TrkC; NT-3) and the low-affinity receptor p75. The secretion of some neurotrophic factors is not triggered until ingrowing axons have reached their synaptic target; thus, it has previously been accepted that neurotrophic factors are unlikely to guide axons during development [151, 193]. However, recent evidence indicates that long distance peripheral sensory axon growth is neurotrophin-dependent [194], but no conclusive studies have confirmed that neurotrophic factors guide axon pathfinding during embryogenesis. Importantly, neurotrophic factors have been shown to behave as guidance molecules in regeneration models. Gradients of NGF and NT-3 can guide sensory neurite extension along distances up to 7 mm in vitro [195]. The ability of neurotrophic factors to elicit guidance signals in vivo was demonstrated by enhanced length of axons growing inside fetal spinal cord transplants at the site of adult spinal cord hemisection injury when neurotrophic factors were applied [196]. Additionally, microinjection of NGF into the brain ventricle of neonatal rats evoked a massive ingrowth of sympathetic fibers into brain tissue toward the source of NGF [197].

#### *4.2.1.2 In vitro systems to study axon chemotaxis*

Since the mechanisms of axon chemotaxis are difficult to elucidate in vivo, many in vitro systems have been developed to investigate neurite guidance. The first systems demonstrating chemotaxis in vitro involved the effects of NGF gradients on sensory neurons, specifically the dorsal root ganglia (DRG) from chicken embryos. DRG are sensory ganglia that lie adjacent to

the spinal cord. DRG send axons to the periphery for the transduction of information, and also send central processes to the spinal cord and brainstem to relay the information [151]. Micropipettes containing 2 to 50 units of NGF placed near growing axons of chick DRG neurons led to axon turning and growth toward the NGF source within 21 minutes [198]. Additionally, a gradient of NGF formed by chamber slides to localize an agarose/NGF mixture was capable of orienting chick DRG neurons toward the source when the concentration was 25 to 1000 ng/mL of β-NGF [199]. In an effort to accurately recapitulate the concentrations and types of factors secreted in vivo, methods were developed to extract target tissue, specifically embryonic rat lumbar spinal cord, and culture the organotypic culture alongside DRG explants [200]. This study confirmed that a diffusible factor, or factors, produced at the embryonic ventral horn were responsible for inhibiting DRG axon innervation of the spinal cord. A second technique aimed at mimicking the mechanisms at which gradients form in vivo, by localized expression of a factor, involved recombinant technologies to achieve heterologous cells expressing netrin-1 and netrin-2, and co-culturing clusters of these cells with embryonic rat dorsal spinal cord explants. This study confirmed that netrin secreted by target tissue guides commissural axons [181].

The systems described above and the subsequent gradients formed can be highly variable and therefore difficult to characterize. Understanding the mechanisms by which growth cones migrate up or down concentration gradients will require well-defined gradients. Recently, engineered systems have attempted to define the concentration gradients of chemotactic factor necessary for guiding neurites. Gradients of NGF were formed in an agarose hydrogel using a gradient-maker equipped with source and sink chambers, and NGF from the source chamber diffused throughout the gel, creating a linear concentration gradient [201]. The gradients were

characterized by sectioning the agarose gel, and quantifying NGF concentration in each 20-μm section. DRG neurons were cultured beneath the NGF gradient within agarose, and guidance was observed when the absolute concentration gradient was above 133 ng/mL/mm [195]. Interestingly, there is not a general consensus in the neuroscience field as to whether the absolute concentration gradient (concentration change per distance), or the fractional concentration gradient (% change across the width of the growth cone), is the accurate measure of successful neurite chemotaxis. The next section will discuss efforts at understanding the gradients required for chemotaxis, with a particular focus on knowledge from leukocyte chemotaxis.

#### *4.2.1.3 Defining the gradients*

It has been well supported experimentally that growth cones are capable of sensing concentration gradients of factors and converting the signal into migration up or down the gradient. The neuron must detect the gradient either through the difference in receptor occupancy on two sides of the growth cone (spatial detection), or changes in the total level of receptor activation with time (temporal detection) [176]. Bacteria use temporal detection during chemotaxis, comparing local concentrations over time and reorienting depending on whether the concentration detected is increasing or decreasing [202]. However, growth cones are much slower than bacteria, extending on average 10-20 μm every 15 minutes, suggesting that spatial detection is likely the mechanism of gradient detection [176, 177]. During leukocyte chemotaxis, the mean concentration of the guidance molecule influences the ability of cells to sense a gradient, and the same school of thought has been adopted for growth cone chemotaxis [203]. Guidance detection is optimal when the concentration at the growth cone is equal to the dissociation constant for the receptor [2, 204]. If the concentration is too low, a small percentage

of receptors will be bound at any given time, yielding little difference in binding. Similarly, if the concentration is too high, a large percentage of receptors will be bound at any given time, again, yielding little difference in binding [177, 203]. Additionally, the percent change in concentration over the distance of the growth cone, or fractional concentration gradient, must be large enough to overcome noise in both the binding process and the intracellular signaling that turns a binding difference into directional information [205]. Furthermore, for mean concentrations far from the dissociation constant for the receptor, the fractional concentration gradient required for guidance is expected to be larger [2]. In vitro assays have shown that growth cones can respond to a gradient of 5-10% across their width in liquid, but the minimum gradients required for detection were not determined [206, 207]. Interestingly, it has been shown that the critical chemorepulsive information to pathfinding Ti1 pioneer growth cones within the developing grasshopper limb is governed by the Sema 2a fractional gradient and not the absolute gradient [208]. Taken together, these experimental and mathematical findings suggest that the mean concentration of the factor and the fractional concentration gradient govern axon chemotaxis.

### *4.2.2 Haptotactic Signals and Mechanisms*

Axons require permissive adhesive environments to grow. Haptotactic guidance cues can be presented as surface-bound gradients, similar to chemotactic mechanisms. Alternatively, the guidance cue can be simply selective adhesion to a permissive substrate within a larger region of non-adhesive molecules. Contact-mediated guidance molecules may be presented as transmembrane proteins on the surface of neuronal or non-neuronal cells, receptors on cells, or extracellular molecules sequestered within the extracellular matrix. Therefore, growth cone interactions with haptotactic molecules can be either cell-cell or cell-substrate interactions.

#### *4.2.2.1 Axon haptotactic molecules*

Many contact-mediated guidance molecules have been identified, including families of cell adhesion molecules (CAMs), ECM molecules, and even diffusible molecules presented by the cell surface or ECM. A brief overview of each class of haptotactic guidance molecules is presented below.

##### *4.2.2.1.1 Cell adhesion molecules (CAMs)*

Two large families of CAMs have been implicated in axon pathfinding, including the immunoglobulin Ig and cadherin superfamilies [5]. Most of the CAMs are transmembrane proteins, and interestingly, many CAMs mediate homophilic adhesion, functioning as a ligand on one cell and a receptor on another [209]. The Ig family of cell adhesion molecules share a common Ig domain (70-110 AA), and usually a FNIII domain (90 AA) [210]. The first cell adhesion molecule to be characterized was neural cell adhesion molecule (NCAM), which was shown to mediate adhesion of cells in the retina and support outgrowth and guidance of mossy fiber tracts in the hippocampus of mice [211, 212]. Genetically modified mice embryos lacking the Ig CAM, L1, showed defects in the guidance of axons of the corticospinal tract, a major motor control pathway projecting from the cortex to the spinal cord. In the absence of L1, a substantial proportion of axons failed to cross the midline to the opposite dorsal column as normal [213]. Importantly, genetic analysis revealed that mutations in L1 are linked to mental retardation in humans [157].

##### *4.2.2.1.2 Extracellular matrix molecules*

Several extracellular matrix molecules have been shown to behave as either promoters or inhibitors of axon growth and extension in vitro, including laminin, fibronectin, tenascin, and a

variety of proteoglycans [214, 215]. Astrocytes expressing laminin influenced axon elongation and nerve pathway formation during embryonic development of the mouse optic nerve. Furthermore, one region of the optic pathway in which retinal ganglion cell axons avoid in vivo did not contain laminin-expressing astrocytes [216]. The contact-adhesion cue may also be a repellant. Chondroitin sulfate proteoglycans (CSPGs) were expressed in the innermost layers of the developing rat retina and moved peripherally with the direction of retinal ganglia axon development. Additionally, the CSPGs always remained at the outer edge of the developing axons. Moreover, retinal ganglia axons were shown to turn so as to avoid outgrowth on the barrier created by CSPG-expressing cells [217].

*4.2.2.1.3 Diffusible molecules*

Interestingly, chemotactic molecules may bind to the extracellular matrix or cell surfaces and behave in a haptotactic mechanism. Neurotrophins are known to bind tightly to the surface of the neuron that secretes them to produce localized synaptic modulation [218]. Nerve growth factor covalently attached to Sepharose beads promoted neurite extension toward the beads, indicating that NGF can exert its effects on neurons by interacting with external membrane structures [219]. In an ensuing study, NGF nonspecifically immobilized to specific regions of a poly-L-lysine substrate resulted in patterned neurite outgrowth, localized to the regions of NGF adsorption [220]. Immunohistochemical localization of netrin-1 in the embryonic chick nervous system revealed that netrin-1 was bound to the tissue along the lateral borders of the cord, suggesting that the effect of netrin-1 on pioneering spinal cord commissural axons is haptotactic [170]. Collectively, these studies indicate that diffusible guidance molecules immobilized to a substrate are active and capable of eliciting a haptotactic guidance signal. Mathematical predictions of

growth cone gradient detection, based on diffusivity and concentration fluctuation, reveal a steeper concentration gradient is required for gradient detection and subsequent axon guidance when a diffusible molecule is presented as a bound ligand [221].

#### *4.2.2.2 In vitro systems to study axon haptotaxis*

Similar to chemotactic guidance signals, many in vitro systems have been engineered to investigate axon haptotaxis. Laminin was micropatterned by adsorption to photolithography defined hydrophobic regions on a quartz substrate. Neurons cultured on the patterned substrates selectively adhered to the laminin-rich regions and neurites extended along the laminin patterns without aberrant sprouting or turning. The flexibility offered by the lithography patterns permitted the investigation of a range of laminin and non-adhesive pattern widths. If laminin patterns were separated by non-adhesive patterns less than 50 μm in width, growth cones were able to cross the non-adhesive tracts to nearby laminin patterns and did not orient [222]. In a separate study, microfluidic techniques were employed to pass laminin through laminar flow microchannels, while adsorbing the protein to a poly-L-lysine substrate in a gradient formed by the microchannels [223]. In this study, rat hippocampal neurons extended axons up the concentration gradient of laminin, if the gradient was greater than 0.06 μg/ml/μm. Another technique to pattern gradients of surface-bound molecules was developed to selectively immobilize the peptide sequence of laminin responsible for neural adhesion and axonal elongation, IKVAV. A photo-linker was first covalently attached to the peptide and subsequently, varying amounts of the peptide were photocrosslinked on a substrate using a laser with varying doses of irradiation [224]. Chick embryo dorsal root ganglia neurons cultured on the IKVAV gradients oriented up the gradients with a 25% concentration difference over 30 μm.

## *4.3 Growth Cone Cytoskeleton Dynamics in Axon Guidance*

During axon elongation and guidance, the growth cone takes on different morphologies controlled by the dynamic nature of both actin and microtubules in the growth cone and axon cytoskeleton. Filopodia are narrow, cylindrical extensions capable of extending tens of microns from the periphery to explore the environment. Lamellipodia are flattened, veil-like extensions at the periphery of the growth cone [225]. In order to understand cytoskeletal arrangements during axon guidance, the cytoskeletal dynamics that occur during axon elongation must first be defined. By monitoring axon elongation in vitro via real-time microscopy, the process of axon elongation was divided into three morphologically distinct stages [226]. The three stages have been termed protrusion, engorgement, and consolidation [225]. During protrusion, both filopodia and lamellipodia elongate, potentially through the polymerization of actin filaments. Engorgement occurs when microtubules invade the protrusions. Vesicles and organelles are also transported into the protrusions, via Brownian motion and directed microtubule based transport. Consolidation occurs when the majority of actin depolymerizes in the neck of the growth cone and the transport of the organelles becomes bidirectional, adding a new distal segment of the axon. During axon guidance, gradients of molecules bias one side of the growth cone to progress through these three stages toward the guidance cue more rapidly than the other side of the growth cone [225], resulting in guided protrusion, engorgement, and consolidation.

Both actin and microtubules are in a constant state of flux, existing sometimes in a stable state and other times as dynamic structures. Actin filaments (F-actin) are helical polymers composed of actin monomers, often referred to as globular actin (G-actin). Actin polymerization occurs at the leading edge of the growth cone and F-actin is retrogradely transported toward the

center of the growth cone. Here, F-actin is depolymerized and recycled for further polymerization [227]. Rho family GTPases (Rho, Rac, and Cdc42) orchestrate actin assembly and disassembly through the activation of effector proteins [166]. Microtubules are polarized structures composed of tubulin dimers assembled into linear arrays of alternating α- and β-tubulin subunits. The microtubule dimers in the nervous system are likely to be heterogeneous polymers composed of several combinations of α/β dimer isotypes [225]. Microtubules are functionally modified via posttranslational modifications, such as tyrosination/detyrosination, acetylation, phosphorylation, polyglutamylation, and polyglycylation [228]. These posttranslational changes are likely to alter binding of microtubule associated proteins which, in turn, influences interactions with other cytoskeletal components and intracellular signaling pathways.

A substantial amount of research has been devoted to understanding how axon guidance molecules modulate these critical cytoskeletal arrangements. Significant evidence suggests axon guidance molecules activate proteins of the Rho family. Binding of netrin to its DCC receptor leads to association of the adapter protein Nck [229] which, in turn, activates Rho GTPases Cdc42 and Rac-1, and presumably actin dynamics [166]. Binding of NGF to trkA induces trans-phosphorylation of TrkA and recruitment of adaptor and effector proteins. GTP-binding proteins activate the MAPK signaling pathway and TrkA activates the PI3-kinase (PI3K) signaling cascade. MAPK has been implicated in mediating the growth and survival effects of neurotrophins. Additionally, PI3K may modulate actin dynamics by regulating the activity of RhoG which can activate Cdc42 and Rac [166]. Moreover, PI3K activation inhibits another downstream signaling pathway, GSK-3β. The inhibition of GSK-3β resulted in localization of

adenomatous polyposis coli (APC) to the tips of microtubules, promoting microtubule assembly and axon elongation [230].

## *4.4 Nerve Regeneration Strategies to Promote Axon Guidance*

Injury to the nervous system is detrimental, and depending on the extent of injury, may cause debilitating results. Peripheral neuropathy can be a result of disease, including diabetes and cancer, or mechanical compression or severance. Injury to the central nervous system is commonly in the form of spinal cord injury (SCI) and oftentimes results in paralysis. Central nervous system injury can also be triggered by the onset of disease, including Parkinson's and Alzheimer's disease. Upon complete transection of a peripheral nerve, macrophages and Schwann cells are recruited to clear myelin and axonal debris. The macrophages and Schwann cells also function to secrete growth promoting cytokines and regeneration is typically initiated. Peripheral nerve regeneration can occur along distances up to a few millimeters with simple suturing techniques or the use of autologous grafts. At the onset of central nervous system injury, the physiological response differs drastically in comparison to the PNS. The recruitment of macrophages to clear myelin debris is a much slower process due to the blood-brain barrier and a lack of cell adhesion molecules [231]. Extracellular matrix proteins at the site of CNS injury are inhibitory for regeneration and form the glial scar, comprised of myelin-associated molecules (Nogo, myelin associated glycoprotein, oligodendrocyte-myelin glycoprotein) and CSPGs. The CNS recruits astrocytes, similar to Schwann cells in the PNS, but they convert to reactive astrocytes at the site of injury by secreting additional inhibitory molecules and contributing to the glial scar [232]. The combination of a plethora of inhibitory molecules, a lack of growth promoting molecules, and alterations in gene expression make the site of injury in the CNS

unfavorable for regeneration and a much more complex system to regenerate. CNS neurons were not believed to have regenerative capacity until 1980, with the demonstration of CNS axon growth into PNS nerve grafts [233]. Currently, there are no clinical methods to regenerate CNS nerves. Only anti-inflammatory drugs, such as methylprednisone, are available to minimize the effects of secondary injury [234]. Tissue engineering strategies to repair PNS injury have shown promise, while the methods to repair CNS injury are still immature. Current tissue engineering strategies will be discussed below, with a particular focus on strategies to promote guidance of axons at a lesion site.

### *4.4.1 Nerve Tissue Engineering Strategies*

Tissue engineering strategies for nerve repair involve many of the processes and endpoints described in Chapter 2. Scaffolds for nerve regeneration have also been termed bridges or conduits. These scaffolds should be designed to provide physical support and bridge the gap created by the lesion, while recruiting progenitor cells into the matrix and blocking inhibitory molecules. The strategy may also incorporate a conductive approach, delivering molecules to promote growth or block inhibition. Additionally, cell transplantation methods have been devised to present growth promoting and cell adhesion molecules. A particular challenge for nerve regenerative strategies is to not only promote the growth of regenerating axons, but achieve efficient and specific guidance of the axons across the lesion site, as guidance of regenerating axons across the length of the lesion will be required to reconnect synapses and achieve functional recovery.

#### *4.4.1.1 Peripheral nervous system tissue engineering*

While there are currently options available for the treatment of PNS injury, the suturing technique cannot be used for injuries greater than a few millimeters due to halted regeneration by tension on the nerve. Autologous grafts are effective, but not ideal, since they require a second nerve injury and multiple surgeries. Tissue engineering strategies have been developed for peripheral nerve regeneration and some FDA approved scaffolds can repair short peripheral nerve defects. Integra Neurosciences Type I collagen tube was shown to bridge 5 mm peripheral nerve gaps in the monkey wrist with physiological recovery similar to suture repair [235]. SaluMedica's SaluBridge Nerve Cuff, a conduit made from polyamide filaments inside silicone tubes, was shown to bridge a 15 mm rat sciatic nerve gap [236]. The Nerve Cuff was employed to repair damaged nerves in the human forearm, showing return of normal sensory and motor functions of the hand [237]. While existing tissue engineering strategies show promise, the ability to regenerate peripheral nerves over long distances remains a challenge.

#### *4.4.1.2 Central nervous system tissue engineering*

The ability to regenerate CNS axons requires the induction of neuron survival and axon elongation, combined with the reduction of survival and growth inhibition factors. The first report demonstrating CNS nerve regeneration was performed by implanting PNS nerve grafts containing Schwann cells at the site of CNS injury [233]. There are, however, unfavorable issues associated with PNS grafts, including multiple surgeries with autologous PNS grafts, immune responses to heterologous PNS grafts, and an inability to engineer PNS grafts for the sustained delivery of therapeutic factors. Nerve bridges to mechanically support a lesion site have been fabricated from synthetic materials (e.g., PLG, PEG) [238, 239] or natural materials (e.g.,

Collagen) [240, 241]. Methods are being designed to effectively deliver growth factors to the site of injury. Gelfoam saturated with neurotrophic factors was placed over a fetal spinal cord tissue transplant at the site of a rat hemisection injury. The delivery of BDNF, NT-3, and NT-4 increased the extent of serotonergic, noradrenergic, and corticospinal axonal ingrowth within the transplant [196]. More controlled and elegant approaches have been developed, but the ability to achieve sustained release of a necessary dose of therapeutic factor over the duration required for regeneration remains a challenge [242]. Recently, nerve bridges delivering non-viral gene therapy vectors to alter gene expression within the spinal cord lesion have demonstrated transgene expression within a rat spinal cord hemisection injury for 2 weeks [238]. Alternative methods to deliver therapeutic factors include implanting Schwann cells [243] or cells that have been genetically modified to express therapeutic factors [244]. These methods have shown promise; however, cell transplantation strategies are often plagued with an inability to support high percentages of cell survival after transplantation. Importantly, the stimulation of survival and outgrowth at the site of injury must be coupled with systems to block inhibitory molecules. Many methods have addressed this requirement, including delivery of small molecules that bind Nogo receptor [245], antibodies to Nogo [246], and enzymes to degrade CSPGs [247]. Recently, siRNA delivery strategies were developed to silence the expression of inhibitory molecules while overcoming disadvantages associated with small molecule delivery [248]. Functional recovery at the site of CNS injury will require a combinatorial approach to support axon survival and outgrowth, block inhibitory molecules, and direct axonal outgrowth. Methods to guide axons in PNS and CNS regenerative strategies are discussed below.

### *4.4.2 Axon Guidance Strategies*

Successful strategies to orient and guide regenerating axons across a lesion will be essential for functional recovery after nerve injury. Investigation of axon guidance during embryogenesis has led to a partial understanding of the extracellular factors that are presented as guidance cues, the mechanisms of guidance signal sensing by the growth cone, and the intracellular signaling events leading to oriented growth. Importantly, neuronal responses to guidance molecules are altered from development to adulthood, complicating the ability to engineer regenerative guidance strategies [249]. Many methods have been developed to fabricate bridges with guidance channels to physically orient axons. These guidance bridges have subsequently been combined with patterned adhesion molecules or glial cells to present both physical and chemical guidance cues. Recently, methods have been devised to achieve gradients of chemotropic factors within guidance bridges.

#### *4.4.2.1 Topographically patterned bridges*

Topographical patterns have been shown to guide axonal outgrowth in vitro. As an axon growth cone reaches the wall of a microchannel, the growth cone migrates parallel to the wall, orienting the axon as it elongates [250]. In vitro demonstrations have led to the onslaught of strategies to fabricate three-dimensional nerve guidance bridges for in vivo transplantation. A guidance conduit fabricated from poly-3-hydroxybutyrate (PHB) sheets resulted in 2-20 μm diameter oriented PHB fibers within the conduit. The conduit was capable of regenerating axons in a rabbit peroneal nerve injury model over a length of 4 cm and regenerating nerve fibers in the PHB conduits were more plentiful than in nerve autograft controls [251]. In a separate study, a silk fibroin nerve guidance conduit (SF-NGC) was fabricated by injection molding a silk fibroin

solution to obtain a single lumen conduit, followed by addition of 20 aligned silk fibroin fibers within the single lumen. The SF-NGC elicited peripheral neurite outgrowth in a 10-mm long sciatic nerve defects in rats, resulting in functional and morphological recovery similar to autografts [252]. A novel technique to engineer guidance bridges involved solvent casting, physical imprinting, and a rolling-fusing method to obtain poly-(L)-lactic acid (PLLA) conduits with multiple intralumenal walls and precise topography along the longitudinal axis. The intralumenal walls in the conduits were 20 μm in width, and the physical parameters of the conduit, such as number of lumens, conduit length, and diameter were all controllable [253].

Of specific importance for the central nervous system, guidance conduits must also present the ability to provide a drug delivery mechanism, both to promote growth and block inhibition. PLG microspheres with encapsulated neurotrophic factors and porogen were loaded into a patterned mold and processed by gas foaming to fabricate porous PLG guidance conduits. The guidance channels within the conduit ranged in diameter between 100 and 250 μm and neurotrophic factor was released from the conduit for at least 42 days while maintaining activity [254].

#### *4.4.2.2 Patterned ECM and glial cell bridges*

Methods to incorporate contact-mediated guidance cues within physical guidance conduits provide the ability to elicit synergistic guidance signals. A guidance conduit of aligned fibronectin fibers was fabricated by precipitating fibronectin out of an acidic solution, manually drawing fibronectin fibers, and freeze-drying the conduit. Once hydrated the fibronectin cables had pores that ranged from 10 to 100 μm, and both Schwann cells and fibroblasts were able to orient along the direction of the fibronectin fibers [255]. In a separate study, silicone conduits

with aligned PLLA filaments and matrigel resulted in longitudinal organization of Schwann cells and axons in a rat sciatic nerve injury model [256]. Further, collagen fibrils were tethered into a silicone guidance conduit and allowed to contract and subsequently align. The oriented collagen fibers demonstrated the ability to guide DRG axon extension in vitro, and regenerate rat sciatic nerve in vivo [257]. Collectively, these techniques show promise for combinatorial approaches with physical and chemical guidance signals. The conduits have shown significant success in peripheral nervous system injury models, but remain to be designed properly for the CNS.

#### *4.4.2.3 Chemotactic gradient bridges*

Investigation is underway to develop guidance bridges containing gradients of chemotactic factors to guide regenerating axons. Recombinant adenoviruses that express NGF were injected into the rat corpus callosum pathway, the structure in the mammalian brain connecting the left and right hemispheres, in multiple sites with varying concentration. Additionally, a 1 mm lesion was made through the corpus callosum at the midline. Three to four days after injection, postnatal dorsal root ganglia were isolated and transplanted into the corpus callosum pathway, 2.8 mm away from the midline. Two weeks following transplantation, robust axon outgrowth was observed crossing the lesion site and along the NGF gradient [258]. This study demonstrates the promise for neurotrophic factor gradients during in vivo regeneration. However, the disadvantages associated with direct injection, such as the inability to achieve controlled gradients in other CNS regions, and the potential requirement for multiple injections, emphasizes the need for guidance bridges capable of localized delivery of a chemotactic gradient. Lipid based microcylinders loaded with NGF were encapsulated within agarose/laminin guidance conduits. NGF released from the microcylinders produced gradients that were capable of guiding

DRG neurites in vitro [259]. Further, linear concentration gradients of immobilized NGF and NT-3 were fabricated in poly(2-hydroxyethylmethacrylate)/poly-(L)-lysine scaffolds by encapsulating the protein, as a gradient, within the precursor solution prior to crosslinking. Immobilized NGF and NT-3 gradients guided DRG neurite outgrowth in vitro [260]. The above systems demonstrate the promise for chemotactic gradients presented by nerve guidance conduits, but a substantial amount of exploration remains to determine the gradients necessary for in vivo regeneration, and the time-scale necessary for gradient presentation. Since proteins are quickly cleared and degraded in vivo, alternative strategies to present chemotactic gradients for extended periods of time may be necessary.

## *4.5 Conclusions*

The intricate and precise connections of the nervous system result from a complex interplay of spatial and temporal patterns of gene expression. Patterned expression of cell adhesion and extracellular matrix molecules, diffusible chemotactic factors, and cell surface receptors guides axon pathfinding. Binding of guidance molecules to growth cone receptors triggers cascades of intracellular signaling pathways that alter cytoskeletal dynamics, resulting in guided axon elongation and migration. This pathfinding is responsible for precise connections that control motor and sensory function. Guidance mechanisms are difficult to visualize and elucidate in vivo; therefore, in vitro systems have been developed to study growth cone response to guidance cues. However, existing in vitro systems do not adequately represent complex formations of guidance cues by spatially patterned gene expression. Advances in biological molecule patterning (reviewed in Chapter 3) combined with gene delivery strategies (reviewed in Chapter 2) may provide methods to recapitulate patterns of gene expression to study growth cone

response in vitro. Tools to repair damaged nerves will require guidance of axons across a lesion for functional recovery. In vitro guidance systems not only enhance knowledge of axon pathfinding during development, but also facilitate the rational design of regeneration strategies.

# Chapter 5

# Spatially Patterned Gene Delivery for Localized Neuron Survival and Neurite Extension

## *5.1 Introduction*

Natural tissues can have complex architectures characterized by the organization of multiple cell types into structures, such as branching networks of the vascular or nervous systems. This cellular organization arises, in part, from spatial patterns in gene expression, which can create concentration gradients of diffusible factors that direct cellular processes. During morphogenesis, gradients of the sonic hedgehog (Shh) [261-263], TGF-β [264-266], and Wingless [267-269] families of proteins direct cellular differentiation. Gradients of platelet-derived growth factor and basic fibroblast growth factor are chemotactic agents for dermal fibroblasts [270, 271] and smooth muscle cells [272], respectively. Additionally, neurons have receptors for diffusible guidance factors such as netrins, semaphorins, and neurotrophic factors that induce and direct axonal elongation [5, 167, 273]. Engineering patterns of gene expression may provide a means to direct cellular processes (e.g., cell migration, neurite extension) for the regeneration of tissues with complex architectures.

Gene delivery from biomaterial scaffolds for tissue engineering offers the potential to support and direct progenitor cell differentiation and migration into functional tissue replacements (described in Chapter 2). Biomaterials serve a central role in the engineering of tissue replacements, and are designed to present a combination of insoluble and soluble signals that promote tissue formation [23, 274, 275]. Gene delivery from a tissue engineering scaffold

represents a versatile approach to induce expression of tissue inductive factors, with expression lasting for days to months [11, 12]. Gene therapy vectors, either virus-derived or non-viral (i.e., synthetic), can be immobilized to tissue culture substrates through either specific (e.g., biotin-avidin) or nonspecific (e.g., electrostatic, van der waals) interactions [91, 276, 277]. This technique, termed substrate-mediated gene delivery or reverse transfection, places complexes directly in the cellular microenvironment for efficient internalization, and high transfection efficiencies can be achieved with less DNA as compared to traditional bolus delivery [278, 279]. Additionally, the immobilization of gene therapy vectors provides the means to spatially restrict complex deposition and potentially pattern gene expression. Patterned gene expression may offer significant advantages over protein patterning, which has been widely used to pattern cellular responses [223, 224, 280-283].

Chapter 5 develops a system to spatially pattern non-viral DNA complexes on a cell adhesive substrate to promote cellular processes within the pattern. Polydimethylsiloxane (PDMS) microchannels were employed to pattern the nonspecific immobilization of cationic lipid/DNA complexes, termed lipoplexes, onto tissue culture polystyrene (TCPS). Treatments were investigated to minimize the interactions between the lipoplexes and PDMS, particularly given the relatively high microchannel volume to TCPS surface area ratio. PDMS microchannels (100 to 1000 μm widths) were treated by either $O_2$ plasma exposure or soaking in a Pluronic L35 solution (hereafter referred to as Pluronic) to render the microchannels hydrophilic, and reduce adsorption of the lipoplexes to PDMS. The microchannel treatments were investigated to achieve efficient and patterned complex binding to the surface, while maintaining complex activity for efficient and patterned transfection. Parameters such as microchannel dimensions and treatment,

and vector concentration were varied to achieve high transfection efficiency. The patterned expression system was investigated for the ability to localize cellular processes using a neuronal co-culture model. Neuron survival and neurite outgrowth were assessed within patterns, and at specific distances outside patterns, of neurotrophic factor expression. This system provides a platform with which to investigate patterns of gene expression in tissue formation, and may be applied for the engineering of functional tissue replacements.

## *5.2 Experimental Procedures*

### *5.2.1 Plasmids*

Plasmid DNA was purified from bacteria culture using Qiagen (Santa Clara, CA) reagents and stored in Tris-EDTA buffer at -20ºC. The plasmid pEGFPLuc has EGFP in the vector backbone with a CMV promoter (Clontech, Mountain View, CA). The plasmid pNGF has full-length mouse NGF in the RK5 vector backbone with a CMV promoter, and was a gift from Dr. Hiroshi Nomoto (Gifu Pharmaceutical University, Japan).

### *5.2.2 Fabrication of Microfluidic Networks*

SU8-100 negative tone photoresist (Microchem; Newton, MA) was spin coated at 1000 rpm for 30 seconds on silicon wafers (Ultrasil; Hayward, CA). After baking, specified regions of the photoresist were polymerized using film transparencies as the photomask (In Tandem Design; Towson, MD) and a Quintel Q-2000 mask aligner (Quintel; San Jose, CA), with UV exposure for 45 seconds. Polydimethylsiloxane (PDMS), also referred to as Dow Corning Sylgard 184 Elastomer, was obtained from Krayden, Inc. (Glenview, IL). PDMS was cured on the photoresist molds at a 10:1 (base:curing agent) ratio at 60ºC for 5 hours. After cooling, the PDMS was

peeled off the molds and ports were punched at either end of the channels. PDMS was treated with either $O_2$ plasma (Harrick Plasma; Ithaca, New York) for 3 minutes or soaked in a 2 mg/ml Pluronic L35 (block copolymer of poly(ethylene oxide)-poly(propylene oxide)-poly(ethylene oxide), gift from BASF Corp.; Mount Olive, NJ) solution in 10 mM $KH_2PO_4$ buffer, rinsed and dried in a sterile hood.

### *5.2.3 Complex Deposition*

DNA in DMEM (Life Technologies; Gaithersburg, MD) was complexed with Lipofectamine™2000 (Life Technologies) in DMEM (DNA:lipid, 1:1) by adding lipid to DNA and pipetting gently. PDMS microchannels were reversibly sealed to tissue culture polystyrene (TCPS) wells and complexes were injected in the microchannels at the inlet port and flowed into the channel via capillary action. After 1 hour incubation, the complexes were removed, the PDMS peeled off, and the surfaces rinsed twice with DMEM. For imaging deposition, plasmid DNA (pEGFPLuc) was fluorescently labeled with tetramethyl rhodamine (Mirus; Madison, WI). The deposited DNA was imaged with fluorescence microscopy, and the average complex diameter was determined using the program ImageJ.

### *5.2.4 Binding Efficiency Quantification*

A nick translation kit (Amersham Pharmacia Biotech; Piscataway, NY) was used to radiolabel pEGFP with $\alpha$-$^{32}$P dATP according to the manufacturer's protocol, with slight modifications [83]. Radiolabeled plasmid was complexed with Lipofectamine 2000 and a known volume of complexes was injected into PDMS microchannels sealed to TCPS. Complexes were removed after 1 hour incubation. The PDMS was peeled away from the surface and the surface was rinsed two times with DMEM. The TCPS, PDMS, and rinses were placed in separate

scintillation vials with 10 mL Biosafe II scintillation cocktail (Research Products; Mt. Prospect, IL). Counts were determined using a scintillation counter and correlated to DNA mass using a standard curve. To normalize for the PDMS surface area, PDMS:TCPS surface area ratios were calculated for each channel width and found to be 1.5, 2, 3, and 6 for 1000, 500, 250, and 100 μm width channels, respectively. The binding efficiencies for each channel width were multiplied by the necessary PDMS surface area correction factor. The corrected binding efficiencies were averaged and statistically analyzed.

### *5.2.5 Patterned Transfection Efficiency*

pEGFPLuc was complexed with Lipofectamine 2000 and incubated in the PDMS microchannels on TCPS for 1 hour. Following two DMEM rinses, HEK293T cells (ATCC; Manassas, VA) in DMEM supplemented with 10% heat inactivated fetal bovine serum (FBS), 1% penicillin-streptomycin, and 1% sodium pyruvate were seeded on the TCPS (2.8 X $10^5$ cells/dish) and cultured for 48 hours at 37ºC and 5% $CO_2$. Cells were fixed with 4% paraformaldehyde (PFA) in phosphate buffer saline (PBS) and stained with 5 μg/ml Hoechst 33258 (Molecular Probes; Eugene, OR). Cells producing the EGFP protein (green) and cell nuclei (blue) were observed using fluorescence microscopy. The number of transfected cells was determined by counting green positive cells in 5 random images per pattern, and the total number of cells in each image was established by counting cell nuclei. Transfection efficiency was defined as the number of transfected cells divided by the total number of cells.

### *5.2.6 In Vitro Neurite Outgrowth*

Plasmid pNGF and pEGFPLuc were co-complexed with Lipofectamine 2000 at varying ratios (20:80, 50:50, and 80:20) and incubated in PDMS microchannels on TCPS as described

above. The EGFP expression allowed for visualization of the patterned transfection. Following two DMEM rinses, HEK293T cells were seeded on the TCPS (8.5 X $10^4$ cells/well). To obtain primary neurons, dorsal root ganglia (DRG) were isolated from E8 white leghorn chicken eggs (Michigan State University Poultry Center; East Lansing, MI) and maintained in HBSS buffer supplemented with 6 g/L glucose until the isolation was complete. DRG were incubated for 30 minutes at 37ºC in 0.25% trypsin (Worthington Biochemical; Lakewood, NJ), followed by trituration with fire-polished glass Pasteur pipettes to dissociate the ganglia. Non-neuronal and neuronal cells were separated by panning for 2 hours at 37ºC. After 8 hour culture of the HEK293T cells, the media was removed and the surfaces were washed with PBS to remove NGF. The dissociated DRG neurons were seeded (5 X $10^4$ cells/well) on the cell layer. Cells were co-cultured for 24 hours in cDMEM at 37ºC and 5% $CO_2$. To minimize convective transport, culture dishes were not disturbed during the culture period. After the 24 hour culture, cells were fixed with 4% PFA. The neurons were stained for the neuron-specific class III β-tubulin by incubating fixed cells in TUJ1 antibody (Covance; Berkely, CA) diluted in 5% normal goat serum (Vector Labs; Burlingame, CA) in PBS for 1 hour followed by incubation in TRITC-conjugated goat anti-mouse secondary antibody (Jackson Immunoresearch; West Grove, PA) in PBS for ½ hour. Cells were counterstained with Hoechst 33258 to visualize cell nuclei.

### *5.2.7 Neuron Survival and Neurite Extension*

Surviving neurons were identified as having sprouting neurites. Neurite lengths were quantified using the tracing program NeuronJ, a plugin to ImageJ [284]. Neuron survival, primary neurite length, and total neurite length were normalized to surface areas at the pattern of transfection and distances away from the pattern. Primary neurites were defined as neurites

extending directly from the cell body. Neurite density was defined as total neurite length divided by the surface area. Quantifications were made from 4 regions at the pattern and averaged.

### *5.2.8 Mathematical Modeling of Concentration Gradients*

Mathematical modeling of NGF diffusion was employed to predict the concentration profile in the culture well. Equation 5-1 describes one-component diffusion in two dimensions in a continuous medium with a term for protein degradation, where D is the diffusivity of the protein:

$$\frac{\partial C}{\partial t} = D\left[\frac{\partial^2 C}{\partial x^2} + \frac{\partial^2 C}{\partial z^2}\right] - kC \tag{5-1}$$

where C is the concentration, D is the diffusivity, and k is the rate constant for protein degradation. The Crank-Nicolson implicit method was employed to solve numerically the second order partial differential equation. The initial condition is a zero concentration throughout the culture (Eqn. 5-2). The boundary conditions indicate a flux (q), which is determined from the protein production rate, within the pattern of transfected cells (Eqn. 5-3), and no flux boundary conditions elsewhere.

$$C(x, z, t = 0) = 0 \tag{5-2}$$

$$-D\frac{\partial C}{\partial z}(x < x_{patt}, z = 0, t) = q \tag{5-3}$$

$$\frac{\partial C}{\partial z}(x > x_{patt}, z = 0, t) = 0 \tag{5-4}$$

$$\frac{\partial C}{\partial z}(x, z = z_{\max}, t) = 0 \tag{5-5}$$

$$\frac{\partial C}{\partial x}(x = 0\ , z, t) = 0 \tag{5-6}$$

$$\frac{\partial C}{\partial x}(x = x_{max}, z, t) = 0 \quad (5\text{-}7)$$

Note that the region of patterned transfection occurs within x = 0 to $x_{patt}$. The boundary in the x-direction ($x_{max}$) was defined as 7.8 mm, the approximate radius of a 24-well tissue culture well. The boundary in the z-direction ($z_{max}$) was set equal to $x_{max}$. Values for the diffusivity of NGF and the production rate of NGF by cells transfected with the pRK5-NGF plasmid were determined from published reports to be 12 X $10^{-7}$ $cm^2/s$ and 1 $ng/cm^3/min$, respectively [285, 286].

### *5.2.9 Statistics*

Statistical analysis was performed using JMP software (SAS Institute, Inc.; Cary, NC). Comparative analyses were executed using one-way ANOVA with Tukey post-tests, at a 95% confidence level. Mean values with standard error of the mean (SEM) are reported. All experiments were performed in triplicate.

## *5.3 Results and Discussion*

### *5.3.1 Patterned Lipoplex Deposition and Binding*

Lipoplexes were deposited on TCPS surfaces using microfluidic devices fabricated by soft lithography. This technique is commonly used to fabricate PDMS microchannels for the patterned deposition of protein or cellular adhesion, but has never been utilized to pattern DNA complexes [121, 122]. PDMS is hydrophobic and strongly adsorbs a range of macromolecules, thus, treatments are commonly employed to render PDMS hydrophilic and reduce adsorption [287]. In these studies, $O_2$ plasma and Pluronic treatments were investigated for their effects on patterned deposition and complex binding. Incubation of lipoplexes within Pluronic treated

PDMS microchannels produced patterns of deposition in widths of 1000 µm (Figure 5-1a), 500 µm (Figure 5-1b), 250 µm (Figure 5-1c), and 100 µm (Figure 5-1d). The width of the pattern matched the width of the microchannel. Pluronic treatment of the channels produced a more dense and homogeneous layer of deposited lipoplexes in a 1000 µm width pattern (Figure 5-1a) as compared to lipoplexes incubated in untreated channels (Figure 5-1e).

The binding efficiency, defined as the amount of DNA bound divided by the amount incubated in the microchannel, was dependent on the channel width and treatment. Higher binding efficiencies were observed with $O_2$ plasma and Pluronic treated microchannels relative to untreated microchannels (Figure 5-2a, $p < 0.05$). $O_2$ plasma and Pluronic treatments increased the binding efficiency to 23%, as compared to 15% with no treatment, presumably by decreasing interactions between PDMS and lipoplexes. $O_2$ plasma exposure introduces silanol groups on the PDMS surface at the expense of methyl groups, but the hydrophilic surface is unstable in

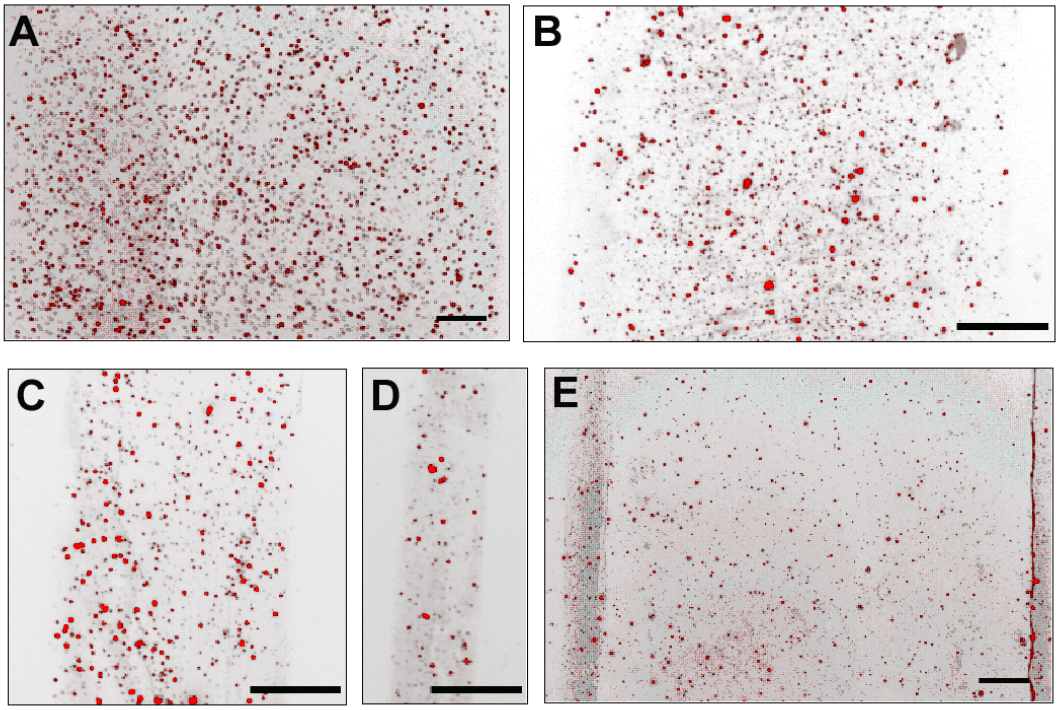


**Figure 5-1: Patterned lipoplex deposition.** Immobilized lipoplexes (red) deposited in Pluronic-treated PDMS microchannels: (A) 1000 μm, (B) 500 μm, (C) 250 μm, and (D) 100 μm. (E) Lipoplexes deposited using untreated microchannels (1000 μm). Scale bars correspond to 100 μm.

ambient air [287, 288]. Pluronic, a block copolymer of poly(ethylene oxide)-poly(propylene oxide)-poly(ethylene oxide) (PEO-PPO-PEO), can anchor to a hydrophobic solid surface, such as PDMS, through interactions with the hydrophobic PPO block [124]. Additionally, the binding efficiency decreased as the channel width decreased (Figure 5-2b, $p < 0.05$). Decreasing the width of the Pluronic treated PDMS microchannel decreased the binding efficiency, from 23% for a 1000 μm channel to 3% for a 100 μm channel. The microchannel volume to TCPS surface area ratio increases with decreasing microchannel width, and normalization of the binding efficiency to the relative PDMS surface area led to similar binding efficiencies for all channel widths (data not shown). Therefore, we conclude that an increase in PDMS surface area contributed to the decrease in binding efficiency, as the Pluronic treatment did not completely eliminate interactions between lipoplexes and PDMS.

### *5.3.2 Spatial Patterns of Gene Expression*

Pluronic treated PDMS microchannels afforded the ability to deposit active lipoplexes, and produced 1000 to 100 μm wide patterns of transgene expression. Nonspecific immobilization of the lipoplexes resulted in localized gene expression (Figures 5-3a-h), with the dimensions of the patterned regions matching the microchannel dimensions. Nonspecific immobilization between lipoplexes and TCPS results in ~ 10% complex release in cell culture media after 24 hours [278]. The correlation between immobilization (Figure 5-1) and transfection (Figure 5-3) observed here may result from either a) lipoplexes internalized directly from the surface, or b) lipoplexes released from the surface that primarily associate with cells in the pattern, with escaping lipoplexes becoming diluted and thus ineffective.

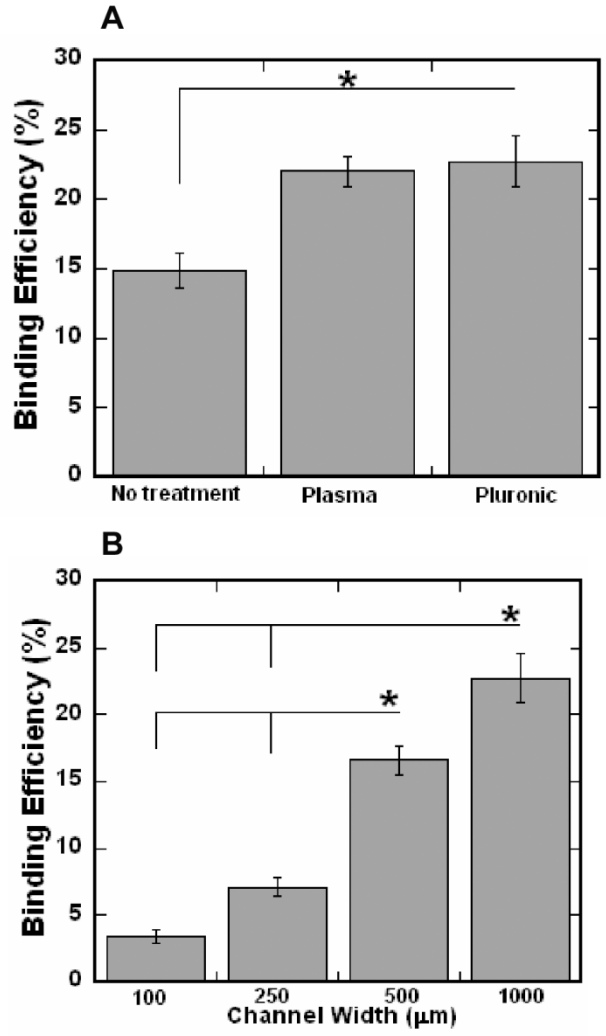


**Figure 5-2: Patterned lipoplex binding efficiency.** Quantification of lipoplex binding efficiency (total bound / total incubated in the channel) using PDMS microchannels, while varying (A) channel treatments (No treatment, $O_2$ plasma, Pluronic) and (B) channel widths (100, 250, 500, 1000 μm). Values are reported as mean ± SEM, (*$p < 0.05$).

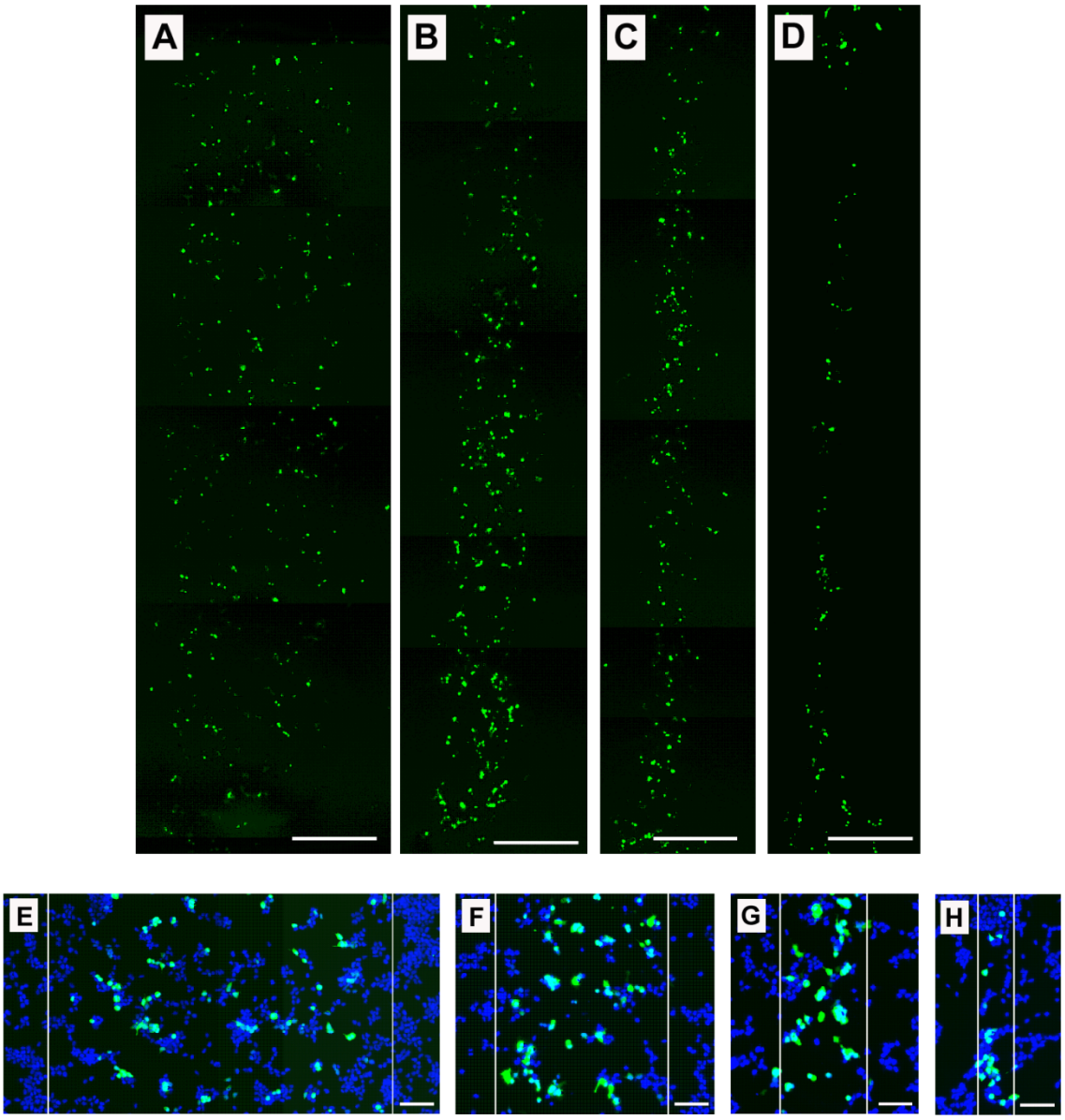


**Figure 5-3: HEK293T cells expressing the reporter gene, EGFP, in a pattern.** EGFP expression (green) within cells cultured on substrates with patterned DNA complex deposition using Pluronic-treated microchannels: (A) 1000 μm, (B) 500 μm, (C) 250 μm, and (D) 100 μm. Higher magnification images present cell nuclei (blue) and transfected cells (green) overlaid: (E) 1000 μm, (F) 500 μm, (G) 250 μm, and (H) 100 μm. White lines indicate pattern boundaries. Scale bars correspond to 500 μm (A-D) and 100 μm (E-H).

The treatment of the microchannel prior to complex deposition was critical to transfecting HEK293T cells cultured on the substrate. Transfection was observed with lipoplexes deposited using Pluronic treated microchannels, but no transfection was observed with untreated or $O_2$ plasma treated microchannels (data not shown). Pluronic mixed with cationic polymers or lipids can increase transfection efficiency compared to polymer or lipid alone [289-291]. Here, loosely bound Pluronic may interact with the lipoplexes to prevent complex aggregation or enhance complex association with the cells. Pluronic may also influence the nonspecific interactions between the lipoplex and substrate. By adsorbing to TCPS, Pluronic may modulate the surface chemistry, and thus influence the binding affinity between the complexes and the surface, which in turn affects transfection efficiency [85].

The vector concentration influenced transfection efficiency in all sized patterns. Relatively high transfection efficiencies (greater than 25%) were achieved using Pluronic treated microchannels for all widths (Figure 5-4). However, high levels of transfection could only be achieved in the smaller channel widths by increasing the concentration of DNA. The decreasing binding efficiency within the narrower channel presumably leads to insufficient quantities on the surface. The vector concentrations in solution that produce the relatively high transfection efficiencies correspond to surface densities of approximately 0.01 to 0.03 μg DNA/cm$^2$ (Figure 5-2). Interestingly, these densities of immobilized lipoplexes were approximately 10-fold lower than that required to achieve comparable transfection efficiencies in tissue culture plates (i.e., without microchannels) (0.2 μg DNA/cm$^2$) [278], further suggesting that Pluronic treatment may increase the delivery efficiency. The range of vector concentrations at which the relatively high

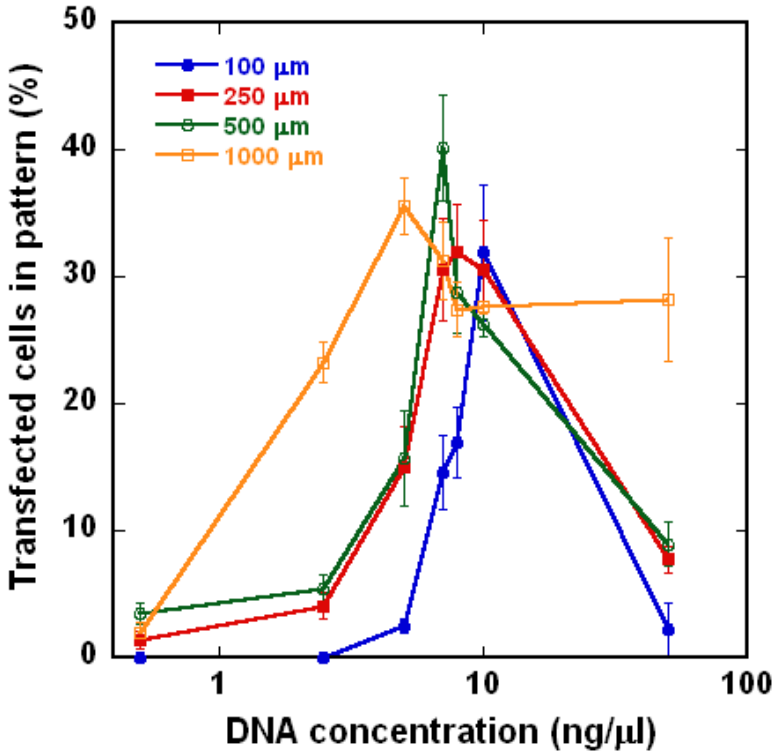


**Figure 5-4: Transfection efficiency was dependent on microchannel width and vector concentration.** Transfection efficiency (% of transfected cells) in the pattern as a function of vector concentration and channel width. Lipoplex deposition was performed within Pluronic-treated microchannels. Values are reported as mean ± SEM.

transfection efficiency is achieved becomes narrower as the pattern width decreases (Figure 5-4). At high DNA concentrations, complex aggregation in small volumes may also hinder transfection. For lipoplexes incubated in the 100 μm channel, increasing the vector concentration (from 10 to 50 ng/μl) increased the average lipoplex diameter on the surface (data not shown).

The use of microfluidic devices is a novel approach to patterning gene expression. Methods to localize DNA delivery have been developed previously, with specifically tethered viral vectors on polyurethane films [91], or mechanical spotting of non-viral vectors [279]. The microfluidics approach can produce complex patterns on a uniform substrate using PDMS microchannels in a range of sizes or shapes. Most importantly, the system can achieve these complex patterns with dimensions on the order of 100 μm, which is a size consistent with many cellular structures within tissues.

### *5.3.3 Localization of Neuron Survival and Neurite Extension*

The method to spatially pattern gene expression was subsequently investigated for directing cellular processes using an in vitro neuronal co-culture model. Patterned transfection of the diffusible neurotrophic factor, nerve growth factor (NGF) could lead to localized and sustained secretion. Previous efforts to localize neurite outgrowth have focused on the patterning of adhesion molecules (e.g., ECM molecules) to guide cellular adhesion and neurite extension [292-295]. One challenge to patterning proteins for guiding cellular processes is nonspecific adsorption of serum or cell-secreted proteins that can mask or displace the immobilized proteins. Gene delivery, in contrast, can sustain transgene expression for timescales ranging from days to months [12], with the persistence of the factors maintaining a stimulus locally to promote the cellular process. We hypothesize that the patterned expression of neurotrophic factors provides

the stimulus to promote neuron survival and neurite outgrowth, and also the directional cue to orient neurite extension.

Primary neurons and HEK293T cells were cultured on patterns (250, 100 μm) with immobilized lipoplexes, which contained a 50:50 mix of pNGF (to promote neurite outgrowth) and pEGFP (to visualize transfected cells). Vector concentrations were selected based on the lowest concentration to yield at least 30% transfection efficiency (250 μm: 8 ng/μl, 100 μm: 10 ng/μl). Patterns of NGF expression were sufficient to localize neuron survival and neurite outgrowth. Neurite extension and neuron survival were apparent directly within the area of patterned transfection for 250 μm (Figures 5-5a, b) and 100 μm (Figures 5-5c, d) width patterns. The absence of pNGF, or cells transfected with an empty vector, did not support either neuron survival or neurite extension (data not shown). Since HEK293T cells did not basally support neuron survival, the behavior of DRG neurons in the co-culture system was directly attributed to the patterns of NGF expression.

Neuron survival and neurite density were assessed at the location of patterned NGF expression, and in 100 μm width increments away from the pattern. Neuron survival (normalized to surface area) was comparable on patterns of 250 and 100 μm width NGF expression (Figure 5-6). Neuron survival decreased significantly in regions adjacent to the 250 and 100 μm patterns (Figure 5-6a, $p < 0.001$). Additionally, the decrease in neuron survival in regions adjacent to the 250 and 100 μm patterns was similar (Figure 5-6a). Neurite density was also similar within the patterned NGF expression for widths of 250 and 100 μm, and decreased significantly in regions

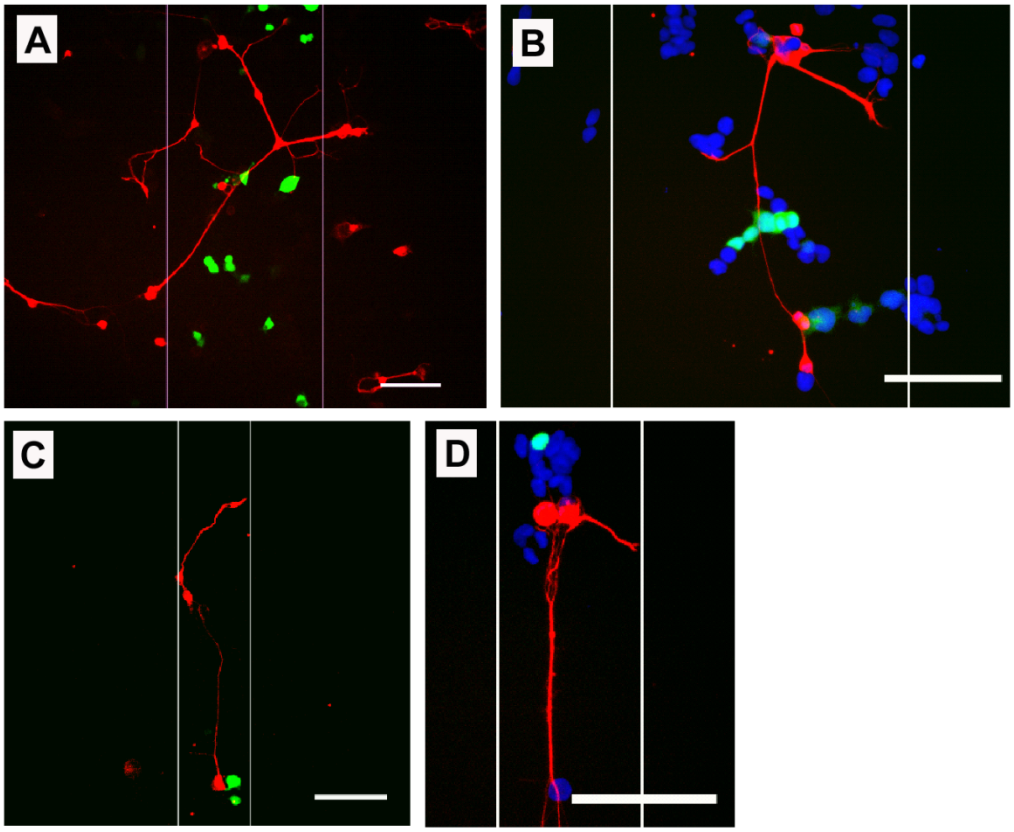


**Figure 5-5: Neurons co-cultured with cells expressing NGF in patterns.** Neurite extension (red) was observed at the region of transfected cells (green): (A, B) 250 μm width, and (C, D) 100 μm width. pNGF:pEGFP ratio of 50:50. White lines indicate pattern boundaries. Cell nuclei (blue) are visible in (B, D). Scale bars correspond to 100 μm.

adjacent to the patterns (Figure 5-6b, $p < 0.001$). The neuronal responses observed here could be due to NGF concentration differences in the cell microenvironment caused by localized production of NGF. Importantly, decreasing the pattern width (from 250 to 100 μm) focused neurite outgrowth within the pattern to a greater extent. With 100 μm patterns of NGF expression, neurite density decreased 97% in regions directly adjacent to the pattern, significantly greater than the 70% decrease observed with 250 μm patterns (Figure 5-6b, $p < 0.01$). Interestingly, the primary neurite density within the pattern (250, 100 μm) was significantly higher than for neuronal co-cultures in the absence of a pattern, or for NGF added to the media (25 ng/ml, the optimum concentration for neuron survival and neurite extension) (Figure 5-7, $p < 0.05$), suggesting that the patterned NGF expression provided a directional cue, which increased the rate of axonal elongation and reduced aberrant sprouting. Higher ratios of pNGF:pEGFP (80:20) increased neuron survival outside the pattern, resulting in neurite extension directed toward the pattern, while lower ratios of pNGF:pEGFP (20:80) decreased neuron survival and neurite density (data not shown).

A partial differential equation model was subsequently adapted to predict concentration profiles that develop from the patterned to the unpatterned region [296]. The patterned expression of diffusible factors creates concentration gradients, with the highest concentrations present within the region of transfected cells, which decrease with increasing distances from the pattern (Figure 5-8a). The experimental results indicate that neuron survival is greatest within the pattern, which corresponds to the highest NGF concentrations, and neurite extension occurs primarily along the patterned region (Figure 5-6). Neurite extension has been reported to occur

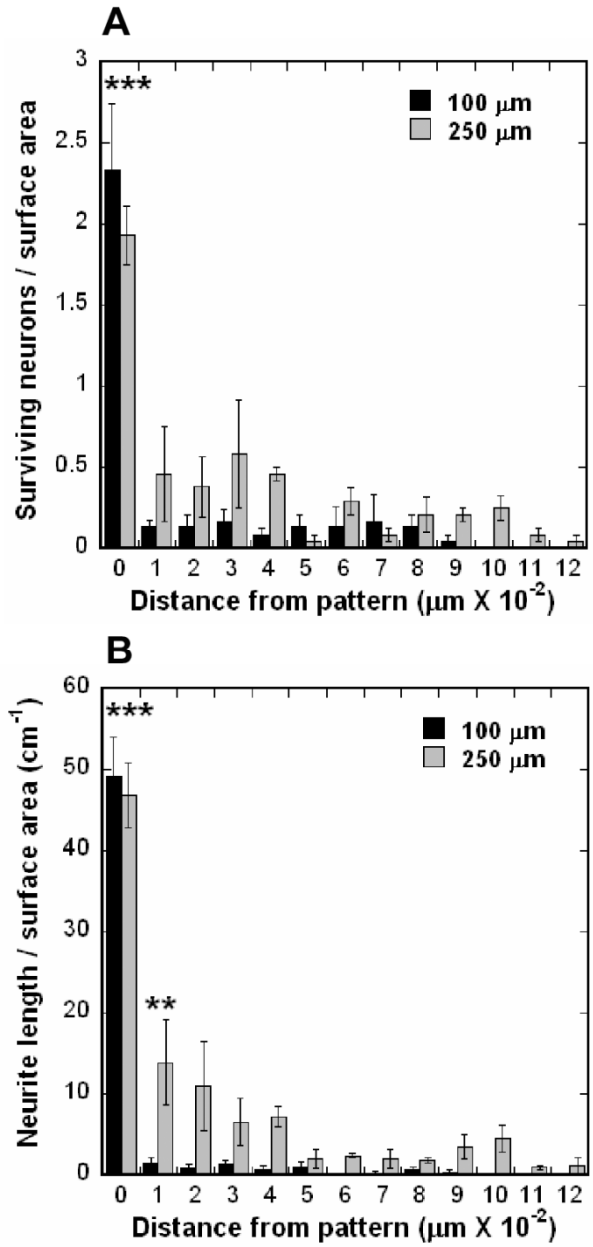


**Figure 5-6: Neuron survival and neurite outgrowth primarily observed within patterns of NGF expression.** (A) Neuron survival, normalized to surface area, and (B) total neurite density quantified within and outside the region of patterned expression. Values are reported as mean ± SEM, (* $p < 0.05$, ** $p < 0.01$, ***$p < 0.001$).

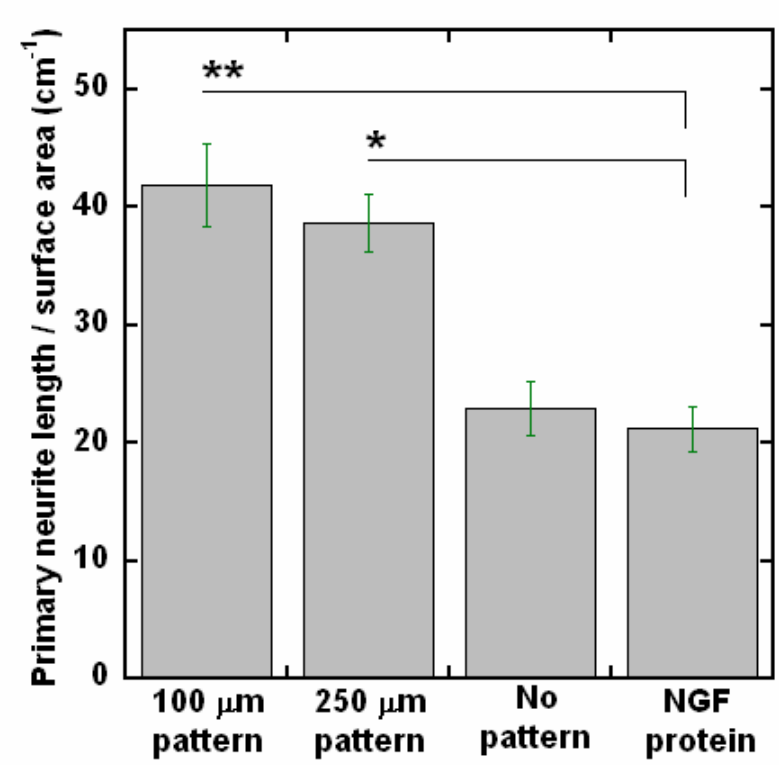


**Figure 5-7: Primary neurite density on patterned NGF expression and non-patterned controls.** The primary neurite density was greater on patterns of NGF expression as compared to co-cultures with NGF expression and no pattern, or co-cultures with NGF added to the media. Values are reported as mean ± SEM, (* $p < 0.05$).

along stable NGF concentrations, and not down concentration gradients [5]. Consistent with these reports, neurites extend along the path of transfected cells that corresponds with the highest predicted NGF concentration. For HEK293T cells seeded on 50:50 pNGF:pEGFP immobilized complexes, an average NGF concentration of 0.4 ng/mL was predicted within the 250 μm pattern, and 0.2 ng/mL was predicted for the 100 μm pattern (Figure 5-8a). The lower concentration results from there being fewer transfected cells within the 100 μm pattern relative to the 250 μm pattern. Experimentally, decreasing the pattern width (from 250 to 100 μm) increased the extent to which neurites were restricted to the pattern (Figure 5-6b), which may result from lower neurotrophin concentrations in the region adjacent to the 100 μm pattern relative to the 250 μm pattern. The average concentration predicted within the 100 μm channel (0.2 ng/mL) was maintained for a distance of ≈700 μm for the 250 μm channel. Thus, the model predicts larger channels create higher concentrations over greater distances than narrower channels.

Mathematical modeling also predicts that increasing the protein production rate by the cells, which could be achieved by increasing the ratio of NGF to GFP plasmid, increases the concentration within the pattern and in adjacent regions (Figure 5-8b, c). This mathematical prediction is consistent with the experimental results with an increasing ratio of NGF:GFP, in which an increased neuron survival was observed outside of the pattern (data not shown). Interestingly, those neurons surviving outside the pattern extended neurites toward the pattern, or up the predicted concentration gradient created by the patterned transfection. Taken together, the NGF concentration gradient can be modulated by the pattern dimensions and the pNGF density,

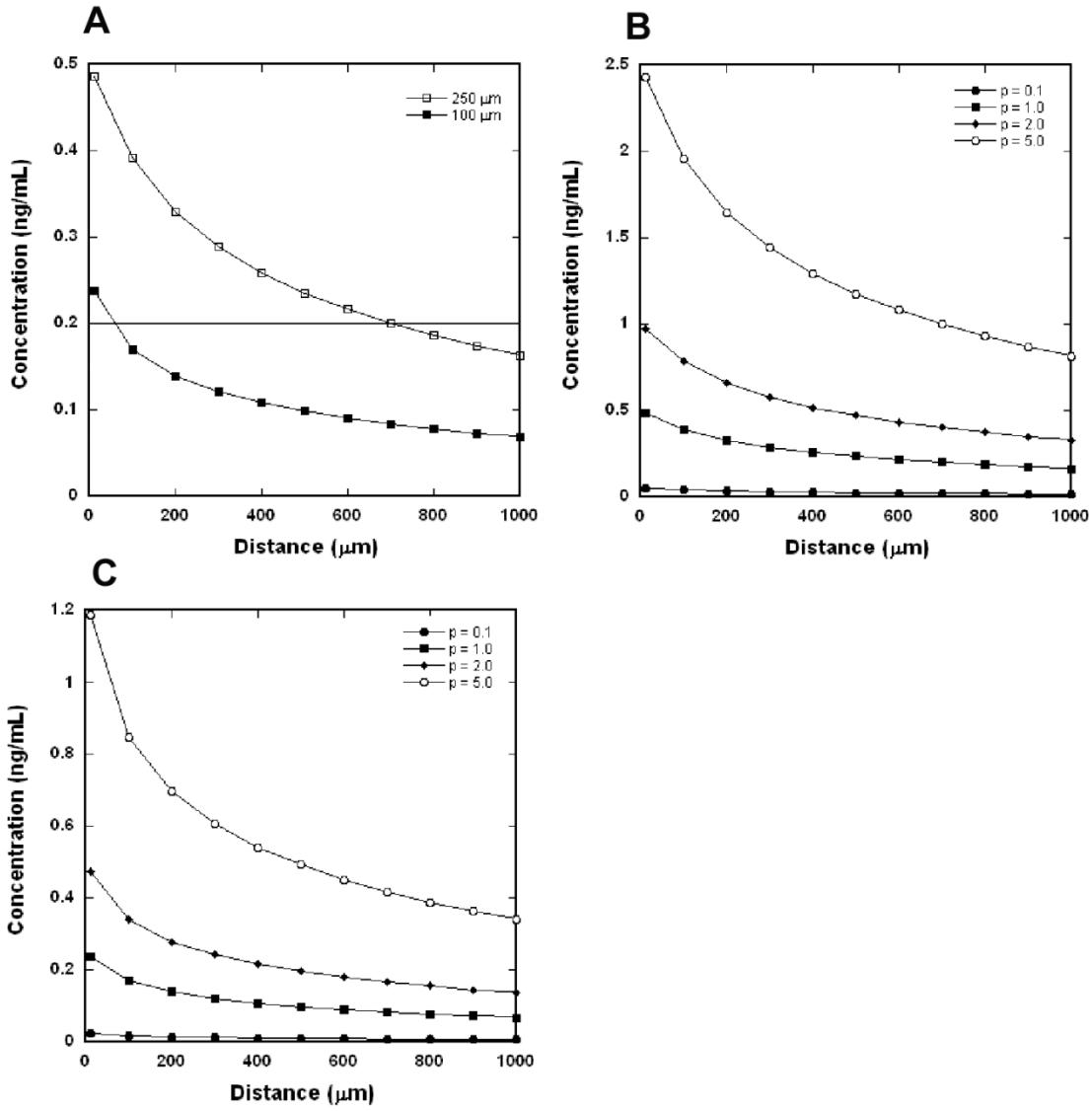


**Figure 5-8: Predicted NGF concentration gradients.** (A) Mathematical model predictions of the NGF concentration profile for channels with widths of 250 and 100 μm. Note that the kinetic constant describing the rate of protein production (p) was estimated to be 1 ng/cm$^3$/min. The production rate was varied and the concentrations modeled for (B) 250 and (C) 100 μm wide patterns. Gradients were modeled for 24 hours, and the reported concentrations are those at the material surface (z=0).

and manipulating the concentration profile can be employed to either localize neurite growth within the pattern or to direct neurite growth towards the pattern.

Convective transport was not incorporated into the model, but could be included to control the concentration gradients. If transport by convection dominated diffusion in our experiments, the secreted NGF would have been distributed throughout the culture media at an expected concentration of approximately 0.005 ng/mL, which does not support significant neuron survival or neurite extension. Diffusion was likely significant, which enabled NGF to accumulate at the cell surface near the region of patterned transfection at concentrations (0.2 – 1.0 ng/mL) that promote neuron survival and neurite outgrowth. For these reasons, the localized neuron survival and neurite extension were attributed to a gradient of NGF that resulted from NGF diffusion from the pattern of expression. In considering the in vivo translation of these results, morphogen gradients predicted in vivo have been suggested to occur mainly by diffusive mechanisms [296]. However, convective transport in conjunction with diffusion can play a role in shaping the morphogen gradients [297].

## *5.4 Conclusions*

In summary, spatial patterns of immobilized lipoplexes can produce patterns of gene expression capable of directing cellular processes. Biomaterial based delivery of protein and DNA has been able to localize drug delivery generally to the implant site and can support the physiological processes that lead to tissue formation. However, the engineering of tissues with complex architectures will require concentrations of inductive factors to be manipulated on smaller length scales (10-100 μm) in order to direct cellular assembly and tissue formation. In this report, we demonstrate that patterned immobilization of gene therapy vectors can regulate

cellular processes on length scales of 100 μm. Patterned gene expression can potentially produce gradients of diffusible proteins for time scales necessary to regenerate functional tissue. We have demonstrated localized neuron survival and neurite outgrowth, but a patterned gene delivery approach can be applied to many cellular responses involved in tissue regeneration, such as directed cellular migration or the patterning of stem cell differentiation that is observed in the niche. The system can be employed in fundamental studies of cellular processes and tissue formation, or applied to the generation of functional tissue replacements.

# Chapter 6

# Spatially Patterned Gene Expression for Guided Neurite Extension

## *6.1 Introduction*

Cellular migration to a desired target is essential for proper cell function during morphogenesis, maintenance, and wound repair [298]. Directed migration of leukocytes (immune responses) [2], endothelial cells (angiogenesis) [3], and fibroblasts (wound healing) [4] result from gradients formed by localized gene expression of guidance molecules by cells positioned at a target. Similarly, the proper development and function of the nervous system is dependent on axon guidance to the intended synaptic target (reviewed in Chapter 4). Guidance cues expressed by target cells have been implicated in pathfinding of circumferential, commissural, and longitudinal axons in the spinal cord and brain [169, 170]. The leading edge of an axon, the growth cone, is responsible for guidance cue detection in the extracellular environment and subsequently directs axons along a specific path [273]. Upon binding to growth cone surface receptors, guidance signals are transduced by cytoplasmic signaling pathways, leading to cytoskeletal rearrangement and directed growth [176].

Axonal guidance molecules are permissive or inhibitory, and exist as soluble factors that diffuse throughout the extracellular space (chemotactic) or nondiffusible factors presented by cells in the microenvironment or extracellular matrix (haptotactic). Groups of functionally specialized cells within target tissues, such as the midline [168], express diffusible guidance molecules and concentration gradients arise from this localized gene expression. While the

importance of chemotaxis in the developing nervous system is widely accepted, the first gradient of a diffusible guidance factor, netrin-1, was only recently visualized directly in the embryonic chick, rat, and mouse spinal cords [178]. Nondiffusible factors such as proteoglycans [217], or cell adhesion molecules [213], are differentially expressed by neuronal and non-neuronal cells and establish a path for axons. Importantly, diffusible factors may also associate with the tissue through ligand binding or nonspecific interactions and elicit a haptotactic signal [183].

Since gradients are difficult to visualize in vivo, and neuronal responses are complex, in vitro assays have been developed to investigate neurite guidance. In vitro gradient cultures have led to the discovery of cell-surface receptors on growth cones responsible for gradient recognition [299] and partial understanding of the intracellular events that lead to cytoskeletal rearrangement of the neurite shaft and oriented growth [225]. However, existing in vitro assays have specific drawbacks. Co-cultures consisting of neurons and either target tissue [300] or a cluster of cells expressing recombinant guidance molecules [181] aim to recapitulate natural gradients, however, the systems are variable and the gradients are not well-defined. In contrast, engineered protein gradients within agarose are well-defined [201], but gradients formed by source/sink chambers may not adequately represent gradients formed by localized expression of diffusible molecules. Moreover, most in vitro guidance assays are acellular, incorporating only the neuron of interest, and the ability of diffusible molecules to associate with non-neuronal cells and their extracellular matrix is oftentimes ignored [301].

Chapter 6 employs a novel, well-characterized patterned gene delivery system to create tunable concentration gradients and investigate directed neurite extension. We hypothesized that

gradients formed by spatially controlled delivery of genes encoding guidance molecules within a complex cellular environment would better mimic gradients that are formed naturally. The ability of diffusible chemotactic factors to bind to the cell culture surface and the subsequent effects on neurite guidance were investigated. Experimentally observed neurite guidance was correlated to predicted concentration gradients, which facilitated comparison to gradients previously fabricated by existing guidance assays.

## *6.2 Experimental Procedures*

### *6.2.1 Plasmids and Reagents*

Plasmid was purified from bacterial culture using Qiagen (Santa Clara, CA) reagents and stored in Tris-EDTA buffer at −20 °C. The plasmid pEGFP-Luc has EGFP in the vector backbone with a CMV promoter and was purchased from Clontech (Mountain View, CA). The plasmid pNGF has full length mouse NGF in the RK5 vector backbone with a CMV promoter and was a gift from Dr. Hiroshi Nomoto (Gifu Pharmaceutical University, Japan). All chemicals were purchased from Sigma-Aldrich (St. Louis, MO) and media components from Invitrogen (Carlsbad, CA) unless otherwise specified.

### *6.2.2 HEK293T Cell Culture*

The human embryonic kidney cell line (HEK293T) was purchased from the American Type Culture Collection (ATCC) (Manassas,VA). HEK293T cells were maintained in T-75 flasks with media change every 48 h and passage every 60 h in DMEM supplemented with 10% heat-inactivated fetal bovine serum, 1% penicillin/streptomycin, and 1% sodium pyruvate at 37 °C

and 5% $CO_2$. For all assays, tissue culture polystyrene wells were precoated with poly-L-lysine (MW 30,000 – 70,000) by incubating a 0.01% solution in wells for 1 h.

### *6.2.3 Patterned Reporter Gene Expression*

Microfluidic networks were fabricated using methods described previously [302]. Briefly, traditional photolithography techniques were employed to fabricate topographically patterned molds. Polydimethylsiloxane (PDMS), also referred to as Dow Corning Sylgard 184 Elastomer (a gift from Dow Corning Corporation; Midland, MI) was cured on the patterned molds and following curing, ports were punched at both ends of the channels to fabricate microchannels with dimensions of 1.0, 0.5, or 0.25 mm W X 5 mm L X 0.25 mm H. Microchannels were soaked for 1 h in a 0.2% Pluronic L35 (a gift from BASF Corporation; Mount Olive, NJ) solution, rinsed, and dried in a sterile hood. To form lipoplexes, plasmid (pEGFP-Luc) in Dulbecco's modified Eagle's medium (DMEM) was complexed with Lipofectamine$^{TM}$ 2000 in DMEM (DNA:lipid 1:1 and vector concentration 2-10 ng/μl) by adding lipid to DNA, pipetting gently, and incubating 10 min. To pattern lipoplex deposition, microchannels were reversibly sealed to PLL-coated wells and complexes were injected in the microchannels. Importantly, the humidity in the culture plate was maintained in order to prevent drying of the complexes during the deposition. After 1 h deposition, complexes were removed from the microchannels and the wells were rinsed with phosphate-buffered saline (PBS). HEK293T cells (4 X $10^4$ cells/$cm^2$) were seeded in wells with patterned lipoplexes and cultured for 48 h using conditions described above. Luciferase transgene levels were measured using the Luciferase Assay System (Promega; Madison, WI). After 48 h culture, cells were lysed and assayed using a luminometer (Turner Biosystems) set for a 3-s delay with signal integration for 10 s. A standard curve was formed

using Luciferase standards and linear regression analysis to convert relative light units (RLU) of each sample to moles. Production rate (p) of luciferase was estimated for each condition and reported in units of pmol/cell/min.

### *6.2.4 Patterned NGF Expression*

Patterned NGF expression was achieved with methods described above and cultures were assessed to determine 1) total NGF secreted by transfected cells and 2) the location of secreted NGF (diffusible versus surface-associated). Lipoplexes were formed with a 7:3 mixture of pNGF (neurotrophic factor of interest) and pEGFP-Luc (to visualize the pattern) and a vector concentration of 10 ng/μl. Lipoplexes were injected into Pluronic-treated microchannels (1.0 mm width) and allowed to deposit for 1 h. HEK293T cells were seeded as above and cultured for 24 or 48 h. At the end of the culture period, the culture media and lysates were analyzed for NGF concentration using a ChemiKine NGF Sandwich ELISA kit (Millipore; Billerica, MA). To assess surface-associated NGF, patterned NGF expression cultures were performed as described above. At the end of the culture period, HEK293T cells were fixed with 2% paraformaldehyde (PFA) in PBS for 10 min. HEK293T cells were stained for NGF with anti-NGF-β (Millipore; Billerica, MA) and ABC-HRP immunostain techniques (Vector Labs; Burlingame, CA). After a 30 s development, cells were washed with PBS and imaged with a Leica DM IL light microscope (Leica; Wetzlar, Germany) equipped with a Spot Insight 2 Megapixel Color Mosaic camera and Spot software (Spot Diagnostic Instruments; Sterling Heights, MI). Images were analyzed for immunostain intensity using Adobe Photoshop with a color threshold set based on the negative control and normalized to the entire surface area occupied by cells.

### *6.2.5 Neurite Outgrowth and Guidance*

A neuronal co-culture model was employed to investigate neurite outgrowth in response to spatial patterns of NGF expression. Patterned NGF expression cultures were performed as described above. At the end of the culture period (9, 24, or 48 h), HEK293T cells were either rinsed with PBS (referred to as *9 h*, *24 h*, and *48 h* cultures) or fixed with 2% PFA for 10 min to halt the secretion of diffusible NGF (referred to as *9 h*, *24 h*, and *48 h surface NGF*). Dorsal root ganglia (DRG) explants were isolated from 8-day chicken embryos (MI State University; East Lansing, MI) and seeded on live or fixed HEK293T cultures 0.5 – 2.5 mm from the center of the pattern of NGF expression (2 explants/well). To assess the response by individual neurons, DRG explants were dissociated using methods described previously [302] and neurons were seeded on HEK293T cultures (1 X $10^4$ cells/$cm^2$). Importantly, the co-cultures were maintained in an isolated incubator and free from convective forces that would disrupt the gradients. 24 h after explant or dissociated neuron seeding, cultures were stained for the neuron-specific class III β-tubulin by incubating fixed cells in TUJ1 antibody (Covance; Berkely, CA) diluted in 5% normal goat serum (Vector Labs; Burlingame, CA) in PBS for 1 h followed by incubation in TRITC-conjugated goat anti-mouse secondary antibody (Jackson Immunoresearch; West Grove, PA) in PBS for 30 min. Co-cultures were imaged on a Leica inverted fluorescence microscope with a cooled CCD camera (Photometrics; Tucson, AZ) using MetaVue (Universal Imaging; Downingtown, PA) acquisition software. Total area occupied by neurites was measured for explants using ImageJ software (NIH) and normalized to explant area. For dissociated neurons, neurite length was quantified using the tracing algorithm in the NeuronJ plug-in for ImageJ [284] and normalized to sprouting neurons.

Neurite guidance was investigated by first performing co-cultures as described above: *9 h, 24 h*, and *48 h* cultures and *9 h, 24 h*, and *48 h surface NGF* cultures with explants or dissociated neurons subsequently seeded at the end of the accessory cell culture period. All co-cultures were assayed 24 h after neuron seeding by fixing and staining for the neuron-specific class III β-tubulin and imaging as described above. To assay neurite guidance from explants, the area occupied by neurites extending toward the pattern of expression was quantified using ImageJ software (NIH) and divided by the entire area occupied by all neurites. To assay neurite guidance from individual neurons, the directional angle of the neurite relative to the pattern of expression was quantified by first drawing two lines: one line was drawn from the neuron cell body perpendicular to the pattern of expression edge, and the second line was drawn from the neuron cell soma to the neurite growth cone. An angle between the two lines was quantified and categorized in 30º increments. 0–90º or – (0–90º) define the 2 quadrants in the direction toward the pattern of expression, while neurites oriented 90–180º or – (90–180º) define the 2 quadrants in the opposite direction. Positive and negative quadrants were defined as symmetrical and equivalent, and therefore were reported as only positive angles. In all cases, the distance the explant or neuron was located from the center of the pattern was measured in Adobe Photoshop.

### *6.2.6 Mathematical Modeling of Concentration Gradients*

Mathematical modeling of NGF diffusion was used to predict the concentration profile in the culture well. Equation 6-1 describes one-component diffusion in three dimensions in a continuous medium with a term for protein degradation:

$$\frac{\partial C}{\partial t} = D\left[\frac{\partial^2 C}{\partial x^2} + \frac{\partial^2 C}{\partial y^2} + \frac{\partial^2 C}{\partial z^2}\right] - kC \tag{6-1}$$

where C is the concentration, D is the diffusivity of the protein, and k is the rate constant for protein degradation. The Crank–Nicolson implicit method was employed to solve numerically the partial differential equation. The initial condition is a zero concentration throughout the culture (Equation 6-2). The boundary conditions indicate a flux (q), which is determined from the protein production rate, within the pattern of transfected cells (Equation 6-3), and no flux boundary conditions elsewhere.

$$C(x, y, z, t = 0) = 0 \tag{6-2}$$

$$-D\frac{\partial C}{\partial z}(x < x_{patt}, y < y_{patt}, z = 0, t) = q \tag{6-3}$$

Note that the region of patterned transfection occurs within x = 0 to $x_{patt}$ and y = 0 to $y_{patt}$. The boundaries in the x-direction ($x_{max}$) and y-direction ($y_{max}$) were defined as 12 mm, the approximate radius of a 12-well tissue culture well. The boundary in the z-direction ($z_{max}$) was set equal to 4 mm, the approximate height of the culture medium. The value for the diffusivity of NGF was determined from published reports to be $2.5 \times 10^{-7}$ $cm^2/s$ [285], and the diffusivity that incorporated reversible binding of the ligand to the accessory cell surface was estimated using Equation 6-4:

$$D_e = \frac{D}{(R+1)} \tag{6-4}$$

Where $D_e$ is the effective diffusion constant, and R is a dimensionless coefficient, calculated by the equation S = RC, where S is the amount of ligand bound to the surface, and C is the amount of soluble NGF (Crank, 1975). The production rate of NGF by cells transfected with the pRK5-NGF plasmid was estimated from ELISA data.

Concentration gradient analysis was performed in terms of the absolute concentration gradient (Equation 6-5) and the fractional concentration gradient (Equation 6-6):

$$\left.\frac{dC}{dx}\right|_n = \frac{C_{n+1} - C_n}{x_{n+1} - x_n} \tag{6-5}$$

$$\left.\frac{dC}{C}\right|_n = \frac{C_{n-1} - C_{n+1}}{C_{n-1}} \tag{6-6}$$

### *6.2.7 Statistics*

Statistical analysis was performed using JMP software (SAS Institute, Cary, NC). Comparative analyses were executed using oneway analysis of variance with Tukey post-tests at a 95% confidence level. $\chi^2$ analysis was used to analyze categorical data. For all co-cultures, the sample set size was n > 20 for explant experiments and n > 200 for neuron experiments for each condition analyzed.

## *6.3 Results*

### *6.3.1 Spatial Patterns of Reporter Gene Expression*

Previously developed techniques combining soft lithography and substrate-mediated gene delivery [302] were utilized to pattern expression of the reporter gene luciferase, while varying pattern width (0.25–1 mm) and vector concentration (2–10 ng/μl). Relative protein expression levels increased with increasing pattern width and vector concentration (Figure 6-1a). The corresponding protein production rates ranged from 6.0 X $10^{-8}$ pmol/cell/min (0.25 mm, 2 ng/μl) to 4.4 X $10^{-7}$ pmol/cell/min (1 mm, 10 ng/μl). According to the model prediction, the ligand concentration remains above zero for the longest distance with a pattern width of 1.0 mm (Figure 6-1b) and a vector concentration of 10 ng/μl (Figure 6-1c). This condition was used throughout

the manuscript for analysis of NGF production, binding, and neuronal response as it enables neurite guidance to be investigated over distances on the order of millimeters.

### *6.3.2 Spatial Patterns of NGF Expression*

Both the amount of NGF secreted by transfected cells and the distribution of NGF were quantified, in order to accurately predict NGF concentration profiles. The amount of soluble NGF in the culture medium was 173 and 364 pg/pattern for 24 and 48 h cultures, respectively (Figure 6-2a). Additional NGF was detected in the cell lysates, and was 2.2 and 6.9 pg/pattern for 24 and 48 h cultures (Figure 6-2a). These results were employed to calculate the NGF production rate ($p = 9.9 \times 10^{-11}$ pmol/cell/min) and effective diffusivity ($D_{e,\ NGF} = 2.45 \times 10^{-7}$ $cm^2/s$) which were inserted into the mathematical model to predict NGF concentration gradients from localized expression. The time points used in the mathematical model coincided with

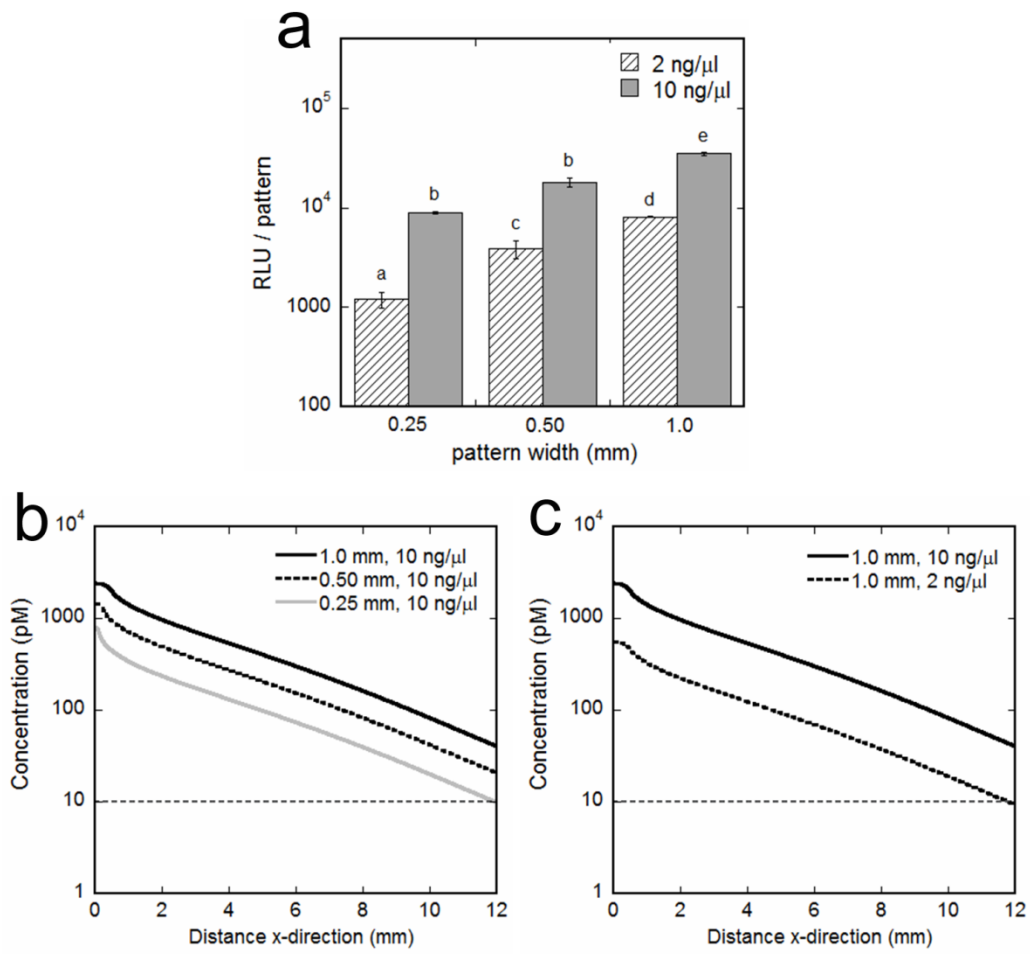


**Figure 6-1: Spatially patterned gene expression.** Quantification of luciferase transgene expression from patterned gene delivery, while varying vector concentration (2 – 10 ng/μL) and channel width (0.25 – 1.0 mm) (a). Values are reported as mean ± SEM, and statistically different values are marked by different letters ($p < 0.05$). Predicted concentration gradients from patterns of gene delivery (b, c). Note that x = 0 is the center of the pattern of expression.

critical time points in the co-culture experiments, where t = 0 h corresponded with the time of neuron cell seeding in which the culture medium was exchanged and the soluble NGF concentration is $C_{NGF}$ = 0 pmol/ml, and t = 24 h corresponded with the time of experimental assay. The predicted NGF concentration profile indicates the NGF concentration was below the approximate maximum concentration for gradient detection (100 nM, 100 times the dissociation constant of the p75 receptor) [171, 203] for all distances and times and remained above the estimated minimum concentration for gradient detection (10 pM, 1% the dissociation constant of the p75 receptor, marked by the dashed line) [203, 204] at x < 1.3 mm for 2 h, x < 2.5 mm for 12 h, and x < 3.7 mm for 24 h (Figure 6-2b).

### *6.3.3 Neurite Outgrowth and Guidance by Spatial Patterns of NGF Expression*

The ability of spatial patterns of NGF expression to induce neurite outgrowth and guidance was investigated by co-culturing DRG explants or dissociated DRG neurons on HEK293T cells with patterned NGF expression, while varying the time between HEK293T cell seeding and DRG seeding (9, 24, and 48 h), referred to hereafter as *9 h*, *24 h*, and *48 h* cultures. A minimum time of 9 h was investigated in order to ensure that transfected cells were producing and secreting NGF at the time the explants or dissociated neurons were seeded. It is important to note that we have previously shown that HEK293T cells alone, without pNGF transfection, do not support neuron survival or neurite extension [302]. Therefore, the neuronal responses observed can be directly attributed to induced NGF expression.

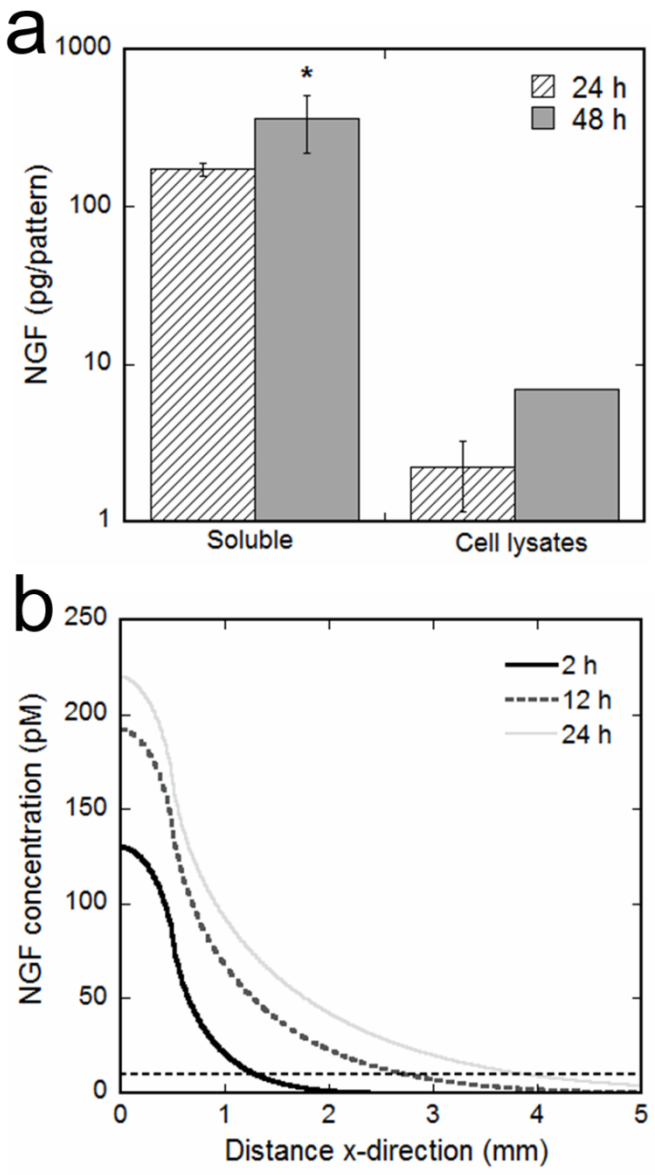


**Figure 6-2: Nerve growth factor expression by spatially patterned gene delivery.** Quantification of NGF production at 24 and 48 h after HEK293T seeding on patterned pNGF lipoplex deposition (a). NGF was detected both soluble in the culture medium and associated with cell lysates. Values are reported as mean ± SEM, and statistically different values are marked by the * ($p < 0.05$). Mathematical model predictions for NGF concentration profiles at 2, 12, and 24 h (b). Note that $x = 0$ is the center of the pattern of expression.

DRG explants seeded on *9 h*, *24 h*, and *48 h* cultures exhibited similar levels of neurite outgrowth (Figure 6-3c). Additionally, DRG explants seeded on *9 h* and *24 h* cultures exhibited neurite guidance toward patterns of NGF expression (Figure 6-3a, b). Quantitative evaluation of neurite guidance showed a higher percent neurite area extended toward the pattern of expression for *9 h* (87.8 ± 2.0%) and *24 h* (76.5 ± 3.9%) cultures, as compared to *48 h* cultures (55.6 ± 4.5%) (Figure 6-3d, $p < 0.05$), when explants were seeded 0.5 – 1.0 mm from the pattern center. Importantly, neurite guidance was also dependent on the distance from the pattern of expression the explant was cultured. A higher percent neurite area extended toward the pattern of expression for explants seeded on *9 h* (75.0 ± 4.2%) and *24 h* (66.1 ± 1.2%) cultures with explants seeded 1.0 – 1.5 mm from the pattern center, with a significant decrease in percent neurite area toward the pattern when explants were seeded 1.5 – 2.5 mm from the pattern center (Figure 6-3d, $p < 0.05$).

Co-cultures with dissociated DRG neurons seeded on spatial patterns of NGF expression were subsequently investigated for neurite growth and guidance. Neurons seeded on *9 h*, *24 h*, and *48 h* cultures exhibited comparable levels of neurite outgrowth (Figure 6-4c). Similar to explants, dissociated neurons seeded on *9 h* and *24 h* cultures also exhibited neurite guidance toward patterns of NGF expression (Figure 6-4a, b). Quantitative analysis of neurite guidance was performed by evaluating neurite orientation relative to the pattern of expression. Neurons seeded on *9 h* and *24 h* cultures extended a significantly higher percent of neurites 0–90º relative to the pattern of expression (92% and 89%, respectively) as compared to *48 h* cultures (55%) (Figure 6-4d, $p < 0.05$), when neurons were positioned 0.5 – 1.0 mm from the pattern of

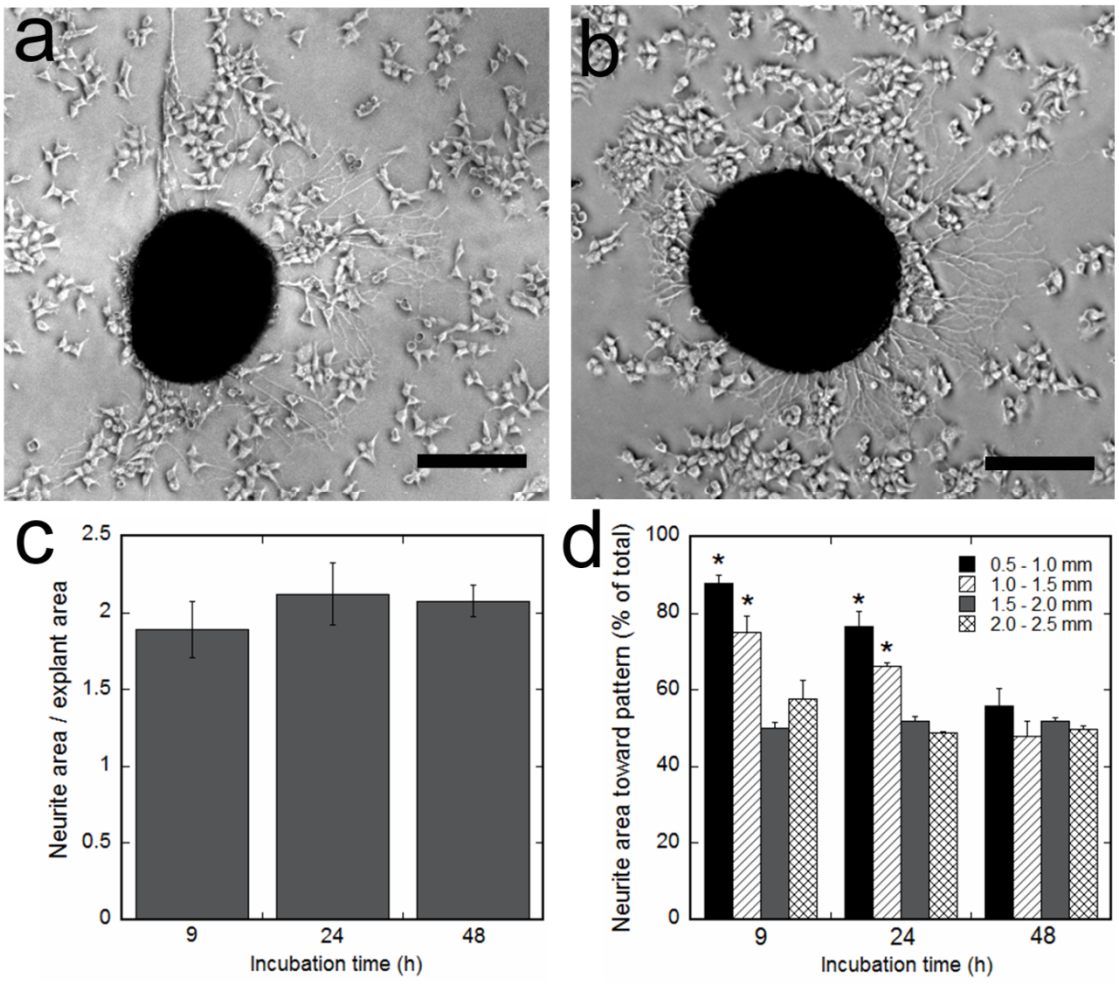


**Figure 6-3: Explants: neurite growth and guidance by patterned NGF expression.** DRG explants were co-cultured on patterned NGF expression. Neurites were guided toward patterns of NGF expression with DRGs cultured 9 h (a) and 24 h (b) after HEK293T seeding. The pattern of expression is to the right of the cultured explant. Scale bars = 250 μm. Quantification of neurite outgrowth while varying the incubation time between cell seedings (c). Quantification of neurite guidance while varying the incubation time between cell seedings and the distance from the pattern center (0.5 – 2.5 mm) (d). Values are reported as mean ± SEM, and statistically different values are marked by * ($p < 0.05$).

expression. A higher percentage of neurites extended 0–90º relative to the pattern of expression for neurons seeded on *9 h* (85%) and *24 h* (83%) cultures with neurons 1.0 – 1.5 mm from the pattern center, with a significant decrease in percentage of neurites 0–90º relative to the pattern of expression when neurons were located 1.5 – 2.5 mm from the pattern center (Figure 6-4d, $p < 0.05$).

### *6.3.4 Characterization of Surface-Associated NGF*

NGF has been shown to non-specifically associate with the extracellular matrix and cell surface proteoglycans, and this surface-associated NGF may contribute to the different neuronal responses observed for the range of accessory cell culture times. We subsequently investigated whether NGF associated with the accessory cell surface and/or extracellular matrix in the co-culture model. Immunocytochemistry revealed that NGF was localized to the surface at the center of patterned expression (Figure 6-5a, d), 0.5 mm from the pattern center (Figure 6-5b, e), and 1.5 mm from the pattern center (not shown) for 24 and 48 h accessory cell cultures, as compared to the negative control (no pNGF) (Figure 6-5c). Quantification of immunostain intensity indicated the percentage of NGF-positive surface area decreased with increasing distance from the pattern (Figure 6-5f, $p < 0.05$). Additionally, the percentage of NGF-positive surface area was higher after 48 h accessory cell culture as compared to 24 h (Figure 6-5f, $p < 0.05$).

### *6.3.5 Neurite Outgrowth and Guidance by Surface-Associated NGF*

The role of surface-associated NGF in promoting and directing neurite outgrowth from patterned NGF expression was investigated by co-culturing neurons on pNGF transfected

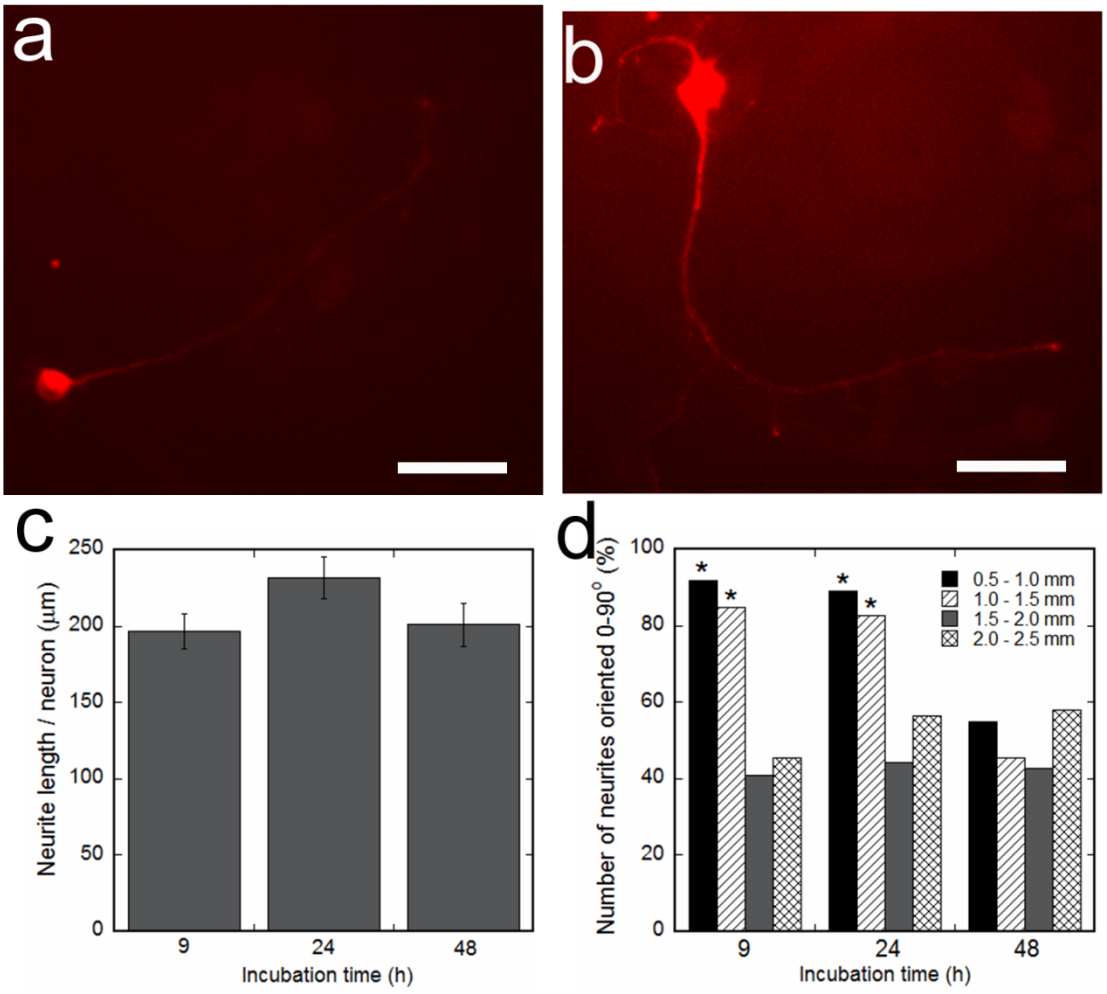


**Figure 6-4: Dissociated neurons: neurite growth and guidance by patterned NGF expression.** Dissociated neurons were co-cultured on patterned NGF expression. Neurites were guided toward patterns of NGF expression with neurons cultured 9 h (a) and 24 h (b) after HEK293T seeding. The pattern of expression is to the right of the dissociated neuron. Scale bars = 50 µm. Quantification of neurite outgrowth while varying the incubation time between cell seedings (c). Quantification of neurite guidance while varying the incubation time between cell seedings and the distance from the pattern center (0.5 – 2.5 mm) (d). Values are reported as mean ± SEM, and statistically different values are marked by * ($p < 0.05$).

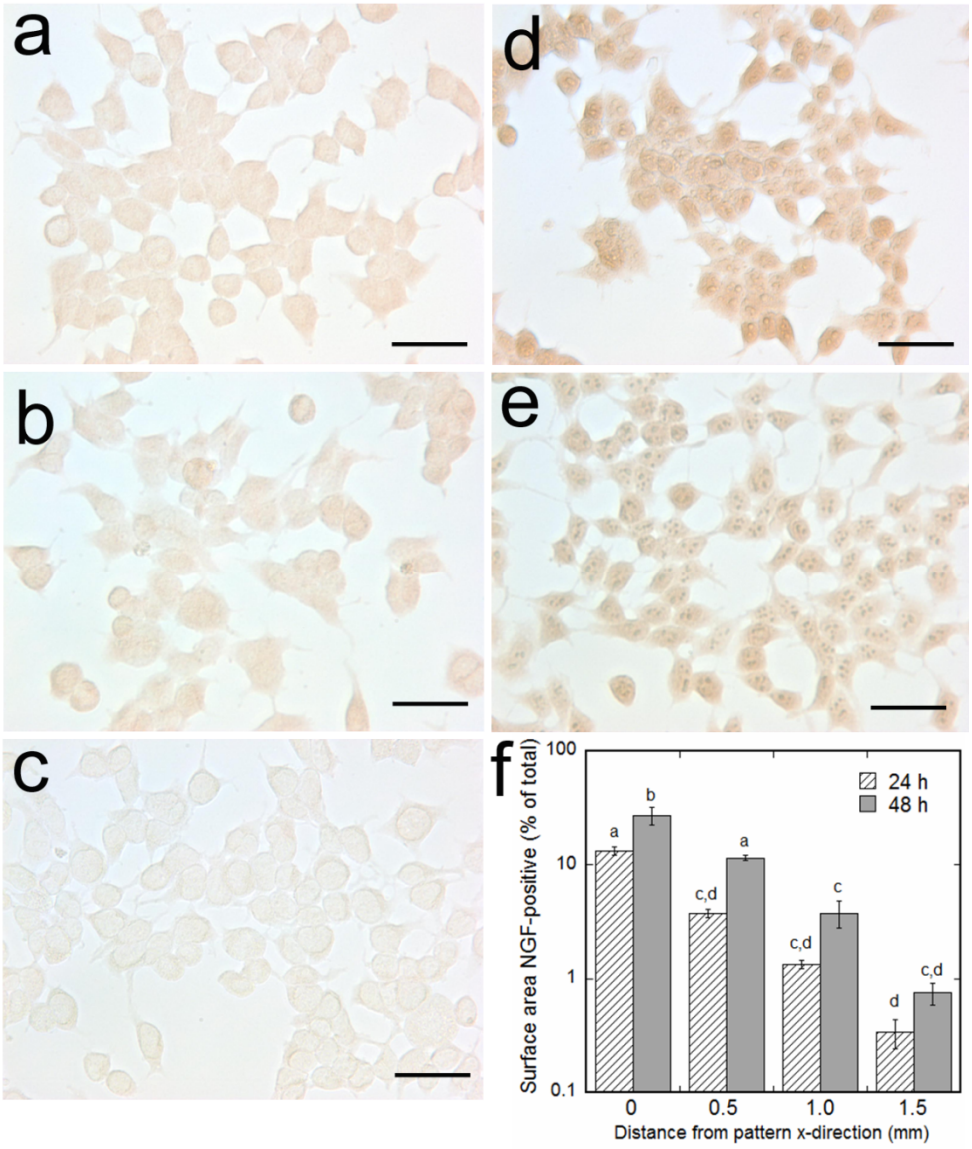


**Figure 6-5: Immunocytochemistry for the detection of surface-associated NGF.** The accessory cell culture surface stains positive for NGF at: the site of patterned gene delivery for 24 and 48 h culture, respectively (a, d), and 0.5 mm from the center of the pattern for 24 and 48 h culture, respectively (b, e), as compared to negative control (no pNGF delivery) (c). Quantification of immunostain intensity versus distance from the pattern center (f). Values are reported as mean ± SEM, and statistically different values are marked by different letters ($p < 0.05$). Scale bars = 50 μm.

accessory cells that had been fixed. Fixation halts NGF production and removes soluble NGF, while retaining NGF in an active form that is associated with the surface. DRG explants or dissociated neurons were cultured on patterned NGF expression with fixed accessory cells 9, 24, and 48 h after HEK293T seeding. The co-cultures on fixed accessory cells are referred to hereafter as *9 h*, *24 h*, and *48 h surface NGF*.

DRG explant survival and neurite outgrowth on surface-associated NGF cultures was dependent on the time between cell seeding and the distance an explant was cultured from the pattern center. Explants did not survive when seeded on *9 h surface NGF*. Explants survived when seeded 0–1.5 mm from the pattern center on *24 h surface NGF*, and 0–2 mm from the pattern center on the *48 h surface NGF* (Figure 6-6a, b). Explants sprouted neurites, and the area occupied by neurites normalized to the explant area was statistically higher with explants cultured on the *48 h surface NGF* (1.2 ± 0.2) as compared to explants seeded on the *24 h surface NGF* (0.62 ± 0.06) (Figure 6-6c, $p < 0.01$). Explants seeded on *24 h* and *48 h surface NGF* did not exhibit neurite guidance, as the area of neurites extending toward the pattern of expression was statistically 50% in all conditions (Figure 6-6d).

Neuron survival and neurite outgrowth from dissociated DRG neurons were also supported by *24 h* and *48 h surface NGF* cultures (Figure 6-7a, b). Neurite length normalized to surviving neurons was higher with neurons seeded on *48 h surface NGF* (200.3 ± 8.4 μm) as compared to neurons seeded on *24 h surface NGF* (100.3 ± 5.0 μm) (Figure 6-7c, $p < 0.01$). Similar to DRG explants, dissociated DRG neurons did not exhibit neurite guidance when seeded on *24 h* and *48 h surface NGF*, with statistically only 50% of neurites oriented 0-90° relative to the pattern of

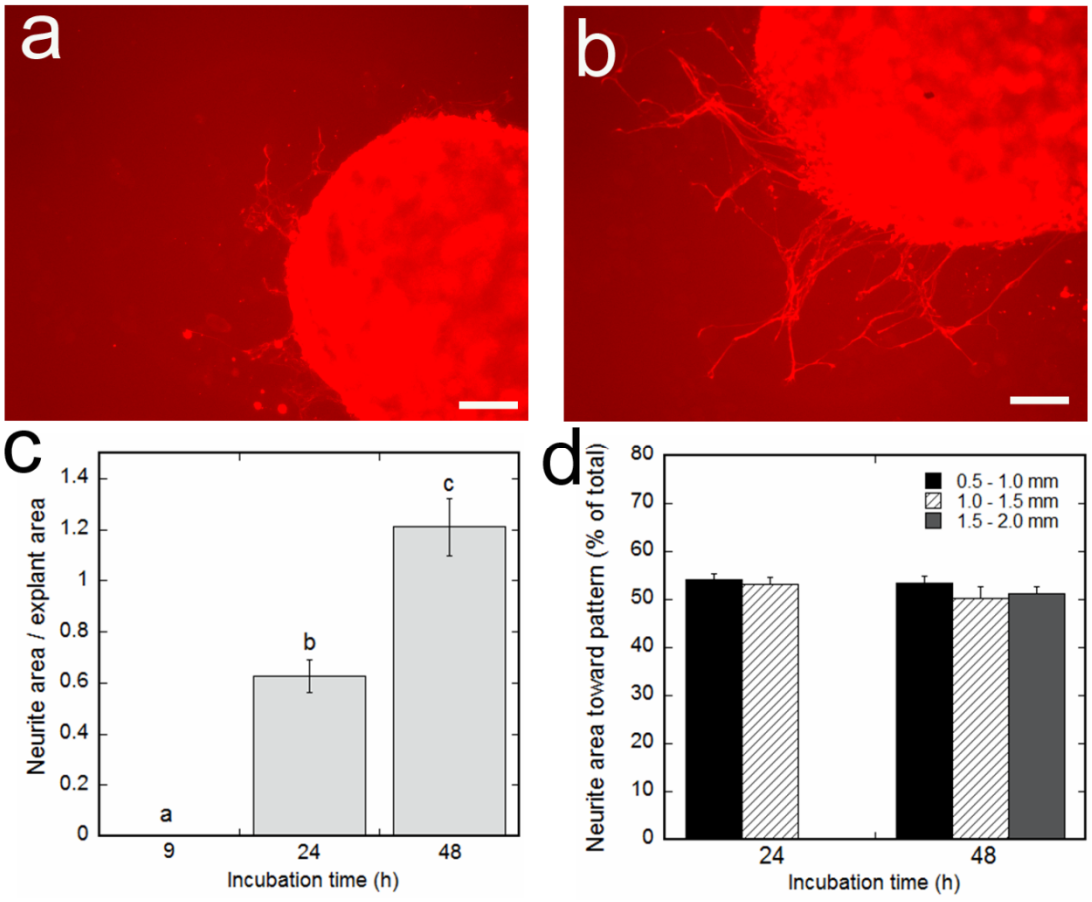


**Figure 6-6: Explants: neurite growth and guidance by surface-associated NGF.** DRG explants were co-cultured on patterned NGF expression directly after HEK293T fixation (to halt production of NGF) at 24 h (a) and 48 h (b) after HEK293T seeding. Scale bars = 100 μm. Quantification of neurite outgrowth while varying the incubation time between cell seedings (c). Quantification of neurite guidance while varying the incubation time between cell seedings and the distance from the pattern center (0.5 – 2.5 mm) (d). Values are reported as mean ± SEM.

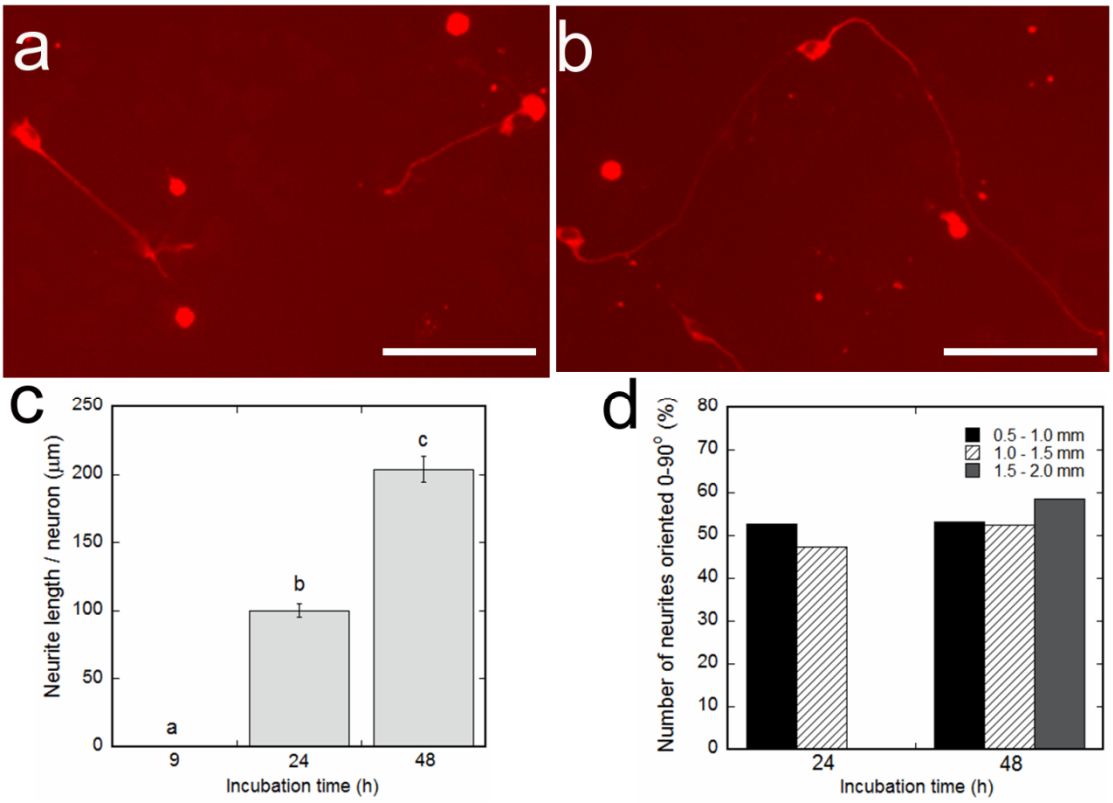


**Figure 6-7: Dissociated neurons: neurite growth and guidance by surface-associated NGF.** Dissociated neurons were co-cultured on patterned NGF expression directly after HEK293T fixation (to halt production of NGF) at 24 h (a) and 48 h (b) after HEK293T seeding. Scale bars = 100 µm. Quantification of neurite outgrowth while varying the incubation time between cell seedings (c). Quantification of neurite guidance while varying the incubation time between cell seedings and the distance from the pattern center (0.5 – 2.5 mm) (d). Values are reported as mean ± SEM.

expression (Figure 6-7d). Importantly, *9 h, 24 h,* and *48 h surface NGF* cultures supplemented with soluble NGF in the culture medium did not demonstrate directed neurite outgrowth from dissociated neurons (data not shown).

## *6.4 Discussion*

In this Chapter, we present a well-defined system of patterned gene expression to investigate neurite guidance in response to concentration gradients formed by localized secretion of NGF. The protein production rate and the resulting concentration gradient were varied by altering pattern width and vector concentration. Patterned gene expression guided neurite outgrowth, with guidance dependent on the distance a neuron was cultured from the pattern and the time between cell seedings. Portions of NGF secreted from patterned expression nonspecifically associated with the surface, which supported neuron survival and neurite outgrowth, with the extent of outgrowth dependent on the time of accessory cell culture, and therefore the amount of NGF bound. Surface-associated NGF alone, however, did not elicit a guidance signal. This is the first report that defines concentration gradients produced by spatial patterns of gene expression necessary for successful neurite guidance. Moreover, these results demonstrate the importance of considering diffusible factor binding in the characterization of gradients that guide neurites. These findings underscore the broad impact a patterned gene expression system may have on the investigation of guidance cues in many tissue development scenarios, as well as in the regeneration of tissues with complex architectures.

The distance a neuron was cultured from the pattern of expression influenced neurite guidance, for *9 h* and *24 h* cultures. Guidance was observed when neurons were cultured 0.5-1.5 mm from the center of patterned NGF expression. Based on knowledge for bacteria and

leukocyte chemotaxis [2], it has been suggested that neurite guidance by chemotactic mechanisms is governed by the mean chemoattractant concentration [203]. If the concentration drops below 1% of the dissociation constant, few of the receptors will be bound at any given time, yielding little difference in binding and the inability of the growth cone to detect the gradient [203]. The dissociation constant of NGF is 1 nM for p75 and 0.1 nM for trkA [303], therefore, the minimal concentration of NGF required for growth cone gradient detection is between 1-10 pM. The mathematical model predicts a total concentration of NGF dropped below 10 pM at x=1.5 mm at t=2 h, and maintained concentrations close to the minimal concentration at x=1.5 mm (C=39 pM at t=12 h, and C=62 pM at t=24 h) for the 24-h time course. This approach to a minimal NGF concentration for guidance detection may partially explain the correlation between guidance and distance.

The predicted concentration profiles were subsequently employed to calculate the absolute and fractional concentration gradients, both of which have been implicated in neurite guidance, for the regions in which guidance was observed (x=0.5-1.5 mm). The absolute concentration gradient ranged from 8.5-0.5 ng/mL/mm at x=0.5-1.5 mm over the 24-h time course (Figure 6-8a). The fractional concentration gradient over the width of the growth cone (≈20 μm) between x=0.5-1.5 mm ranged from 8.0-5.3%, 4.7-2.1%, and 4.0-1.5% for 2, 12, and 24 h, respectively (Figure 6-8b).

The absolute and fractional concentration gradients formed by patterned gene expression were discrepant with what has been previously shown to guide neurites by gradients engineered

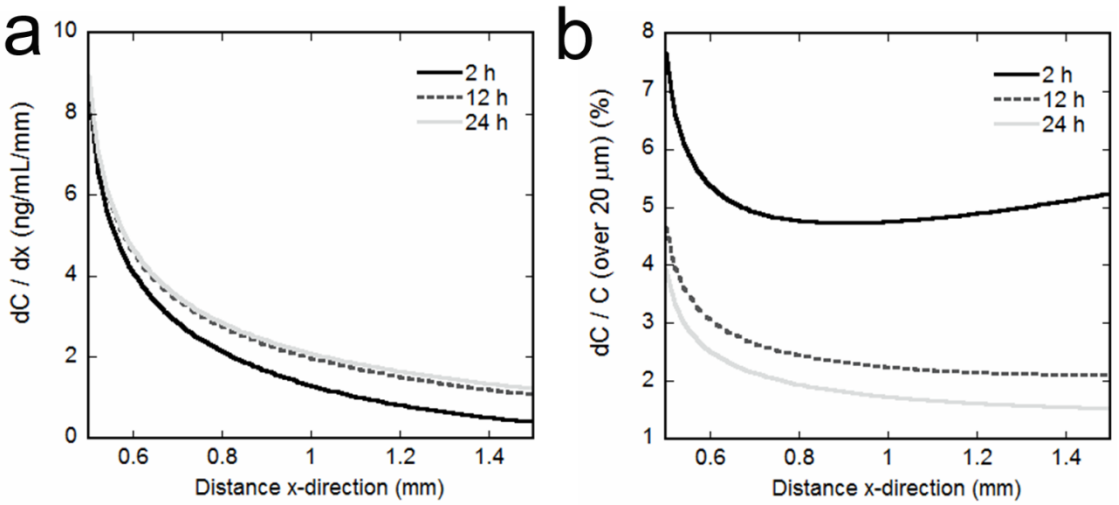


**Figure 6-8: Predicted NGF concentration gradients.** The predicted absolute concentration gradients (a) and fractional concentration gradients (b) within the region of observed neurite guidance (x = 0.5 – 1.5 mm) for t = 2, 12, and 24 h.

with purified proteins. The absolute concentration gradient produced by patterned expression (8.5-0.5 ng/mL/mm) was well below the suggested requirement for neurite guidance with engineered NGF gradients in agarose (133 ng/mL/mm) [195]. However, it has been suggested that the critical chemorepulsive information to pathfinding Ti1 pioneer growth cones within the developing grasshopper limb is governed by the Sema 2a fractional gradient and not the absolute gradient [208]. Fractional gradients produced by patterned expression were primarily steeper (8.0-1.5%) than engineered protein gradients that have previously been shown to guide neurites (3.3, 0.80, and 0.45%) [201]. Interestingly, these findings coincide with observations from leukocyte chemotaxis that lower mean concentrations require steeper fractional gradients to elicit a guidance cue [2]. These results are consistent with the hypothesis that engineered protein gradients do not adequately represent gradients formed by spatial patterns of gene expression and subsequent diffusion within a complex cellular environment.

The soluble NGF gradients from patterned expression provided a guidance signal for neurite outgrowth, while surface-associated NGF contributed to neuron survival and neurite outgrowth, but did not direct extension. Noteworthy is that the guidance cue by soluble NGF gradients was abolished when neurons were seeded 48 h after accessory cells. Since the culture medium was exchanged before neurons were seeded and NGF production rates were similar for the 48 h period, the predicted soluble NGF gradients were similar for *9 h*, *24 h*, and *48 h* cultures, and therefore, the lack of a guidance signal could not be explained by differences in soluble gradients. As a result, the ability of NGF to associate with the surface, and in turn, influence neurite outgrowth and guidance was investigated. Surface-associated NGF after 24 and 48 h accessory cell cultures supported neuron survival and neurite outgrowth, and neurons seeded on *48 h surface NGF* extended longer neurites, with neurite lengths comparable to neurons seeded on *9 h* cultures. Importantly, surface-associated NGF alone did not elicit a guidance cue. Previously, immobilized NGF within poly(2-hydroxyethylmethacrylate) gels guided neurites [260]. Predictions for neurite guidance by haptotactic mechanisms suggest a need for steeper concentration gradients when chemotactic factors are adsorbed to a substrate [221]. The surface bound NGF gradients formed by diffusion from localized expression and association with the surface were not sufficient to elicit a haptotactic guidance signal. Moreover, the presentation of NGF after adsorption to the surface may differ from NGF encapsulated within synthetic hydrogels, and in turn may alter the haptotactic capability of immobilized NGF. Since surface-associated NGF alone did not elicit a guidance signal, and the amount of bound NGF was significantly higher after 48 h of accessory cell culture as compared to 24 h, surface-associated NGF may contribute to the disappearance of the guidance signal during the *48 h* culture. The

relatively high surface concentration in the *48 h* culture may mask the soluble concentration gradient, rendering the soluble NGF gradient ineffective at guiding neurites.

The binding of diffusible factors to the extracellular matrix has been implicated in cell migration and differentiation during morphogenesis [304], with heparin-binding growth factors binding to ECM proteoglycans [305]. While NGF has a low affinity for heparan sulfate, the incorporation of NGF into a hydrogel loaded with heparin reduced the ligand diffusion rate and slowed release [306], suggesting that NGF may interact with accessory cell proteoglycans in the patterned expression system presented here. Furthermore, NGF is a sticky protein and has been shown to nonspecifically adsorb to various surfaces [307]. Previously, NGF bound to nitrocellulose paper [308] or adsorbed to pol-l-glutamate surfaces [220] supported neuron survival and neurite extension, substantiating that nonspecifically adsorbed NGF retains activity.

Patterned gene delivery may be useful in repairing damaged nerves, as axon guidance across a lesion and to a target is essential for functional recovery. Nerve guidance bridges have been designed to present topographical guidance cues [254], and have shown promise in both PNS and CNS injury models [309, 310]. The CNS, however, is not a conducive environment for regeneration, and at the onset of injury, is plagued by widespread changes in gene expression, many of which involve guidance cues and their receptors [311]. Spatially patterned gene delivery within spinal cord bridges provides a novel method to alter gene expression at the injury site and present guidance signals over an extended period of time. Plasmid delivery from guidance bridges elicited reporter gene expression at a rat spinal cord hemisection for two weeks, demonstrating the promise for gene delivery in spinal cord regeneration strategies [238].

The patterned gene expression system described in this report offers significant advantages over existing in vitro neurite guidance assays. Gradients formed by localized secretion of diffusible factors within a complex cellular environment mimic the manner in which gradients are formed naturally, and therefore better recapitulate guidance signals as compared to protein gradients from source/sink methods or pipette assays. While target tissue cultures represent the natural formation of gradients, the cultures and resultant concentration profiles have inherent variability and are difficult to characterize. We present a well-characterized system in terms of protein production from the source, protein binding to the surface, and predicted concentration gradients from patterns of expression. The protein production rates can be varied by simple changes in system conditions, and nonviral DNA delivery strategies provide the flexibility to investigate any therapeutic factor by readily exchanging plasmids without altering the delivery system. This flexibility enables the investigation of other diffusible guidance factors with different concentration requirements for guidance, and can be used to study migration of other cell types (e.g., fibroblasts) in response to localized expression of guidance factors.

## *6.5 Conclusions*

In summary, patterned gene expression produced soluble NGF gradients capable of guiding neurite growth, with the extent of guidance dependent on the distance neurons were cultured from the pattern and the amount of NGF bound to the surface. The patterned expression system presented here allowed for comparison to existing in vitro gradient assays, and we have demonstrated that absolute and fractional gradients formed by localized expression within a cellular environment that direct neurite outgrowth differ from engineered gradients with purified proteins in an acellular environment. Spatially patterned gene expression provides a well-defined

and tunable method to investigate cellular responses to gradients of guidance molecules, and may be applied to the regeneration of tissues with complex architectures.

# Chapter 7

# Patterned PLG Substrates for Localized DNA Delivery and Directed Neurite Extension

## *7.1 Introduction*

Injury to a nerve results in paralysis below the lesion, and nerve regeneration across the lesion is a first step towards regaining function. In the spinal cord, neurons have the potential to regenerate, but growth is limited by the extracellular environment [312-314]. An approach to manipulate the local environment involves the implantation of biomaterial scaffolds that are termed bridges. Bridges implanted at the lesion function to maintain a continuous path for regeneration, promote infiltration of permissive cell types that can secrete inductive factors, support axonal elongation, and reduce scar formation [315, 316]. Recently, bridges have been engineered with channels that may function to physically guide extending neurites and segregate functional pathways [250, 254, 317, 318]. The physical boundaries provided by the channels can produce longer and oriented neurites, which may otherwise be random [250]. While bridges support axonal growth, the density of axons remains significantly less than native tissue (for review, see [316]).

Neurotrophic factors, such as nerve growth factor (NGF), neurotrophin-3 (NT-3), and brain derived neurotrophic factor (BDNF), delivered at a lesion can enhance the density of axons growing through the lesion [319, 320]. Injured neurons remain responsive to the neurotrophins, yet the local concentration produced endogenously is insufficient to promote regeneration [321]. Delivering these factors can act directly on the neurons to promote survival and axonal

elongation. Neurotrophic factors have been delivered via protein injection and the transplantation of ex-vivo engineered cells [322]. These methods of protein delivery are met by limitations, such as clearance, degradation, and instability, and do not maintain therapeutic concentrations of neurotrophic factors for sustained periods of time. More recently, bridges capable of controlled release have been developed with the potential to provide a more controlled and localized dose relative to traditional delivery methods [254, 322].

Gene delivery is a versatile alternative to direct protein delivery, with the potential for delivery from biomaterials to provide localized inductive expression of proteins for extended times [12]. An approach to delivering DNA from a tissue engineering scaffold involves immobilization of the vector to the scaffold, a process termed substrate-mediated delivery [323]. DNA is complexed with a cationic lipid or polymer for immobilization by specific and/or non-specific interactions between the vector and substrate [45, 278]. Substrate-mediated delivery places DNA at or near the biomaterial surface, which can promote internalization by those cells adhering to the scaffold [277]. This delivery approach enables scaffolds to be fabricated by any technique and in any geometry for subsequent immobilization without affecting the DNA stability. Additionally, immobilization provides a means to spatially localize gene transfer, which may be useful for recreating the architecture of complex tissues.

In this Chapter, the delivery of genes encoding for neurotrophic factors was combined with physical guidance barriers to promote neuron survival and neurite outgrowth and simultaneously direct extending neurites in vitro. Two-dimensional poly(lactide-co-glycolide) (PLG) scaffolds with topographical patterns were fabricated via compression molding on poly(dimethyl siloxane) (PDMS) templates. PLG has been widely used as bridges for spinal cord repair, or conduits for

peripheral nerve regeneration [315]. Non-viral DNA complexes were created by mixing plasmid DNA with a cationic polymer, poly(ethylene imine) (PEI). These non-viral DNA complexes were immobilized to the PLG surface and both transfection efficiency and transgene expression were investigated as a function of channel width and DNA amount. DNA encoding NGF was subsequently non-specifically immobilized to the PLG microchannels and an in vitro co-culture model was employed to assess neuron survival and neurite extension [286]. Additionally, the ability to localize gene transfer to the channel in order to tailor channels for specific axonal populations was investigated. This study identifies design parameters for applying the delivery mechanism to three-dimensional structures for the promotion of nerve regeneration.

## *7.2 Experimental Procedures*

### *7.2.1 Fabrication of Flat PLG Disks*

PLG (75:25 mol ratio of $_{D,L}$-lactide to glycolide *i.v.* = 0.6 – 0.8) (Boehringer Ingelheim Chemical, Petersburg, VA) pellets were heated to 82˚C and pressed into a flat disk using a 5 kg weight. The temperature was slowly decreased from 82˚C to 37˚C and the disks were placed at 37˚C overnight. Disks had a radius of approximately 1.55 cm and were stored at room temperature until use.

### *7.2.2 Fabrication of Patterned PLG Disks*

Templates containing the desired pattern were constructed using photolithography. SU8-100 negative tone photoresist (Microchem, Newton, MA) was spin coated at 1000 rpm for 30 seconds on silicon wafers (Ultrasil, Hayward, CA). After baking, specific regions of the photoresist were polymerized using film transparencies as the photomask (In Tandem Design,

Towson, MD) and a Quintel Q-2000 mask aligner (Quintel, San Jose, CA), with UV exposure for 45 seconds. The photoresist was patterned with raised lines that were 250 µm wide, 150 µm high, and 10 mm long. The distance between the lines varied in the following order: 100, 150, and 250 µm, and this distance between the lines determined the channel width. A second pattern was fabricated to achieve uniform channels on a single disk. In this case, the distance between the lines was held constant at either 100, 150, or 250 µm. PDMS (Krayden, Glenview, IL), also referred to as Dow Corning Sylgard 184 Elastomer, was cured on the photoresist molds at a 10:1 (base to curing agent) ratio at 60ºC for 5 hours. After cooling, the PDMS was peeled from the silicon wafer, leaving a template of the fabricated pattern. To fabricate patterned PLG disks, the PDMS template was coated with PLG pellets, heated, and the polymer was molded as described in Section 2.1. Patterned disks were stored at room temperature until use.

### *7.2.3 DNA Complex Immobilization*

Prior to complex immobilization, PLG disks (flat and patterned) were attached to the bottom of wells of a 24-well tissue culture plate with autoclaved silicon grease. Disks were incubated with 50% fetal bovine serum (FBS) in phosphate buffered saline (PBS) for 4 hours at room temperature. Plasmid was complexed with polyethylenimine (PEI) (25 kDa, Aldrich, St. Louis, MO) in a total volume of 300 µl to form PEI/DNA complexes at 3 fixed DNA amounts: 1, 3, and 6 µg by dropwise addition of PEI to plasmid and subsequent mixing. The amount of PEI was varied to achieve an N/P ratio of 25 while both DNA and PEI were diluted with 150mM NaCl. Complexes were incubated at room temperature for 10 minutes, and then incubated on the PLG disks at room temperature for 1 hour. For gene delivery within each channel, the complexes (≈ 10 µL) were deposited into individual channels using a mouth pipette. The complexes quickly

adsorbed to the PLG, therefore, multiple depositions (n = 5) were performed sequentially. For imaging deposition, plasmid (pEGFPLuc) was fluorescently labeled with tetramethyl rhodamine using the manufacturer's protocol (Mirus, Madison, WI). The deposited DNA was imaged with fluorescence microscopy (Leica) and complex size was measured using the NIH program *Image J* (available at http://rsb.info.nih.gov/nih-image).

### *7.2.4 Cell Culture and Transfection*

Transfection studies were performed with HEK293T cells (ATCC, Manassas, VA) cultured at 5% $CO_2$ and 37˚C in Dulbecco's Modified Eagle Medium (DMEM) supplemented with 10% heat inactivated FBS, 1% penicillin-streptomycin and 1% sodium pyruvate (cDMEM). Cells were seeded at a density of 100,000 cells per PLG disk (flat and patterned). For substrate-mediated delivery, cells were seeded directly following complex immobilization. Transfection was analyzed following a 48 hour culture.

Transfection was characterized through the extent of transgene expression (luciferase levels) and the number of transfected cells (β-galactosidase expression). The dual reporter plasmid pEGFPLuc, (Clontech, Mountain View, CA) which contains both EGFP and luciferase driven by a CMV promoter was used to determine the extent of transgene expression. Luciferase transgene levels were measured using the Luciferase Assay System (Promega, Madison, WI). After 48 hours in culture, cells were lysed and assayed using a luminometer (Turner Biosystems) set for a 3-s delay with signal integration for 10 s. Luciferase activity was normalized to the total amount of protein. To assess luciferase activity within individual sized channels, pEGFPLuc complexes were immobilized to disks with uniform sized channels. Before cell lysis, the cells cultured on top of the channels were removed by scraping, as to achieve an accurate quantification of

expression by cells cultured within the channels. The reporter plasmid ß-galactosidase (pNGVL1-nt-LacZ) (National Gene Vector Labs, Ann Arbor, MI) was used to determine the number of transfected cells. Expression was visualized using X-gal stain, and the total number of transfected cells was counted from five random pictures of the PLG surface. The total number of cells within each image was determined by staining with 5 μg/ml Hoechst 33258 (Molecular Probes, Eugene, OR) and counting the cells using cell counting software, CellC version 1.11 (available at http://www.cs.tut.fi/sgn/csb/cellc/).

### *7.2.5 In Vitro Neurite Outgrowth*

The plasmid encoding for NGF (pNGF) has full-length mouse NGF in the RK5 vector backbone with a CMV promoter, and was a gift from Dr. Hiroshi Nomoto (Gifu Pharmaceutical University, Japan). pNGF was complexed with PEI (N/P = 25) and immobilized to the PLG substrates as described in Section 2.3. Following two PBS rinses, HEK293T cells were cultured on the PLG substrates. To obtain primary neurons, dorsal root ganglia (DRG) were isolated from E8 white leghorn chicken embryos (Michigan State University Poultry Center, East Lansing, MI) and maintained in Hank's balanced salt solution (HBSS) buffer supplemented with 6 g/L glucose until the isolation was complete. DRG were incubated for 30 minutes at 37ºC in 0.25% trypsin (Worthington Biochemical, Lakewood, NJ), followed by trituration with fire-polished glass Pasteur pipettes to dissociate the ganglia. Non-neuronal and neuronal cells were separated by panning for 2 hours at 37ºC. After 8 hour culture of the HEK293T cells, the media was removed, the surfaces were washed with PBS, and dissociated DRG neurons were seeded (5 X $10^4$ cells/well) on the cell layer. Control conditions included DRG neurons co-cultured with HEK293T cells with no DNA deposited and various concentrations of recombinant rat β-NGF

(R&D Systems, Minneapolis, MN) (0.1, 1.0, 10, and 25 ng/mL) added to the culture media at the time of DRG seeding. Cells were co-cultured for 48 hours in cDMEM at 37ºC, 5% $CO_2$ and fixed with 4% paraformaldehyde (PFA) after the culture period. The neurons were stained for neuron-specific class III β-tubulin by incubating fixed cells in TUJ1 antibody (Covance, Berkely, CA) diluted in 5% normal goat serum (Vector Labs, Burlingame, CA) in PBS for 1 hour followed by incubation in TRITC-conjugated goat anti-mouse secondary antibody (Jackson Immunoresearch, West Grove, PA) in PBS for 30 minutes. Cells were counterstained with Hoechst 33258 to visualize cell nuclei. Neurons and HEK293Ts were visualized with confocal microscopy (Leica Laser Confocal Microscope).

### *7.2.6 Neuron Survival and Neurite Length Quantification*

Surviving neurons were identified as having sprouting neurites. Primary and secondary neurite length were measured using *Image J* with a Neuron J plug-in [284]. Primary neurites were defined as extending directly from the neuron cell soma. Secondary neurites were defined as extending from a primary neurite. Quantifications were made from five regions of each disk or channel size and averaged.

### *7.2.7 Statistics*

Statistical analysis was performed using JMP software (SAS Institute, Cary, NC). Comparative analyses were executed using one-way ANOVA with Tukey post-tests, at a 95% confidence level. Mean values with standard error of the mean (SEM) are reported. All experiments were performed in triplicate.

## 7.3 Results

### 7.3.1 Cellular Transfection on PLG Substrates

Initial studies evaluated the transfection efficiency and transgene expression with polyplexes nonspecifically immobilized to compression molded, flat PLG disks. Three DNA amounts (1, 3 and 6 µg) were incubated on the substrate for immobilization, with approximately 3% of the DNA remaining immobilized to the surface after washing [277]. Transfected cells were homogeneously distributed across the PLG disks (Figure 7-1a). Transfection efficiency (percent of transfected cells) by immobilized polyplexes on PLG increased with increasing DNA amounts on the surfaces (Figure 7-1b, $p < 0.05$). Efficiency $(33 \pm 2)\%$ was maximal with 6 µg DNA incubated on PLG surfaces. Protein expression on PLG disks increased from $1.3 \times 10^5$ RLU/mg protein to $7.1 \times 10^6$ RLU/mg protein, when the DNA amount incubated on the surface increased from 1 to 6 µg (Figure 7-1c, $p < 0.05$).

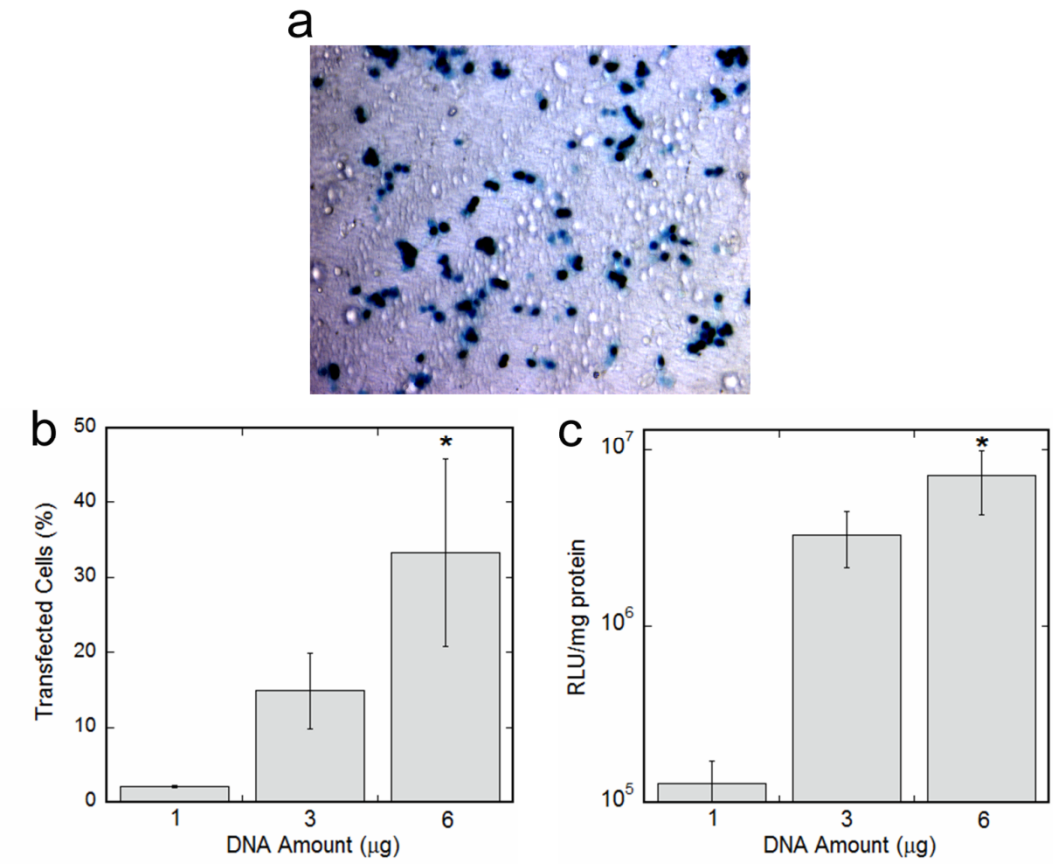


**Figure 7-1: Cellular transfection on flat PLG disks.** X-gal staining of transfected HEK293T cells on a transparent PLG disk (a). Scale bar represents 100 μm. Comparison of transfection efficiency (b) and transgene expression (c) on PLG disks with varying DNA amounts. The symbol * indicates statistical significance, $p < 0.05$.

### *7.3.2 Complex Immobilization and Cellular Transfection on Patterned PLG*

PLG disks with topographical patterns were capable of DNA immobilization and subsequent surface transfection depending on channel width. Each patterned PLG disk contained a double pattern of 100, 150, and 250 µm channels (Figure 7-2a) or 6 uniform sized channels (Figure 7-2b), spaced by 250 µm wide and 150 µm high walls. Complexes deposited on the PLG substrate were homogeneously distributed independent of the channel width. The number of complexes with a diameter greater than 2 µm within the 100 and 150 µm channels was significantly increased relative to either the flat PLG disks or the 250 µm channels, suggesting that complexes may have aggregated in the smaller channels (Figure 7-2c-f). Cellular transfection within all sized channels (100, 150, and 250 µm) was achieved by immobilization of DNA complexes (Figure 7-3a-c). For incubation of 3 µg DNA on the surface, transfection efficiency within all channel sizes (~ 5%) was less than on flat PLG disks (~ 15%) (Figure 7-3d, $p < 0.05$). A significant increase in transfection efficiency was observed in all channel widths when the DNA amount was increased from 3 to 6 µg (Figure 7-3d, $p < 0.05$), similar to the result shown with flat PLG disks. For 6 µg DNA incubated, transfection efficiency increased to (16± 2)% in the 100 µm channel and (30 ± 2)% in the 150 µm channel (Figure 7-3d). Additionally, transfection efficiency in the 250 µm channel (52 ± 7)% was significantly higher than efficiency in the smaller channels (Figure 7-3d, $p < 0.05$). For 6 µg DNA incubated, protein expression also increased with channel width from 5.6 X $10^5$ RLU/mg protein (100 µm channel) to 4.0 X $10^6$ RLU/mg protein (250 µm channel) (Figure 7-3e, $p < 0.05$).

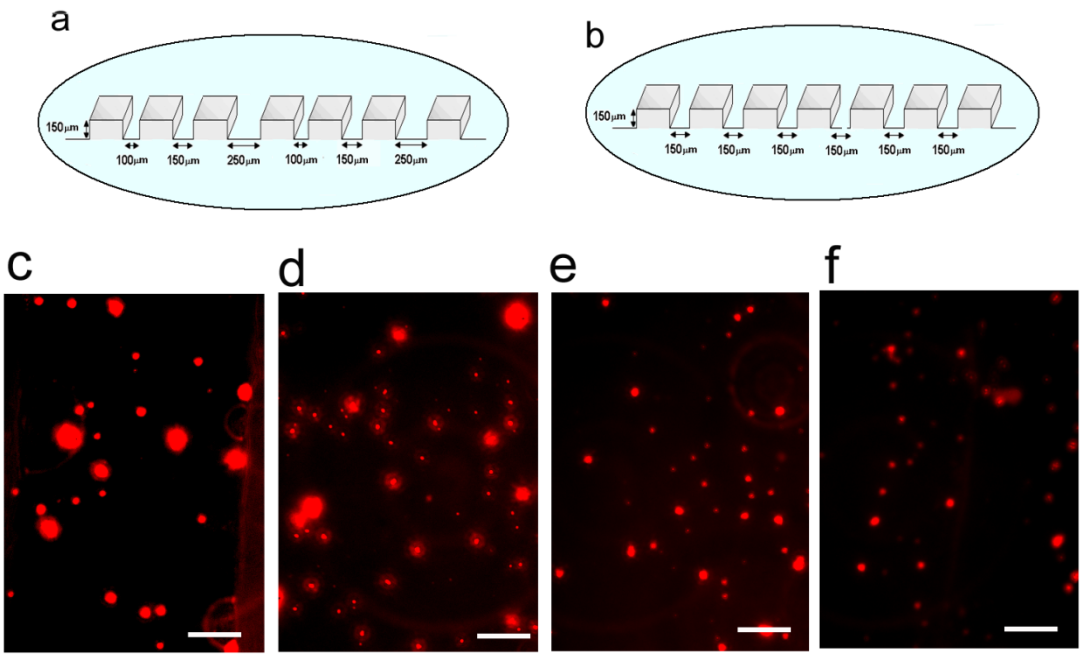


**Figure 7-2**: **DNA complex deposition within PLG microchannels.** Schematic of patterned PLG disks fabricated by compression molding (a, b). Fluorescently labeled DNA complexes within 100 (c), 150 (d), and 250 (e) μm channels and on flat PLG disks (f). Scale bars represent 100 μm.

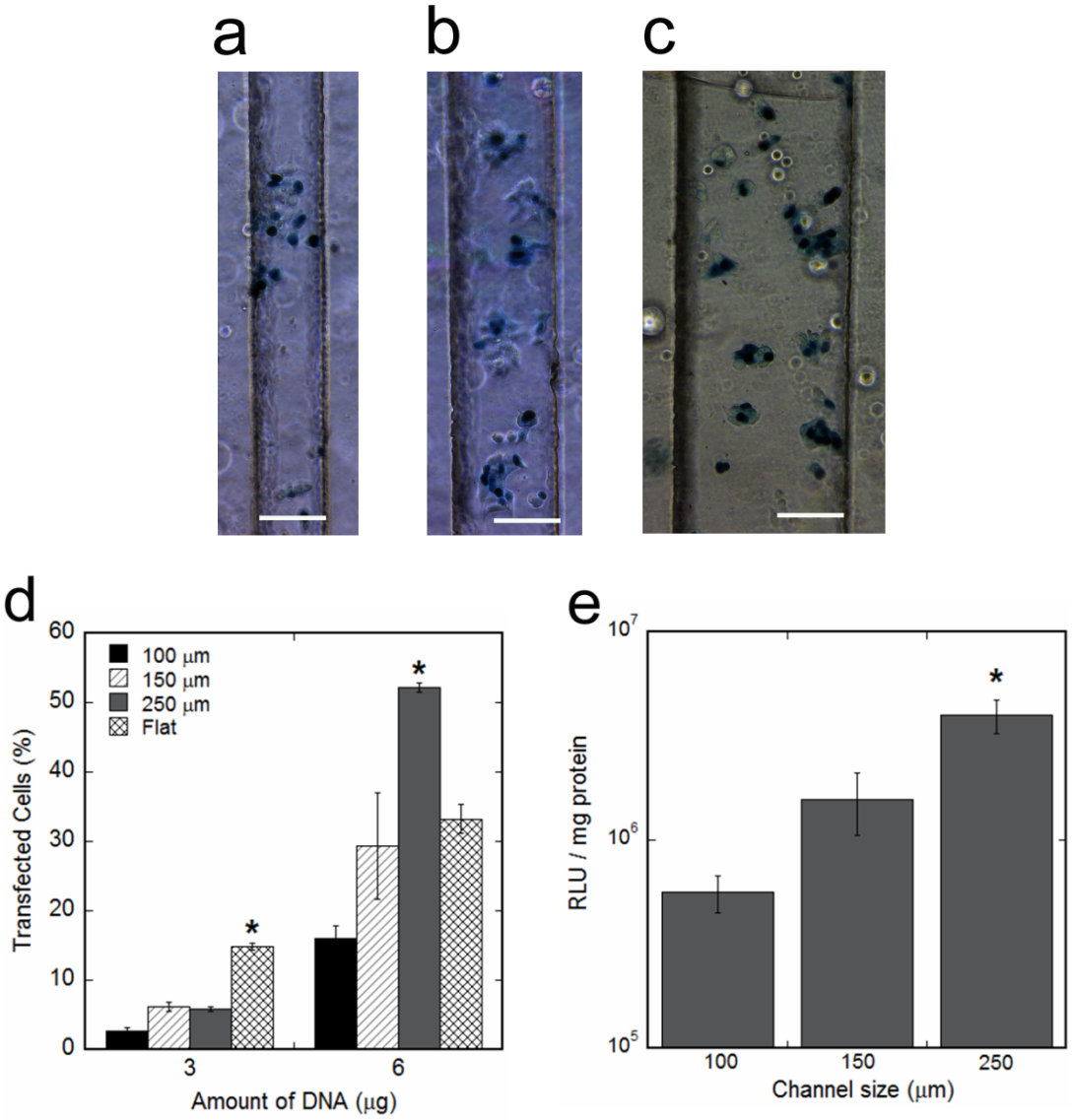


**Figure 7-3: Cellular transfection within PLG microchannels**. X-gal staining of transfected HEK293T cells within 100 (a), 150 (b), and 250 (c) μm channels. Scale bars represent 100 μm. Comparison of transfection efficiency (d) and transgene expression (e) within the different width channels. The symbol * indicates statistical significance, $p < 0.05$.

### *7.3.3 Neuronal Co-Culture on Flat PLG Substrates*

Primary neurons were co-cultured with HEK293T cells on flat PLG disks and assessed for neuron survival and neurite extension. pNGF (6 µg) was incubated on the PLG surface, the condition that yielded the highest percent transfected cells and protein expression level (Figure 7-1). Significant neuron survival and neurite extension was present on surfaces with pNGF/PEI complexes deposited (Figure 7-4a), but not on surfaces with either pLUC/PEI complexes (Figure 7-4b), or in the absence of a vector (Figure 7-4c). HEK293T cells were chosen for the co-culture model as they do not basally support neuron survival and neurite extension (Figure 7-4c); thus, the neuronal response resulted from the production and secretion of NGF by the HEK293T cells. Neuron survival on pNGF/PEI-PLG disks (35.6 ± 5.2)% was higher than on disks with no DNA (2.0 ± 0.9)% or disks with immobilized pLUC/PEI complexes (1.7 ± 1.1)% (Figure 7-4d, $p < 0.001$). Furthermore, neuron survival on pNGF-PLG disks was comparable to survival on disks with 25 ng/mL NGF added to the cell culture media (Figure 7-4d). In addition to neuron survival, total neurite extension per surface area was higher on pNGF-PLG disks (81.4 ± 7.2 $cm^{-1}$), compared to disks with no DNA (1.9 ± 0.9 $cm^{-1}$) or pLUC-PLG disks (1.7 ± 0.8 $cm^{-1}$), and comparable to PLG disks with 25 ng/ml NGF (72.3 ± 8.4 $cm^{-1}$) (Figure 7-4e, $p < 0.001$). The distribution of primary and secondary neurite density was subsequently investigated. Primary neurites extend directly from the neuron cell soma, while secondary neurites branch from primary neurites. Primary and secondary neurite densities were quantified by measuring the total length of primary and secondary neurites and normalizing to the surface area. The primary neurite density on flat PLG disks with pNGF transfected cells was 26.5 ± 3.2 $cm^{-1}$, while the secondary neurite density was 24.3 ± 3.6 $cm^{-1}$.

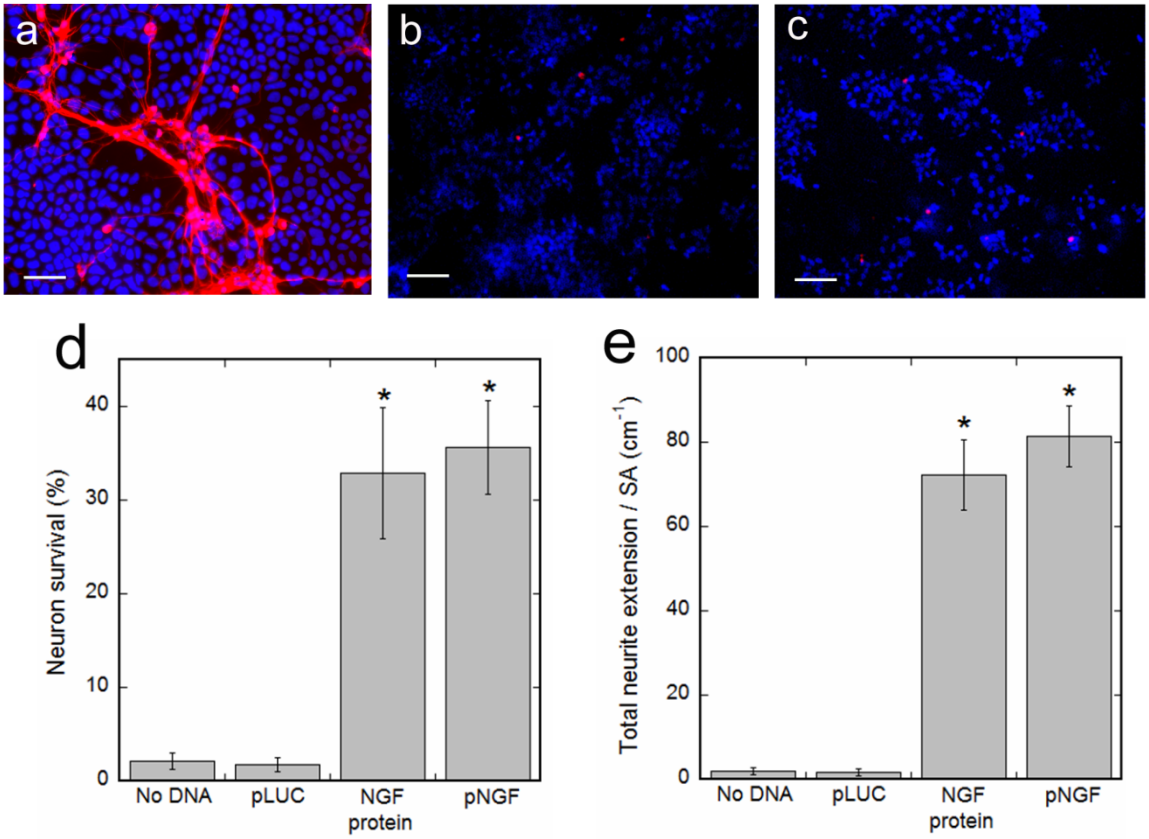


**Figure 7-4: Neuronal co-cultures on flat PLG disks.** Neurite extension on PLG disks with: surface immobilized pNGF/PEI complexes (a), surface immobilized pLUC/PEI complexes (b), and no DNA (c). TUJ1 (red) and Hoechst 33258 nuclear stain (blue) images shown are overlaid. Scale bars represent 100 µm. Quantification of neuron survival (d) and total neurite extension normalized to surface area (e) on pNGF-PLG disks and control disks. The symbol * indicates statistical significance, $p < 0.001$.

### *7.3.4 Neuronal Co-Culture on Patterned PLG*

The ability to direct neurite extension was assessed by co-culturing primary neurons and HEK293T cells in the PLG channels, with 6 µg pNGF incubated. Neurons attached to the surface and sprouted neurites in channels of all sizes (Figure 7-5a-d). Additionally, neurites in the 100 µm channel have neurites that contact and extend parallel to the channel wall (Figure 7-5a), suggesting guidance by the wall. The larger channel widths display greater branching, with less neurites growing along the channel wall (Figure 7-5b,c). Interestingly, neurites that did not contact the channel wall in the 100 µm channels also exhibited less branching than those in the 250 µm channels. The primary neurite density in the 100 µm channel (89.2 ± 11.2 $cm^{-1}$) was significantly greater than all other conditions (Figure 7-5e, $p < 0.05$). The primary neurite densities in the 150 µm (60.2 ± 2.2 $cm^{-1}$) and 250 µm (47.3 ± 4.1 $cm^{-1}$) channels were significantly greater than that on the flat PLG disk (26.5 ± 3.2 $cm^{-1}$) (Figure 7-5e, $p < 0.05$). Additionally, the ratio of primary to secondary neurite density decreased (from 2.3 to 1.2) as the channel size increased (from 100 to 250 µm).

To evaluate whether the differences in primary neurite outgrowth between different width channels could be attributed to variations in NGF concentration, neurons were cultured in the channels and NGF was added to the cell culture media to a final concentration ranging between 0.1 and 25 ng/mL. For a given channel width, the primary neurite density and degree of secondary sprouting did not change with varying NGF concentration (Figure 7-5f). Primary neurite density was significantly greater in the 100 µm channels as compared to the 250 µm channels for each NGF concentration (Figure 7-5f, $p < 0.05$). Interestingly, the ratio of primary

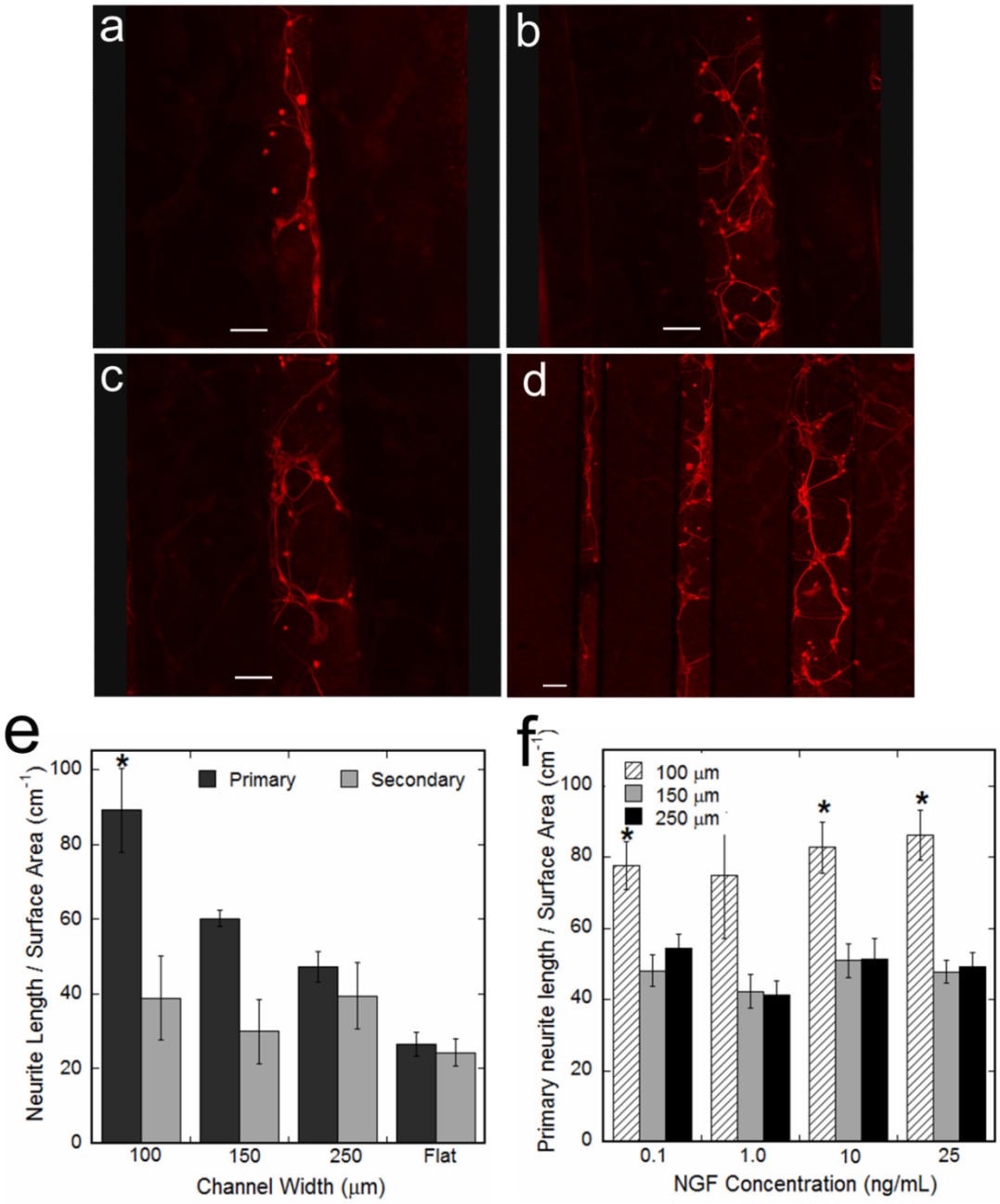


**Figure 7-5: Neuronal co-cultures within PLG microchannels.** Fluorescence imaging of neurons cultured within PLG channels with immobilized pNGF/PEI complexes: 100 µm (a), 150 µm (b), 250 µm (c), and all channel widths (d). Scale bars represent 100 µm. Length of primary and secondary neurites per surface area within the PLG channels and on flat PLG disks with immobilized pNGF/PEI complexes (e). Length of primary neurites per surface area within PLG channels with various NGF concentrations added to the culture media (f). The symbol * indicates statistical significance, $p < 0.05$.

neurite density in the 100 versus 250 µm channel was greater when neurons were co-cultured with pNGF transfected cells (1.9) as compared to neurons with NGF added to the media (1.45).

### *7.3.5 Patterned Cellular Transfection in PLG Channels*

Subsequent studies investigated the ability of substrate-mediated delivery to transfect cells only within the channel, and to enable transfection with different plasmids within each channel. Techniques were developed to isolate DNA/PEI complexes encoding for different plasmids within each channel of the patterned PLG disk. DNA/PEI complexes encoding for DsRed (pDsRed/PEI) and EGFP (pEGFP/PEI) were pipetted individually into separate PLG channels. This deposition procedure maintained the activity of the complexes, as transfected cells were observed within the channels. Importantly, cells cultured in the channel with immobilized pDsRed expressed DsRed efficiently with no visual evidence of EGFP expression. Similarly, channels with immobilized pEGFP did not exhibit cellular expression of DsRed (Figure 7-6).

## *7.4 Discussion*

Bridges for nerve regeneration must provide signals that promote neuron survival and neurite extension, while simultaneously directing regenerating neurites across the injury. Bridges that provide neurotrophic factors at therapeutic concentrations while providing guidance could enable novel approaches for regeneration. This report demonstrates the ability to immobilize DNA complexes within PLG channels for localized secretion of neurotrophic factors. PLG was fabricated with channels of widths ranging from 100 to 250 µm. The dimensions of the channels mimic the channels within three-dimensional PLG scaffolds fabricated for in vivo spinal cord implantation [254]. Nonspecifically adsorbed complexes yielded efficient transfection within the

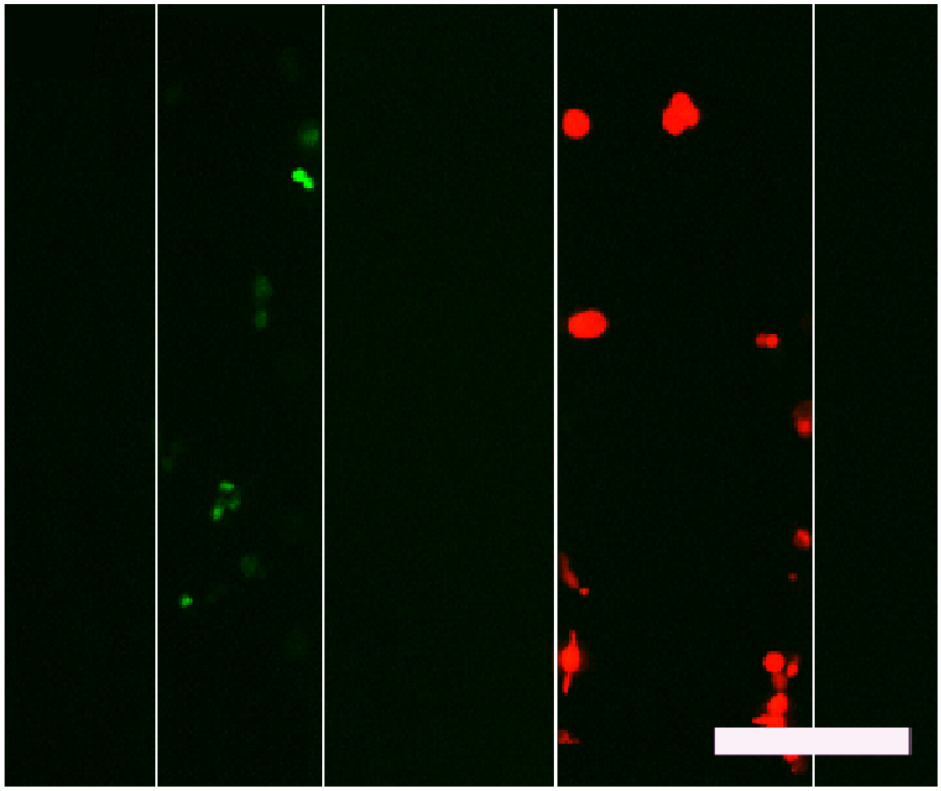

**Figure 7-6: Localized transfection in PLG channels.** Complexes encoding for EGFP or DsRed were deposited into separate PLG channels. DsRed (red) and EGFP (green) images are overlaid. Scale bar represents 100 μm.

channels, with efficiencies comparable to that on flat PLG disks, with transfection dependent upon the channel width and DNA amount. NGF secreted by the transfected cells supported neuron survival and neurite extension, and the size of the channel influenced the ability of the guidance channels to direct neurite extension.

The width of the channels influenced transfection efficiency and protein expression by cells cultured on the substrates. For incubation with 6 μg DNA, transfection efficiency and transgene expression in 100 μm channels were significantly lower than in 250 μm channels (Figure 7-3d,e). An increased number of large complexes were present in the smaller channels relative to the 250 μm channel (Figure 7-2), which may result from aggregation of the complexes and thus reducing the transfection efficiency [324, 325]. The greater surface area in the 250 μm channels relative to smaller channels may enable complexes to deposit independently. Complexes in the smaller channels presumably aggregate when they deposit adjacent to or on neighboring complexes, which could limit either cellular internalization or trafficking.

Neurons cultured in the 100 μm PLG channels extended longer primary neurites and exhibited significantly less branching as compared to neurons in larger channels. Primary neurites extend directly from the neuron cell soma and secondary neurites branch from the primary, which is hypothesized to occur in the absence of guidance cues in order to explore the environment [326]. As branching occurs, the growth of a primary neurite slows and is followed by cytoskeleton rearrangement and extension of a secondary growth cone [250]. A higher ratio of primary neurites is desired, as branching results in several shorter neurites, and longer primary neurites are more likely to cross a lesion. Primary neurite extension was greater and branching was minimal in the 100 μm channel, suggesting a directional cue within the channel. This

directional cue may be physical guidance resulting from the channel walls. The closer spacing of the walls in the 100 µm channel relative to larger channels increases the probability that a neurite will contact the wall and extend parallel to it. Previously, channels 20-30 µm wide (the same order of magnitude as filopodia) directed neurites down the channel, potentially by limiting the angles at which the microtubules and actin filaments accumulate and assemble within the neurite shaft and growth cone [250].

Transfected accessory cells cultured within channel walls resulted in localized secretion of NGF at the PLG surface. Neurons can extend neurites across micropatterned grooves to span the channel [327]; however, neurites spanning the channel were not observed in this report. Neurotrophic factor expression on the polymer likely maintains the neurites at the surface, and can also facilitate physical guidance. Furthermore, localized secretion of the therapeutic factor will concentrate the secreted protein and can potentially maintain the protein at a therapeutic level. Neurons cultured in the 100 µm channels exhibited an increase in primary neurite density as compared to the larger channels, which was independent of the NGF concentration (Figure 7-5f). Additionally, the extent of this increase in primary neurite density was higher when neurons were co-cultured with pNGF transfected cells as compared to neurons with NGF added to the media. Together, these results suggest the pNGF transfected cells may also direct extending neurites, in addition to the guidance by the channel walls.

The system presented here may offer specific advantages over previously developed methods to promote and direct neurite extension. Patterning adhesion molecules (e.g., ECM proteins) can guide cellular adhesion and neurite extension [293-295]. A challenge in patterning adhesive proteins or peptides to guide cellular processes in vivo is the nonspecific adsorption of various

proteins present in serum, or proteins deposited by the cells, which can mask or displace the immobilized molecules. Alternatively, physical barriers have been fabricated using a photolithographic technique to pattern polyimide walls with widths ranging from 20 to 60 µm [250]. While the physical barriers with smaller widths provided a more efficient physical guidance, regenerating neurites in vivo are likely to grow in bundles, and may require channels on the order of 100 µm in diameter [328]. Importantly, physical barriers or patterned ECM can provide necessary directional cues, but do not maintain therapeutic levels of growth promoting signals, which is a factor limiting regeneration in vivo. The developed system provides physical guidance, while simultaneously altering the expression profile of cells cultured in the channels. Gene delivery from tissue engineering scaffolds can alter gene expression for time scales on the order of months [12]. Here, the sustained expression can maintain therapeutic concentrations with transfected cells localized to the PLG in order to provide a path across the lesion.

The immobilization of DNA complexes to the PLG enabled the localization of individual genes at specific channels, which has not be demonstrated to our knowledge and would be challenging using traditional drug delivery methods. The ability to localize protein production to specific regions of a tissue engineering scaffold may facilitate the regeneration of complex tissues, such as the spinal cord. The white matter of the spinal cord contains several distinct tracts, both motor and sensory, that respond differentially to various neurotrophic factors, such as NGF, neurotrophins (NT-3, NT-4/5), glial-derived and brain-derived neurotrophic factor (GDNF and BDNF) [329]. For example, NGF promotes the growth of sensory neurons [330], while combinations of BDNF, GDNF, and NT-3 promote the growth of axons within the corticospinal tract [331]. Tissue engineering strategies for spinal cord regeneration may require that factor

delivery be spatially controlled to target the various axon populations within the spinal cord. In this report, the patterned deposition of DNA complexes produced localized expression of the proteins, with no cells in the EGFP channel expressing DsRed, and vice versa (Figure 7-6). The system presented here extends the capabilities of substrate-mediated delivery on patterned PLG, and has implications for tailoring individual channels to recreate the complex architecture of the spinal cord.

## *7.5 Conclusions*

PLG substrates that promote and direct axonal elongation were developed using topographically patterned PLG and gene delivery. Gene delivery by immobilization to the PLG surface resulted in transfection efficiency and transgene expression dependent upon the channel width and DNA amount. An in vitro neuronal co-culture model demonstrated that neurons cultured in smaller width PLG microchannels exhibited a greater degree of directionality and less secondary sprouting than larger channels. Additionally, surface immobilization enabled gene transfer to be localized to specific regions of the polymer, which may facilitate the regeneration of complex tissues. These studies have identified design principles for translation to three-dimensional constructs and in vivo nerve regeneration.

# Chapter 8

# Non-viral Gene Delivery Transfection Profiles Influence Neuronal Processes in an In Vitro Co-culture Model

## *8.1 Introduction*

Gene delivery from biomaterials has been employed to achieve localized expression of proteins for extended times, with many applications in disease treatment and tissue regeneration. The biomaterial serves to maintain DNA concentration locally, and sustained release provides prolonged opportunities for cellular transfection. These delivery systems present applications for gene therapy, for the treatment of cancer [332, 333] or inherited genetic disorders [334], and tissue regeneration [12]. In regenerative medicine, the biomaterial (scaffold) functions to maintain a physical space at a lesion site, while promoting cellular processes (e.g., adhesion, migration) necessary to regenerate healthy tissue [16]. Gene delivery from the tissue engineering scaffold can induce expression of tissue inductive factors to further stimulate the cellular processes required for regeneration [11].

Non-viral gene delivery from tissue engineering scaffolds has been employed to induce expression of tissue inductive factors, such as BMP-4 for bone regeneration [335], VEGF for angiogenesis [12], and TGF-β1 for wound healing [65]. Non-viral vectors are delivered as plasmid or plasmid condensed with cationic lipids or polymers (i.e. complexes) to facilitate internalization and trafficking [35]. Vectors are delivered to progenitor cells surrounding or infiltrating the scaffold, and transfected cells behave as bioreactors, secreting the protein of

interest. The factors act in a paracrine manner to stimulate adjacent cells to promote the desired responses. Although the duration of expression can influence the response, the number and distribution of transfected cells and the expression level are also critical design considerations [104]. Since transfected cells secrete diffusible proteins, their number, distribution, and expression level determine the concentration profile of inductive factors within the tissue. Concentration gradients of inductive factors are linked to proper cellular organization and tissue architecture during embryogenesis [269], and tissue regeneration strategies must recapitulate tissue architecture to regain function.

The ability of localized gradients to alter tissue structure has been characterized in the nervous system during development and regeneration. Gradients of neurotrophic factors, such as nerve growth factor (NGF) and neurotrophin-3 (NT-3), guide axon extension in vitro [336, 337]. The leading edge of an axon, the growth cone, is responsible for gradient detection in the extracellular environment and subsequently directs axons along a specific path [273]. Non-viral gene delivery provides a method to achieve localized secretion and gradients of neurotrophic factors. However, the manner to deliver genes encoding for neurotrophic factors to direct axon extension is poorly understood. The local concentration at the growth cone is a critical factor, as neurotrophic factors released from an individual cell can alter the structure of nearby neurites on an exquisitely local scale [338].

Chapter 8 investigates neuronal responses to varying NGF transfection profiles produced by non-viral gene delivery in vitro. We hypothesized that varying the extent of transgene expression and percentage of transfected cells will alter the neurotrophic factor gradients formed by localized expression and secretion. Different transfection profiles were established by altering

the type and amount of complexing agent and the amount of DNA administered to HEK293T cells. A co-culture model of transfected accessory cells and neurons was employed to investigate neuron survival and neurite outgrowth, branching, and guidance in response to the different transfection profiles. The gradients that develop from transfected cells were mathematically modeled and correlated to responses observed experimentally. The in vitro system presented in this Chapter provides insight into the rational design of tissue engineering scaffolds for nerve regeneration, and can be applied to the regeneration of many tissues with complex architectures.

## *8.2 Experimental Procedures*

### *8.2.1 Plasmids and Reagents*

Plasmid was purified from bacterial culture using Qiagen (Santa Clara, CA) reagents and stored in Tris-EDTA buffer at −20 °C. The plasmid pEGFP-Luc has EGFP in the vector backbone with a CMV promoter and was purchased from Clontech (Mountain View, CA). The plasmid pNGF has full length mouse NGF in the RK5 vector backbone with a CMV promoter and was a gift from Dr. Hiroshi Nomoto (Gifu Pharmaceutical University, Japan). All chemicals were purchased from Sigma-Aldrich (St. Louis, MO) and media components from Invitrogen (Carlsbad, CA) unless otherwise specified.

### *8.2.2 HEK293T Cell Culture*

The human embryonic kidney cell line (HEK293T) was purchased from the American Type Culture Collection (ATCC) (Manassas,VA). HEK293T cells were maintained in T-75 flasks with media change every 48 h and passage every 60 h in DMEM supplemented with 10% heat-inactivated fetal bovine serum, 1% penicillin/streptomycin, and 1% sodium pyruvate at 37 °C

and 5% $CO_2$. For all assays, tissue culture polystyrene wells were precoated with poly-L-lysine (MW 30,000 – 70,000) by incubating a 0.01% solution in wells for 1 h.

### *8.2.3 Establishment of Transfection Profiles*

HEK293T cells (3 X $10^4$ cells/well) were seeded in 24-wells and cultured for 16 h using conditions described above. Poly(ethylene imine) complexes (polyplexes) were formed by diluting the desired amount of PEI (25 kDa, branched) (N/P 10 or 25) or plasmid (pEGFP-Luc, 0.15 or 0.3 μg/well) in tris-buffered saline, mixing by vortex, and incubating for 15 min. Lipofectamine$^{TM}$2000 complexes (lipoplexes) were formed by diluting the desired amount of LF$^{TM}$2000 (Invitrogen) (1:1 plasmid:lipid) or plasmid (pEGFP-Luc, 0.5 μg/well) in DMEM, mixed by gentle pipetting, and incubated for 20 min. 16 h after HEK293T seeding, nonviral complexes were added to the culture medium and the cells were incubated for 24 h. After incubation, cultures were assayed for either transfection efficiency or extent of transgene expression. To assay transfection efficiency, cultures were imaged on a Leica inverted fluorescence microscope with a cooled CCD camera (Photometrics; Tucson, AZ) using MetaVue (Universal Imaging; Downingtown, PA) acquisition software for EGFP positive cells, followed by Hoechst 33258 imaging of the cell population. EGFP positive cells and total cells were counted using ImageJ software (NIH). To assay extent of transgene expression, cells were lysed and assayed using a luminometer (Turner Biosystems) set for a 3-s delay with signal integration for 10 s. Luciferase levels were normalized to total protein in the sample, quantified by the BCA protein assay (Pierce; Rockford, IL).

### *8.2.4 Quantification of NGF Expression*

To assay NGF expression, transfection profiles cultures were performed as described above, with replacement of the pEGFP-Luc plasmid with pRK5-NGF. 24 h after the addition of nonviral complexes, the culture media were analyzed for NGF concentration using a ChemiKine NGF Sandwich ELISA kit (Millipore; Billerica, MA).

### *8.2.5 Neuronal Responses to Transfection Profiles*

A neuronal co-culture model was employed to investigate neuronal responses to the different NGF transfection profiles. NGF transfection profile cultures were performed as described above. 8 h after the addition of complexes, HEK293T cells were rinsed with PBS. Dorsal root ganglia (DRG) explants were isolated from 8-day chicken embryos (MI State University; East Lansing, MI), dissociated using methods described previously [302], and seeded on HEK293T cultures. 48 h after neuron seeding, cultures were stained for the neuron-specific class III β-tubulin by incubating fixed cells in TUJ1 antibody (Covance; Berkely, CA) diluted in 5% normal goat serum (Vector Labs; Burlingame, CA) in PBS for 1 h followed by incubation in TRITC-conjugated goat anti-mouse secondary antibody (Jackson Immunoresearch; West Grove, PA) in PBS for 30 min. Co-cultures were imaged on a Leica inverted fluorescence microscope with a cooled CCD camera (Photometrics; Tucson, AZ) using MetaVue (Universal Imaging; Downingtown, PA) acquisition software. Neurite length was quantified using the tracing algorithm in the NeuronJ plug-in for ImageJ [284] and normalized to either surface area or sprouting neurons.

To assess growth cone morphology, cultures were performed as described above, with the exception of using poly-l-lysine coated glass chamber wells, in order to image with relatively

high magnification. Co-cultures were imaged on the Leica inverted fluorescence microscope, at high magnification. Growth cone morphology was quantified by tracing the length of the growth cone in ImageJ (NIH).

### *8.2.6 Mathematical Modeling of Concentration Gradients*

Mathematical modeling of NGF diffusion was used to predict the concentration gradient surrounding a transfected cell for each transfection profile, using methods described previously [339]. Briefly, Equation 8-1 describes one-component diffusion in three dimensions in a continuous medium with a term for protein degradation:

$$\frac{\partial C}{\partial t} = D\left[\frac{\partial^2 C}{\partial x^2} + \frac{\partial^2 C}{\partial y^2} + \frac{\partial^2 C}{\partial z^2}\right] - kC \tag{8-1}$$

where C is the concentration, D is the diffusivity of the protein, and k is the rate constant for protein degradation. The Crank–Nicolson implicit method was employed to solve numerically the partial differential equation. The initial condition is a zero concentration throughout the culture (Equation 8-2). The boundary conditions indicate a flux (q), which is determined from the protein production rate, from an individual transfected cell (Equation 8-3), and no flux boundary conditions elsewhere.

$$C(x, y, z, t = 0) = 0 \tag{8-2}$$

$$-D\frac{\partial C}{\partial z}(x = x_{trans}, y = y_{trans}, z = 0, t) = q \tag{8-3}$$

Note that the location of a single transfected cell is defined at $x = x_{trans}$ and $y = y_{trans}$. The average distance between two transfected cells was calculated from experimentally quantified cell confluency and transfection efficiency. The boundaries in the x- and y-directions were defined as the average distance between transfected cells for each condition. The boundary in the z-

direction was set equal to 4 mm, the approximate height of the culture medium. The production rate of NGF by cells transfected with the pRK5-NGF plasmid was estimated from ELISA data. The value for the diffusivity of NGF was determined from published reports to be $2.5 \times 10^{-7}$ $cm^2/s$ [285], and the diffusivity that incorporated reversible binding of the ligand to the accessory cell surface was estimated using Equation 8-4:

$$D_e = \frac{D}{(R+1)} \tag{8-4}$$

Where $D_e$ is the effective diffusion constant, and R is a dimensionless coefficient, calculated by the equation S = RC, where S is the amount of ligand bound to the surface, and C is the local free concentration (Crank, 1975).

Concentration gradient analysis was performed in terms of the absolute concentration gradient (Equation 8-5) and the fractional concentration gradient (Equation 8-6):

$$\left.\frac{dC}{dx}\right|_n = \frac{C_{n+1} - C_n}{x_{n+1} - x_n} \tag{8-5}$$

$$\left.\frac{dC}{C}\right|_n = \frac{C_{n-1} - C_{n+1}}{C_{n-1}} \tag{8-6}$$

## *8.2.7 Statistics*

Statistical analysis was performed using JMP software (SAS Institute, Cary, NC). Comparative analyses were executed using oneway analysis of variance with Tukey post-tests, at a 95% confidence level. For each experiment, all conditions were performed in triplicate. All experiments were performed in duplicate.

## *8.3 Results*

### *8.3.1 Development of Transfection Profiles*

Three distinct transfection profiles, in terms of transfection efficiency (percent of EGFP expressing cells) (Figure 8-1a-c) and extent of transgene expression (luciferase reporter gene levels), were developed (Table 8-1). The transfection profiles were defined as *profile 1*, *profile 2*, and *profile 3*. Relatively low transfection efficiency was achieved by complexing plasmid with the cationic polymer, poly(ethylene imine) (PEI) (*profile 1* and *profile 2*), while high transfection efficiency was achieved by complexing plasmid with the cationic lipid, Lipofectamine2000 (*profile 3*). The extent of transgene expression increased 500-fold from *profile 1* to *profile 2* by increasing the N/P ratio (10 to 25) and the amount of plasmid administered (0.15 to 0.30 μg/well), while maintaining relatively low transfection efficiency. *Profile 3* returned a significantly higher extent of transgene expression as compared to *profile 1*, and a marginally higher extent of transgene expression as compared to *profile 2* by increasing the amount of plasmid administered and complexing with Lipofectamine2000.

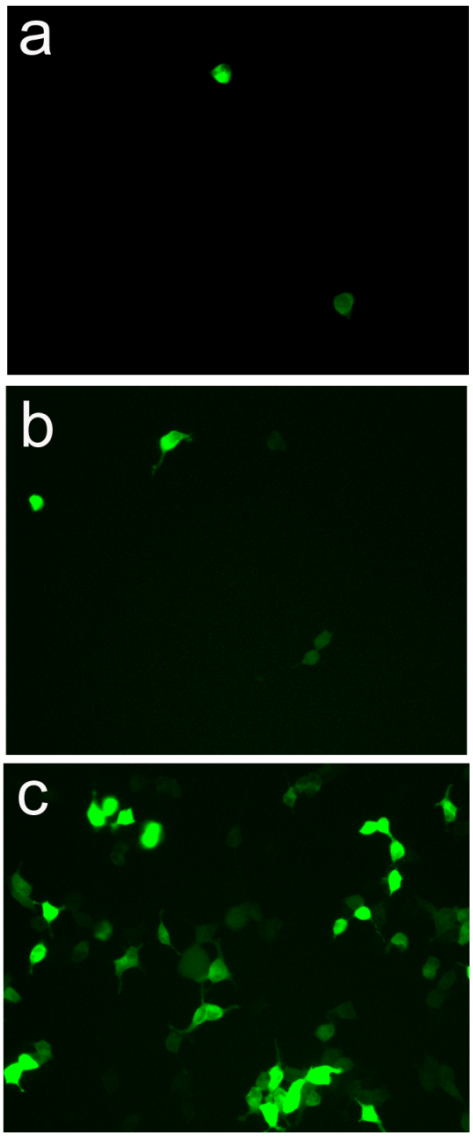


**Figure 8-1: Three transfection profiles.** EGFP expressing HEK293T cells (green), with *profile 1* (a), *profile 2* (b), and *profile 3* (c).

| | Complexing Agent | DNA amount (μg/well) | Transfection efficiency (% of total) | Transgene expression (RLU/mg) |
|---|---|---|---|---|
| Profile 1 | PEI, N/P = 10 | 0.15 | $1.3 \pm 0.3^{a}$ | $1.5\ (\pm 0.2) \times 10^{4a}$ |
| Profile 2 | PEI, N/P = 25 | 0.30 | $2.9 \pm 0.9^{a}$ | $7.3\ (\pm 3.2) \times 10^{7b}$ |
| Profile 3 | LF2000, 1:1 | 0.50 | $40 \pm 2.3^{b}$ | $3.9\ (\pm 0.2) \times 10^{8b}$ |

**Table 8-1:** Characterization of three distinct transfection profiles. Values are reported as mean ± SEM. Significant differences are indicated by different letters ($p < 0.05$).

### *8.3.2 NGF Expression and Diffusion*

The developed transfection profiles were employed to determine expression levels of the neurotrophic factor, NGF. As expected, *profile 1* returned a relatively low NGF concentration after 24 h culture (0.17 ± 0.03 ng/ml) as compared to *profile 2* (4.2 ± 0.9 ng/ml) and *profile 3* (40.4 ± 0.9 ng/ml) (Figure 8-2). NGF expression levels were combined with the previously calculated transfection efficiencies to determine the average NGF production rate by a single transfected cell for each transfection profile (Table 8-2). Transfection efficiencies were also employed to estimate the average distance between two transfected cells for each profile.

We hypothesized that localized secretion and diffusion of NGF from a transfected cell would result in a concentration gradient extending from the transfected cell. To evaluate this hypothesis, the values from Table 8-2 were incorporated into a three-dimensional mathematical model of NGF diffusion from a transfected cell for the three transfection profiles. NGF concentration gradients were predicted for the three transfection profiles, and the maximum NGF concentrations, occurring at the sites of production, were 1.2 ng/ml (*profile 1*, Figure 8-3a), 20 ng/ml (*profile 2*, Figure 8-3b), and 107 ng/ml (*profile 3*, Figure 8-3c) at the time of assay, 48 h. Note that the number of peaks in each graph varies, depending on the number of transfected cells that occur over the distance x and y = 1 mm. The distance between two transfected cells

influenced the minimum NGF concentrations, since the gradient from one transfected cell overlapped the nearest transfected cell, and the predicted minimum NGF concentrations were 0.3 ng/ml (*profile 1*, Figure 8-3a), 8.9 ng/ml (*profile 2*, Figure 8-3b), and 99 ng/ml (*profile 3*, Figure 8-3c).

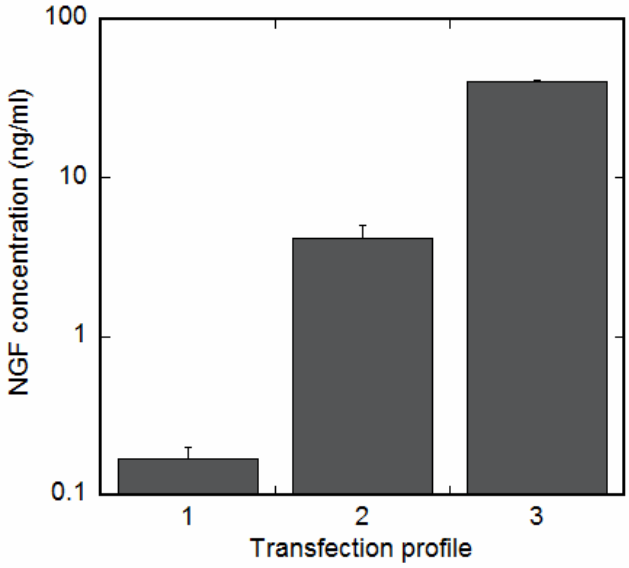


**Figure 8-2: Nerve growth factor expression by different transfection profiles.** Quantification of NGF production 24 h after non-viral DNA complexes were added to the culture medium. Values are reported as mean ± SEM.

| | NGF production rate (pg/cell/min) | Distance between transfected cells (μm) |
|---|---|---|
| Profile 1 | $7.1 \times 10^{-5}$ | 481 |
| Profile 2 | $9.3 \times 10^{-4}$ | 350 |
| Profile 3 | $6.8 \times 10^{-4}$ | 96 |

**Table 8-2:** Calculated NGF production rates and estimated distance between transfected cells for three transfection profiles.

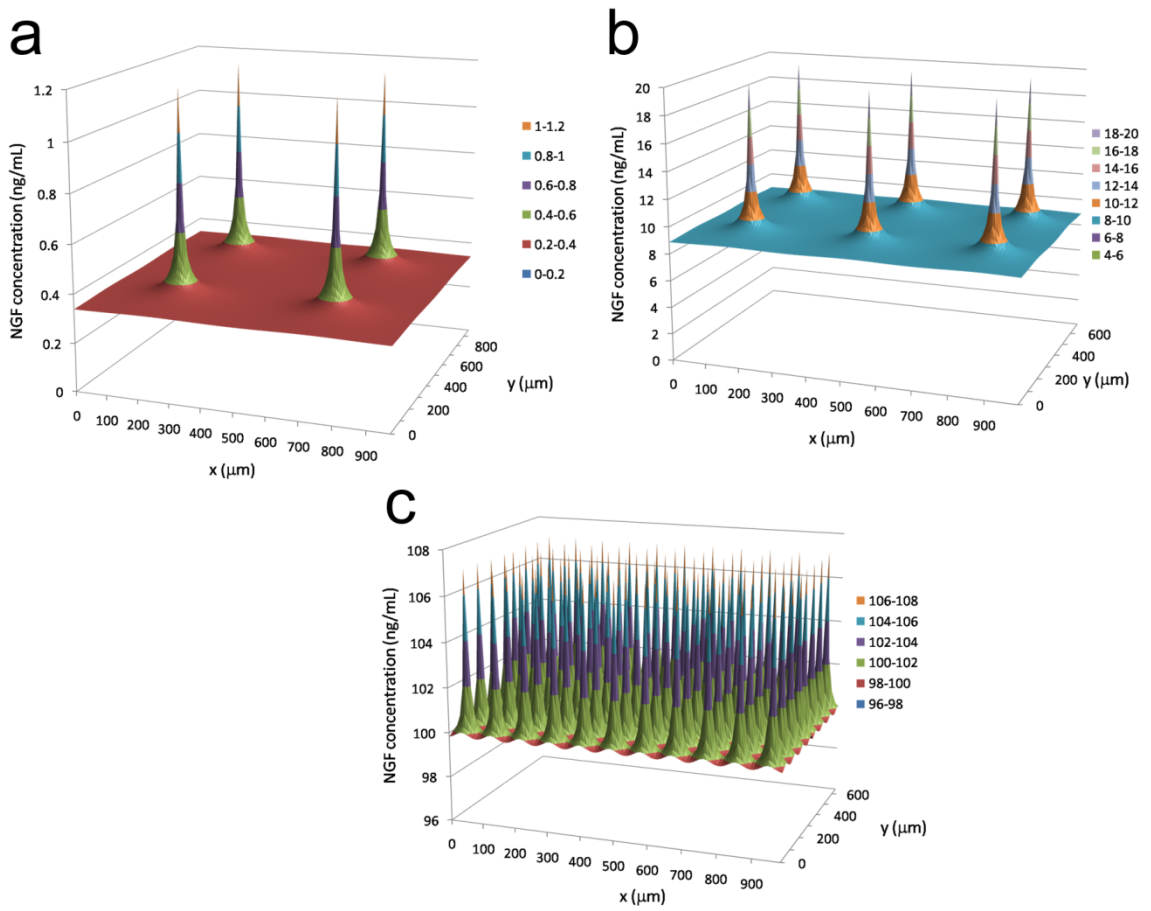


**Figure 8-3: Predicted concentration gradients.** Mathematical model predictions for NGF concentration profiles at 48 h after nonviral DNA complexes were added to the culture medium for *profile 1* (a), *profile 2* (b), and *profile 3* (c).

### *8.3.3 Neuronal Responses to Transfection Profiles*

To investigate neuronal responses to different microenvironmental concentrations of NGF, DRG neurons were co-cultured with HEK293T cells expressing NGF with the three established transfection profiles. Importantly, we have established previously that HEK293T cells alone, without pNGF transfection, do not support neuron survival or neurite extension. Therefore, any neuronal responses observed can be directly attributed to NGF expression. Neurons cultured on *profile 1* generally exhibited a unipolar morphology, with primary neurites extending from one end of the cell soma, and few branches (Figure 8-4a). Neurons cultured on *profile 2* and *profile 3* exhibited unipolar and bipolar neurite outgrowth, with many branches creating a dense arbor (Figure 8-4b, c).

Subsequently, neuron survival and neurite outgrowth were quantitatively evaluated. Total neurite outgrowth, normalized to surface area, was significantly higher on *profile 3* ($76.0 \pm 10.1$ $cm^{-1}$) as compared to *profile 1* ($28.9 \pm 5.4$ $cm^{-1}$) and *profile 2* ($19.1 \pm 1.6$ $cm^{-1}$) (Figure 8-5a, $p < 0.05$). Additionally, neuron survival was significantly higher with neurons cultured on *profile 3* as compared to *profile 1* and *profile 2* (data not shown). Interestingly, extent of neurite outgrowth per sprouting neuron was higher with neurons cultured on *profile 1* ($290.9 \pm 3.7$ μm) as compared to *profile 2* ($128.9 \pm 13.4$ μm) and *profile 3* ($170.4 \pm 22.3$ μm) (Figure 8-5b, $p < 0.05$). The greater extent of neurite outgrowth per neuron in *profile 1* was due to greater primary neurite outgrowth (Figure 8-5b, $p < 0.05$), as the extent of branching per neuron was similar for the three profiles (Figure 8-5b).

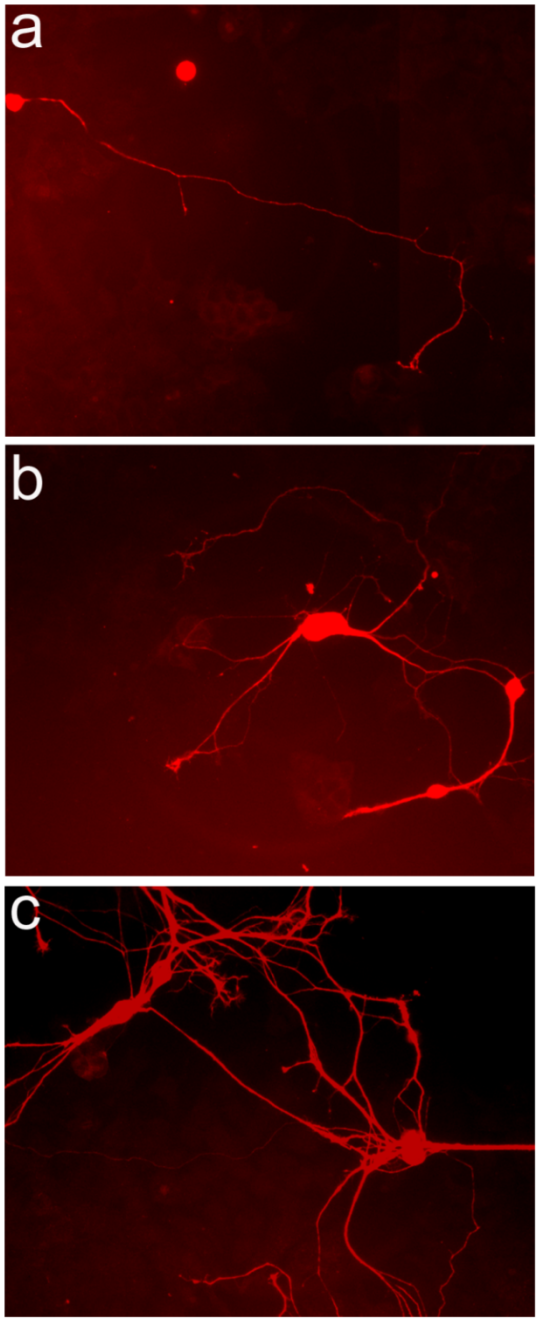


**Figure 8-4: Neurons co-cultured on three transfection profiles.** Neurons co-cultured on HEK293T cells expressing NGF with three distinct transfection profiles: *profile 1* (a), *profile 2* (b), and *profile 3* (c).

Neurite outgrowth was evaluated further by quantifying the average length of a single neurite for the three profiles. Primary neurites were significantly longer with neurons cultured on *profile 1* (219.8 ± 14.9 μm) as compared to *profile 2* (68.3 ± 6.2 μm) and *profile 3* (58.0 ± 6.5 μm) (Figure 8-5c, $p < 0.05$). The average length of a branching neurite was higher with neurons cultured on *profile 1* (71.2 ± 13.7 μm) as compared to *profile 2* (36.0 ± 6.6 μm) and *profile 3* (26.7 ± 2.0 μm) (Figure 8-5c, $p < 0.05$). The average number of primary neurites extending from a neuron was 1.2 ± 0.1 for *profile 1*, which confirmed a unipolar morphology (Figure 8-5d). The average number of primary neurites per neuron increased with neurons cultured on *profile 2* (1.5 ± 0.1) and *profile 3* (2.2 ± 0.1), demonstrating a transition to a bipolar morphology (Figure 8-5d, $p < 0.05$). The average number of branching neurites per neuron was similar for *profile 1* (0.65 ± 0.05) and *profile 2* (0.69 ± 0.11), and increased with neurons cultured on *profile 3* (1.6 ± 0.1) (Figure 8-5d, $p < 0.05$).

To assess the source for differences in neurite outgrowth observed by the transfection profiles, co-cultures were performed without pNGF transfection, but with varying doses of NGF added to the culture medium. Eliminating transfected cells allowed for the investigation of neuronal responses initiated by changes in mean NGF concentration, and not the differences in microenvironmental concentrations of NGF caused by transfection and resultant concentration gradients. Similar to transfection profiles, the total neurite outgrowth, normalized to surface area, increased with increasing NGF concentration (0.10 to 50 ng/ml) (Figure 8-6a, $p < 0.05$). Additionally, neuron survival increased with increasing NGF concentration (data not shown). However, extent of neurite outgrowth normalized to sprouting neurons was similar for all NGF

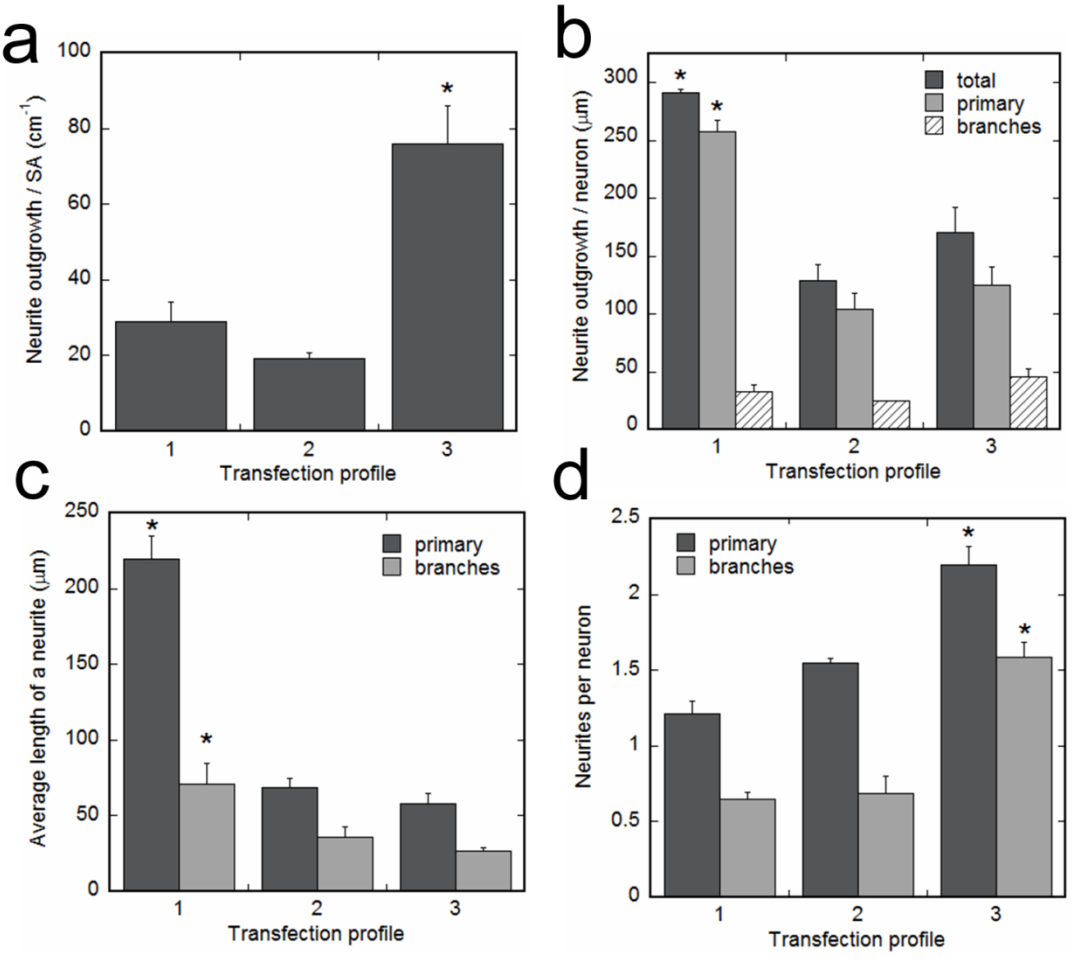


**Figure 8-5: Quantification of neurite outgrowth from neurons co-cultured on three transfection profiles.** Neurite outgrowth and branching was quantified with neurons cultured on HEK293T cells with three distinct transfection profiles. Neurite outgrowth normalized to surface area (a). Neurite outgrowth normalized to sprouting neurons (b). Average length of primary and branching neurites (c). Average number of neurites per neuron (d). Values are reported as mean ± SEM. Significant differences are indicated by * ($p < 0.05$).

concentrations (0.10 to 50 ng/ml) (Figure 8-6b). Additionally, the average length of a primary neurite and a branching neurite were statistically similar for all NGF concentrations (Figure 8-6c). The average number of primary neurites extending from a neuron ranged between 1.2 and 1.7 for all NGF concentrations, indicative of both unipolar and bipolar morphologies. The average number of branching neurites per neuron ranged between 0.35 and 0.70 for all NGF concentrations (Figure 8-6d).

### *8.3.4 Growth Cone Morphology*

To further evaluate the response triggered by varying transfection profiles, the growth cone morphology was investigated. Growth cones extending from neurites cultured on *profile 1* exhibited an elongated morphology, marked by long filopodia (Figure 8-7a) as compared to growth cones extending from neurites cultured on *profile 2* (Figure 8-7b) and *profile 3* (Figure 8-7c), which were marked by short filopodia. Quantitative evaluation of growth cone morphology revealed growth cones were longer when neurons were cultured on *profile 1* ($25.8 \pm 3.7$ μm) as compared to *profile 2* ($14.1 \pm 1.6$ μm) and *profile 3* ($11.9 \pm 0.4$ μm) (Figure 8-7d, $p < 0.05$).

## *8.4 Discussion*

In this manuscript, a range of transfection profiles were employed to investigate neuronal responses to various gradients formed around NGF-expressing cells. Transfection efficiency, extent of transgene expression, and the resultant concentration gradients were altered by changing the type and amount of complexing agent and the amount of plasmid delivered.

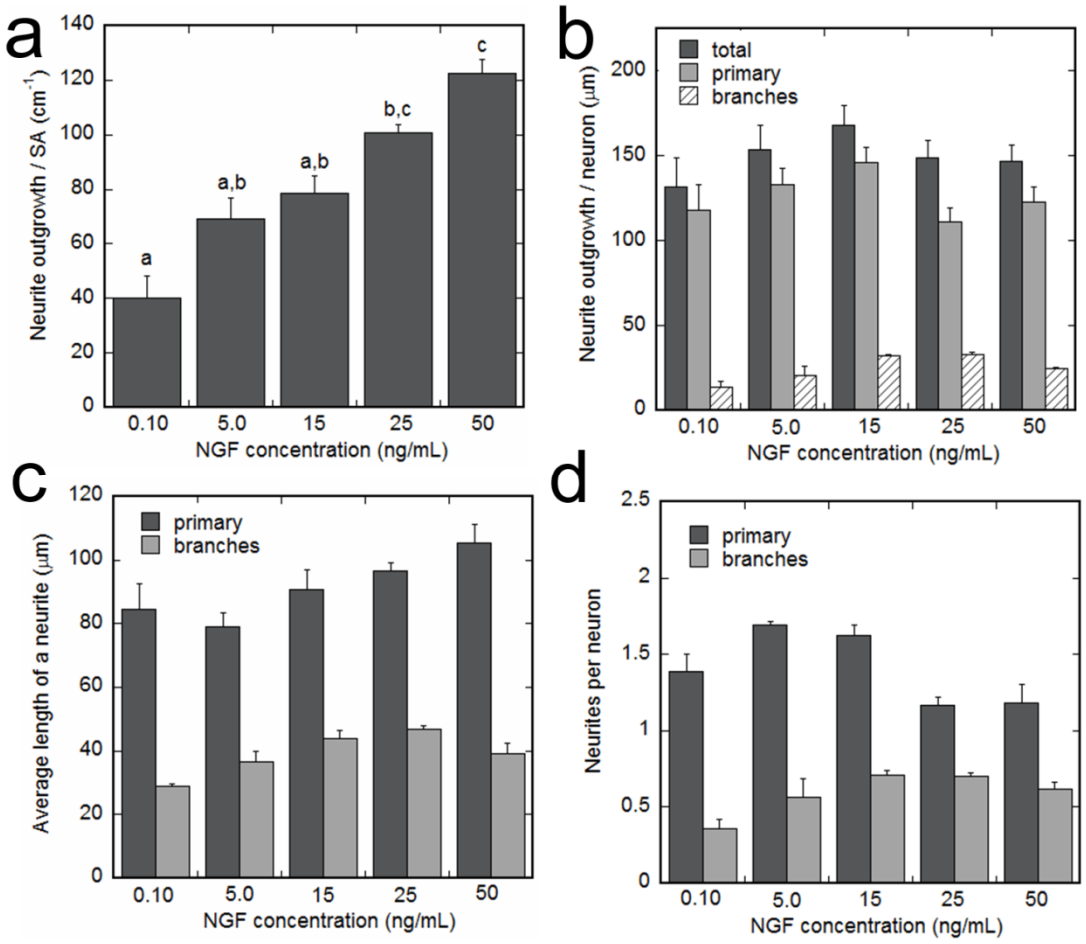


**Figure 8-6: Quantification of neurite outgrowth from neurons co-cultured on non-transfected accessory cells.** Neurite outgrowth and branching was quantified with neurons cultured on HEK293T cells with NGF supplemented culture medium. Neurite outgrowth normalized to surface area (a). Neurite outgrowth normalized to sprouting neurons (b). Average length of primary and branching neurites (c). Average number of neurites per neuron (d). Values are reported as mean ± SEM. Significant differences are indicated by different letters ($p < 0.05$).

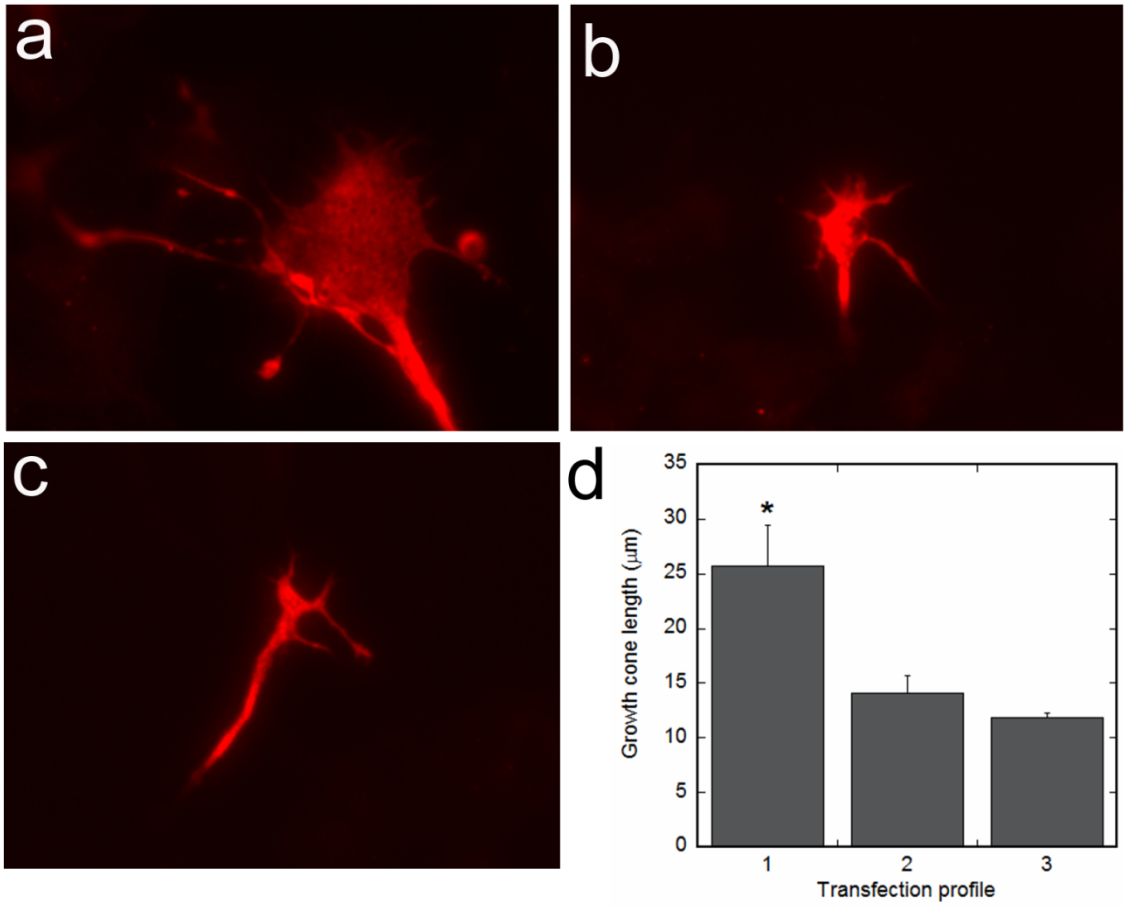


**Figure 8-7: Neurite growth cone morphology.** Neurite growth cones extending from neurons co-cultured on HEK293T cells expressing NGF with distinct transfection profiles, *profile 1* (a), *profile 2* (b), and *profile 3* (c). Quantification of filopodia length (d). Values are reported as mean ± SEM. Significant differences are indicated by * ($p < 0.05$).

Transfected cells expressing NGF supported neuron survival and neurite outgrowth, with the extent of survival and outgrowth directly dependent on the mean concentration of NGF in the culture medium. Neurons cultured on *profile 3* extended a higher number of neurites per neuron as compared to *profile 1* and *profile 2*. However, neurons cultured on *profile 1* extended significantly longer neurites as compared to neurons cultured on *profile 2*, *profile 3*, and non-transfected accessory cells with NGF added to the culture medium. Moreover, neurons cultured on *profile 1* exhibited elongated growth cone morphology, marked by longer filopodia, as compared to neurons cultured on *profile 2* and *profile 3*. These findings highlight the importance of considering both transfection efficiency and extent of transgene expression, rather than the mean concentration of a therapeutic factor, when applying gene delivery for tissue engineering. We highlight the importance in nerve tissue engineering strategies, but the *in vitro* system presented here can be applied to any regenerative strategy in which concentration gradients play a role, such as VEGF delivery for blood vessel formation [104] or PDGF delivery to recruit fibroblasts for wound healing [340].

Extent of neuron survival and neurite outgrowth, normalized to the culture surface area, was determined by the mean NGF concentration in the medium. Neurons cultured on *profile 3* exhibited higher levels of neurite outgrowth and neuron survival as compared to *profile 1* and *profile 2*. This difference was directly attributed to the mean NGF concentration in the medium, since co-cultures with non-transfected accessory cells and NGF supplemented medium exhibited higher neuron survival and neurite outgrowth with increasing NGF concentration. Additionally, NGF is a well known neurotrophic factor capable of eliciting survival and outgrowth cues [341].

The number of neurites extending from neurons and the extent of neurite outgrowth normalized to sprouting neurons varied with the different transfection profiles. The number of primary neurites per neuron was significantly higher on *profile 3* as compared to *profile 1* and *profile 2*, but decreased with increasing mean NGF concentration with non-transfected accessory cells. Additionally, the number of branches per neuron was significantly higher with *profile 3*, as compared to *profile 1* and *profile 2*, but did not change with non-transfected accessory cells supplemented with NGF. The differences in number of neurites for the different transfection profiles, therefore, could not be attributed to changes in mean NGF concentration. Moreover, the number of primary and branching neurites on *profile 3* was significantly higher as compared to non-transfected accessory cells with NGF supplemented medium, indicating the transfection profile is eliciting the responses observed with *profile 3*. Relatively high microenvironmental NGF concentrations in *profile 3*, as characterized by mathematical modeling, may initiate the higher number of primary and branching neurites. Conversely, total neurite outgrowth per sprouting neuron was significantly higher with *profile 1* as compared to *profile 2* and *profile 3*. Total neurite outgrowth remained consistent with varying mean NGF concentrations between 0.1 – 50 ng/ml, a range that includes the mean concentrations for the different transfection profiles. Additionally, neurite outgrowth per sprouting neuron was significantly higher with *profile 1* as compared to neurons cultured on non-transfected accessory cells with NGF supplemented culture medium, indicating transfection *profile 1* initiates the response.

The average length of primary and branching neurites and growth cone morphology varied with the different transfection profiles. Both primary and branching neurites were longer with neurons cultured on *profile 1* as compared to *profile 2* and *profile 3*, but did not change with non-

transfected accessory cells with varying mean NGF concentration in the culture medium. Moreover, primary and branching neurites extending from neurons cultured on *profile 1* were significantly longer than with neurons cultured on non-transfected accessory cells with NGF supplemented medium, regardless the dose, further indicating that the transfected cells in *profile 1* were eliciting the response. Longer neurites indicate the presence of a guidance cue in *profile 1*, suggesting the guidance cue directs neurites along a specific path without the need to pause and explore the extracellular environment. Moreover, the higher number of branching neurites observed in *profile 3* suggests the absence of a guidance cue in *profile 3*, since primary neurites must pause and extend branches to explore the environment. Growth cones extending from primary neurites with neurons cultured on *profile 1* exhibited elongated morphology, characteristic of polarized filopodia, as compared to growth cones from primary neurites with neurons cultured on *profile 2* and *profile 3*, which exhibited shorter filopodia, characteristic of paused neurites [342]. In the presence of a soluble guidance cue, filopodial numbers have been shown to be greater in the direction of the gradient [343] and highly motile growth cones adopt an elongated morphology [342]. The growth cone morphology detected in *profile 1* further supports the hypothesis that a guidance cue is present.

Experimental observations with number of branching neurites per neuron, average length of neurites, and growth cone morphology were consistent with a guidance cue provided by transfection *profile 1*. Gradients of NGF have been shown to direct neurites via a chemotactic guidance signal, and the NGF gradients that form around transfected cells in *profile 1* may guide neurites. Mathematical modeling was employed to calculate the absolute and fractional concentration gradients, both of which have been implicated in neurite guidance, for each

transfection profile. The absolute concentration gradient outside a single cell remained consistent over the 48 h time course, and ranged between 50-0.01 ng/ml/mm for *profile 1*, 660-0.5 ng/ml/mm for *profile 2*, and 480-20 ng/ml/mm for *profile 3* (Figure 8-8a). The fractional concentration gradient over the approximate width of the growth cone, 20 μm, varied along the 48 h time course. At t = 5 h the fractional concentration gradient ranged between 70-0.2% for *profile 1*, 64-0.1% for *profile 2*, and 16-0.7% for *profile 3*, and at t = 48 h ranged between 55-0.1% for *profile 1*, 44-0.1% for *profile 2*, and 6-0.2% for *profile 3* (Figure 8-8b). The absolute and fractional concentration gradients formed by transfected cells are within ranges that have previously been shown to guide neurites by spatial patterns of NGF expression. Absolute concentration gradients between 8-0.5 ng/ml/mm were shown to guide neurite extension [339], values well below the absolute gradients formed by a transfected cell in all three transfection profiles. Additionally, the fractional concentration gradients for all profiles and all time points were primarily above what has previously been shown to guide neurites with spatial patterns of gene expression (8.0-1.5%) [339]. Since the gradients achieved in all profiles should be capable of guiding neurites, the relatively high NGF expression levels in *profile 2* and *profile 3* may explain the absence of a guidance cue. Knowledge from leukocyte chemotaxis suggests that a chemotactic guidance signal is most effective if the mean concentration is kept near the dissociation constant for the ligand's receptor [2]. The dissociation constant for the p75 NGF receptor is 1 nM, and the dissociation constant for the trkA NGF receptor is 0.1 nM [303]. In

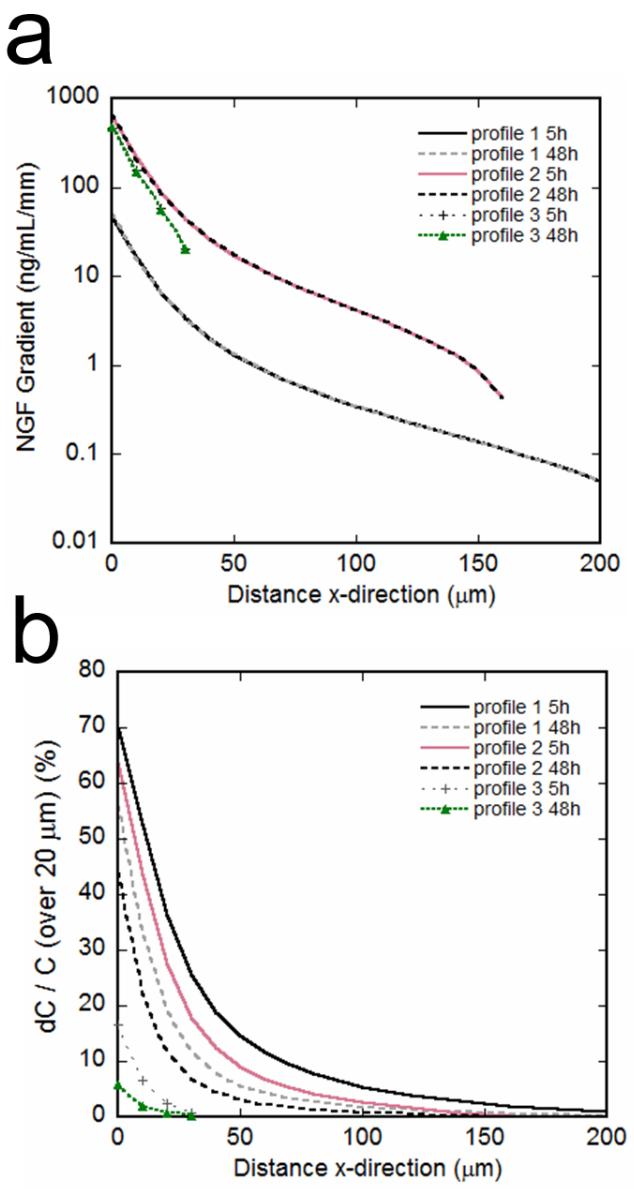


**Figure 8-8: Predicted NGF concentration gradients.** The predicted absolute concentration gradients (a) and fractional concentration gradients (b) from a single HEK293T cell expressing NGF with three distinct transfection profiles. Note that x = 0 is at the center of a transfected cell.

*profile 2*, microenvironmental concentrations reach 0.8 nM, well above the dissociation constant for the trkA receptor. In *profile 3*, microenvironmental concentrations reach 4 nM, a concentration well above the dissociation constants for both NGF receptors.

In this Chapter, we demonstrate that NGF microenvironmental concentrations resulting from pNGF transfected cells govern neuronal behavior, which is an important consideration in the design of gene delivery scaffolds for nerve regeneration. Relatively high levels of NGF expression and high percentage of transfected cells supported increased neuron survival, extent of neurite outgrowth, and number of extending neurites. Relatively low levels of NGF expression supported longer neurite lengths, presumably by the NGF gradients that formed around transfected cells. In nerve regeneration strategies, the stimulation of neuron survival and neurite outgrowth is critical. However, the local sprouting of axons is not necessarily indicative that neurons have become competent to sustain longer-distance elongation of axons [344]. Also critical in nerve regeneration strategies is the guidance of growing axons across the entire length of a lesion site to ultimately restore function. After peripheral nervous system injury, adult neurons have an inherent ability to switch from a branching morphology to an elongating morphology, extending longer neurites to span an injury site [344, 345]. This change in morphology is triggered by differences in gene expression after injury [346, 347], that do not readily occur in the central nervous system (CNS) after injury [348], and turning on those genes in the CNS leads to longer axon extension [349]. We present a method to promote elongation and minimal branching without altering gene expression within neurons, since gene therapy to neurons has proven to be difficult [350]. Moreover, different classes of neurons within the central nervous system, such as spinal sensory, corticospinal, and noradrenergic neurons, are

responsive to different neurotrophic factors or combinations of factors, such as NGF, NT-3, and BDNF, and additionally have been shown to behave as neurotropic factors at the site of injury [196, 351]. The system presented in this manuscript can be employed to identify ideal transfection profiles for different classes of CNS neurons. Importantly, current tissue engineering strategies to guide regenerating axons, such as patterned adhesion molecules [293, 352] or engineered protein gradients [353], may not be relevant in vivo for an extended period of time required to guide axons across a lesion, due to quick clearance of proteins or masking of adhesion molecules by nonspecific adsorption of proteins present in serum, or proteins deposited by the cells. Non-viral gene delivery from tissue engineering scaffolds has promoted transgene expression for up to 105 days [12], and therefore holds promise for providing long-term guidance signals. Importantly, gene delivery from nerve guidance bridges containing topographical guidance cues achieved transgene expression within a rat spinal cord hemisection injury model [238]. The combination of topographical guidance cues with the proper transfection profiles to guide axons may provide long term and synergistic axon guidance signals within a nerve lesion site [354].

We highlight the importance of considering transfection profiles when developing therapeutic strategies for nerve guidance, however, the *in vitro* system developed in this manuscript can be applied to many other tissue regeneration systems. Ozawa *et al.* [104] demonstrated that high levels of VEGF secretion by retrovirally transduced myoblasts induced the growth of abnormal blood vessels. Decreasing the number of cells transplanted, which decreased the total dose of VEGF, served to reduce the region in which abnormal blood vessel formation was observed. However, transplantation of cells that were selected for low VEGF

expression resulted in the formation of normal, mature vascular structures. The result was hypothesized to occur by the existence of gradients forming around VEGF-expressing myoblasts. The in vitro system presented in this work may be employed to define the VEGF concentration gradients capable of supporting healthy blood vessel growth. Moreover, the migration of various cell types, such as fibroblasts, macrophages, and keratinocytes are guided by gradients of factors, such as PDGF and IL-8, and contribute to the regulation of epithelialization, tissue remodeling, and angiogenesis during cutaneous wound healing [3]. The in vitro system presented in this work may be employed to determine proper transfection profiles to guide diverse cell types during wound healing. The controlled method to alter transfection profiles presented in this research, combined with well-characterized concentration gradients, provides a platform to investigate tissue responses to localized expression of therapeutic factors.

## *8.5 Conclusions*

In this Chapter, transfection profiles were developed, in terms of transfection efficiency and extent of transgene expression, by altering the type and amount of non-viral complexing agent, and amount of DNA administered. Mathematical modeling of NGF diffusion confirmed that concentration gradients form around NGF-expressing cells in each transfection profile. The NGF gradients produced by transfected cells in *profile 1* were capable of guiding neurites, as evidenced by the average length of neurites and growth cone morphology. We have demonstrated that the extent of NGF expression governs the ability of gradients to guide neurites. The in vitro system presented in this manuscript provides a tunable method to investigate cellular responses to varying transfection profiles, which may influence the architecture of regenerating tissue.

# Chapter 9

# Non-viral Vector Delivery from PEG-Hyaluronic Acid Hydrogels

## *9.1 Introduction*

The physical properties of natural and synthetic hydrogels are similar to those of the natural extracellular matrix, making these biomaterials appealing for numerous tissue engineering applications [355, 356]. Many naturally occurring biopolymers, such as hyaluronic acid (HA) [356] and collagen [357, 358], are generally considered to be biocompatible and can be used alone or in combination with synthetic polymers such as poly(ethylene glycol) (PEG). The natural polymers provide specific biological interactions or functionality, whereas the synthetic polymers can modulate the physical properties and can be synthesized cost effectively and reproducibly [356]. These polymers form 3D networks by crosslinking either chemically (e.g., acrylation), physically, or ionically [359, 360]. These crosslinking techniques are generally mild, allowing for the encapsulation of cells and other bioactive molecules. By manipulating the polymer composition and the cross-link density, hydrogels can be created with a range of physical properties and degradation rates.

The functionality of hydrogels used for tissue engineering can be enhanced by creating gels capable of localized delivery of therapeutic drugs, proteins, or genes. The controlled release of these bioactive molecules to surrounding tissue can be employed to promote the cellular processes (e.g., proliferation, differentiation) involved in tissue formation [361, 362]. For gene delivery in particular, localized release of plasmid or DNA complexes can transfect cells for the

sustained production of tissue inductive proteins [363, 364]. Hydrogels formed from a range of polymers have been employed for the controlled release of non-viral vectors, such as naked plasmid or cationic polymer/DNA complexes [358, 365-370]. For many hydrogels, release occurs primarily by diffusion, which can be influenced by physical properties such as water content, swelling ratio, and mesh size. The chemical composition of the hydrogel or the vector can also influence delivery, as vectors can reversibly associate with biomaterials to influence their transport and cellular internalization [361, 371, 372]. The different non-viral vectors can vary substantially in the properties, such as size and charge [371, 373], that will influence transport through a hydrogel. Naked plasmid is highly negatively charged and has a large hydrodynamic radius, but the delivery efficiency can be low due to plasmid degradation or ineffective internalization or trafficking. Complexation of the plasmid with cationic polymers or lipids can protect the plasmid against degradation, and package the plasmid to facilitate cellular internalization and trafficking. This complexation process, involving the self-assembly of the cationic polymer or lipid with the negatively charged phosphate backbone of DNA, may produce complexes with properties significantly different from the plasmid [371].

Hydrogels previously used as DNA delivery scaffolds rely on the release of the vectors as the hydrogel degrades, and oftentimes result in low levels of expression lasting only a few days [374]. Substrate-mediated gene delivery increases the local concentration of DNA within the cellular microenvironment and can overcome barriers to non-viral gene delivery, such as mass transport and complex aggregation [371]. Transgene expression can be enhanced with substrate-mediated gene delivery by modifying the interactions between the vector and substrate. In particular, negatively charged hydrophilic surfaces have been shown to increase vector binding

and transgene expression [85]. To incorporate substrate-mediated gene delivery into a hydrogel delivery system, the hydrogel must maintain the vectors within the matrix without quick release. Additionally, cells must infiltrate the hydrogel and be placed directly in the microenvironment with the hydrogel-associated vectors.

In this Chapter, the release of plasmid and DNA complexes from hydrogels was investigated. The composition of both the hydrogel and vector, and degradation rate of the hydrogel were systematically manipulated. Hydrogels were formed from a combination of PEG and HA. PEG was used for regulating and maintaining the hydrogel stability, while HA was chosen to alter the backbone charge and enable hydrogel degradation by the enzyme hyaluronidase (HAase) [375, 376]. The biopolymers were modified with acrylate groups to enable hydrogel formation by photocrosslinking, a relatively mild technique that can maintain the bioactivity of encapsulated vectors. Hydrogels with varying ratios of PEG and HA were formed containing either plasmid or DNA complexed with the cationic polymer polyethylenimine. Initial studies characterized the physical properties of the hydrogels, such as swelling ratio and degradation. Subsequently, the release rate of encapsulated plasmid and complexes was determined in the absence or presence of hyaluronidase to degrade HA. Photocrosslinking was combined with lithography techniques to spatially pattern DNA vectors within the hydrogel, which may expand their utility in numerous tissue engineering applications. Hydrogels were implanted into a subcutaneous mouse model to investigate cellular infiltration and in vivo DNA delivery.

## 9.2 Experimental Procedures

### 9.2.1 Materials and Methods

Hyaluronic acid was a generous gift from Genzyme Corporation (1.33 x $10^6$ Da, Cambridge, MA). N-hydroxysulfonosuccinimide sodium salt (sulfo-NHS), N-(3-dimethylaminopropyl)-N-ethylcarbodiimide hydrochloride (EDC), and adipic acid dihydrazide (AAD) were purchased from Sigma (St. Louis, MO). NHS-PEG Acryl (MW 3400) was purchased from Nektar Therapeutics (San Carlos, CA). Irgacure 2959 was purchased from Ciba Specialty Chemicals Corp. (Tarrytown, NY). Dual expression plasmid encoding for luciferase (LUC) and enhanced green fluorescent protein (EGFP) with a CMV promoter was purified from bacteria culture using Qiagen (Santa Clara, CA) reagents and stored in Tris-EDTA buffer (10 mM Tris, 1 mM EDTA, pH 7.4). Branched polyethylenimine (PEI, 25 kDa) was purchased from Aldrich (St. Louis, MO). All other reagents were purchased from Fisher Scientific (Fair Lawn, NJ) unless otherwise mentioned.

### 9.2.2 Synthesis and Characterization of Acrylated Hyaluronic Acid

HA/PEG hydrogels were created through modification of both HA and PEG with acrylate groups, which can crosslink the polymers following activation by exposure to UV light. HA-Acryl was obtained by a two-step process that involves the initial modification of hyaluronic acid with adipic acid dihydrazide (HA-AAD) as previously described [377], which was subsequently modified with NHS-PEG-Acryl. HA-AAD was characterized using a trinitrobenzene sulfonic acid (TNBS) assay (Pierce, Rockford, IL) to determine the percent of carboxyl groups replaced with hydrazide groups. HA-AAD was then dissolved in dd$H_2O$ (10 mg/ml HA-AAD), and 0.04 molar equivalents of NHS-PEG-Acryl were added and stirred for 16 hours at room temperature.

The reaction mixture was purified by dialysis, lyophilized, and stored at 4 $^{o}$C until use. Proton NMR spectroscopy was used to determine percent acrylation of the final product. NMR spectra were obtained using an INOVA 400 NMR (400 MHz). $D_2O$ (Acros Organic, Springfield, NJ) was used as a solvent for all samples, and the analysis was performed on an average of 16 scans.

### *9.2.3 Hydrogel Formation*

Solutions containing HA-Acryl and 4-arm PEG-Acryl (SunBio, Seoul, Korea) were prepared in PBS with 1% (wt/vol) of the water soluble photoinitiator, I2959 [378]. Unmodified Type 1 rat-tail collagen was also added at a concentration of 0.2 mg/ml, which was incorporated to support cell adhesion in vitro. The polymer solutions (100 μl) were placed in a 96 well plate, and exposed to UV light to initiate crosslinking. Plates were placed 2 cm from a UV lamp that had a wavelength centered at 365 nm (Spectroline Model SB 100P, Westbury, NY) for 2-7 minutes. Gelation was determined by sufficient stability for removal from the well. DNA was incorporated by mixing either plasmid or DNA/PEI complexes prior to gelation. For plasmid alone, pEGFP-LUC plasmid solution (50 μl of 1 mg/ml) was added. For the encapsulation of DNA complexes, complexes were formed as described in Bengali et al [371] and added to the biopolymer solutions. The final concentration of the DNA within the hydrogel was 33.3 μg/ml.

### *9.2.4 Determination of Hydrogel Physical Properties*

Hydrogels were prepared from 100 μl polymer solutions containing 1% (wt/vol) I2959, 0.2 mg/ml collagen and varying concentrations of HA-Acryl and 4-arm PEG-Acryl (Table 9-1). Hydrogels were allowed to swell overnight in dd$H_2O$ and were then blotted to remove excess water and weighed to obtain the swollen hydrogel mass, $M_s$. These hydrogels were then dried by heating to temperatures between 90-100 $^{o}$C to determine the final dry mass, $M_d$. Water content

and swelling ratios were then determined from the swollen and dry hydrogel masses. The percent water content was determined by Equation 9-1:

$$\left(\frac{M_s - M_d}{M_s}\right)\times 100 = \text{water content} \tag{9-1}$$

The mass based swelling ratio, $Q_M$, was calculated by dividing the hydrogel mass after swelling, $M_s$, by the mass after the hydrogel has dried, $M_d$. The volumetric based swelling ratio, $Q_v$, was then calculated from $Q_M$ according to Equation 9-2:

$$Q_v = 1 + \frac{\rho_p}{\rho_s}(Q_M - 1) \tag{9-2}$$

where $\rho_p$ is the density of the dry polymer and $\rho_s$ is the density of the solvent (1 g/cm$^3$ for water). Values for $\rho_p$ were calculated by estimating the molar volume for the PEG-Acryl/HA-Acryl polymer segment and dividing by the molecular weight of the segment [379].

The average molecular weight between crosslinks ($\overline{M}_c$) was subsequently calculated from Equation 9-3. In this case $\nu$, is the specific volume of the dry polymer (0.893 cm$^3$/g for PEG and 0.813 cm$^3$/g for HA), V1 is the molar volume of the solvent (18 mol/cm$^3$), and $\chi$ is the Flory polymer-solvent interaction parameter (0.426 for PEG and 0.473 for HA) [380, 381]. Parameters $\nu$ and $\chi$ were calculated using the weighted average of each parameter based on the polymer composition of the gel.

$$\overline{M}_c = \frac{V1}{\overline{\nu}}\times\left(\frac{1}{2} - \chi\right)\times(Q_v)^{5/3} \tag{9-3}$$

The crosslink density, $\nu_e$, was then calculated according to Equation 9-4.

$$\nu_e = \frac{\rho_p}{\overline{M}_c} \tag{9-4}$$

### *9.2.5 Hydrogel Degradation and DNA Release*

Gels were placed in a 48 well plate with 1 ml of PBS, either in the absence or presence of 150 U/ml HAase. Bovine testicular hyaluronidase was used for HA degradation studies, with concentration chosen based on previous reports [377, 382]. For plasmid release, the solution above the hydrogel was sampled (200 µl) with replacement. The removed solution was used to determine HA content and the DNA concentration. A carbazole assay was used to quantify HA levels in solution as a measure of hydrogel degradation [383]. For plasmid incorporation and release, concentrations were determined by fluorometry and the DNA integrity was characterized by gel electrophoresis. For DNA/PEI complexes, DNA concentrations were determined by radiolabeling, achieved with a nick translation kit (Amersham Pharmacia Biotech, Piscataway, NJ) following the manufacturer's protocol [357]. Release studies with hydrogels with encapsulated DNA/PEI complexes were performed as described above. The removed sample was added to 5 ml of scintillation cocktail (Bio-safe II) to determine the quantity of DNA. The activity of the collected sample was then measured in a scintillation counter. The counts were correlated to DNA mass using a standard curve. The percentage of DNA released was calculated as the ratio of the cumulative release at a given time divided by the initial amount encapsulated.

### *9.2.6 Spatially Patterned DNA Vectors*

Layer-by-layer lithography techniques were employed to patterned DNA vectors within hydrogels. Hydrogel precursor solutions (HA-acryl, 4-arm PEG-acryl) were injected into soft-lithography patterned PDMS molds and exposed to UV light for 2 minutes. The topographically patterned feature from the PDMS mold was subsequently filled with hydrogel precursor solution containing rhodamine-labeled DNA complexes (HA-acryl, 4-arm PEG-acryl, Rho-DNA/PEI

complexes). The hydrogel was again exposed to UV light for 2 minutes. Patterned complexes were imaged using a Leica inverted fluorescence microscope with a cooled CCD camera (Photometrics; Tucson, AZ) using MetaVue (Universal Imaging; Downingtown, PA) acquisition software.

### *9.2.7 In Vivo Transfection Studies*

Hydrogels loaded with plasmid (200 – 400 μg) were implanted subcutaneously into male CD1 mice (20–22 g). Conditions examined include hydrogels fabricated with various amount of polyethylene glycol (PEG) (2-10%), various amounts of hyaluronic acid (0-4%), and different ECM molecules (5% attached fibronectin or blended collagen). In vivo luciferase expression was monitored using an IVIS imaging system (Xenogen Corp., Alameda, CA, USA), which includes a cooled CCD camera. For imaging, the animals were injected ip with d-luciferin (Molecular Therapeutics, Inc., MI, USA; 150 mg/kg body wt, 20 mg/ml in PBS) using 28-gauge insulin syringes. Note that the animals increased in weight during the experiment, and the volume of d-luciferin injected increased proportional to the weight of the animal. The animals were placed in a light-tight chamber and bioluminescence images were acquired (every 5 min for a total of 20 min) until the peak light emission was confirmed.

Hydrogels were retrieved 7 days postimplantation, fixed in 4% paraformaldehyde overnight at 48C, and subsequently immersed in 10 and 30% sucrose solutions. Tissue blocks were embedded in OCT and frozen. Sections were cut (10 μm) and mounted on poly-L-lysine-coated slides. After blocking, sections were incubated with primary rabbit anti-luciferase antibody (Cortex Biochem, CA, USA) diluted (1:100) in PBS/0.1% BSA for 1 h at 378C. For PCNA staining, tissue sections were incubated with primary rabbit anti-PCNA polyclonal antibody

(Abcam, MA, USA; 1:50 dilution) and subsequently with biotinylated goat anti-rabbit secondary antibody (Vector Laboratories; 1:200 dilution). Diaminobenzidine (DAB) substrate kit (Vector Laboratories) was used for staining proliferating cells, and tissue sections were counterstained with hematoxylin.

### *9.2.8 Statistical Analysis*

Release profiles were analyzed to determine statistically significant differences in the maximal amount released. The percent release for the final collected time point was averaged and the means compared by ANOVA followed by Tukey-Kramer post test. A value of p less than 0.05 was considered statistically significant. Statistical analyses were performed using the statistical package JMP (SAS, Cary, NC).

## *9.3 Results*

### *9.3.1 Hydrogel Formation*

Hydrogels were formed with PEG content ranging from 2% to 8% and HA content ranging from 1% to 4% (wt/vol). The extent of modification of HA carboxyl groups with hydrazide groups was 37 ± 4%. The extent of acrylation was determined by NMR to be 15 ± 2% of the total carboxyl groups modified with NHS-PEG-Acryl. Mixtures of acryl-modified HA and PEG-Acryl formed hydrogels following exposure to UV light; however, the UV exposure time differed among hydrogels and was dependent upon the composition. Hydrogels containing 6% or greater PEG required between 2 and 3 min. exposure, while hydrogels containing 4% or less PEG required 5 to 7 min. (Table 9-1). The physical properties of the hydrogel were also dependent on the polymer concentrations. The mass and volumetric swelling ratios decrease with

increasing PEG concentrations ($p < 0.05$). In regards to the HA concentration, the mean values for mass and volumetric swelling ratios had a decreasing trend as the HA concentration decreased, though the differences were not statistically significant ($p < 0.1$). The water content for all hydrogels was greater than 94%; however, the water content decreased as the PEG content increased. Using the values obtained from the swelling ratio, the crosslink density and molecular weight between crosslinks were calculated (Table 9-1).

### *9.3.2 HA Degradation*

Hydrogels containing 6% or greater PEG maintained their stable 3-dimensional structures in the presence of hyaluronidase (HAase), whereas lower PEG contents led to dissolution on time scales of several weeks. Hydrogels containing 6% or greater PEG are referred to as mechanically

| HA (%) | PEG (%) | Exposure Time (min) | Mass Based Swelling Ratio | Volume Based Swelling Ratio | Mol. Wt. between Crosslinks ($10^6$, g/mol) | Crosslink Density ($10^{-6}$, mol/cm$^3$) |
|---|---|---|---|---|---|---|
| 1 | 2 | 7 | 90 ± 7 | 199 ± 15 | 16 ± 1 | 0.72 ± 0.05 |
| 4 | 4 | 5 | 64 ± 12 | 141 ± 26 | 10 ± 2 | 1.1 ± 0.2 |
| 2 | 4 | 5 | 45 ± 4 | 81 ± 7 | 5.1 ± 0.5 | 2.3 ± 0.3 |
| 2 | 6 | 2.5 | 31 ± 4 | 54 ± 7 | 2.5 ± 0.3 | 4.5 ± 0.5 |
| 1 | 6 | 2.5 | 28 ± 1 | 48 ± 2 | 1.98 ± 0.01 | 5.7 ± 0.1 |
| 2 | 8 | 2 | 21 ± 1 | 36 ± 2 | 1.33 ± 0.07 | 8.6 ± 0.5 |
| 1 | 8 | 2 | 18 ± 1 | 30 ± 2 | 0.93 ± 0.02 | 12.2 ± 0.3 |

**Table 9-1:** Conditions for hydrogel formation, along with physical property measurements and calculations.

stable, as these hydrogels retained their three-dimensional structure for at least 50 days in the presence or absence of HAase. Hydrogels with 4% PEG or less are referred to as fully degradable hydrogels, as these gels led to complete dissolution, the lack of 3 dimensional structures determined by inspection, over times of approximately 30 to 50 days. Gels with higher

HA contents correlated with shorter times to dissolution. Percent cumulative HA degradation is defined as the quantity of released uronic acids divided by the quantity of uronic acids present in unmodified HA.

The release of HA for both mechanically stable and fully degradable hydrogels generally exhibited the greatest release during the initial 2 days, and the cumulative amount released was dependent upon hydrogel degradation. For HA and DNA release, representative curves are illustrated in the figures, with values that characterize curves from all conditions listed in a table. No significant difference in the amount of HA released was observed between days 2 and 5, with the exception of the fully degradable gel composed of 2% PEG and 1% HA and 4% PEG and 2% HA incubated in PBS (Figure 9-1, Table 9-2). The release kinetics were independent of the presence of HAase, though HAase significantly increased the cumulative amount of HA released relative to PBS alone for gels with at least 2% HA ($p < 0.05$). Mechanically stable hydrogels incubated in PBS had a cumulative HA release at day 5 ranging from approximately 4% to 25% of the original HA content, while the presence of HAase increased this percentage release to approximately 53% to 69%. The cumulative amount of HA released at day 5 was significantly different ($p < 0.05$) for mechanically stable gels in the presence of PBS relative to 150 U/ml HAase. The mean cumulative HA release at day 5 for fully degradable hydrogels in PBS ranged from 50% to 65% of the original HA content, with HAase increasing this range from 60% to 81%. In comparing fully degradable and mechanically stable hydrogels, the fully degradable gels produced HA release measurements which were significantly different than those obtained for mechanically stable gels at time points of both days 2 and 5 for gels in the presence of PBS. However, no difference was observed between these gels at day 2 in 150 U/ml HAase.

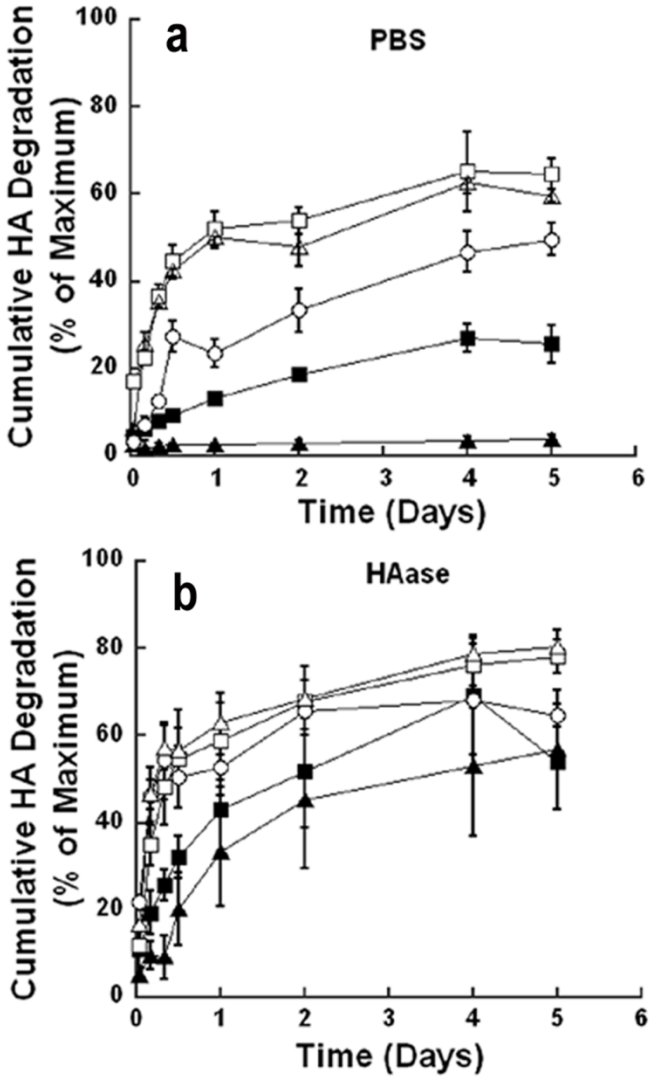


**Figure 9-1: Representative release profiles for cumulative HA degradation.** Degradation studies are performed in either PBS (a) or 150 U/ml HAase (b). The percentages of PEG and HA in the hydrogel are: PEG6:HA1 (■), and PEG8:HA1 (▲) for mechanically stable gels and PEG2:HA1 (□), PEG4:HA2 (○), and PEG4:HA4 (Δ) for fully degradable gels. In this and subsequent figures PEG6:HA21 indicates a gel formed with a composition of 6% PEG and 1% HA.

| Solvent | HA (%) | PEG (%) | Initial Burst (%) | Initial Rate (%/hr) | Cumulative Release (%) |
|---|---|---|---|---|---|
| PBS | 1 | 2 | 52 ± 4 | 1.86 | 65 ± 9 |
| | 4 | 4 | 50 ± 3 | 2.70 | 63 ± 2 |
| | 2 | 4 | 23 ± 3 | 1.06 | 50 ± 4 |
| | 2 | 6 | 12.3 ± | 0.31 | 17.2 ± 0.1 |
| | 1 | 6 | 13.2 ± | 0.36 | 27 ± 3 |
| | 2 | 8 | 4.2 ± 0.4 | 0.12 | 9 ± 1 |
| | 1 | 8 | 2.5 ± 0.5 | 0.014 | 4.0 ± 0.9 |
| HAase | 1 | 2 | 52 ± 4 | 1.86 | 65 ± 9 |
| | 4 | 4 | 50 ± 3 | 2.70 | 62 ± 2 |
| | 2 | 4 | 63 ± 4 | 2.65 | 84 ± 2 |
| | 2 | 6 | 44 ± 16 | 1.83 | 69 ± 13 |
| | 1 | 6 | 43 ± 9 | 1.56 | 69 ± 13 |
| | 2 | 8 | 33 ± 7 | 1.48 | 53 ± 8 |
| | 1 | 8 | 34 ± 13 | 1.12 | 57 ± 14 |

**Table 9-2:** Characteristics of HA release from HA-based hydrogels. Hydrogels varied in HA:PEG ratio. Studies were performed either in PBS alone, or in the presence of a HAase.

### *9.3.3 Plasmid Release*

For mechanically stable hydrogels, the majority of plasmid was released within the initial 2 days, and the maximal cumulative release was dependent upon the PEG content. Hydrogels containing 6% PEG and 2% HA in the presence of PBS and gels containing 8% PEG and 2% HA in the presence of 150 U/ml HAase had an increased plasmid release between days 2 and 10, though the quantities were relatively small (≈10%). The mean cumulative release for mechanically stable gels in PBS ranged from 20% to 60% of the initial DNA loaded, and gels with a lower PEG content exhibited a greater plasmid release. Incubation of the hydrogels in 150 U/ml HAase had a cumulative release ranging from 25% to 78% (Figure 9-2a, b, Table 9-3). However, the presence of HAase significantly increased the cumulative release at day 10 relative to PBS for hydrogels containing 8% PEG and 2% HA. Additionally, hydrogels containing 2% HA had significantly increased release of plasmid compared to hydrogels containing 1% HA ($p < 0.05$). Increasing the PEG content or decreasing the HA content led to lower amounts of cumulative plasmid release. The integrity of the encapsulated plasmid was retained during encapsulation and release, though a shift in the relative amount of plasmid in the open and supercoiled conformation was observed (Figure 9-3). In all cases, two distinct bands appeared, representing the relaxed and supercoiled forms of the DNA, both of which are transfection competent [365].

The release profile for plasmid from fully degradable hydrogels was similar to the mechanically stable hydrogels, though with greater cumulative release observed. Plasmid release occurred within the initial 2 days (Figure 9-2a), without significant increases thereafter. The mean cumulative release for hydrogels in PBS ranged from 26% to 74% of the initial DNA loaded. The hydrogel composed of 2% PEG and 1% HA had significantly greater release than the other

hydrogels. In the presence of HAase, the release profile was similar for all hydrogel conditions, with a mean maximal release ranging from 65% to 80% of the initial DNA loading. The presence of HAase increased the cumulative amount released relative to PBS for the 4% PEG / 4% HA containing hydrogels ($p < 0.05$, Figure 9-2b, Table 9-3). The quantities of cumulative plasmid release from fully degradable gels were significantly greater ($p < 0.05$) than quantities released from mechanically stable gels at day 2, with the exception of hydrogels containing 6% PEG and 2% HA. The integrity of the released DNA had similar integrity to that obtained with the mechanically stable hydrogels (data not shown).

### *9.3.4 DNA Complex Release*

In contrast to plasmid, DNA/PEI complexes incorporated into the hydrogels were primarily retained within the hydrogel. In mechanically stable hydrogels, approximately 1.5% to 4.8% of the initial DNA was released (Figure 9-4a, Table 9-3), and the presence of HAase increased the release by approximately 3% (Figure 9-4b, Table 9-3). Release from the degradable hydrogels was significantly greater than that from the mechanically stable hydrogels (Figure 9-4, $p < 0.05$). However, the quantity released reached only approximately 6.3% to 14% of the initial DNA by incubation with either PBS or HAase (Figure 9-4a, b, Table 9-3). The release of complexes is significantly lower than that obtained for plasmid alone, for both mechanically stable and fully degradable hydrogels ($p < 0.001$).

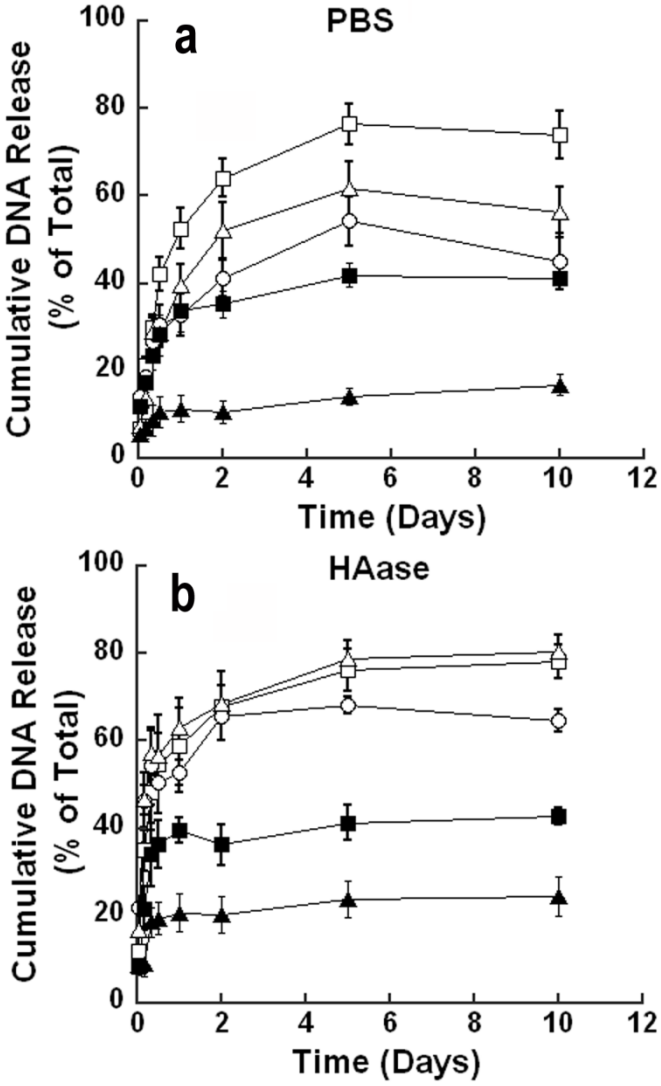


**Figure 9-2: Representative release profiles for cumulative plasmid release from HA-based gels.** Release studies performed in the presence of PBS (a) or 150 U/ml HAase (b. The percentages of PEG and HA in the hydrogel are: PEG6:HA1 (■), and PEG8:HA1 (▲) for mechanically stable gels and PEG2:HA1 (□), PEG4:HA2 (○), and PEG4:HA4 (Δ) for fully degradable gels.

| Solvent | Composition | | Plasmid | | | DNA Complexes | | |
|---|---|---|---|---|---|---|---|---|
| | HA (%) | PEG (%) | Initial Burst (%) | Initial Rate (%/hr) | Cum. Release (%) | Initial Burst (%) | Initial Rate (%/hr) | Cum. Release (%) |
| PBS | 1 | 2 | 53 ± 5 | 1.88 | 76 ± 5 | 10 ± 2 | 0.00 | 10 ± 2 |
| | 4 | 4 | 40 ± 5 | 1.75 | 62 ± 6 | 5 ± 1 | 0.00 | 6 ± 1 |
| | 2 | 4 | 33 ± 5 | 0.97 | 54 ± 6 | 5 ± 1 | 0.00 | 6 ± 1 |
| | 2 | 6 | 51 ± 6 | 1.56 | 59 ± 4 | 1.3 ± 0.2 | 0.01 | 2.1 ± 0.2 |
| | 1 | 6 | 34 ± 5 | 1.09 | 43 ± 2 | 0.5 ± 0.02 | 0.01 | 2.1 ± 0.1 |
| | 2 | 8 | 24 ± 3 | 0.43 | 47 ± 7 | 2.2 ± 0.4 | 0.00 | 2.4 ± 0.4 |
| | 1 | 8 | 2 ± 3 | 0.29 | 20 ± 3 | 1.1 ± 0.2 | 0.00 | 2.4 ± 0.6 |
| HAase | 1 | 2 | 59 ± 11 | 2.87 | 78 ± 4 | 6.3 ± 0.4 | 0.00 | 8 ± 1 |
| | 4 | 4 | 63 ± 5 | 2.62 | 81 ± 4 | 12.4 ± 0.4 | 0.00 | 14 ± 1 |
| | 2 | 4 | 53 ± 3 | 1.38 | 68 ± 2 | 4.9 ± 0.4 | 0.00 | 10 ± 2 |
| | 2 | 6 | 71 ± 6 | 2.16 | 78 ± 5 | 1.7 ± 0.3 | 0.00 | 2.7 ± 0.4 |
| | 1 | 6 | 40 ± 3 | 1.47 | 47 ± 1 | 0.8 ± 0.1 | 0.01 | 1.6 ± 0.1 |
| | 2 | 8 | 35 ± 2 | 0.55 | 41 ± 1 | 1.2 ± 0.1 | 0.00 | 4.8 ± 0.7 |
| | 1 | 8 | 11 ± 4 | 0.66 | 21 ± 4 | 1.4 ± 0.1 | 0.00 | 2.4 ± 0.3 |

**Table 9-3:** Characteristics of plasmid and complexed DNA release from HA-based hydrogels varying in HA:PEG ratio. Studies were performed either in PBS alone, or with HAase in PBS.

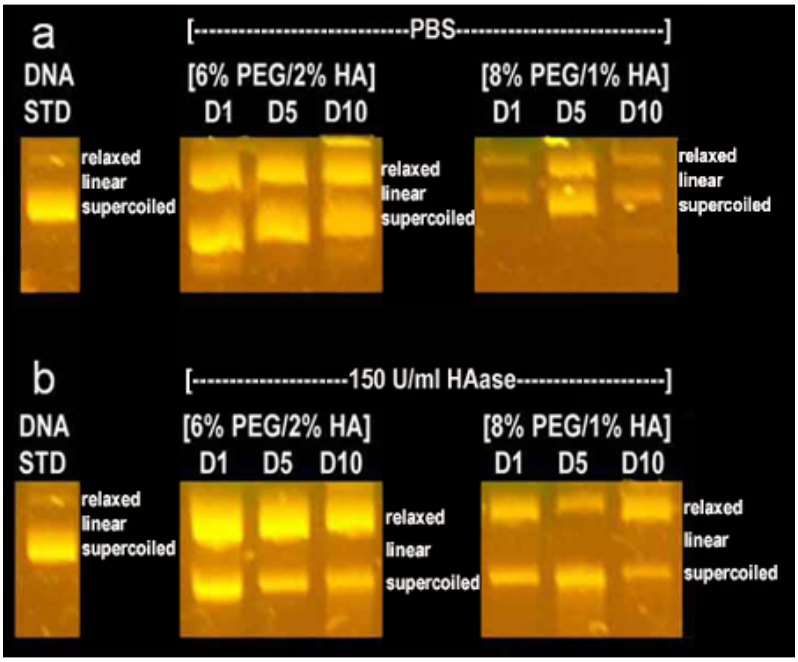


**Figure 9-3: DNA integrity.** Gel electrophoresis for plasmid released from mechanically stable hydrogels in the presence of a) PBS and b) 150 U/mL HAase at days 1, 5, and 10 compared to the original pGFP-LUC DNA prior to encapsulation (DNA STD).

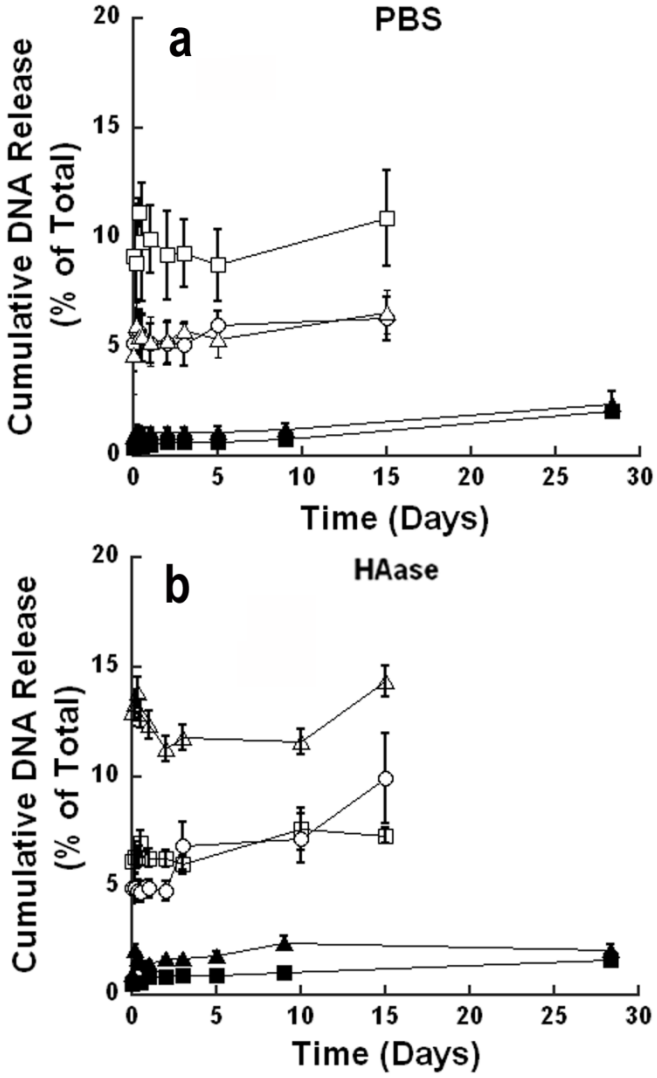


**Figure 9-4: Representative release profiles for cumulative release of DNA complexes from HA-based gels.** Release studies performed in the presence of PBS (a) or 150 U/ml HAase (b. The percentages of PEG and HA in the hydrogel are: PEG6:HA1 (■), and PEG8:HA1 (▲) for mechanically stable gels and PEG2:HA1 (□), PEG4:HA2 (○), and PEG4:HA4 (Δ) for fully degradable gels.

### *9.3.5 Spatial Patterns of DNA Vectors*

Layer-by-layer lithography was employed to spatially pattern DNA vectors within the hydrogel. After photocrosslinking within a PDMS mold, a pattern of rhodamine-labeled DNA vectors was observed within the PEG hydrogel, measuring 1 X 0.25 X 10 mm (Figure 9-5).

### *9.3.6 In Vivo Gene Delivery and Cell Infiltration*

Feasibility studies were performed to determine the potential of these hydrogels for delivery of non-viral vectors in vivo. Hydrogels fabricated with less than 4% PEG did not result in transgene expression (Table 9-4). Additionally, hydrogels fabricated with 4% PEG and 1-4% HA

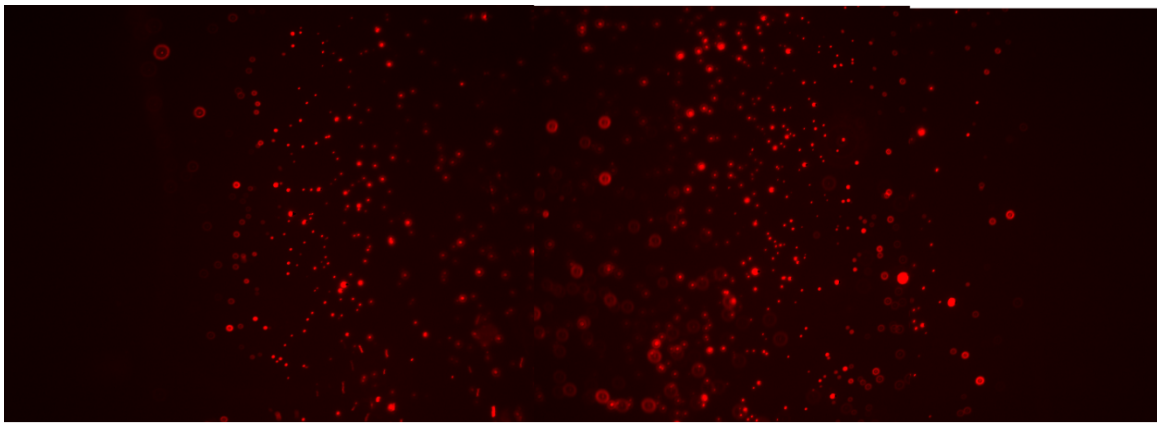

**Figure 9-5: Spatially patterned DNA vectors.** Soft lithography molds were utilized to spatially crosslink PEG hydrogels with fluorescently labeled DNA vectors.

| PEG (%) | HA (%) | ECM | DNA dose (μg) | Transgene Expression at t = 48 h | n |
|---|---|---|---|---|---|
| 2 | 1 | collagen | 400 | no | 3 |
| 4 | 0 | collagen | 400 | no | 3 |
| 4 | 0 | fibronectin | 400 | yes | 4 |
| 4 | 2 | collagen | 400 | no | 3 |
| 4 | 4 | collagen | 400 | no | 3 |
| 4 | 4 | fibronectin | 400 | no | 3 |
| 6 | 1 | collagen | 400 | no | 3 |
| 8 | 1 | collagen | 400 | no | 3 |
| 10 | 0 | fibronectin | 400 | yes | 3 |
| 10 | 4 | fibronectin | 400 | yes | 4 |

**Table 9-4:** Characterization of transgene expression by hydrogels implanted in a subcutaneous mouse model.

did not support transgene expression. Only 4% PEG/5% fibronectin (Figure 9-6) and 10% PEG/5% fibronectin (data not shown) hydrogels resulted in transgene expression in a mouse subcutaneous model for 48 h. Hydrogels were subsequently investigated for the ability to support cellular infiltration. For all hydrogel formulations, cells did not infiltrate the hydrogel, but adhered to the outer edges (Figure 9-7).

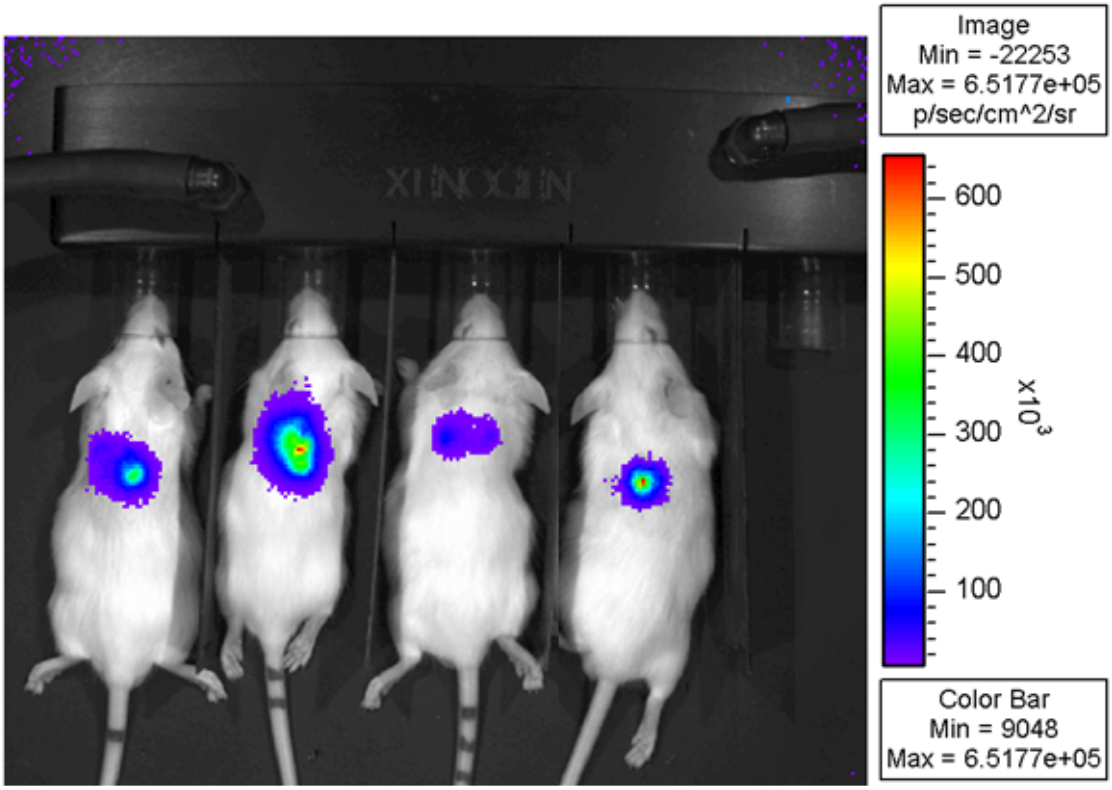


**Figure 9-6: In vivo gene delivery from PEG/HA hydrogels.** Bioluminescence imaging of firefly luciferase expression for hydrogels (4% PEG, 5% FN) fabricated with 400 μg of pLuc input to the process. Images show light emission for a single mouse at t = 48 h.

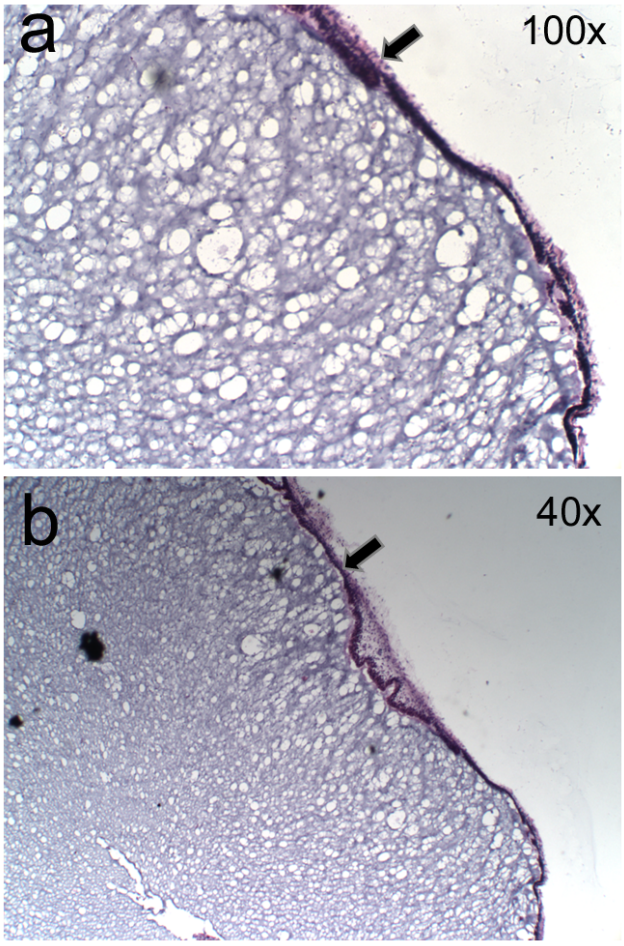


**Figure 9-7: Immunohistochemistry of in vivo implanted PEG/HA hydrogels.** Representative sections of hydrogel (4% PEG, 4% HA, 5% FN) retrieved 7 days post-implantation. Cells did not infiltrate the hydrogel. A layer of cells outline the hydrogel (marked by the arrow).

## *9.4 Discussion*

The formation of hydrogels using varied concentrations of both synthetic and natural polymers allowed for a range of hydrogel physical properties and localized release of non-viral gene therapy vectors. Hydrogels were formed by photocrosslinking mixtures of acryl modified PEG and HA. Hydrogels with 6% or greater PEG were mechanically stable for more than 50 days, while hydrogels containing 4% or less PEG were fully degradable, with times to complete dissolution ranging from 30-50 days depending on PEG concentration. For hydrogels with encapsulated plasmid, the cumulative release was reduced at higher PEG contents, and increased with increasing HA content. Only fully degradable hydrogels formed with a high quantity of HA had an increased cumulative release induced by the enzyme hyaluronidase. Hydrogels with encapsulated plasmid supported transgene expression in a subcutaneous mouse model for 48 h. Additionally, DNA/PEI complexes incorporated into the hydrogel were primarily retained, with less than 14% of the complexes released during the initial 3 weeks. The photocrosslinkable hydrogels were employed to spatially pattern DNA vectors within the three-dimensional matrix, demonstrating the utility for the hydrogels in spatially patterning gene delivery.

Hydrogels formed by combining synthetic and natural polymers can be tailored to produce a range of physical properties. In our system, the synthetic polymer PEG is non-degradable and provides stability to the hydrogel, whereas the natural polymer HA provides for cellular interactions, and can be degraded enzymatically [375, 376, 384]. HA is a natural component of many connective tissues, has a significant role in wound healing, and has been used in regenerative medicine [375, 376]. The hydrogels described herein were more than 94% water, similar to previous reports [377]. Enzymatic degradation of HA was initiated by HAase, a cell

secreted enzyme [385], which allows hydrogel degradation in response to cell growth. Hydrogels with a relatively high PEG content are mechanically stable, which may be desirable for tissue growth in vitro or in vivo, in which maintaining the three-dimensional structure may be necessary. However, altering the physical composition through increased HA and decreased PEG can produce hydrogels that are fully degradable, which would be replaced by infiltrating cells. Hydrogels with controllable stability to provide either stable or degradable hydrogels are under development for a variety of biomedical applications [386].

The combination of PEG and HA provides physical properties for the hydrogels that differ from the properties of either pure PEG or pure HA. Literature reports indicate that pure PEG hydrogels (80-85% degree of modification, MW=20,000) with PEG concentrations ranging between 10-70% wt/vol have values for $Q_m$ and crosslink density ranging from 15 to 45 and 6 x $10^{-7}$ to 7 x $10^{-6}$ mol/cm$^3$ respectively [387]. However, pure HA hydrogels (7-11% degree of modification, MW=2 x $10^6$) with HA concentrations ranging between 0.5-2% wt/vol have values for $Q_m$ and crosslink density ranging from 42 to 52 and 1.45 x $10^{-6}$ to 2.07 x $10^{-6}$ mol/cm$^3$, respectively [381]. In this report, hydrogels formed from the combination of PEG and HA have values for $Q_m$ ranging from 18 to 90 with crosslink density ranging from 0.7 x $10^{-6}$ to 12 x $10^{-6}$ mol/cm$^3$. The broader range of values for HA/PEG hydrogels relative to the pure hydrogels reflects the varied molecular weight of PEG and HA and the range of polymer concentrations used for hydrogel formation. Addition of viscoelastic HA, which has a MW of $10^3$ kDa, significantly enhances the swelling ratio of hydrogels composed primarily of PEG (MW = 10 kDa) [376]. In this report, increasing the PEG concentration decreased the swelling ratio, which is consistent with previous observations of PEG hydrogels [388]. Increasing the polymer

concentration would influence both the number of crosslinks and may cause increased entanglement, leading to a decreased swelling ratio [388, 389]. However an increased swelling, which corresponds to a decreased cross-link density of the hydrogel, was observed with an increasing HA content. This reduced cross-link density may result from the semiflexible random coil configuration of HA, which restricts availability of potential cross-link sites on the HA [390] and has been reported for HA concentrations used herein.

The presence of HAase affected the overall quantity of released HA, though the hydrogel composition influenced the degradation profile. The cumulative HA release likely did not reach 100% due to modification of the HA, which prevents complete degradation. Additionally, some HA fragments may remain attached to the hydrogel. In PBS, HA release likely occurs because a portion of the HA polymer is not covalently crosslinked to the hydrogel network. Characterization of the released HA indicated that the extent of acrylation was unchanged, and that the molecular weight of the released HA had decreased relative to measurements of HA-Acryl prior to crossslinking. Photoinitiation and photocrosslinking can partially degrade HA [391]. Additionally, HA is well hydrated with an extended coiled structure that leads to entanglement of individual HA molecules even at low concentrations [392, 393]. This coiled structure and entanglement may produce intra-HA crosslinking (i.e. acryl groups within HA react) or limit reaction with the external PEG acryl groups, which would produce unattached fragments that could diffuse from the gel. In the presence of HAase, degraded HA is due to both the release of HA that is not covalently crosslinked and HA which has undergone enzymatic hydrolysis.

The release of plasmid from the hydrogel was dependent upon its physical structure and degradation. Previous reports of PEG:HA hydrogels used for protein delivery demonstrated a decreasing normalized diffusivity with increasing PEG and HA concentrations [394]. The decreasing diffusivity correlated with the decreasing water content of the hydrogel, a result reflected in our studies in which mechanically stable hydrogels possessing decreased water content had slower rates of plasmid release. For example, the most significant difference in the maximal plasmid release for the mechanically stable gels was observed between gels with greatest difference in PEG:HA ratios, which also corresponded to the greatest difference in the swelling ratio (i.e. 6% PEG, 2% HA compared with 8% PEG, 1% HA). The decreasing water content correlates with a decreasing mesh size of the hydrogel. Importantly, the decreasing mesh size slowed release rather than prevented release, likely due to the conformational flexibility of the plasmid. Plasmid with 6000 base pairs, a typical size for use in gene delivery, has been reported as having a hydrodynamic radius of 175 nm [395], which is substantially larger than the reported mesh sizes for PEG hydrogels. However, plasmid may traverse the hydrogel by reptation rather than move as a fixed structure [396]. DNA entrapped within the pores may undergo random segmental motion to traverse between pores of the hydrogel.

Degradation of HA by HAase increases the maximal release of plasmid for both mechanically stable and fully degradable hydrogels. This degradation would reduce the cross-link density and increase the mesh size, thereby increasing transport through the hydrogel. Increasing the quantity of degradable segments will decrease the stability of the hydrogel, yet will increase transport through the hydrogel and thus increase the quantity released [365]. These observations have been reported previously with PEG-based hydrogels containing hydrolytically

degradable PLA (poly lactic acid) linkages, which provide a sustained release based on the hydrolysis of the lactic acid segments [365]. In this report, HA-based hydrogels are employed that degrade through enzyme action. Thus, cells infiltrating into the HA-based hydrogels will secrete HAase to degrade the hydrogel, and may provide release based on cellular demand or activity [369]. HAase affected release most significantly for gels containing 4% PEG and 4% HA, which were more susceptible to enzymatic degradation of HA crosslinks than the other gels. Similar to cumulative HA degradation, cumulative plasmid release never reached 100%. The fully degradable had a cumulative release of approximately 90%, with no measurable amount of DNA remaining in the gel upon completion of the release study.

DNA/PEI complexes encapsulated in HA:PEG hydrogels were bioactive and had substantially lower quantities released relative to naked plasmid, which may result from a combination of the complex size and the interactions between the hydrogel and complex. In vitro transfection was observed, which confirmed the activity of the complexes and illustrates the feasibility of using these hydrogels for non-viral vector delivery. Complexation of plasmid with the cationic polymer PEI is typically employed to reduce the negative surface charge of the plasmid, protect the plasmid from degradation, and promote cellular internalization and trafficking. DNA/PEI complexes (N:P ratio of 25) have hydrodynamic diameters 121 ± 10 nm [371] and are likely restricted in their ability to change conformations and thus may have limited mobility. Alternatively, the transport of DNA complexes may be affected by non-specific interactions with the hydrogel. Naked plasmid and complexed DNA have substantial differences in zeta potential, with approximate values of –36.4 mV and +21.2 mV (N/P = 10), respectively [371, 397]. These values for zeta potential suggest that the complexes and plasmid may have

different interactions with the hydrogel. HA has exposed hydroxyl and carboxyl groups that can impart a net negative charge, which would repel plasmid to enhance transport but may attract complexes and hinder diffusion. Similar observations have been noted with protein release, in which ionic interactions between the hydrogel and the protein were manipulated to obtain either retention or release [398]. Additionally, studies with cell culture substrates have indicated that DNA/PEI complexes are retained on the biomaterial, with cells able to internalize the immobilized complex. Thus, the limited release of DNA/PEI complexes likely results from a combination of size exclusion and nonspecific interactions, and demonstrates that the release dynamics be manipulated through the properties of the hydrogel and the encapsulated factors.

The integrity of the encapsulated plasmid was maintained by crosslinking with short exposure times of long wavelength UV light (365 nm). When investigated by gel electrophoresis, plasmid released from the PEG/HA hydrogels had two distinct bands pertaining to both the supercoiled and relaxed forms, with both forms known to be transfection competent [365]. Previous studies investigating plasmid integrity in photopolymerized hydrogels indicate that radicals formed by the photoinitiator can damage plasmids when crosslinked with long range UV light [365]. Short range UV light results in either a linear conformation or simply degraded fragments [370]. However, long range UV only causes a shift in conformation from supercoiled to open forms, both of which are transfection competent DNA. Short exposure of DNA to 365 nm light has shown to produce a 5% decrease in the supercoiled conformation, and does not linearize plasmids [370].

DNA delivery from hydrogel matrices provides chemical and mechanical signals that are necessary to regenerate healthy tissue. However, natural tissues have complex architectures that

must be regenerated to regain function. Patterns of gene expression guide cellular processes (e.g., migration, differentiation) during development, leading to healthy complex structures. Patterned gene expression may provide a mechanism to present signals capable of guiding cellular processes during regeneration. The ability of spatially patterned gene delivery to guide cell migration in two dimensions has recently been demonstrated [302], but the regeneration of complex tissue architectures will require spatial patterns of gene expression in three dimensions. Layer-by-layer lithography was employed in this Chapter to spatially pattern DNA vectors within hydrogels. Future studies should address the ability to localize DNA delivery within the hydrogel.

Hydrogels implanted subcutaneous resulted in expression of the luciferase transgene for 2 days when the hydrogel content was at least 4% PEG and included 5% fibronectin. Since lower PEG content gels did not result in transgene expression, matrix stiffness may govern transfection. Previously, increased hydrogel stiffness was shown to increase efficiency of non-viral gene delivery [399]. Additionally, since collagen-incorporated PEG gels did not result in transgene expression, cellular adhesion and/or vector interactions with fibronectin may regulate transfection. Previously, fibronectin coated substrates enhanced transfection, potentially by targeting caveolae-mediated endocytosis [84]. The relatively short duration of transgene expression could be due to fast plasmid release from the hydrogels. Methods to retain plasmids within the hydrogel should be explored to increase extent and time of transgene expression. The hydrogels developed in this Chapter did not support cellular infiltration in vivo, suggesting that cells at the outer edge of the hydrogel expressed the transgene. Future studies should explore crosslinking strategies that support cellular infiltration and migration.

## *9.5 Conclusions*

Hydrogels composed of HA combined with synthetic polymers have been created via a variety of techniques, supporting their use as a support for cell growth and drug delivery, and this Chapter focuses on their suitability for delivery of gene therapy vectors. PEG:HA hydrogels were formed by photopolymerization, with the relative composition of the hydrogel determining the stability in the presence of matrix degrading enzymes. Encapsulated plasmid was released at rates that depended on the hydrogel composition, with faster release from hydrogels with higher HA content. For encapsulated DNA/PEI complexes, release was substantially lower, likely resulting from limited mobility and non-specific interactions with the hydrogel. The hydrogels demonstrated gene delivery in vivo, although duration of transgene expression was relatively short. These hydrogels are highly tunable, and can be employed to identify the design parameters that promote efficient substrate-mediated gene delivery in three dimensions. Hydrogels with controllable stability and the capability for localized delivery of gene therapy vectors can both support and promote cellular processes (e.g., proliferation, differentiation) involved in tissue formation and could find utility for a variety of biomedical applications [355].

# Chapter 10

# Conclusions and Future Directions

## *10.1 Introduction*

The ultimate goal of tissue engineering is to stimulate and direct progenitor cell or transplanted cell processes to regenerate healthy tissues. Tissue engineering scaffolds have been utilized to study the regeneration of bone, cartilage, nerve, heart, and many other tissues that have been disrupted by disease or injury. Advances have been made in the field of tissue engineering in the past decade, including the development of novel materials and fabrication techniques to address several requirements of the scaffold, such as biocompatibility, specific mechanical properties, and mild fabrication strategies to incorporate proteins, peptides, nucleic acids, or cells. In order to regain tissue function, the scaffold must also direct cellular processes into complex structures that mimic natural tissue architecture. Design characteristics of the tissue engineering scaffold have aimed to recapitulate this architecture, by presenting physical barriers and patterned peptides or proteins. Additionally, spatial patterns of gene expression guide cellular processes into complex structures during development, and may provide a means to recapitulate the complex architectures of natural tissues. In order to establish complex cellular structures in vivo, the guidance signals must be presented on time scales from weeks to months, and length scales from mm to cm.

This thesis aimed to develop and understand spatially patterned gene delivery in vitro to investigate guided cellular processes. The next sections of this Chapter describe conclusions

drawn from this thesis and future directions necessary to further advance the field, working toward the ultimate goal of directing cellular processes to regenerate healthy tissues.

## *10.2 Spatially Patterned Gene Delivery to Investigate Neurite Guidance*

Complex spatiotemporal patterns of gene expression guide cell differentiation and migration into organized functional structures during tissue development and repair. Patterned gene expression results in concentration gradients of guidance molecules which facilitates cell orientation and instruction. Since gradients are difficult to characterize in vivo, there exists a significant need for in vitro assays capable of recapitulating in vivo gradients. To date, in vitro biological patterning techniques fail to present guidance molecules and gradients similar to the manner in which they exist in vivo. The spatially patterned gene delivery system developed in this thesis defines concentration gradients that form from localized secretion and diffusion within a complex cellular environment, similar to the manner in which gradients form naturally.

### *10.2.1 Conclusions*

Biological patterning strategies were combined with substrate-mediated gene delivery to localize DNA vectors to a tissue culture surface. Methods to maximize DNA vector binding to TCPS surfaces were employed (Chapter 5). Both Pluronic and $O_2$ plasma treatment increased binding efficiency to TCPS by decreasing adsorption to PDMS. However, transfection efficiency was enhanced by Pluronic treatment as compared to $O_2$ plasma treatment. Loosely bound Pluronic may interact with the lipoplexes to prevent complex aggregation or enhance complex association with the cells. Pluronic may also influence the nonspecific interactions between the lipoplex and substrate thereby enhancing transfection. Protein production rates by localized

expression were varied by altering vector concentration and channel width (Chapter 6). The concentration gradients that arise from localized secretion and diffusion were characterized by three-dimensional mathematical modeling. The production rates, and subsequently concentration gradients, can be altered by simple changes in system conditions. Additionally, non-viral DNA delivery strategies provide the flexibility to investigate any therapeutic factor by readily exchanging plasmids without altering the delivery method. The flexibility of the system developed in this thesis allows for the investigation of gradients of almost any chemotactic factor with, potentially, any concentration requirement for guidance.

The spatially patterned gene expression system developed in this thesis was employed to investigate neuronal responses to localized expression of the neurotrophic factor, NGF. Patterns of NGF expression 100-250 μm in width resulted in localized neuron survival and neurite extension primarily confined to the regions of expression (Chapter 5). NGF concentrations within patterns approached a minimum concentration required for survival. Furthermore, neurites remained localized to the pattern, as to not extend to regions of lower NGF concentration. Patterns of NGF expression 1 mm in width allowed for investigation of neurite guidance by increasing the mean NGF concentration and, subsequently, increasing the distance to explore response (Chapter 6). The extent of neurite guidance was dependent on the distance a neuron was cultured from the pattern and the amount of NGF bound to the surface. Accumulation of NGF on the surface masked the guidance signal provided by soluble NGF. The soluble gradients capable of guiding neurites were 8.5-0.5 ng/mL/mm (absolute gradient) and 8.0-1.5% (fractional gradient); values that differed substantially from previously engineered NGF gradients.

Collectively, these results demonstrate the importance of using spatially patterned gene expression to define concentration gradients capable of guiding cellular processes.

### *10.2.2 Future Directions*

The spatially patterned gene expression system presented in this thesis provides a method to achieve concentration gradients of neurite guidance factors in vitro that represent the manner in which gradients develop in vivo. Admittedly, the environment responsible for presenting gradients of guidance cues in vivo is significantly more complex than the in vitro system developed herein. Nerve guidance cues are expressed in vivo by a combination of neuronal and non-neuronal (glial) cells. For the purpose of initial investigations, the in vitro system presented in this thesis is simplified by using only one accessory cell type that is not located in the nervous system. Cells in the nervous system may have receptors for chemotactic molecules and, therefore, may internalize the ligand [400] which could alter the concentration profiles drastically. Moreover, cell types in the nervous system may also present different ECM molecules that are more or less conducive to ligand binding [401]. Understanding the effects of both receptor and extracellular surface binding of guidance molecules on the concentration profiles developed from patterned expression will be critical to the utility of this system for fundamental chemotaxis studies. Strategies such as radioactivity or flow cytometry can be employed to quantify the relative amounts of ligand internalized by cells or immobilized to the culture surface with different cell types present in the nervous system. Internalization and binding coefficients can be placed in the mathematical model to predict new concentration profiles [296]. With this additional level of complexity in vivo, combinations of factors may be necessary to elicit a guidance signal [402]. Slight modifications to photolithographic masks that

produce the PDMS molds will allow patterning of several gene expression profiles to investigate combinations of guidance factors, both chemotactic and haptotactic. Additionally, biological patterning techniques have recently been applied to high-throughput investigations [403]. Adapting a high-throughput strategy to patterned gene expression may support the investigation of several cell types and several guidance molecules, and all combinations thereof, to determine optimum guidance capabilities.

An important goal in tissue engineering strategies is to achieve vascularization of the implanted scaffold to support oxygen and nutrient transport to regenerating tissues. The patterned gene expression system presented in this thesis can also be applied to investigate fundamental studies of chemotaxis during wound healing and angiogenesis [3]. Gradients of PDGF guide fibroblast migration to the wound site to produce new extracellular matrix necessary to support further cell ingrowth [271, 404]. Gradients of IL-8 support endothelial cell chemotaxis to wound sites and, thus, mediate angiogenesis [405]. Moreover, specific microenvironmental levels of VEGF support the formation of healthy blood vessels, presumably by concentration gradients that guide cell migration [104]. The patterned gene expression system presented in this thesis can provide a fundamental understanding of how gradients guide cell migration to wound sites and the organization of healthy blood vessels. Information gained from the in vitro system can be applied to the rational design of tissue engineering strategies capable of instructing angiogenesis.

The patterned gene expression system presented herein can also be applied to the development of structurally organized bone and cartilage tissues. In particular, mesenchymal stem cells (MSCs) can be induced to differentiate exclusively into adipocytic, chondrocytic, or

osteocytic lineages. MSCs are thought to be recruited in the body for repair of injured tissues, and, therefore, are ideal candidates for cell-based therapies for regeneration [406]. Importantly, the mechanisms of targeted migration of mesenchymal stem cells to injury sites are poorly understood [407]. Patterned gene expression can be employed to understand targeted MSC migration, and knowledge obtained from this system can be incorporated into the rational design of bone and cartilage tissue engineering strategies. During endochondral bone formation, cartilage serves as the morphological template for vascular invasion and bone tissue production. Regenerative strategies should duplicate some of the events of chondrogenesis and endochondral ossification through temporal and spatial presentation of growth factors to initiate the appropriate cascade of cellular events required for proper bone formation [408]. Patterned gene expression provides a means to control spatial presentation of growth factors that can be applied to fabricate systems capable of regenerating structurally organized bone tissues.

## *10.3 Patterned Gene Delivery for Nerve Regeneration*

Tissue engineering strategies aim to support and stimulate tissue formation that has been lost due to injury or disease. Tissue engineering scaffolds function to maintain a space at a lesion site and support cellular organization, while drug delivery is incorporated to present factors that are critical to promote cell processes (adhesion, migration, differentiation, proliferation). Gene delivery from scaffolds aims to overcome disadvantages associated with traditional protein delivery, and can present therapeutic factors at elevated and sustained levels [11, 12]. Many tissues rely on a complex architecture to function properly, and tissue regeneration strategies must reestablish the architecture to regain function. In this thesis, patterned gene delivery

strategies were combined with topographically patterned tissue regenerative scaffolds to investigate synergistic guidance signals to organize regenerating neurites.

### *10.3.1 Conclusions*

Biological patterning strategies were combined with substrate-mediated gene delivery to fabricate topographically patterned PLG microchannels capable of delivering genes to accessory cells cultured within the microchannels. PLG patterns were fabricated by compression molding PLG onto PDMS molds (Chapter 7). The microchannels were fabricated with 100, 150, and 250 μm widths, design parameters similar to three-dimensional PLG scaffolds [254]. DNA vectors were localized within the microchannels by mouth pipetting, and both transfection efficiency and extent of transgene expression decreased with decreasing channel width. Localized delivery of pNGF to accessory cells cultured inside the channel maintained elevated levels of NGF at the channel floor, the optimum placement of neurons and neurites. Neurons cultured inside the 100 μm channels extended longer primary neurites than those cultured in 150 and 250 μm channels. Importantly, guidance in the 100 μm channel was a result of physical guidance cues by the channel wall and guidance signals provided by the pNGF transfected cells. Surface immobilization allowed for the delivery of distinct plasmids from each channel, which may enable channels to be tailored for specific nerve tracts.

The guidance cue provided by single pNGF transfected cells within the PLG scaffold were investigated independent of the physical guidance cues. Transfection profiles were developed in terms of transfection efficiency and extent of transgene expression to vary microenvironmental concentrations of NGF and gradients that extend from single pNGF transfected cells (Chapter 8). Mathematical modeling confirmed NGF diffusion from a single transfected cell produced

gradients outside the cell. The maximum NGF levels were defined by the production rate, and the minimum NGF levels were defined by both the production rate and the average distance between NGF-expressing cells. Transfected cells expressing low levels of NGF were required to guide neurites. These studies demonstrated the mean microenvironmental NGF concentration governs guidance by single NGF-expressing cells. The knowledge gained from these studies can be applied to the rational design of gene delivery nerve guidance bridges.

### *10.3.2 Future Directions*

Studies presented in this thesis demonstrated the capability to immobilize DNA vectors within PLG microchannels. Localized NGF expression within PLG microchannels elicited physical guidance by the channel walls and chemical guidance by NGF gradients from single transfected cells. Neurite orientation by single transfected cells, however, may be imprecise and may not provide the shortest path for neurite extension across a lesion. A higher degree of neurite orientation may be achieved by NGF gradients from a cluster of cells (Chapters 5 and 6) within the PLG microchannel. NGF gradients produced by a cluster of NGF-expressing cells are capable of precisely guiding neurites over a distance up to 1 mm (Chapter 6). Axon chemotaxis in vivo has been shown to occur over distances less than or equal to 1 mm, and chemotaxis over longer distances occurs by a series of intermediate targets [5]. To achieve axon guidance across an entire lesion (several millimeters to centimeters), a series of NGF-expressing cell clusters within PLG microchannels may be required as intermediate targets. Series of localized DNA vectors within PLG microchannels may be achieved by enhanced microfluidic strategies or microprinting techniques. Importantly, axons must also be guided out of the intermediate target to sense the subsequent NGF gradients and continue along a directed path. Based on studies

presented in Chapter 8, the transfection profile within the cluster of NGF-expressing cells can be altered to achieve a mean NGF concentration capable of optimizing axon guidance through the intermediate targets.

The optimum bridge for nerve regeneration will include three critical regions: the on-ramp, the surface of the bridge, and the off-ramp [314]. Each of these regions will have specific design requirements. The studies presented in this thesis focus on neurite guidance at the surface of the bridge, however, spatially patterned gene delivery can also be incorporated into the design of both the on- and off-ramps. First, neurons rostral to a nerve lesion will require elevated levels of survival cues to achieve optimum neuron survival and a high density of axons entering the scaffold (on-ramp). To achieve maximum neuron survival, high concentrations of neurotrophic factors will be required, contrary to the concentration requirement for axon guidance within the scaffold. Spatial patterns of viral vector delivery at the onset of the injury may increase neurotrophic factor expression and maximize survival. Moreover, the region caudal to the injury site is marked by inhibitory cues and the glial scar that prevent axon extension into host tissue (off-ramp). Spatial patterns of genes encoding factors to block inhibitory cues at the end of the injury may enhance axon extension into host tissue. Furthermore, spatial patterns of neurotrophic factor expression at the scaffold / host tissue interface may further support axon guidance out of the scaffold and into the host tissue.

## *10.4 Gene Delivery from Photopolymerizable Hydrogels*

Patterns of gene expression that guide tissue formation during embryogenesis are presented within a complex three-dimensional extracellular matrix. The composition and functions of adhesions in three-dimensional matrices differ from focal adhesions on two-dimensional

substrates, with three-dimensional adhesions displaying enhanced cell biological activities and narrowed integrin usage [142]. Presumably, differences in cell adhesion in three dimensions versus two dimensions translate to differences in cell migration, proliferation, and differentiation. These differences in cell processes are important to consider when investigating cellular responses to patterns of gene expression.

Layer-by-layer lithography can be utilized to pattern DNA vectors within three-dimensional photopolymerizable PEG hydrogels. Traditionally, gene delivery from hydrogels has been focused on the release of vectors by diffusion to the surrounding tissue [74, 409, 410]. In order to establish techniques to achieve patterned gene delivery within hydrogels, strategies must first be devised to achieve controlled DNA delivery within a hydrogel matrix. Substrate-mediated gene delivery provides a method to immobilize vectors within a matrix, but has not been applied in three dimensions. The hydrogel developed in this thesis provides a platform to investigate substrate-mediated gene delivery mechanisms in three dimensions, and has been applied to the spatial patterning of DNA vectors.

### *10.4.1 Conclusions*

Hydrogels were formed by photocrosslinking acryl-modified hyaluronic acid (HA) with a 4-arm poly(ethylene glycol) (PEG) acryl (Chapter 9). Hyaluronic acid was incorporated into the original hydrogel design to provide 1) cell-instructed degradation and infiltration and 2) functional groups ($COO^-$) capable of retaining positively charged DNA vectors within the hydrogel matrix. The polymer content, and relative composition of HA and PEG, modulated the swelling ratio, water content, and degradation, which can influence transport of the vector through the hydrogel. Plasmids were stably incorporated into the hydrogel, with a majority of the

release occurring during the initial two days. For incubation in buffer, the cumulative release increased with a decreasing PEG or increasing HA content, with approximately 20% to 80% released during the first week depending on the hydrogel composition. Hydrogels incubated in hyaluronidase, an enzyme that degrades HA, significantly increased plasmid release for hydrogels containing 4% PEG and 4% HA-Acryl. The encapsulation of plasmid complexed with poly(ethylene imine) had less than 14% of the complexes released from the hydrogel both in the presence and absence of hyaluronidase. The limited release of the complexes likely results from the complex size and interactions between the vector and hydrogel. Layer-by-layer lithography was employed to spatially pattern DNA vectors within specific regions of the photopolymerized hydrogels. Rhodamine-labeled DNA complexes were immobilized to a 1 X 0.25 X 10 mm rectangular pattern. While three-dimensional patterned gene delivery was beyond the scope of this thesis, the photopolymerizable hydrogels presented herein can be utilized in future studies to investigate 3D patterned substrate-mediated gene delivery.

The hydrogels were investigated for the ability to instruct cellular infiltration and transfect cells migrating into the hydrogel in vivo. Transgene expression was observed for a maximum of 2-4 days. The highest extent of transgene expression was observed with hydrogels containing greater than 4% PEG and minimal HA, suggesting that hydrogel rigidity governed transfection. Additionally, the highest extent of transgene expression was observed with hydrogels containing 5% covalently attached fibronectin, suggesting that cellular adhesion to the hydrogel also governed transfection. Immunohistochemistry revealed that cells did not migrate into the hydrogel after 7 days, demonstrating that HA was not adequately crosslinked into the matrix, or cells were not secreting necessary levels of hyaluronidase to degrade the matrix. Collectively,

these results provide insight into necessary design requirements to achieve substrate-mediated gene delivery in three dimensions.

### *10.4.2 Future Directions*

Hydrogels were developed in this thesis to study substrate-mediated gene delivery in three dimensions. Prior to exploring patterned gene delivery in hydrogels, a fundamental understanding of the mechanisms of three-dimensional substrate-mediated gene delivery must be established. Cellular infiltration is critical for in vivo utility of this system. The hyaluronic acid incorporated into the hydrogel did not support cellular infiltration in vivo. Modifications to the hydrogel design will, therefore, be necessary to establish a scaffold that supports cellular infiltration and migration. Natural hydrogels (collagen, fibrin) provide the necessary functionalities to support cellular processes [411]. However, critical to the investigation of substrate-mediated gene delivery mechanisms is a chemically and mechanically tailorable scaffold. PEG hydrogels can be crosslinked with proteolytically degradable sequences specific for various cell secreted proteases involved in natural matrix remodeling [67, 94]. With a hydrogel that supports cellular migration, the mechanisms of substrate-mediated gene delivery in three dimensions can be explored. Factors that have been shown to regulate substrate-mediated gene delivery in two dimensions include vector/substrate interactions (hydrophilic, ionic) [85] and cell/substrate interactions (adhesion molecules) [84]. The PEG hydrogel presented in this thesis provides photopolymerizable groups to present molecules (ionic groups, adhesion peptides) to investigate the effects of these factors on substrate-mediated delivery in three dimensions.

Studies conducted in this thesis demonstrate the ability to spatially pattern DNA vectors in three-dimensional hydrogels. The reality of spatially patterned gene expression in three dimensions may be more complex due to cell migration and proliferation and vector retention. Two-dimensional substrate-mediated gene delivery has demonstrated that nonspecific interactions between the substrate and DNA vectors maintain the vectors in a spatial pattern. Theoretically, the hydrogels can be designed to retain DNA vectors locally in the same manner without the vectors diffusing out of the pattern. Also important for the success of the two-dimensional patterning system presented in this thesis is the immediate placement of the cells in the microenvironment with the patterned vectors. A three-dimensional hydrogel may rely on the migration of cells into the hydrogel before coming in contact with the patterned vectors, which could take several days in vivo. Future studies will need to address the activity of DNA vectors over time and whether vector retention is sustainable to maintain the patterns for the time scale necessary for cells to infiltrate. Additionally, cellular proliferation and migration in the two-dimensional patterned gene delivery system presented herein was slow enough at the time of assay that the pattern of expression was not dramatically disturbed by transfected cells migrating out of the pattern. However, a cell-instructed degradable hydrogel to support cellular migration and proliferation may lead to disruption of the pattern, depending on the time scale of assay. To realize three-dimensional patterning, methods to maintain transfected cells within the pattern need to be developed. A first step toward understanding the effects of migration on gradients may be utilizing a PLG bridge as the scaffold with spatially patterned DNA delivering hydrogels within the bridge. Cellular transfection and migration away from the hydrogels can be monitored to evaluate the degree of gradient disruption. The percentage of transfected cells migrating out of

the pattern may be relatively small and may not disrupt the desired cell response to gradients. Additional methods to alter migration rates include altering the specificity of MMP degradable sequences used to crosslink PEG gels [412] and modifying the strength of cellular adhesion [413].

Once the ability to spatially pattern gene expression within a hydrogel is realized, the scaffold can be used to investigate combinatorial nerve regeneration strategies. Patterned gene expression can be employed to guide regenerating axons through a lesion site. The hydrogel can be designed to target the migration of supporting neuronal cells, which will present positive regeneration signals, assist in axon bundling, and modulate nerve signal propagation. Spatial patterns of gene expression can produce gradients of chemotropic factors extending from the hydrogel edge to guide infiltration of glial cells that support regeneration. Additionally, MMP-sensitive substrates can be crosslinked into the hydrogel to target infiltration of supporting cells and inhibit reactive astrocyte infiltration [414].

In summary, strategies have been developed in this thesis to spatially pattern gene expression. The systems have been characterized in terms of protein production rates and concentration gradients that arise from localized secretion and diffusion. Gradients formed by a cluster of NGF-expressing cells, as well as single NGF-expressing cells, are capable of guiding neurite extension. The systems have been employed to explore fundamental questions in nerve guidance, as well as the potential for spatially patterned gene expression in nerve regeneration strategies. The ability to localize DNA vectors in a PEG hydrogel has been demonstrated, but further mechanistic evaluations of substrate-mediated gene delivery in three dimensions will be required before three dimensional patterns of gene expression are realized. While this thesis has

focused on nerve regeneration, spatially patterned gene expression can be utilized to investigate many tissue development scenarios, as well as the rational design of tissue regeneration scaffolds.

# Chapter 11

## References


1. Zecca, M., Basler, K., and Struhl, G. (1996). Direct and long-range action of a wingless morphogen gradient. *Cell* 87: 833-844.

2. Devreotes, P. N., and Zigmond, S. H. (1988). Chemotaxis in Eukaryotic Cells - a Focus on Leukocytes and Dictyostelium. *Annual Review of Cell Biology* 4: 649-686.

3. Gillitzer, R., and Goebeler, M. (2001). Chemokines in cutaneous wound healing. *Journal of Leukocyte Biology* 69: 513-521.

4. Postlethwaite, A. E., and Seyer, J. M. (1991). Fibroblast Chemotaxis Induction by Human Recombinant Interleukin-4 - Identification by Synthetic Peptide Analysis of 2 Chemotactic Domains Residing in Amino-Acid-Sequences 70-88 and 89-122. *Journal of Clinical Investigation* 87: 2147-2152.

5. Tessier-Lavigne, M., and Goodman, C. S. (1996). The molecular biology of axon guidance. *Science* 274: 1123-1133.

6. Gurdon, J. B., and Bourillot, P. Y. (2001). Morphogen gradient interpretation. *Nature* 413: 797-803.

7. Chen, C. S., Mrksich, M., Huang, S., Whitesides, G. M., and Ingber, D. E. (1998). Micropatterned surfaces for control of cell shape, position, and function. *Biotechnology Progress* 14: 356-363.

8. Patel, N., et al. (1998). Spatially controlled cell engineering on biodegradable polymer surfaces. *Faseb Journal* 12: 1447-1454.

9. Mapili, G., Lu, Y., Chen, S. C., and Roy, K. (2005). Laser-layered microfabrication of spatially patterned functionalized tissue-engineering scaffolds. *Journal of Biomedical Materials Research Part B-Applied Biomaterials* 75B: 414-424.

10. Nath, N., Hyun, J., Ma, H., and Chilkoti, A. (2004). Surface engineering strategies for control of protein and cell interactions. *Surface Science* 570: 98-110.

11. Shea, L. D., Smiley, E., Bonadio, J., and Mooney, D. J. (1999). DNA delivery from polymer matrices for tissue engineering. *Nat Biotechnol* 17: 551-554.

12. Jang, J. H., Rives, C. B., and Shea, L. D. (2005). Plasmid delivery in vivo from porous tissue-engineering scaffolds: transgene expression and cellular transfection. *Mol Ther* 12: 475-483.

13. Langer, R., and Vacanti, J. P. (1993). Tissue engineering. *Science* 260: 920-926.

14. Lysaght, M. J., and Hazlehurst, A. L. (2004). Tissue engineering: the end of the beginning. *Tissue Eng* 10: 309-320.

15. Langer, R. (1998). Drug delivery and targeting. *Nature* 392: 5-10.

16. Murphy, W. L., and Mooney, D. J. (1999). Controlled delivery of inductive proteins, plasmid DNA and cells from tissue engineering matrices. *J Periodontal Res* 34: 413-419.

17. Bonadio, J., Goldstein, S. A., and Levy, R. J. (1998). Gene therapy for tissue repair and regeneration. *Adv. Drug Del. Rev.* 33: 53-69.

18. Pannier, A. K., and Shea, L. D. (2004). Controlled release systems for DNA delivery. *Mol Ther* 10: 19-26.

19. Gafni, Y., Turgeman, G., Liebergal, M., Pelled, G., Gazit, Z., and Gazit, D. (2004). Stem cells as vehicles for orthopedic gene therapy. *Gene Ther* 11: 417-426.

20. Deasy, B. M., and Huard, J. (2002). Gene therapy and tissue engineering based on muscle-derived stem cells. *Curr Opin Mol Ther* 4: 382-389.

21. De Rosa, G., Quaglia, F., La Rotonda, M. I., Appel, M., Alphandary, H., and Fattal, E. (2002). Poly(lactide-co-glycolide) microspheres for the controlled release of oligonucleotide/polyethylenimine complexes. *J Pharm Sci* 91: 790-799.

22. Devroe, E., and Silver, P. A. (2004). Therapeutic potential of retroviral RNAi vectors. *Expert Opin Biol Ther* 4: 319-327.

23. Langer, R., and Tirrell, D. A. (2004). Designing materials for biology and medicine. *Nature* 428: 487-492.

24. Sakiyama-Elbert, S. E., and Hubbell, J. A. (2001). Functional Biomaterials: Design of Novel Biomaterials. *Ann Rev Mater Res* 31: 183-201.

25. Quick, D. J., and Anseth, K. S. (2003). Gene delivery in tissue engineering: a photopolymer platform to coencapsulate cells and plasmid DNA. *Pharm Res* 20: 1730-1737.

26. Lu, L., et al. (2000). In vitro and in vivo degradation of porous poly(DL-lactic-co-glycolic acid) foams. *Biomaterials* 21: 1837-1845.

27. Luu, Y. K., Kim, K., Hsiao, B. S., Chu, B., and Hadjiargyrou, M. (2003). Development of a nanostructured DNA delivery scaffold via electrospinning of PLGA and PLA-PEG block copolymers. *Journal of Controlled Release* 89: 341-353.

28. Jang, J. H., and Shea, L. D. (2003). Controllable delivery of non-viral DNA from porous scaffolds. *J Control Release* 86: 157-168.

29. Hubbell, J. A. (1999). Bioactive biomaterials. *Curr Opin Biotechnol* 10: 123-129.

30. Saltzman, W. M., and Olbricht, W. L. (2002). Building drug delivery into tissue engineering. *Nat Rev Drug Discov* 1: 177-186.

31. Nishikawa, M., and Huang, L. (2001). Nonviral vectors in the new millennium: Delivery barriers in gene transfer. *Human Gene Therapy* 12: 861-870.

32. Herweijer, H., and Wolff, J. A. (2003). Progress and prospects: naked DNA gene transfer and therapy. *Gene Ther* 10: 453-458.

33. Ledley, F. (1996). Pharmaceutical Approach to Somatic Gene Therapy. *Pharmaceutical Research* 13: 1595-1613.

34. Chen, Y., et al. (2001). Identification of methylated CpG motifs as inhibitors of the immune stimulatory CpG motifs. *Gene Ther* 8: 1024-1032.

35. Segura, T., and Shea, L. D. (2001). Materials for non-viral gene delivery. *Ann Rev Mater Res* 31: 25-46.

36. Loser, P., Huser, A., Hillgenberg, M., Kumin, D., Both, G. W., and Hofmann, C. (2002). Advances in the development of non-human viral DNA-vectors for gene delivery. *Curr Gene Ther* 2: 161-171.

37. Kootstra, N. A., and Verma, I. M. (2003). Gene therapy with viral vectors. *Annu Rev Pharmacol Toxicol* 43: 413-439.

38. Zaharoff, D. A., Barr, R. C., Li, C. Y., and Yuan, F. (2002). Electromobility of plasmid DNA in tumor tissues during electric field-mediated gene delivery. *Gene Ther* 9: 1286-1290.

39. Alden, T. D., et al. (1999). In vivo endochondral bone formation using a bone morphogenetic protein 2 adenoviral vector. *Hum Gene Ther* 10: 2245-2253.

40. Musgrave, D. S., Bosch, P., Ghivizzani, S., Robbins, P. D., Evans, C. H., and Huard, J. (1999). Adenovirus-mediated direct gene therapy with bone morphogenetic protein-2 produces bone. *Bone* 24: 541-547.

41. Beer, S. J., Matthews, C. B., Stein, C. S., Ross, B. D., Hilfinger, J. M., and Davidson, B. L. (1998). Poly (lactic-glycolic) acid copolymer encapsulation of recombinant adenovirus reduces immunogenicity in vivo. *Gene Ther* 5: 740-746.

42. Ochiya, T., Nagahara, S., Sano, A., Itoh, H., and Terada, M. (2001). Biomaterials for gene delivery: atelocollagen-mediated controlled release of molecular medicines. *Curr Gene Ther* 1: 31-52.

43. Scherer, F., Schillinger, U., Putz, U., Stemberger, A., and Plank, C. (2002). Nonviral vector loaded collagen sponges for sustained gene delivery in vitro and in vivo. *J Gene Med* 4: 634-643.

44. Levy, R. J., et al. (2001). Localized adenovirus gene delivery using antiviral IgG complexation. *Gene Therapy* 8: 659-667.

45. Segura, T., and Shea, L. D. (2002). Surface-tethered DNA complexes for enhanced gene delivery. *Bioconjugate Chemistry* 13: 621-629.

46. Xie, Y., Yang, S. T., and Kniss, D. A. (2001). Three-dimensional cell-scaffold constructs promote efficient gene transfection: implications for cell-based gene therapy. *Tissue Eng* 7: 585-598.

47. Samuel, R. E., et al. (2002). Delivery of plasmid DNA to articular chondrocytes via novel collagen-glycosaminoglycan matrices. *Hum Gene Ther* 13: 791-802.

48. Kim, A., Checkla, D. M., Dehazya, P., and Chen, W. L. (2003). Characterization of DNA-hyaluronan matrix for sustained gene transfer. *Journal of Controlled Release* 90: 81-95.

49. Batycky, R. P., Hanes, J., Langer, R., and Edwards, D. A. (1997). A theoretical model of erosion and macromolecular drug release from biodegrading microspheres. *J Pharm Sci* 86: 1464-1477.

50. Bonadio, J., Smiley, E., Patil, P., and Goldstein, S. (1999). Localized, direct plasmid gene delivery in vivo: prolonged therapy results in reproducible tissue regeneration. *Nat Med* 5: 753-759.

51. Pascher, A., et al. (2004). Gene delivery to cartilage defects using coagulated bone marrow aspirate. *Gene Ther* 11: 133-141.

52. Berry, M., et al. (2001). Sustained effects of gene-activated matrices after CNS injury. *Mol Cell Neurosci* 17: 706-716.

53. Tyrone, J. W., et al. (2000). Collagen-embedded platelet-derived growth factor DNA plasmid promotes wound healing in a dermal ulcer model. *J Surg Res* 93: 230-236.

54. Klugherz, B. D., et al. (2000). Gene delivery from a DNA controlled-release stent in porcine coronary arteries. *Nat Biotechnol* 18: 1181-1184.

55. Cohen-Sacks, H., et al. (2004). Delivery and expression of pDNA embedded in collagen matrices. *J Control Release* 95: 309-320.

56. Hijjawi, J., et al. (2004). Platelet-derived growth factor B, but not fibroblast growth factor 2, plasmid DNA improves survival of ischemic myocutaneous flaps. *Arch Surg* 139: 142-147.

57. Ochiya, T., et al. (1999). New delivery system for plasmid DNA in vivo using atelocollagen as a carrier material: the Minipellet. *Nat Med* 5: 707-710.

58. Kushibiki, T., Tomoshige, R., Fukunaka, Y., Kakemi, M., and Tabata, Y. (2003). In vivo release and gene expression of plasmid DNA by hydrogels of gelatin with different cationization extents. *J Control Release* 90: 207-216.

59. Fang, J., et al. (1996). Stimulation of new bone formation by direct transfer of osteogenic plasmid genes. *Proc Natl Acad Sci U S A* 93: 5753-5758.

60. Chandler, L. A., et al. (2000). Matrix-enabled gene transfer for cutaneous wound repair. *Wound Repair Regen* 8: 473-479.

61. Chandler, L. A., et al. (2000). FGF2-Targeted adenovirus encoding platelet-derived growth factor-B enhances de novo tissue formation. *Mol Ther* 2: 153-160.

62. Doukas, J., et al. (2001). Matrix immobilization enhances the tissue repair activity of growth factor gene therapy vectors. *Hum Gene Ther* 12: 783-798.

63. Gu, D. L., et al. (2004). Adenovirus encoding human platelet-derived growth factor-B delivered in collagen exhibits safety, biodistribution, and immunogenicity profiles favorable for clinical use. *Mol Ther* 9: 699-711.

64. Perlstein, I., et al. (2003). DNA delivery from an intravascular stent with a denatured collagen-polylactic-polyglycolic acid-controlled release coating: mechanisms of enhanced transfection. *Gene Ther* 10: 1420-1428.

65. Lee, P. Y., Li, Z., and Huang, L. (2003). Thermosensitive hydrogel as a Tgf-beta1 gene delivery vehicle enhances diabetic wound healing. *Pharm Res* 20: 1995-2000.

66. Li, Z., et al. (2003). Controlled gene delivery system based on thermosensitive biodegradable hydrogel. *Pharm Res* 20: 884-888.

67. Lutolf, M. P., et al. (2003). Repair of bone defects using synthetic mimetics of collagenous extracellular matrices. *Nat Biotechnol* 21: 513-518.

68. Alsberg, E., Anderson, K. W., Albeiruti, A., Rowley, J. A., and Mooney, D. J. (2002). Engineering growing tissues. *Proc Natl Acad Sci U S A* 99: 12025-12030.

69. Bryant, S. J., Durand, K. L., and Anseth, K. S. (2003). Manipulations in hydrogel chemistry control photoencapsulated chondrocyte behavior and their extracellular matrix production. *J Biomed Mater Res* 67A: 1430-1436.

70. Williams, C. G., Kim, T. K., Taboas, A., Malik, A., Manson, P., and Elisseeff, J. (2003). In vitro chondrogenesis of bone marrow-derived mesenchymal stem cells in a photopolymerizing hydrogel. *Tissue Eng* 9: 679-688.

71. Taylor, S. J., McDonald, J. W., 3rd, and Sakiyama-Elbert, S. E. (2004). Controlled release of neurotrophin-3 from fibrin gels for spinal cord injury. *J Control Release* 98: 281-294.

72. Meilander, N. J., Pasumarthy, M. K., Kowalczyk, T. H., Cooper, M. J., and Bellamkonda, R. V. (2003). Sustained release of plasmid DNA using lipid microtubules and agarose hydrogel. *J Control Release* 88: 321-331.

73. Jozkowicz, A., et al. (2003). Delivery of high dose VEGF plasmid using fibrin carrier does not influence its angiogenic potency. *International Journal of Artificial Organs* 26: 161-169.

74. Quick, D. J., and Anseth, K. S. (2004). DNA delivery from photocrosslinked PEG hydrogels: encapsulation efficiency, release profiles, and DNA quality. *J Control Release* 96: 341-351.

75. Eliaz, R. E., and Szoka, F. C., Jr. (2002). Robust and prolonged gene expression from injectable polymeric implants. *Gene Ther* 9: 1230-1237.

76. Nof, M., and Shea, L. D. (2002). Drug-releasing scaffolds fabricated from drug-loaded microspheres. *Journal of Biomedical Materials Research* 59: 349-356.

77. Huang, Y. C., Connell, M., Park, Y., Mooney, D. J., and Rice, K. G. (2003). Fabrication and in vitro testing of polymeric delivery system for condensed DNA. *J Biomed Mater Res* 67A: 1384-1392.

78. Baltzer, A. W., et al. (2000). Genetic enhancement of fracture repair: healing of an experimental segmental defect by adenoviral transfer of the BMP-2 gene. *Gene Ther* 7: 734-739.

79. Okubo, Y., Bessho, K., Fujimura, K., Iizuka, T., and Miyatake, S. I. (2000). Osteoinduction by bone morphogenetic protein-2 via adenoviral vector under transient immunosuppression. *Biochem Biophys Res Commun* 267: 382-387.

80. Sailaja, G., HogenEsch, H., North, A., Hays, J., and Mittal, S. K. (2002). Encapsulation of recombinant adenovirus into alginate microspheres circumvents vector-specific immune response. *Gene Ther* 9: 1722-1729.

81. Siemens, D. R., Austin, J. C., Hedican, S. P., Tartaglia, J., and Ratliff, T. L. (2000). Viral vector delivery in solid-state vehicles: gene expression in a murine prostate cancer model. *J Natl Cancer Inst* 92: 403-412.

82. Doukas, J., et al. (2002). Delivery of FGF genes to wound repair cells enhances arteriogenesis and myogenesis in skeletal muscle. *Mol Ther* 5: 517-527.

83. Segura, T., Volk, M. J., and Shea, L. D. (2003). Substrate-mediated DNA delivery: role of the cationic polymer structure and extent of modification. *Journal of Controlled Release* 93: 69-84.

84. Bengali, Z., Rea, J. C., and Shea, L. D. (2007). Gene expression and internalization following vector adsorption to immobilized proteins: dependence on protein identity and density. *Journal of Gene Medicine* 9: 668-678.

85. Pannier, A. K., Anderson, B. C., and Shea, L. D. (2005). Substrate-mediated delivery from self-assembled monolayers: Effect of surface ionization, hydrophilicity, and patterning. *Acta Biomaterialia* 1: 511-522.

86. Bielinska, A. U., et al. (2000). Application of membrane-based dendrimer/DNA complexes for solid phase transfection in vitro and in vivo. *Biomaterials* 21: 877-887.

87. Kofron, M. D., and Laurencin, C. T. (2004). Development of a calcium phosphate co-precipitate/poly(lactideco-glycolide) DNA delivery system: release kinetics and cellular transfection studies. *Biomaterials* 25: 2637-2643.

88. Segura, T., Chung, P., and Shea, L. D. (in press). DNA Delivery from Hyaluronic Acid-Collagen Hydrogels via a Substrate-Mediated Approach. *Biomaterials*.

89. Klugherz, B. D., et al. (2002). Gene delivery to pig coronary arteries from stents carrying antibody-tethered adenovirus. *Human Gene Therapy* 13: 443-454.

90. Abrahams, J. M., Song, C. X., DeFelice, S., Grady, M. S., Diamond, S. L., and Levy, R. J. (2002). Endovascular microcoil gene delivery using immobilized anti-adenovirus antibody for vector tethering. *Stroke* 33: 1376-1382.

91. Stachelek, S. J., et al. (2004). Localized gene delivery using antibody tethered adenovirus from polyurethane heart valve cusps and intra-aortic implants. *Gene Therapy* 11: 15-24.

92. Ozbas-Turan, S., Aral, C., Kabasakal, L., Keyer-Uysal, M., and Akbuga, J. (2003). Co-encapsulation of two plasmids in chitosan microspheres as a non-viral gene delivery vehicle. *J Pharm Pharm Sci* 6: 27-32.

93. Kai, E., and Ochiya, T. (2004). A method for oral DNA delivery with N-acetylated chitosan. *Pharm Res* 21: 838-843.

94. Seliktar, D., Zisch, A. H., Lutolf, M. P., Wrana, J. L., and Hubbell, J. A. (2004). MMP-2 sensitive, VEGF-bearing bioactive hydrogels for promotion of vascular healing. *J Biomed Mater Res* 68A: 704-716.

95. Mason, D. J. (2004). Glutamate signalling and its potential application to tissue engineering of bone. *Eur Cell Mater* 7: 12-25; discussion 25-16.

96. Gronthos, S., Chen, S., Wang, C. Y., Robey, P. G., and Shi, S. (2003). Telomerase accelerates osteogenesis of bone marrow stromal stem cells by upregulation of CBFA1, osterix, and osteocalcin. *J Bone Miner Res* 18: 716-722.

97. Lee, J. Y., et al. (2002). Enhancement of bone healing based on ex vivo gene therapy using human muscle-derived cells expressing bone morphogenetic protein 2. *Hum Gene Ther* 13: 1201-1211.

98. Moutsatsos, I. K., et al. (2001). Exogenously regulated stem cell-mediated gene therapy for bone regeneration. *Mol Ther* 3: 449-461.

99. Eliopoulos, N., Al-Khaldi, A., Crosato, M., Lachapelle, K., and Galipeau, J. (2003). A neovascularized organoid derived from retrovirally engineered bone marrow stroma leads to prolonged in vivo systemic delivery of erythropoietin in nonmyeloablated, immunocompetent mice. *Gene Ther* 10: 478-489.

100. Hirata, K., et al. (2003). Transplantation of skin fibroblasts expressing BMP-2 promotes bone repair more effectively than those expressing Runx2. *Bone* 32: 502-512.

101. Kofron, M. D., Zhang, J. X., Lieberman, J. R., and Laurencin, C. T. (2003). Genetically modified mesodermal-derived cells for bone tissue engineering. *IEEE Eng Med Biol Mag* 22: 57-64.

102. Murray, M., and Fischer, T. (2001). Transplantation and gene therapy: Combined approaches for repair of spinal cord injury. *Neuroscientist* 7: 28-41.

103. Cao, L., et al. (2004). Olfactory ensheathing cells genetically modified to secrete GDNF to promote spinal cord repair. *Brain* 127: 535-549.

104. Ozawa, C. R., et al. (2004). Microenvironmental VEGF concentration, not total dose, determines a threshold between normal and aberrant angiogenesis. *J Clin Invest* 113: 516-527.

105. Rebar, E. J., et al. (2002). Induction of angiogenesis in a mouse model using engineered transcription factors. *Nat Med* 8: 1427-1432.

106. Varga, C. M., Hong, K., and Lauffenburger, D. A. (2001). Quantitative analysis of synthetic gene delivery vector design properties. *Mol Ther* 4: 438-446.

107. Zabner, J., Fasbender, A. J., Moninger, T., Poellinger, K. A., and Welsh, M. J. (1995). Cellular and molecular barriers to gene transfer by a cationic lipid. *J Biol Chem* 270: 18997-19007.

108. Hannon, G. J., and Rossi, J. J. (2004). Unlocking the potential of the human genome with RNA interference. *Nature* 431: 371-378.

109. Barron, A. E., Blanch, H. W., and Soane, D. S. (1994). A Transient Entanglement Coupling Mechanism for DNA Separation by Capillary Electrophoresis in Ultradilute Polymer-Solutions. *Electrophoresis* 15: 597-615.

110. Gordon, E. M., Barrett, R. W., Dower, W. J., Fodor, S. P. A., and Gallop, M. A. (1994). Applications of Combinatorial Technologies to Drug Discovery .2. Combinatorial Organic-Synthesis, Library Screening Strategies, and Future-Directions. *Journal of Medicinal Chemistry* 37: 1385-1401.

111. Pannier, A. K., Ariazi, E. A., Bellis, A. D., Bengali, Z., Jordan, V. C., and Shea, L. D. (2007). Bioluminescence Imaging for assessment and normalization in transfected cell Arrays. *Biotechnology and Bioengineering* 98: 486-497.

112. Christman, K. L., et al. (2006). Submicron streptavidin patterns for protein assembly. *Langmuir* 22: 7444-7450.

113. Rozkiewicz, D. I., et al. (2006). Covalent microcontact printing of proteins for cell patterning. *Chemistry-a European Journal* 12: 6290-6297.

114. Dewez, J. L., et al. (1998). Adhesion of mammalian cells to polymer surfaces: from physical chemistry of surfaces to selective adhesion on defined patterns. *Biomaterials* 19: 1441-1445.

115. Hand, A. (2006). High-Index Lenses Push Immersion Beyond 32 nm. In *Semiconductor International*.

116. Schena, M., Shalon, D., Davis, R. W., and Brown, P. O. (1995). Quantitative Monitoring of Gene-Expression Patterns with a Complementary-DNA Microarray. *Science* 270: 467-470.

117. Lockhart, D. J., et al. (1996). Expression monitoring by hybridization to high-density oligonucleotide arrays. *Nature Biotechnology* 14: 1675-1680.

118. Fodor, S. P. A., Read, J. L., Pirrung, M. C., Stryer, L., Lu, A. T., and Solas, D. (1991). Light-Directed, Spatially Addressable Parallel Chemical Synthesis. *Science* 251: 767-773.

119. Chee, M., et al. (1996). Accessing genetic information with high-density DNA arrays. *Science* 274: 610-614.

120. Michel, R., et al. (2002). Selective molecular assembly patterning: A new approach to micro- and nanochemical patterning of surfaces for biological applications. *Langmuir* 18: 3281-3287.

121. Whitesides, G. M., Ostuni, E., Takayama, S., Jiang, X., and Ingber, D. E. (2001). Soft lithography in biology and biochemistry. *Annual review of biomedical engineering* 3: 335-373.

122. Xia, Y. N., and Whitesides, G. M. (1998). Soft lithography. *Annual Review of Materials Science* 28: 153-184.

123. Trimbach, D. C., Al-Hussein, M., de Jeu, W. H., Decre, M., Broer, D. J., and Bastiaansen, C. W. M. (2004). Hydrophilic elastomers for microcontact printing of polar inks. *Langmuir* 20: 4738-4742.

124. Lee, S., Iten, R., Muller, M., and Spencer, N. D. (2004). Influence of molecular architecture on the adsorption of poly(ethylene oxide)-poly(propylene oxide)-poly(ethylene oxide) on PDMS surfaces and implications for aqueous lubrication. *Macromolecules* 37: 8349-8356.

125. Patrito, N., McLachlan, J. M., Faria, S. N., Chan, J., and Norton, P. R. (2007). A novel metal-protected plasma treatment for the robust bonding of polydimethylsiloxane. *Lab on a Chip* 7: 1813-1818.

126. Qin, M., et al. (2007). Two methods for glass surface modification and their application in protein immobilization. *Colloids and Surfaces B-Biointerfaces* 60: 243-249.

127. Csucs, G., Michel, R., Lussi, J. W., Textor, M., and Danuser, G. (2003). Microcontact printing of novel co-polymers in combination with proteins for cell-biological applications. *Biomaterials* 24: 1713-1720.

128. Whitesides, G. M., and Laibinis, P. E. (1990). Wet Chemical Approaches to the Characterization of Organic-Surfaces - Self-Assembled Monolayers, Wetting, and the Physical Organic-Chemistry of the Solid Liquid Interface. *Langmuir* 6: 87-96.

129. Mrksich, M., Dike, L. E., Tien, J., Ingber, D. E., and Whitesides, G. M. (1997). Using microcontact printing to pattern the attachment of mammalian cells to self-assembled monolayers of alkanethiolates on transparent films of gold and silver. *Experimental cell research* 235: 305-313.

130. Zhang, S. G., et al. (1999). Biological surface engineering: a simple system for cell pattern formation. *Biomaterials* 20: 1213-1220.

131. Sharma, V., Dhayal, M., Govind, Shivaprasad, S. M., and Jain, S. C. (2007). Surface characterization of plasma-treated and PEG-grafted PDMS for micro fluidic applications. *Vacuum* 81: 1094-1100.

132. Liu, J. K., Sun, X. F., and Lee, M. L. (2007). Adsorption-resistant acrylic copolymer for prototyping of microfluidic devices for proteins and peptides. *Analytical Chemistry* 79: 1926-1931.

133. Saadi, W., Wang, S. J., Lin, F., and Jeon, N. L. (2006). A parallel-gradient microfluidic chamber for quantitative analysis of breast cancer cell chemotaxis. *Biomedical Microdevices* 8: 109-118.

134. Caelen, I., Bernard, A., Juncker, D., Michel, B., Heinzelmann, H., and Delamarche, E. (2000). Formation of gradients of proteins on surfaces with microfluidic networks. *Langmuir* 16: 9125-9130.

135. Terrill, R. H., Balss, K. M., Zhang, Y. M., and Bohn, P. W. (2000). Dynamic monolayer gradients: Active spatiotemporal control of alkanethiol coatings on thin gold films. *Journal of the American Chemical Society* 122: 988-989.

136. Sharma, S., Tan, W., and Desai, T. A. (2005). Improving the integrity of three-dimensional vascular patterns by poly(ethylene glycol) conjugation. *Bioconjugate Chem* 16: 18-22.

137. Takayama, S., Ostuni, E., LeDuc, P., Naruse, K., Ingber, D. E., and Whitesides, G. M. (2001). Laminar flows - Subcellular positioning of small molecules. *Nature* 411: 1016-1016.

138. Jackman, R. J., Duffy, D. C., Cherniavskaya, O., and Whitesides, G. M. (1999). Using elastomeric membranes as dry resists and for dry lift-off. *Langmuir* 15: 2973-2984.

139. Piner, R. D., Zhu, J., Xu, F., Hong, S. H., and Mirkin, C. A. (1999). "Dip-pen" nanolithography. *Science* 283: 661-663.

140. Lee, K. B., Park, S. J., and Mirkin, C. A. (2002). Protein nanoarrays generated by Dip-Pen Nanolithography. *Abstracts of Papers of the American Chemical Society* 223: C94-C94.

141. Wilson, D. L., Martin, R., Hong, S., Cronin-Golomb, M., Mirkin, C. A., and Kaplan, D. L. (2001). Surface organization and nanopatterning of collagen by dip-pen nanolithography. *Proceedings of the National Academy of Sciences of the United States of America* 98: 13660-13664.

142. Cukierman, E., Pankov, R., Stevens, D. R., and Yamada, K. M. (2001). Taking cell-matrix adhesions to the third dimension. *Science* 294: 1708-1712.

143. Bryant, S. J., Nuttelman, C. R., and Anseth, K. S. (2000). Cytocompatibility of UV and visible light photoinitiating systems on cultured NIH/3T3 fibroblasts in vitro. *Journal of Biomaterials Science-Polymer Edition* 11: 439-457.

144. Tsang, V. L., and Bhatia, S. N. (2004). Three-dimensional tissue fabrication. *Advanced drug delivery reviews* 56: 1635-1647.

145. Revzin, A., et al. (2001). Fabrication of poly(ethylene glycol) hydrogel microstructures using photolithography. *Langmuir* 17: 5440-5447.

146. Liu, V. A., and Bhatia, S. N. (2002). Three-dimensional photopatterning of hydrogels containing living cells. *Biomedical Microdevices* 4: 257-266.

147. Tsang, V. L., et al. (2007). Fabrication of 3D hepatic tissues by additive photopatterning of cellular hydrogels. *Faseb Journal* 21: 790-801.

148. Park, A., Wu, B., and Griffith, L. G. (1998). Integration of surface modification and 3D fabrication techniques to prepare patterned poly(L-lactide) substrates allowing regionally selective cell adhesion. *Journal of Biomaterials Science-Polymer Edition* 9: 89-110.

149. Kim, S. S., et al. (1998). Survival and function of hepatocytes on a novel three-dimensional synthetic biodegradable polymer scaffold with an intrinsic network of channels. *Annals of Surgery* 228: 8-13.

150. Hahn, M. S., Miller, J. S., and West, J. L. (2006). Three-dimensional Biochemical and Biomechanical Patterning of Hydrogels for Guiding Cell Behavior. *Advanced Materials* 18: 2679-2684.

151. Purves, D., Augustine, G. J., Fitzpatrick, D., Katz, L., LaMantia, A. S., and McNamara, J. O., Eds. (1997). *Neuroscience*, Sinauer Associates, Inc, Sunderland, MA.
152. Lodish, H., Berk, A., Zipursky, S. L., Matsudaira, P., Baltimore, D., and Darnell, J. E. (1999). *Molecular Cell Biology*, W. H. Freeman and Company, New York, New York.

153. Hatten, M. E. (1999). Central nervous system neuronal migration. *Annual Review of Neuroscience* 22: 511-539.

154. Wen, Z. X., and Zheng, J. Q. (2006). Directional guidance of nerve growth cones. *Current Opinion in Neurobiology* 16: 52-58.

155. Hannula-Jouppi, K., et al. (2005). The axon guidance receptor gene ROBO1 is a candidate gene for developmental dyslexia. *PLoS genetics* 1: e50.

156. Holtmaat, A. J., et al. (2003). Transient downregulation of Sema3A mRNA in a rat model for temporal lobe epilepsy. A novel molecular event potentially contributing to mossy fiber sprouting. *Experimental neurology* 182: 142-150.

157. Wong, E. V., Kenwrick, S., Willems, P., and Lemmon, V. (1995). Mutations in the cell adhesion molecule L1 cause mental retardation. *Trends Neurosci* 18: 168-172.

158. Cajal, S. R. y. (1890). A quelle epoque apparaissent les expansions des cellules nerveuses de la moelle epiniere du poulet? *Anatomomischer Anzeiger* 21-22: 609-639.

159. Tanaka, E., and Sabry, J. (1995). Making the connection: cytoskeletal rearrangements during growth cone guidance. *Cell* 83: 171-176.

160. Harrison, R. G. (1910). The outgrowth of the nerve fiber as a mode of protoplasmic movement. *The Journal of experimental zoology* 9: 787-846.

161. Kalil, K., and Dent, E. W. (2005). Touch and go: guidance cues signal to the growth cone cytoskeleton. *Curr Opin Neurobiol* 15: 521-526.

162. Cajal, R. y. (1892). La rétine des vertébrés. *La Cellule* 9: 119.
163. Campenot, R. B. (1977). Local control of neurite development by nerve growth factor. *Proceedings of the National Academy of Sciences of the United States of America* 74: 4516-4519.

164. Ebendal, T., and Jacobson, C. O. (1977). Tissue explants affecting extension and orientation of axons in cultured chick embryo ganglia. *Experimental cell research* 105: 379-387.

165. Cook, G., Tannahill, D., and Keynes, R. (1998). Axon guidance to and from choice points. *Curr Opin Neurobiol* 8: 64-72.

166. Huber, A. B., Kolodkin, A. L., Ginty, D. D., and Cloutier, J. F. (2003). Signaling at the growth cone: ligand-receptor complexes and the control of axon growth and guidance. *Annu Rev Neurosci* 26: 509-563.

167. Mueller, B. K. (1999). Growth cone guidance: first steps towards a deeper understanding. *Annu Rev Neurosci* 22: 351-388.

168. Colamarino, S. A., and Tessier-Lavigne, M. (1995). The Role of the Floor Plate in Axon Guidance. *Annual Review of Neuroscience* 18: 497-529.

169. Serafini, T., et al. (1996). Netrin-1 is required for commissural axon guidance in the developing vertebrate nervous system. *Cell* 87: 1001-1014.

170. MacLennan, A. J., et al. (1997). Immunohistochemical localization of netrin-1 in the embryonic chick nervous system. *Journal of Neuroscience* 17: 5466-5479.

171. Tessier-Lavigne, M., and Placzek, M. (1991). Target Attraction - Are Developing Axons Guided by Chemotropism. *Trends in Neurosciences* 14: 303-310.

172. Thompson, H., Camand, O., Barker, D., and Erskine, L. (2006). Slit proteins regulate distinct aspects of retinal ganglion cell axon guidance within dorsal and ventral retina. *J Neurosci* 26: 8082-8091.
173. Wiesendanger, R., and Wiesendanger, M. (1982). The corticopontine system in the rat. II. The projection pattern. *The Journal of comparative neurology* 208: 227-238.

174. Wiesendanger, R., and Wiesendanger, M. (1982). The corticopontine system in the rat. I. Mapping of corticopontine neurons. *The Journal of comparative neurology* 208: 215-226.

175. Heffner, C. D., Lumsden, A. G. S., and Oleary, D. D. M. (1990). Target Control of Collateral Extension and Directional Axon Growth in the Mammalian Brain. *Science* 247: 217-220.

176. Song, H. J., and Poo, M. M. (2001). The cell biology of neuronal navigation. *Nature Cell Biology* 3: E81-E88.

177. Goodhill, G. J. (1998). Mathematical guidance for axons. *Trends Neurosci* 21: 226-231.

178. Kennedy, T. E., Wang, H., Marshall, W., and Tessier-Lavigne, M. (2006). Axon guidance by diffusible chemoattractants: A gradient of netrin protein in the developing spinal cord. *Journal of Neuroscience* 26: 8866-8874.

179. Mortimer, D., Fothergill, T., Pujic, Z., Richards, L. J., and Goodhill, G. J. (2008). Growth cone chemotaxis. *Trends Neurosci* 31: 90-98.

180. Serafini, T., Kennedy, T. E., Galko, M. J., Mirzayan, C., Jessell, T. M., and Tessierlavigne, M. (1994). The Netrins Define a Family of Axon Outgrowth-Promoting Proteins Homologous to C-Elegans Unc-6. *Cell* 78: 409-424.

181. Kennedy, T. E., Serafini, T., Delatorre, J. R., and Tessierlavigne, M. (1994). Netrins Are Diffusible Chemotropic Factors for Commissural Axons in the Embryonic Spinal-Cord. *Cell* 78: 425-435.

182. Richards, L. J., Koester, S. E., Tuttle, R., and O'Leary, D. D. (1997). Directed growth of early cortical axons is influenced by a chemoattractant released from an intermediate target. *J Neurosci* 17: 2445-2458.
183. Deiner, M. S., Kennedy, T. E., Fazeli, A., Serafini, T., TessierLavigne, M., and Sretavan, D. W. (1997). Netrin-1 and DCC mediate axon guidance locally at the optic disc: Loss of function leads to optic nerve hypoplasia. *Neuron* 19: 575-589.

184. Chan, S. S., et al. (1996). UNC-40, a C. elegans homolog of DCC (Deleted in Colorectal Cancer), is required in motile cells responding to UNC-6 netrin cues. *Cell* 87: 187-195.

185. Hamelin, M., Zhou, Y., Su, M. W., Scott, I. M., and Culotti, J. G. (1993). Expression of the UNC-5 guidance receptor in the touch neurons of C. elegans steers their axons dorsally. *Nature* 364: 327-330.

186. Song, H. J., Ming, G. L., and Poo, M. M. (1997). cAMP-induced switching in turning direction of nerve growth cones. *Nature* 388: 275-279.

187. Mark, M. D., Lohrum, M., and Puschel, A. W. (1997). Patterning neuronal connections by chemorepulsion: the semaphorins. *Cell and tissue research* 290: 299-306.

188. Messersmith, E. K., Leonardo, E. D., Shatz, C. J., Tessier-Lavigne, M., Goodman, C. S., and Kolodkin, A. L. (1995). Semaphorin III can function as a selective chemorepellent to pattern sensory projections in the spinal cord. *Neuron* 14: 949-959.

189. He, Z., and Tessier-Lavigne, M. (1997). Neuropilin is a receptor for the axonal chemorepellent Semaphorin III. *Cell* 90: 739-751.

190. Feiner, L., Koppel, A. M., Kobayashi, H., and Raper, J. A. (1997). Secreted chick semaphorins bind recombinant neuropilin with similar affinities but bind different subsets of neurons in situ. *Neuron* 19: 539-545.

191. Levi-Montalcini, R. (1952). Effects of mouse tumor transplantation on the nervous system. *Annals of the New York Academy of Sciences* 55: 330-344.

192. Cohen, S., Levi-Montalcini, R., and Hamburger, V. (1954). A Nerve Growth-Stimulating Factor Isolated from Sarcom as 37 and 180. *Proceedings of the National Academy of Sciences of the United States of America* 40: 1014-1018.

193. Davies, A. M., Bandtlow, C., Heumann, R., Korsching, S., Rohrer, H., and Thoenen, H. (1987). Timing and site of nerve growth factor synthesis in developing skin in relation to innervation and expression of the receptor. *Nature* 326: 353-358.

194. Markus, A., Patel, T. D., and Snider, W. D. (2002). Neurotrophic factors and axonal growth. *Curr Opin Neurobiol* 12: 523-531.

195. Cao, X., and Shoichet, M. S. (2003). Investigating the synergistic effect of combined neurotrophic factor concentration gradients to guide axonal growth. *Neuroscience* 122: 381-389.

196. Bregman, B. S., McAtee, M., Dal, H. N., and Kuhn, P. L. (1997). Neurotrophic factors increase axonal growth after spinal cord injury and transplantation in the adult rat. *Experimental neurology* 148: 475-494.

197. Menesini Chen, M. G., Chen, J. S., and Levi-Montalcini, R. (1978). Sympathetic nerve fibers ingrowth in the central nervous system of neonatal rodent upon intracerebral NGF injections. *Archives italiennes de biologie* 116: 53-84.

198. Gundersen, R. W., and Barrett, J. N. (1979). Neuronal Chemotaxis - Chick Dorsal-Root Axons Turn toward High-Concentrations of Nerve Growth-Factor. *Science* 206: 1079-1080.

199. Letourneau, P. C. (1978). Chemotactic Response of Nerve-Fiber Elongation to Nerve Growth-Factor. *Developmental Biology* 66: 183-196.

200. Fitzgerald, M., Kwiat, G. C., Middleton, J., and Pini, A. (1993). Ventral spinal cord inhibition of neurite outgrowth from embryonic rat dorsal root ganglia. *Development* 117: 1377-1384.

201. Cao, X., and Shoichet, M. S. (2001). Defining the concentration gradient of nerve growth factor for guided neurite outgrowth. *Neuroscience* 103: 831-840.

202. Adler, J. (1975). Chemotaxis in bacteria. *Annual review of biochemistry* 44: 341-356.

203. Goodhill, G. J. (1997). Diffusion in axon guidance. *European Journal of Neuroscience* 9: 1414-1421.

204. Zigmond, S. H. (1981). Consequences of Chemotactic Peptide Receptor Modulation for Leukocyte Orientation. *Journal of Cell Biology* 88: 644-647.

205. Tranquillo, R. T., and Lauffenburger, D. A. (1987). Stochastic model of leukocyte chemosensory movement. *Journal of mathematical biology* 25: 229-262.

206. Lohof, A. M., Quillan, M., Dan, Y., and Poo, M. M. (1992). Asymmetric modulation of cytosolic cAMP activity induces growth cone turning. *J Neurosci* 12: 1253-1261.

207. Zheng, J. Q., Felder, M., Connor, J. A., and Poo, M. M. (1994). Turning of nerve growth cones induced by neurotransmitters. *Nature* 368: 140-144.

208. Isbister, C. M., Mackenzie, P. J., To, K. C. W., and O'Connor, T. P. (2003). Gradient steepness influences the pathfinding decisions of neuronal growth cones in vivo. *Journal of Neuroscience* 23: 193-202.

209. Cunningham, B. A., Hemperly, J. J., Murray, B. A., Prediger, E. A., Brackenbury, R., and Edelman, G. M. (1987). Neural cell adhesion molecule: structure, immunoglobulin-like domains, cell surface modulation, and alternative RNA splicing. *Science* 236: 799-806.

210. Walsh, F. S., and Doherty, P. (1997). Neural cell adhesion molecules of the immunoglobulin superfamily: role in axon growth and guidance. *Annual review of cell and developmental biology* 13: 425-456.

211. Hoffman, S., et al. (1982). Chemical characterization of a neural cell adhesion molecule purified from embryonic brain membranes. *The Journal of biological chemistry* 257: 7720-7729.

212. Cremer, H., Chazal, G., Goridis, C., and Represa, A. (1997). NCAM is essential for axonal growth and fasciculation in the hippocampus. *Molecular and cellular neurosciences* 8: 323-335.

213. Cohen, N. R., Taylor, J. S. H., Scott, L. B., Guillery, R. W., Soriano, P., and Furley, A. J. W. (1998). Errors in corticospinal axon guidance in mice lacking the neural cell adhesion molecule L1. *Current Biology* 8: 26-33.

214. Lander, A. D. (1987). Molecules that make axons grow. *Mol Neurobiol* 1: 213-245.

215. Hynes, R. O., and Lander, A. D. (1992). Contact and adhesive specificities in the associations, migrations, and targeting of cells and axons. *Cell* 68: 303-322.

216. Liesi, P., and Silver, J. (1988). Is Astrocyte Laminin Involved in Axon Guidance in the Mammalian Cns. *Developmental Biology* 130: 774-785.

217. Snow, D. M., Watanabe, M., Letourneau, P. C., and Silver, J. (1991). A chondroitin sulfate proteoglycan may influence the direction of retinal ganglion cell outgrowth. *Development* 113: 1473-1485.

218. Blochl, A., and Thoenen, H. (1995). Characterization of nerve growth factor (NGF) release from hippocampal neurons: evidence for a constitutive and an unconventional sodium-dependent regulated pathway. *The European journal of neuroscience* 7: 1220-1228.

219. Frazier, W. A., Boyd, L. F., and Bradshaw, R. A. (1973). Interaction of nerve growth factor with surface membranes: biological competence of insolubilized nerve growth factor. *Proceedings of the National Academy of Sciences of the United States of America* 70: 2931-2935.

220. Gundersen, R. W. (1985). Sensory Neurite Growth Cone Guidance by Substrate Adsorbed Nerve Growth-Factor. *Journal of Neuroscience Research* 13: 199-212.

221. Goodhill, G. J., and Urbach, J. S. (1999). Theoretical analysis of gradient detection by growth cones. *Journal of Neurobiology* 41: 230-241.

222. Clark, P., Britland, S., and Connolly, P. (1993). Growth cone guidance and neuron morphology on micropatterned laminin surfaces. *Journal of cell science* 105 ( Pt 1): 203-212.

223. Dertinger, S. K., Jiang, X., Li, Z., Murthy, V. N., and Whitesides, G. M. (2002). Gradients of substrate-bound laminin orient axonal specification of neurons. *Proceedings of the National Academy of Sciences of the United States of America* 99: 12542-12547.

224. Adams, D. N., Kao, E. Y., Hypolite, C. L., Distefano, M. D., Hu, W. S., and Letourneau, P. C. (2005). Growth cones turn and migrate up an immobilized gradient of the laminin IKVAV peptide. *J Neurobiol* 62: 134-147.

225. Dent, E. W., and Gertler, F. B. (2003). Cytoskeletal dynamics and transport in growth cone motility and axon guidance. *Neuron* 40: 209-227.

226. Goldberg, D. J., and Burmeister, D. W. (1986). Stages in axon formation: observations of growth of Aplysia axons in culture using video-enhanced contrast-differential interference contrast microscopy. *The Journal of cell biology* 103: 1921-1931.

227. Gallo, G., and Letourneau, P. C. (2004). Regulation of growth cone actin filaments by guidance cues. *J Neurobiol* 58: 92-102.

228. Luduena, R. F. (1998). Multiple forms of tubulin: different gene products and covalent modifications. *International review of cytology* 178: 207-275.

229. Li, X., et al. (2002). The adaptor protein Nck-1 couples the netrin-1 receptor DCC (deleted in colorectal cancer) to the activation of the small GTPase Rac1 through an atypical mechanism. *The Journal of biological chemistry* 277: 37788-37797.

230. Zhou, F. Q., Zhou, J., Dedhar, S., Wu, Y. H., and Snider, W. D. (2004). NGF-induced axon growth is mediated by localized inactivation of GSK-3beta and functions of the microtubule plus end binding protein APC. *Neuron* 42: 897-912.

231. Avellino, A. M., Hart, D., Dailey, A. T., MacKinnon, M., Ellegala, D., and Kliot, M. (1995). Differential macrophage responses in the peripheral and central nervous system during wallerian degeneration of axons. *Experimental neurology* 136: 183-198.

232. McKeon, R. J., Schreiber, R. C., Rudge, J. S., and Silver, J. (1991). Reduction of neurite outgrowth in a model of glial scarring following CNS injury is correlated with the expression of inhibitory molecules on reactive astrocytes. *J Neurosci* 11: 3398-3411.

233. Richardson, P. M., McGuinness, U. M., and Aguayo, A. J. (1980). Axons from CNS neurons regenerate into PNS grafts. *Nature* 284: 264-265.

234. McDonald, J. W. (1999). Repairing the damaged spinal cord. *Scientific American* 281: 64-73.

235. Archibald, S. J., Shefner, J., Krarup, C., and Madison, R. D. (1995). Monkey median nerve repaired by nerve graft or collagen nerve guide tube. *J Neurosci* 15: 4109-4123.

236. Lundborg, G., Dahlin, L., Dohi, D., Kanje, M., and Terada, N. (1997). A new type of "bioartificial" nerve graft for bridging extended defects in nerves. *Journal of hand surgery (Edinburgh, Scotland)* 22: 299-303.

237. Lundborg, G., Rosen, B., Dahlin, L., Danielsen, N., and Holmberg, J. (1997). Tubular versus conventional repair of median and ulnar nerves in the human forearm: early results from a prospective, randomized, clinical study. *The Journal of hand surgery* 22: 99-106.

238. De Laporte, L., Yang, Y., Zelivyanskaya, M., Cummings, B. J., Anderson, A. J., and Shea, L. D. (2008). Plasmid releasing multiple channel bridges for transgene expression after spinal cord injury. *submitted*.

239. Borgens, R. B., Shi, R., and Bohnert, D. (2002). Behavioral recovery from spinal cord injury following delayed application of polyethylene glycol. *The Journal of experimental biology* 205: 1-12.

240. Joosten, E. A., Bar, P. R., and Gispen, W. H. (1995). Collagen implants and cortico-spinal axonal growth after mid-thoracic spinal cord lesion in the adult rat. *J Neurosci Res* 41: 481-490.

241. Spilker, M. H., Yannas, I. V., Kostyk, S. K., Norregaard, T. V., Hsu, H. P., and Spector, M. (2001). The effects of tubulation on healing and scar formation after transection of the adult rat spinal cord. *Restorative neurology and neuroscience* 18: 23-38.

242. Blesch, A., Lu, P., and Tuszynski, M. H. (2002). Neurotrophic factors, gene therapy, and neural stem cells for spinal cord repair. *Brain research bulletin* 57: 833-838.

243. Xu, X. M., Chen, A., Guenard, V., Kleitman, N., and Bunge, M. B. (1997). Bridging Schwann cell transplants promote axonal regeneration from both the rostral and caudal stumps of transected adult rat spinal cord. *Journal of neurocytology* 26: 1-16.

244. Nakahara, Y., Gage, F. H., and Tuszynski, M. H. (1996). Grafts of fibroblasts genetically modified to secrete NGF, BDNF, NT-3, or basic FGF elicit differential responses in the adult spinal cord. *Cell transplantation* 5: 191-204.

245. Ahmed, Z., et al. (2006). Schwann cell-derived factor-induced modulation of the NgR/p75NTR/EGFR axis disinhibits axon growth through CNS myelin in vivo and in vitro. *Brain* 129: 1517-1533.

246. Caroni, P., and Schwab, M. E. (1988). Antibody against myelin-associated inhibitor of neurite growth neutralizes nonpermissive substrate properties of CNS white matter. *Neuron* 1: 85-96.

247. Barritt, A. W., et al. (2006). Chondroitinase ABC promotes sprouting of intact and injured spinal systems after spinal cord injury. *J Neurosci* 26: 10856-10867.

248. Ahmed, Z., et al. (2005). Disinhibition of neurotrophin-induced dorsal root ganglion cell neurite outgrowth on CNS myelin by siRNA-mediated knockdown of NgR, p75NTR and Rho-A. *Molecular and cellular neurosciences* 28: 509-523.

249. Filbin, M. T. (2006). Recapitulate development to promote axonal regeneration: good or bad approach? *Philosophical transactions of the Royal Society of London* 361: 1565-1574.

250. Mahoney, M. J., Chen, R. R., Tan, J., and Saltzman, W. M. (2005). The influence of microchannels on neurite growth and architecture. *Biomaterials* 26: 771-778.

251. Young, R. C., Wiberg, M., and Terenghi, G. (2002). Poly-3-hydroxybutyrate (PHB): a resorbable conduit for long-gap repair in peripheral nerves. *British journal of plastic surgery* 55: 235-240.

252. Yang, Y., et al. (2007). Development and evaluation of silk fibroin-based nerve grafts used for peripheral nerve regeneration. *Biomaterials* 28: 5526-5535.

253. Li, J., and Shi, R. (2007). Fabrication of patterned multi-walled poly-l-lactic acid conduits for nerve regeneration. *J Neurosci Methods* 165: 257-264.

254. Yang, Y., et al. (2005). Neurotrophin releasing single and multiple lumen nerve conduits. *J Control Release* 104: 433-446.

255. Ahmed, Z., Underwood, S., and Brown, R. A. (2003). Nerve guide material made from fibronectin: assessment of in vitro properties. *Tissue Eng* 9: 219-231.

256. Cai, J., Peng, X., Nelson, K. D., Eberhart, R., and Smith, G. M. (2004). Synergistic improvements in cell and axonal migration across sciatic nerve lesion gaps using bioresorbable filaments and heregulin-beta1. *J Biomed Mater Res A* 69: 247-258.

257. Phillips, J. B., Bunting, S. C., Hall, S. M., and Brown, R. A. (2005). Neural tissue engineering: a self-organizing collagen guidance conduit. *Tissue Eng* 11: 1611-1617.

258. Jin, Y., Ziemba, K. S., and Smith, G. M. (2007). Axon growth across a lesion site along a preformed guidance pathway in the brain. *Experimental neurology*.

259. Yu, T. T., and Shoichet, M. S. (2005). Guided cell adhesion and outgrowth in peptide-modified channels for neural tissue engineering. *Biomaterials* 26: 1507-1514.

260. Moore, K., Macsween, M., and Shoichet, M. (2006). Immobilized concentration gradients of neurotrophic factors guide neurite outgrowth of primary neurons in macroporous scaffolds. *Tissue Engineering* 12: 267-278.

261. Dillon, R., Gadgil, C., and Othmer, H. G. (2003). Short- and long-range effects of Sonic hedgehog in limb development. *Proceedings of the National Academy of Sciences of the United States of America* 100: 10152-10157.

262. Marti, E., Bumcrot, D. A., Takada, R., and McMahon, A. P. (1995). Requirement of 19K form of Sonic hedgehog for induction of distinct ventral cell types in CNS explants. *Nature* 375: 322-325.

263. Briscoe, J., and Ericson, J. (1999). The specification of neuronal identity by graded Sonic Hedgehog signalling. *Semin Cell Dev Biol* 10: 353-362.

264. Liem, K. F., Jr., Tremml, G., Roelink, H., and Jessell, T. M. (1995). Dorsal differentiation of neural plate cells induced by BMP-mediated signals from epidermal ectoderm. *Cell* 82: 969-979.

265. Hofmann, C., Luo, G., Balling, R., and Karsenty, G. (1996). Analysis of limb patterning in BMP-7-deficient mice. *Dev Genet* 19: 43-50.

266. Tickle, C. (1999). Morphogen gradients in vertebrate limb development. *Semin Cell Dev Biol* 10: 345-351.
267. Strigini, M., and Cohen, S. M. (2000). Wingless gradient formation in the Drosophila wing. *Curr Biol* 10: 293-300.

268. Neumann, C. J., and Cohen, S. M. (1997). Long-range action of Wingless organizes the dorsal-ventral axis of the Drosophila wing. *Development* 124: 871-880.

269. Zecca, M., Basler, K., and Struhl, G. (1996). Direct and long-range action of a wingless morphogen gradient. *Cell* 87: 833-844.

270. Schneider, I. C., and Haugh, J. M. (2005). Quantitative elucidation of a distinct spatial gradient-sensing mechanism in fibroblasts. *The Journal of cell biology* 171: 883-892.

271. Singer, A. J., and Clark, R. A. (1999). Cutaneous wound healing. *N Engl J Med* 341: 738-746.

272. Jackson, C. L., and Reidy, M. A. (1993). Basic fibroblast growth factor: its role in the control of smooth muscle cell migration. *Am J Pathol* 143: 1024-1031.

273. Song, H. J., and Poo, M. M. (1999). Signal transduction underlying growth cone guidance by diffusible factors. *Curr Opin Neurobiol* 9: 355-363.

274. Jang, J. H., Houchin, T. H., Shea, L. D. (2004). Gene delivery from polymer scaffolds for tissue engineering. *Expert Reviews in Medical Devices* 1: 127-138.

275. Lutolf, M. P., and Hubbell, J. A. (2005). Synthetic biomaterials as instructive extracellular microenvironments for morphogenesis in tissue engineering. *Nat Biotechnol* 23: 47-55.

276. Segura, T., Chung, P. H., and Shea, L. D. (2005). DNA delivery from hyaluronic acid-collagen hydrogels via a substrate-mediated approach. *Biomaterials* 26: 1575-1584.

277. Jang, J. H., Bengali, Z., Houchin, T. L., and Shea, L. D. (2006). Surface adsorption of DNA to tissue engineering scaffolds for efficient gene delivery. *Journal of Biomedical Materials Research Part A* 77A: 50-58.

278. Bengali, Z., et al. (2005). Gene delivery through cell culture substrate adsorbed DNA complexes. *Biotechnology and Bioengineering* 90: 290-302.

279. Ziauddin, J., and Sabatini, D. M. (2001). Microarrays of cells expressing defined cDNAs. *Nature* 411: 107-110.

280. Gunawan, R. C., et al. (2005). Regiospecific control of protein expression in cells cultured on two-component counter gradients of extracellular matrix proteins. *Langmuir* 21: 3061-3068.

281. Luo, Y., and Shoichet, M. S. (2004). A photolabile hydrogel for guided three-dimensional cell growth and migration. *Nat Mater* 3: 249-253.

282. DeLong, S. A., Moon, J. J., and West, J. L. (2005). Covalently immobilized gradients of bFGF on hydrogel scaffolds for directed cell migration. *Biomaterials* 26: 3227-3234.

283. Vepari, C. P., and Kaplan, D. L. (2006). Covalently immobilized enzyme gradients within three-dimensional porous scaffolds. *Biotechnol Bioeng* 93: 1130-1137.

284. Meijering, E., Jacob, M., Sarria, J. C. F., Steiner, P., Hirling, H., and Unser, M. (2004). Design and validation of a tool for neurite tracing and analysis in fluorescence microscopy images. *Cytometry Part A* 58A: 167-176.

285. Stroh, M., Zipfel, W. R., Williams, R. M., Webb, W. W., and Saltzman, W. M. (2003). Diffusion of nerve growth factor in rat striatum as determined by multiphoton microscopy. *Biophys J* 85: 581-588.

286. Whittlesey, K. J., and Shea, L. D. (2006). Nerve growth factor expression by PLG-mediated lipofection. *Biomaterials* 27: 2477-2486.

287. Papra, A., Bernard, A., Juncker, D., Larsen, N. B., Michel, B., and Delamarche, E. (2001). Microfluidic networks made of poly(dimethylsiloxane), Si, and Au coated with polyethylene glycol for patterning proteins onto surfaces. *Langmuir* 17: 4090-4095.

288. McDonald, J. C., et al. (2000). Fabrication of microfluidic systems in poly(dimethylsiloxane). *Electrophoresis* 21: 27-40.

289. Liu, F., Yang, J. P., Huang, L., and Liu, D. X. (1996). Effect of non-ionic surfactants on the formation of DNA/emulsion complexes and emulsion-mediated gene transfer. *Pharmaceutical Research* 13: 1642-1646.

290. Gebhart, C. L., Sriadibhatla, S., Vinogradov, S., Lemieux, P., Alakhov, V., and Kabanov, A. V. (2002). Design and formulation of polyplexes based on pluronic-polyethyleneimine conjugates for gene transfer. *Bioconjugate Chem* 13: 937-944.

291. Nguyen, H. K., et al. (2000). Evaluation of polyether-polyethyleneimine graft copolymers as gene transfer agents. *Gene Therapy* 7: 126-138.

292. Miller, C., Shanks, H., Witt, A., Rutkowski, G., and Mallapragada, S. (2001). Oriented Schwann cell growth on micropatterned biodegradable polymer substrates. *Biomaterials* 22: 1263-1269.

293. Kam, L., Shain, W., Turner, J. N., and Bizios, R. (2001). Axonal outgrowth of hippocampal neurons on micro-scale networks of polylysine-conjugated laminin. *Biomaterials* 22: 1049-1054.

294. Miller, C., Jeftinija, S., and Mallapragada, S. (2002). Synergistic effects of physical and chemical guidance cues on neurite alignment and outgrowth on biodegradable polymer substrates. *Tissue Eng* 8: 367-378.

295. Heller, D. A., et al. (2005). Patterned networks of mouse hippocampal neurons on peptide-coated gold surfaces. *Biomaterials* 26: 883-889.

296. Lander, A. D., Nie, Q., and Wan, F. Y. (2002). Do morphogen gradients arise by diffusion? *Dev Cell* 2: 785-796.

297. Helm, C. L., Fleury, M. E., Zisch, A. H., Boschetti, F., and Swartz, M. A. (2005). Synergy between interstitial flow and VEGF directs capillary morphogenesis in vitro through a gradient amplification mechanism. *Proceedings of the National Academy of Sciences of the United States of America* 102: 15779-15784.

298. Singer, S. J., and Kupfer, A. (1986). The Directed Migration of Eukaryotic Cells. *Annual Review of Cell Biology* 2: 337-365.

299. Gallo, G., Lefcort, F. B., and Letourneau, P. C. (1997). The trkA receptor mediates growth cone turning toward a localized source of nerve growth factor. *Journal of Neuroscience* 17: 5445-5454.

300. Chamley, J. H., Goller, I., and Burnstoc.G (1973). Selective Growth of Sympathetic-Nerve Fibers to Explants of Normally Densely Innervated Autonomic Effector Organs in Tissue-Culture. *Developmental Biology* 31: 362-379.

301. Heron, P. M., Sutton, B. M., Curinga, G. M., Smith, G. M., and Snow, D. M. (2007). Localized gene expression of axon guidance molecules in neuronal co-cultures. *Journal of Neuroscience Methods* 159: 203-214.

302. Houchin-Ray, T., Whittlesey, K. J., and Shea, L. D. (2007). Spatially patterned gene delivery for localized neuron survival and neurite extension. *Molecular Therapy* 15: 705-712.

303. Tse, T. H. Z., Chan, B. P., Chan, C. M., and Lam, J. (2007). Mathematical modeling of guided neurite extension in an engineered conduit with multiple concentration gradients of nerve growth factor (NGF). *Annals of Biomedical Engineering* 35: 1561-1572.

304. The, I., Bellaiche, Y., and Perrimon, N. (1999). Hedgehog movement is regulated through tout velu-dependent synthesis of a heparan sulfate proteoglycan. *Molecular Cell* 4: 633-639.
305. Ramirez, F., and Rifkin, D. B. (2003). Cell signaling events: a view from the matrix. *Matrix Biology* 22: 101-107.

306. Sakiyama-Elbert, S. E., and Hubbell, J. A. (2000). Controlled release of nerve growth factor from a heparin-containing fibrin-based cell ingrowth matrix. *Journal of Controlled Release* 69: 149-158.

307. Pearce, F. L., Banthorp.Dv, Cook, J. M., and Vernon, C. A. (1973). Adsorption of Nerve Growth-Factor onto Surfaces - Implications for Assay in Tissue-Culture. *European Journal of Biochemistry* 32: 569-575.

308. Pettmann, B., Manthorpe, M., Powell, J. A., and Varon, S. (1988). Biological-Activities of Nerve Growth-Factor Bound to Nitrocellulose Paper by Western Blotting. *Journal of Neuroscience* 8: 3624-3632.

309. Hadlock, T., Sundback, C., Hunter, D., Cheney, M., and Vacanti, J. P. (2000). A polymer foam conduit seeded with Schwann cells promotes guided peripheral nerve regeneration. *Tissue Eng* 6: 119-127.

310. Xu, X. M., Zhang, S. X., Li, H., Aebischer, P., and Bunge, M. B. (1999). Regrowth of axons into the distal spinal cord through a Schwann-cell-seeded mini-channel implanted

into hemisected adult rat spinal cord. *The European journal of neuroscience* 11: 1723-1740.

311. Curinga, G., and Smith, G. M. (2008). Molecular/genetic manipulation of extrinsic axon guidance factors for CNS repair and regeneration. *Experimental neurology* 209: 333-342.

312. Yiu, G., and He, Z. (2006). Glial inhibition of CNS axon regeneration. *Nat Rev Neurosci* 7: 617-627.

313. David, S., and Lacroix, S. (2003). Molecular approaches to spinal cord repair. *Annu Rev Neurosci* 26: 411-440.

314. Geller, H. M., and Fawcett, J. W. (2002). Building a bridge: Engineering spinal cord repair. *Experimental neurology* 174: 125-136.

315. Schmidt, C. E., and Leach, J. B. (2003). Neural tissue engineering: strategies for repair and regeneration. *Annu Rev Biomed Eng* 5: 293-347.

316. Zhang, N., Yan, H., and Wen, X. (2005). Tissue-engineering approaches for axonal guidance. *Brain Res Brain Res Rev* 49: 48-64.

317. Moore, M. J., et al. (2006). Multiple-channel scaffolds to promote spinal cord axon regeneration. *Biomaterials* 27: 419-429.

318. Friedman, J. A., Windebank, A. J., Moore, M. J., Spinner, R. J., Currier, B. L., and Yaszemski, M. J. (2002). Biodegradable polymer grafts for surgical repair of the injured spinal cord. *Neurosurgery* 51: 742-751; discussion 751-742.

319. Bunge, M. B. (2001). Bridging areas of injury in the spinal cord. *Neuroscientist* 7: 325-339.

320. Bregman, B. S., et al. (2002). Transplants and neurotrophic factors increase regeneration and recovery of function after spinal cord injury. *Prog Brain Res* 137: 257-273.

321. Boyd, J. G., and Gordon, T. (2003). Neurotrophic factors and their receptors in axonal regeneration and functional recovery after peripheral nerve injury. *Mol Neurobiol* 27: 277-324.

322. Whittlesey, K. J., and Shea, L. D. (2004). Delivery systems for small molecule drugs, proteins, and DNA: the neuroscience/biomaterial interface. *Exp Neurol* 190: 1-16.

323. Segura, T., Volk, M. J., and Shea, L. D. (2003). Substrate-mediated DNA delivery: role of the cationic polymer structure and extent of modification. *J Control Release* 93: 69-84.

324. Lee, H., Jeong, J. H., and Park, T. G. (2002). PEG grafted polylysine with fusogenic peptide for gene delivery: high transfection efficiency with low cytotoxicity. *J Control Release* 79: 283-291.

325. Koyama, Y., et al. (2003). Novel poly(ethylene glycol) derivatives with carboxylic acid pendant groups: synthesis and their protection and enhancing effect on non-viral gene transfection systems. *J Biomater Sci Polym Ed* 14: 515-531.

326. Kalil, K., Szebenyi, G., and Dent, E. W. (2000). Common mechanisms underlying growth cone guidance and axon branching. *J Neurobiol* 44: 145-158.

327. Goldner, J. S., Bruder, J. M., Li, G., Gazzola, D., and Hoffman-Kim, D. (2006). Neurite bridging across micropatterned grooves. *Biomaterials* 27: 460-472.

328. Anderson, M. J., and Waxman, S. G. (1983). Regeneration of spinal neurons in inframammalian vertebrates: morphological and developmental aspects. *J Hirnforsch* 24: 371-398.

329. Jones, L. L., Oudega, M., Bunge, M. B., and Tuszynski, M. H. (2001). Neurotrophic factors, cellular bridges and gene therapy for spinal cord injury. *J Physiol* 533: 83-89.

330. Ramer, M. S., Priestley, J. V., and McMahon, S. B. (2000). Functional regeneration of sensory axons into the adult spinal cord. *Nature* 403: 312-316.

331. Zhou, L., and Shine, H. D. (2003). Neurotrophic factors expressed in both cortex and spinal cord induce axonal plasticity after spinal cord injury. *J Neurosci Res* 74: 221-226.

332. Megeed, Z., Haider, M., Li, D., O'Malley, B. W., Jr., Cappello, J., and Ghandehari, H. (2004). In vitro and in vivo evaluation of recombinant silk-elastinlike hydrogels for cancer gene therapy. *J Control Release* 94: 433-445.

333. Beer, S. J., Hilfinger, J. M., and Davidson, B. L. (1997). Extended release of adenovirus from polymer microspheres: Potential use in gene therapy for brain tumors. *Advanced drug delivery reviews* 27: 59-66.

334. Dao, M. A., Hashino, K., Kato, I., and Nolta, J. A. (1998). Adhesion to fibronectin maintains regenerative capacity during ex vivo culture and transduction of human hematopoietic stem and progenitor cells. *Blood* 92: 4612-4621.

335. Huang, Y. C., Simmons, C., Kaigler, D., Rice, K. G., and Mooney, D. J. (2005). Bone regeneration in a rat cranial defect with delivery of PEI-condensed plasmid DNA encoding for bone morphogenetic protein-4 (BMP-4). *Gene Ther* 12: 418-426.

336. Gundersen, R. W., and Barrett, J. N. (1979). Neuronal chemotaxis: chick dorsal-root axons turn toward high concentrations of nerve growth factor. *Science* 206: 1079-1080.

337. Paves, H., and Saarma, M. (1997). Neurotrophins as in vitro growth cone guidance molecules for embryonic sensory neurons. *Cell and tissue research* 290: 285-297.

338. Horch, H. W., and Katz, L. C. (2002). BDNF release from single cells elicits local dendritic growth in nearby neurons. *Nature Neuroscience* 5: 1177-1184.

339. Houchin-Ray, T., Huang, A., West, E., Zelivyanskaya, M., and Shea, L. D. (2008). Spatially Patterned Gene Expression for Guided Neurite Extension. *submitted.*

340. Siegbahn, A., Hammacher, A., Westermark, B., and Heldin, C. H. (1990). Differential-Effects of the Various Isoforms of Platelet-Derived Growth-Factor on Chemotaxis of Fibroblasts, Monocytes, and Granulocytes. *Journal of Clinical Investigation* 85: 916-920.

341. Levi-Montalcini, R. (1982). Developmental neurobiology and the natural history of nerve growth factor. *Annu Rev Neurosci* 5: 341-362.

342. Dent, E. W., and Kalil, K. (2001). Axon branching requires interactions between dynamic microtubules and actin filaments. *J Neurosci* 21: 9757-9769.
343. Zheng, J. Q., Wan, J. J., and Poo, M. M. (1996). Essential role of filopodia in chemotropic turning of nerve growth cone induced by a glutamate gradient. *Journal of Neuroscience* 16: 1140-1149.

344. Smith, D. S., and Skene, J. H. P. (1997). A transcription-dependent switch controls competence of adult neurons for distinct modes of axon growth. *Journal of Neuroscience* 17: 646-658.

345. Fu, S. Y., and Gordon, T. (1997). The cellular and molecular basis of peripheral nerve regeneration. *Molecular Neurobiology* 14: 67-116.

346. Caroni, P. (1997). Intrinsic neuronal determinants that promote axonal sprouting and elongation. *Bioessays* 19: 767-775.

347. Skene, J. H. P. (1989). Axonal Growth-Associated Proteins. *Annual Review of Neuroscience* 12: 127-156.

348. Fernandes, K. J. L., Fan, D. P., Tsui, B. J., Cassar, S. L., and Tetzlaff, W. (1999). Influence of the axotomy to cell body distance in rat rubrospinal and spinal motoneurons: Differential regulation of GAP-43, tubulins, and neurofilament-M. *Journal of Comparative Neurology* 414: 495-510.

349. Bomze, H. M., Bulsara, K. R., Iskandar, B. J., Caroni, P., and Skene, J. H. P. (2001). Spinal axon regeneration evoked by replacing two growth cone proteins in adult neurons. *Nature Neuroscience* 4: 38-43.

350. Slack, R. S., and Miller, F. D. (1996). Viral vectors for modulating gene expression in neurons. *Current Opinion in Neurobiology* 6: 576-583.

351. Tuszynski, M. H., Gabriel, K., Gage, F. H., Suhr, S., Meyer, S., and Rosetti, A. (1996). Nerve growth factor delivery by gene transfer induces differential outgrowth of sensory, motor, and noradrenergic neurites after adult spinal cord injury. *Experimental neurology* 137: 157-173.
352. Schmalenberg, K. E., and Uhrich, K. E. (2005). Micropatterned polymer substrates control alignment of proliferating Schwann cells to direct neuronal regeneration. *Biomaterials* 26: 1423-1430.

353. Kapur, T. A., and Shoichet, M. S. (2003). Chemically-bound nerve growth factor for neural tissue engineering applications. *J Biomater Sci Polym Ed* 14: 383-394.

354. Houchin-Ray, T., Swift, L. A., Jang, J. H., and Shea, L. D. (2007). Patterned PLG substrates for localized DNA delivery and directed neurite extension. *Biomaterials* 28: 2603-2611.

355. Sakiyama-Elbert, S. E., and Hubbell, J. A. (2001). Functional Biomaterials: Design of Novel Biomaterials. *Annual Review of Material Research* 31: 183-201.

356. Drury, J. L., and Mooney, D. J. (2003). Hydrogels for Tissue Engineering: Scaffold Design Variables and Applications. *Biomaterials* 24: 4337-4351.

357. Segura, T., Volk, M. J., and Shea, L. D. (2003). Substrate-Mediated DNA Delivery: Role of the Cationic Polymer Structure and Extend of Modification. *Journal of Controlled Release* 93: 69-84.

358. Segura, T., Chung, P. H., and Shea, L. D. (2005). DNA Delivery from Hyaluronic Acid-Collagen Hydrogels Via a Substrate-Mediated Approach. *Biomaterials* 26: 1575-1584.

359. Hennink, W. E., and van Nostrum, C. F. (2002). Novel Crosslinking Methods to Design Hydrogels. *Advanced Drug Delivery Reviews* 54: 13-36.

360. Kuo, K. C., and Ma, P. X. (2001). Ionically Crosslinked Alginate Hydrogels as Scaffolds for Tissue Engineering: Part 1. Structure, Gelation Rate and Mechanical Properties. *Biomaterials* 22: 511-521.

361. Pannier, A. K., and Shea, L. D. (2004). Controlled Release Systems for DNA Delivery. *Molecular Therapy* 10: 19-26.
362. Sershen, S., and West, J. (2002). Implantable, Polymeric Systems for Modulated Drug Delivery. *Advanced Drug Delivery Reviews* 54: 1225-1235.

363. Salvay, D. M., and Shea, L. D. (2006). Inductive Tissue Engineering with Protein and DNA-Releasing Scaffolds. *Molecular Biosystems* 2: 36-48.

364. Pack, D. W., Hoffman, A. S., Pun, S., and Stayton, P. S. (2005). Design and Development of Polymers for Gene Delivery. *Nature Review Drug Discovery* 4: 581-593.

365. Quick, D. J., and Anseth, K. S. (2004). DNA Delivery from Photocrosslinked PEG Hydrogels Encapsulation Efficiency, Release Profiles, and DNA Quality. *Journal of Controlled Release* 96: 341-351.

366. Kasper, F. K., et al. (2005). *In vitro* Release of Plasmid DNA from Oligo(poly(ethylene glycol) fumarate) Hydrogels. *Journal of Controlled Release* 104: 521-539.

367. Chun, K. W., Lee, J. B., Kim, S. H., and Park, T. G. (2005). Controlled Release of Plasmid DNA from Photo-cross-linked Pluronic Hydrogels. *Biomaterials* 26: 3319-3326.

368. Megeed, Z., Haider, M., Li, D., O'Malley, B. W., Cappello, J., and Ghandehari, H. (2004). *In vitro* and *in vivo* Evaluation of Recombinant Silk-elastinlike Hydrogels for Cancer Gene Therapy. *Journal of Controlled Release* 94: 433-445.

369. Meilander-Lin, N. J., Cheung, P. J., Wilson, D. L., and Bellamkonda, R. V. (2005). Sustained *in vivo* Gene Delivery from Agarose Hydrogel Prolongs Nonviral Gene Expression in Skin. *Tissue Engineering* 11: 546-555.

370. Quick, D. J., and Anseth, K. S. (2003). Gene Delivery in Tissue Engineering: A Photopolymer Platform to Coencapsulate Cells and Plasmid DNA. *Pharmaceutical Research* 20: 1730-1737.

371. Bengali, Z., et al. (2005). Gene Delivery Through Cell Culture Substrate Adsorbed DNA Complexes. *Biotechnology and Bioengineering* 90: 290-302.

372. Scherer, F., Schillinger, U., Putz, U., Stemberger, A., and Plank, C. (2002). Nonviral Vector Loaded Collagen Sponges for Sustained Gene Delivery in vitro and in vivo. *The Journal of Gene Medicine* 4: 634-643.

373. Honore´, I., Grosse, S., Frison, N., Favatier, F., Monsigny, M., and Fajac, I. (2005). Transcription of Plasmid DNA: Influence of Plasmid DNA/Polyethylenimine Complex Formation. *Journal of Controlled Release* 107: 537–546.

374. Fukunaka, Y., Iwanaga, K., Morimoto, K., Kakemi, M., and Tabata, Y. (2002). Controlled release of plasmid DNA from cationized gelatin hydrogels based on hydrogel degradation. *J Control Release* 80: 333-343.

375. Chen, J., and Abatangelo, G. (1999). Functions of Hyaluronan in Wound Repair. *Wound Repair and Regeneration* 7: 79-89.

376. Price, R., Myers, S., Leigh, I. M., and Navsaria, H. A. (2005). The Role of Hyaluronic Acid in Wound Healing - Assesment of Clinical Evidence. *The American Journal of Clinical Dermatology* 6: 393-402.

377. Segura, T., Anderson, B. C., Chung, P. H., Webber, R. E., Shull, K. R., and Shea, L. D. (2005). Crosslinked Hyaluronic Acid Hydrogels: A Strategy to Functionalize and Pattern. *Biomaterials* 26: 359-371.

378. Bryant, S. J., Nuttelman, C. R., and Anseth, K. S. (2000). Cytocompatiblity of UV and Visible Light Photoinitiating Systems on Cultured NIH/3T3 Fibroblasts in vitro. *Journal of Biomaterial Science Polymer Edition* 11: 439-457.

379. Van Krevelen, D. W. (1990). *Properties of Polymers: Their Correlation with Chemical Structure; Their Numerical Estimation and Prediction from Additive Group Contributions,* Elsevier Science Publishers, Amsterdam.

380. Raeber, G. P., Lutolf, M. P., and Hubbell, J. A. (2005). Molecularly Engineered PEG Hydrogels: A Novel Model System for Proteolytically Mediated Cell Migration. *Biophysical Journal* 89: 1374–1388.

381. Leach, J. B., Bivens, K. A., Patrick, J., Charles W., and Schmidt, C. E. (2003). Photocrosslinked Hyaluronic Acid Hydrogels: Natural, Biodegradable Tissue Engineering Scaffolds. *Biotechnology and Bioengineering* 82: 578-589.

382. Hiltunen, E. L. J., et al. (2002). Elevated Hyaluronan Concentration without Hyaluronidase Activation in Malignant Epithelial Ovarian Tumors. *Cancer Research* 62: 6410–6413.

383. Bitter, T., and Muir, H. M. (1962). A Modified Uronic Acid Carbazole Reaction. *Analytical Biochemistry* 4: 330-334.

384. Lui, Y., Shu, X. Z., and Prestwich, G. (2005). Biocompatibility and Stability of Disulfide-Crosslinked Hyaluronan Films. *Biomaterials* 26: 4737-4746.

385. Kreil, G. (1995). Hyaluronidases - A Group of Neglected Enzymes. *Protein Science* 4: 1666-1669.

386. Park, Y. D., Tirelli, N., and Hubbell, J. A. (2003). Photopolymerized Hyaluronic Acid-Based Hydrogels and Interpenetrating Networks. *Biomaterials* 24: 893-900.

387. Andreopoulos, F. M., Beckman, E. J., and Russell, A. J. (1998). Light-Induced Tailoring of PEG-Hydrogel Properties. *Biomaterials* 19: 1343-1352.

388. Cruise, G. M., Scharp, D. S., and Hubbell, J. A. (1998). Characterization of Permeability and Network Structure of Interfacially Photopolymerized Poly(ethylene glycol) Diacrylate Hydrogels. *Biomaterials* 19: 1287-1294.

389. Park, H., and Park, K. (1996). Hydrogels and Biodegradable Polymers for Bioapplications. In *Hydrogels and Biodegradable Polymers for Bioapplications* (R. M. Ottenbrite, S. J. Huang and K. Park, Eds.), pp. 2-10. American Chemical Society, Washington DC.

390. Cowman, M. K., et al. (2005). Extended, Relaxed, and Condensed Conformations of Hyaluronan Observed by Atomic Force Microscopy. *Biophysical Journal* 88: 590–602.
391. Lapcik, L., Chabrecek, P., and Stasko, A. (1991). Photodegradation of Hyaluronic Acid - EPR and Size Exclusion Chromatography Study. *Biopolymers* 31: 1429-1435.

392. Laurent, T. C., and Gergely, J. (1955). Light Scattering Studies on Hyaluronic Acid. *Journal of Biological Chemistry* 212: 325-332.

393. Laurent, T. C., Björk, I., Pietruszkiewicz, A., and Persson, H. (1963). On the Interaction Between Polysaccharides and Other Macromolecules. 2. Transport of Globular Particles through Hyalurounic Acid Solutions. *Biochimica et Biophysica Acta* 78: 351-359.

394. Leach, J. B., and Schmidt, C. E. (2005). Characterization of Protein Release from Photocrosslinkable Hyaluronic Acid-Polyethylene Glycol Hydrogel Tissue Engineering Scaffolds. *Biomaterials* 26: 125–135.

395. Ledley, F. D. (1996). Pharmaceutical Approach to Somatic Gene Therapy. *Pharmaceutical Research* 13: 1595-1614.

396. Jabbari, E. (2004). Release Characteristics of a Model Plasmid DNA Encapsulated in Biodegradable Poly(ethylene glycol fumarate)/Acrylamide Hydrogel Microspheres. *Journal of Microencapsulation* 21: 525–538.

397. Nishikawa, M., Takemura, S., Takakura, Y., and Hashida, M. (1998). Targeted Delivery of Plasmid DNA to Hepatocytes *in vivo*: Optimization of the Pharmacokinetics of Plasmid DNA Galactosylated Poly(L-Lysine) Complexes by Controlling Their Physicochemical Properties. *The Journal of Pharmacology and Experimental Therapeutics* 287: 408–415.

398. Mellott, M. B., Searcy, K., and Pishko, M. V. (2001). Release of Protein from Highly Cross-linked Hydrogels of Poly(ethylene glycol) Diacrylate Fabricated by UV Polymerization. *Biomaterials* 22: 929-941.

399. Kong, H. J., Lui, J., Riddle, K., Matsumoto, T., Leach, K., and Mooney, D. J. (2005). Non-viral Gene Delivery Regulated by Stiffness of Cell Adhesion Substrates. *Nature Materials* 4: 460-464.

400. Rudge, J. S., et al. (1994). Neurotrophic Factor Receptors and Their Signal-Transduction Capabilities in Rat Astrocytes. *European Journal of Neuroscience* 6: 693-705.

401. McKeon, R. J., Jurynec, M. J., and Buck, C. R. (1999). The chondroitin sulfate proteoglycans neurocan and phosphacan are expressed by reactive astrocytes in the chronic CNS glial scar. *Journal of Neuroscience* 19: 10778-10788.

402. Kantor, D. B., et al. (2004). Semaphorin 5A is a bifunctional axon guidance cue regulated by heparan and chondroitin sulfate proteoglycans. *Neuron* 44: 961-975.

403. Bailey, S. N., Wu, R. Z., and Sabatini, D. M. (2002). Applications of transfected cell microarrays in high-throughput drug discovery. *Drug Discovery Today* 7: S113-S118.

404. Pierce, G. F., Mustoe, T. A., Altrock, B. W., Deuel, T. F., and Thomason, A. (1991). Role of Platelet-Derived Growth-Factor in Wound-Healing. *Journal of Cellular Biochemistry* 45: 319-326.

405. Strieter, R. M., et al. (1995). The Functional-Role of the Elr Motif in Cxc Chemokine-Mediated Angiogenesis. *Journal of Biological Chemistry* 270: 27348-27357.

406. Sharma, B., and Elisseeff, J. H. (2004). Engineering structurally organized cartilage and bone tissues. *Annals of Biomedical Engineering* 32: 148-159.

407. Son, B. R., et al. (2006). Migration of bone marrow and cord blood mesenchymal stem cells in vitro is regulated by stromal-derived factor-1-CXCR4 and hepatocyte growth factor-c-met axes and involves matrix metalloproteinases. *Stem Cells* 24: 1254-1264.

408. Caplan, A. I. (2000). Tissue engineering designs for the future: New logics, old molecules. *Tissue Engineering* 6: 1-8.

409. Li, Z. H., et al. (2003). Controlled gene delivery system based on thermosensitive biodegradable hydrogel. *Pharmaceutical Research* 20: 884-888.

410. Kushibiki, T., Tomoshige, R., Fukunaka, Y., Kakemi, M., and Tabata, Y. (2003). In vivo release and gene expression of plasmid DNA by hydrogels of gelatin with different cationization extents. *Journal of Controlled Release* 90: 207-216.

411. Lv, Q., Hu, K., Feng, Q., and Cui, F. (2008). Fibroin/collagen hybrid hydrogels with crosslinking method: Preparation, properties, and cytocompatibility. *Journal of Biomedical Materials Research Part A* 84A: 198-207.

412. Nagase, H., and Fields, G. B. (1996). Human matrix metalloproteinase specificity studies using collagen sequence-based synthetic peptides. *Biopolymers* 40: 399-416.

413. Gobin, A. S., and West, J. L. (2002). Cell migration through defined, synthetic extracellular matrix analogues. *Faseb Journal* 16: 751-+.

414. Rosenberg, G. A., et al. (2001). Immunohistochemistry of matrix metalloproteinases in reperfusion injury to rat brain: activation of MMP-9 linked to stromelysin-1 and microglia in cell cultures. *Brain Research* 893: 104-112.